

AD-A162 765

STUDY OF TRANSPORT PROPERTIES AND STRUCTURE OF  
EXTENDED-CHAIN POLYMERS (U) VIRGINIA UNIV  
CHARLOTTESVILLE DEPT OF MATERIALS SCIENCE

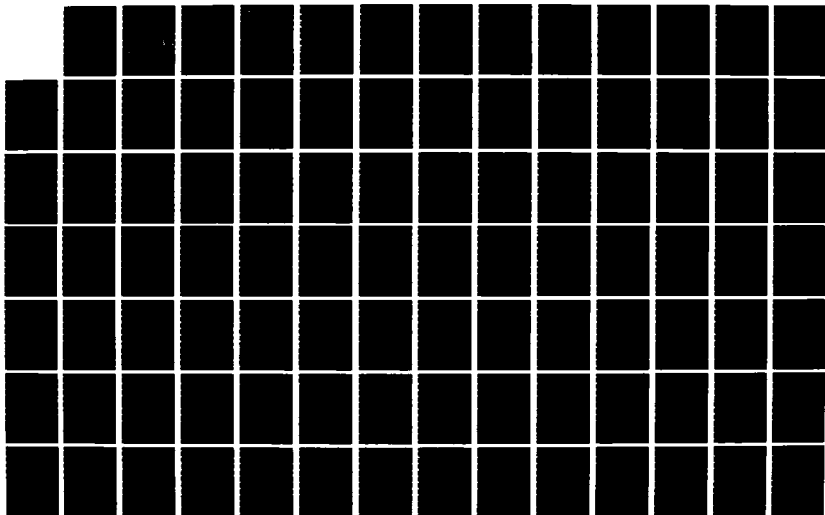
1/3

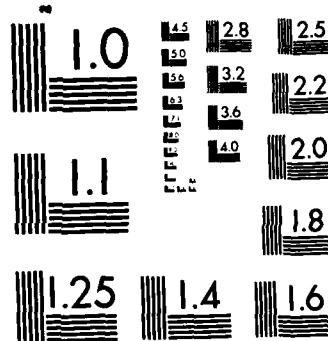
UNCLASSIFIED

R E BARKER ET AL SEP 85

F/G 11/9

NL





MICROCOPY RESOLUTION TEST CHART  
NATIONAL BUREAU OF STANDARDS-1963-A

AEOSR-TR- 85-1111

Final Report

Grant No. 80-0014A,B

STUDY OF TRANSPORT PROPERTIES AND STRUCTURE  
OF EXTENDED-CHAIN POLYMERS

For the period October 1, 1979 - March 31, 1983

Submitted to:

U.S. Air Force Office of Scientific Research  
Bolling Air Force Base  
Washington, D.C. 20332

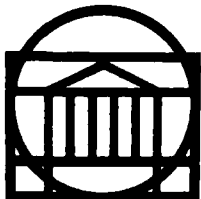
Attention: Mr. Donald R. Ulrich  
Building 410 NC

Submitted by:

R. E. Barker, Jr.  
Professor

K. R. Lawless  
Professor and Chairman

AD-A162 765



DTIC FILE COPY

Report No. UVA/525631/MS86/103  
September 1985

DTIC  
ELECTE  
DEC 30 1985  
S A

SCHOOL OF ENGINEERING AND  
APPLIED SCIENCE

DEPARTMENT OF MATERIALS SCIENCE

Approved for public release,  
distribution unlimited

UNIVERSITY OF VIRGINIA  
CHARLOTTESVILLE, VIRGINIA 22901

85 12 30 029

Final Report

Grant No. 80-0014A,B

STUDY OF TRANSPORT PROPERTIES AND STRUCTURE  
OF EXTENDED-CHAIN POLYMERS

For the period October 1, 1979 - March 31, 1983

Submitted to:

U.S. Army Office of Scientific Research  
Bolling Air Force Base  
Washington, D.C. 20332

Attention: Mr. Donald R. Ulrich  
Building 410 NC

Submitted by:

R. E. Barker, Jr.  
Professor

K. R. Lawless  
Professor and Chairman

Department of Materials Science  
SCHOOL OF ENGINEERING AND APPLIED SCIENCE  
UNIVERSITY OF VIRGINIA  
CHARLOTTESVILLE, VIRGINIA

Report No. UVA/525631/MS86/103  
September 1985

Copy No. \_\_\_\_\_



Unclassified

SECURITY CLASSIFICATION OF THIS PAGE (When Data Entered)

REPORT DOCUMENTATION PAGE		READ INSTRUCTIONS BEFORE COMPLETING FORM
1. REPORT NUMBER <b>AFOSR-TR- 85-1111</b>	2. GOVT ACCESSION NO. <b>AD-A163 765</b>	3. RECIPIENT'S CATALOG NUMBER
4. TITLE (and Subtitle) Study of Transport Properties and Structure in Extended Chain Polymers		5. TYPE OF REPORT & PERIOD COVERED Final Report October 1979 - March 1983
		6. PERFORMING ORG. REPORT NUMBER
7. AUTHOR(s) R. Edward Barker, Jr. and Kenneth R. Lawless (with Daniel Y. Chen on Part II)		8. CONTRACT OR GRANT NUMBER(s) AFOSR-80-0014
9. PERFORMING ORGANIZATION NAME AND ADDRESS Department of Materials Science Thornton Hall, University of Virginia Charlottesville, Virginia 22901		10. PROGRAM ELEMENT, PROJECT, TASK AREA & WORK UNIT NUMBERS <b>2303/A3</b> <b>61102E</b>
11. CONTROLLING OFFICE NAME AND ADDRESS U.S. Air Force Office of Scientific Research / NC Bolling AFB, Washington, D.C. 20332-6448		12. REPORT DATE September 1985
		13. NUMBER OF PAGES <b>284</b>
14. MONITORING AGENCY NAME & ADDRESS (if different from Controlling Office)		15. SECURITY CLASS. (of this report) Unclassified
		15a. DECLASSIFICATION/DOWNGRADING SCHEDULE
16. DISTRIBUTION STATEMENT (of this Report)  <b>Approved for public release, distribution unlimited</b>		
17. DISTRIBUTION STATEMENT (of the abstract entered in Block 20, if different from Report)		
18. SUPPLEMENTARY NOTES		
19. KEY WORDS (Continue on reverse side if necessary and identify by block number) Poly para phenylene benzobisthiazole (PPBT)      Thermal conductivity Extended chain polymers      Transport properties Electrical conductivity      Diffusion Ionic conductivity      Sorption Electrode systems		
20. ABSTRACT (Continue on reverse side if necessary and identify by block number) The broad objective of the work was to relate charge, heat, and mass transport in the Air Force's extended chain polymers (especially poly-para-phenylene benzobisthiazole PBT) to other electrical, thermal, mechanical and microstructural properties of the polymers and also to compare these very unusual, highly anisotropic Air Force materials with other materials when it is scientifically relevant or when potential applications may be involved. Special techniques were developed for (continued on back)		

DD FORM 1473

1 JAN 73

EDITION OF 1 NOV 65 IS OBSOLETE

Unclassified

SECURITY CLASSIFICATION OF THIS PAGE (When Data Entered)

Unclassified

20. ABSTRACT

making transport-property determinations on samples in the form of thin fibers and small area films. Two types of miniature cells were developed in the study of PBT transport properties, and an application for a patent has been filed through the legal offices of the Air Force. A very promising area of the research relates to an anisotropic version of the Barker-Sharbaugh weak electrolyte model for ionic conduction in polymers. Theoretically and experimentally there is substantial overlap with the work on diffusion and solubility. A new technique which has been termed the diffusion controlled-differential current (DCDC) method evolved from experiments related to the weak electrolyte model. This DCDC-technique looks promising as a new analytical tool.

The results for PBT turned out to be especially interesting because the ratio of ionic conductivities parallel and perpendicular to the chain axis was very large ( $10^3$  at 300K) and temperature dependent (smaller ratio at a higher temperature). Special techniques for the thermal conductivity allowed the axial and perpendicular thermal conductivities to be determined. The perpendicular value  $K_{22}$  was approximately 200 mW/m°C (fairly typical for an isotropic polymer) but the axial value  $K_{11} \approx 1000$  mW/m°C may be large enough to suggest practical applications. Sorption of water and common organic vapors was small but not negligible. A dual sorption model had to be invoked to explain the observations.

Unclassified

## FOREWORD

The research described in this report was performed in the Materials Science Department at the University of Virginia. The work was initiated under Grant AFOSR-80-0014, entitled, "Study of Inter-relationships Between Microstructural and Transport Properties in Extended Chain Aromatic Polymers," and was administered under the direction of the Air Force Office of Scientific Research, Bolling Air Force Base, Washington, D.C. 20332. The original grants spanned the period October 1, 1979 through September 31, 1982. A no-cost extension until March 31, 1983 was approved. Due to the fact that three of the GRAs affiliated with the grant during its total duration were not U.S. citizens, the Export Control Law sometimes interfered with the most efficient pursuit of the research objectives, not only by restricting the non-citizens' access to relevant reports from other AF grantees, but also by inhibiting our discussions during seminars on the research. The research has involved a considerable degree of interdependence with Air Force personnel and other USAFOSR and AFWPL grantees and we take this opportunity to express our appreciation to all who provided us with samples and helpful information and cooperation, often beyond the call of duty and at critical times as a lengthy series of improbable circumstances delayed the normal presentation of this report. In these regards we would especially mention Dr. E. C. Chenevey and Dr. J. R. Leal of the Celanese Research Company, Dr. D. Bhaumik, Prof. J. E. Mark and Dr. W. J. Welsh of the University of Cincinnati, Professors S. L. Hsu, F. E.

AIR FORCE OFFICE OF SCIENTIFIC RESEARCH  
NOTICE OF  
THIS  
OFFICE  
OF  
AFWPL  
OF  
OF

Karasz, R. S. Porter, and E. L. Thomas of the University of  
Massachusetts, Dr. J. F. Wolfe of Stanford Research Institute, Dr. T.  
E. Helminiak of WPAFB, and Dr. D. R. Ulrich of AFOSR.



		<input checked="" type="checkbox"/>
		<input type="checkbox"/>
		<input type="checkbox"/>
Library Codes		
Dist	Average d/or Special	
A-1		

## TABLE OF CONTENTS

	<u>Page</u>
REPORT DOCUMENTATION FORM.....	ii
FOREWORD .....	iii
PART I SUMMARY OF GRANT PROGRESS	
I. Introduction .....	3
II. Results .....	5
III. Professional Personnel and Interactions ...	66
IV. New Discoveries and Inventions .....	68
V. Concluding Remarks .....	70
PART II TECHNICAL NARRATIVE: CHARGE TRANSPORT IN EXTENDED CHAIN POLYMERS	
I. Introduction .....	76
II. Background .....	87
III. Experimental Instrumentation and Techniques .....	144
IV. Experimental Results and Discussion .....	171
V. Weak Electrolyte Model (Ionic Conduction) .....	208
VI. I <sub>2</sub> Doping Experiments (Electronic Conduction .	217
VII. Future Research Possibilities and Applications .....	230
VIII. Conclusions .....	248
References .....	251
Appendices .....	256

PART I  
SUMMARY OF GRANT PROGRESS

## CONTENTS

	<u>Page</u>
PART I SUMMARY OF GRANT PROGRESS	
I. Introduction .....	3
A. Objectives .....	3
B. Status of Research .....	4
II. Results .....	5
A. Cumulative List of Publications and Presentations under Grant AFOSR 80-0014 ..	5
B. Published Reprints and Abstracts .....	9
C. Summary of Results for Thermal Conductivity .....	50
D. Summary of Results for Vapor Diffusion and Solubility in PPBT .....	59
III. Professional Personnel and Interactions ...	66
A. Professional Personnel .....	66
B. Interactions .....	67
IV. New Discoveries and Inventions .....	68
V. Concluding Remarks .....	70

## I. INTRODUCTION

### A. Objectives

The overall goals of this research were to conduct studies of three of the five transport properties (see below) of the Air Force's new rigid extended chain polymers (in particular polyparaphenylene benzobisthiazole, PPBT or PBT) and to relate the transport properties to certain structural features and processing conditions.

Transport properties (diffusion, thermal conductivity, electrical conductivity, etc.) have proved remarkably fruitful in providing insight into the nature of many polymeric materials. However, prior to this study little had been done in the way of systematic studies of these properties for the kinds of rod-like polymers of interest to the Air Force. This lack of information was in part due to the difficult nature of some of the needed experiments. The difficulties arose because of the small amounts of material available, to its surface features, and to its extreme anisotropy.

There are five important types of phenomena which can be classified as transport processes in polymers. These are:

1. Diffusion and Permeation  
(of small vapor and gas molecules, segmental movements, etc.)
2. Electrical Conduction  
(similar to diffusion but involving charge carriers in an electric field)
3. Sound and Mechanical Impulses
4. Thermal Conduction  
(similar to sound but at very much higher dominant frequencies)



## 5. Viscoelastic Creep

(bearing some obvious, and some subtle, relations to 1, 3, and 4).

In the research performed under Grant AFOSR 80-0014, the major concern has been with diffusion (and permeation), electrical conduction (and some related dielectric properties), and thermal conductivity. Eventually research in the other two areas should be undertaken in a subsequently funded study.

### B. Status of Research

As will be detailed in other sections of this report, the research has achieved the goal of providing better understanding of the nature of transport properties in highly anisotropic polymeric systems. Due to the very limited amounts of PPBT available, and the physical forms available, many of the measurements turned out to be much more difficult than originally thought so that a set of special measuring techniques evolved which should be useful for other experimenters in different fields. The work has led to one Ph.D. dissertation (Daniel Y. Chen) and two M.S. theses (Wu Song Huang and Larry J. Adams). Counting the dissertation and theses the research under Grant USAFOSR 80-0014 has led to a total of 24 publications and presentations and an application for a patent (AF/JACPD - File S/N 06/528,309). More importantly, the research has produced a new theoretical formalism for predicting the anisotropy in the ionic conductivity from the dielectric permittivity tensor and certain other material parameters such as the moisture sorption coefficient. This theory appears to provide a good nutrient for future research and is connected with the development of a new experimental technique: Diffusion Controlled Differential Current (DCDC).

In addition to the measurement of the ionic conductivity tensor components for a variety of environmental conditions, the research also has led to interesting and useful results for the thermal conductivity tensor components and for the diffusion and sorption coefficients for benzene and water, and in the case of water, for the effects of a number of complex metallic salts. In the case of the thermal conductivity, an extensive examination of suitable techniques was conducted before a successful combination was discovered. The Kohlrausch method and its adaptation by I. L. Kalnin, M. J. Ram, and R. Dix (AFML-TR-72-151, November 1972) to measure the thermal conductivity of graphite fibers was not suitable for PPBT because the combination of electrical and thermal conductivities for the two materials is quite different. The most useful method for our experiments was a modification of the de Senarmont technique in conjunction with a miniature thin film apparatus.

## II. RESULTS

### A. Cumulative List of Publications and Presentations under Grant AFOSR 80-0014

(1) D. Y. Chen and R. E. Barker, Jr., "Techniques for the Measurement of the Axial Electrical Conductivity of Polymer Fibers," presented at the 58th Meeting, Virginia Academy of Science, Charlottesville, VA, May 13-16, 1980. Abstract published in Va. J. Sci., 31, 129 (1980).

(2) L. J. Adams and R. E. Barker, Jr., "Preliminary Attempts to Determine the Axial Thermal Conductivity of Small Polymer Fibers," presented at the 58th Meeting, Virginia Academy of Science, Charlottesville, VA, May 13-16, 1980). Abstract published in Va. J. Sci., 31, 128 (1980).

(3) R. E. Barker, Jr., "Considerations of Transport Property Investigations in Ordered Polymers," Air Force Ordered Polymers Review, Dayton, Ohio, January 8, 1980.

(4) R. E. Barker, Jr., "Non-Ohmic Processes in Polymers," Invited talk, Polymer Research Center, University of Cincinnati, April 3, 1980.

(5) R. E. Barker, Jr., "Review of Study on the Relationships between Structure and Transport Properties in Extended-Chain Aromatic Polymers," Air Force Order Polymers Review, Dayton, Ohio, September 22-24, 1980.

(6) D. Y. Chen and R. E. Barker, Jr., "Current-Voltage Characteristics of Small Diameter Poly(p-phenylene benzobisthiazole) Fibers," presented at the DHPP session of the March Meeting of the Am. Phys. Soc., Phoenix, Arizona, March 16-20, 1981. Abstract published in Bulletin Am. Phys. Soc., 26, 434 (1981).

(7) R. E. Barker, Jr., D. Y. Chen, and L. J. Adams, "Problems in the Determination of Anisotropic Transport Properties in Very Thin Polymer Fibers," presented at the 1980 Annual Conference on Electrical Insulation and Dielectric Phenomena (National Research Council - Assembly of Engineering), Boston, Mass., October 26-29, 1980. 1980 Annual Report CEIDP, National Academy Press, Washington, D.C., I.S.B.N. 0-309-03126-5, pp. 357-383 (1980).

(8) R. E. Barker, Jr. and L. J. Adams, "Thermal Conduction in Polymers and its Relation to Electrical Systems," presented at the North American Thermal Analysis Society Symposium on "Application of Thermal Analysis to the Electronics and Electrical Industries," October 26-29, 1980, Boston, Mass.

(9) D. Y. Chen and R. E. Barker, Jr., "Electrical Conductivity of Highly Anisotropic Fibers and Films of Poly (paraphenylene benzobisthiazole)," presented at the 59th Annual Meeting of the Virginia Academy of Science, Old Dominion University, Norfolk, Virginia, May 14, 1981. Abstract published in Va. J. Sci., 32, 131 (Fall 1981).

(10) W. S. Huang and R. E. Barker, Jr., "Development of Techniques to Study Vapor Diffusion and Solubility in Fibers and Films of Poly (paraphenylene benzobisthiazole)," presented at the 59th Annual Meeting of the Virginia Academy of Science, Old Dominion University, Norfolk, Virginia, May 14, 1981. Abstract published in Va. J. Sci., 32, 131 (Fall 1981).

(11) L. J. Adams and R. E. Barker, Jr., "Techniques for the Determination of the Thermal Conductivity of Small Fibers and Films," presented at the 59th Annual Meeting of the Virginia Academy of Science, Old Dominion University, Norfolk, Virginia, May 14, 1981. Abstract published in Va. J. Sci., 32, 130 (Fall 1981).

(12) R. E. Barker, Jr. and D. Y. Chen, "Electrical Conductivity of Anisotropic Poly (paraphenylene benzobisthiazole)," presented at the 1981 Annual Conference on Electrical Insulation and Dielectric Phenomena (sponsored by the IEEE Electrical Insulation Society), Whitehaven, Pennsylvania, October 26-28, 1981. Paper published in the 1981 Annual Report CEIDP, IEEE Service Center, 81CH1668-3, pp. 351-359 (1981).

(13) R. E. Barker, Jr., D. Y. Chen, and W. S. Huang, "The Anisotropic Transport of Charged and Neutral Species in Extended Chain Polymers," presented at the DHPP Session of the March Meeting

of the Am. Phys. Soc., Dallas, Texas, March 8-12, 1982. Abstract published in Bulletin Am. Phys. Soc., 27, 169 (1982).

(14) D. Y. Chen and R. E. Barker, Jr., "Evidence for the Applicability of an Anisotropic Version of the Weak-Electrolyte Theory of Ionic Conductivity in Extended Chain Polymers," presented at the 60th Annual Meeting of the Virginia Academy of Science, Virginia Polytechnic Institute, Blacksburg, Virginia, April 22, 1982. Abstract published in Va. J. Sci., 33(3), 159 (1982).

(15) W. S. Huang and R. E. Barker, Jr., "Dual Sorption Model for Diffusion in Poly (p-phenylene benzobisthiazole)," presented at the 60th Annual Meeting of the Virginia Academy of Science, Virginia Polytechnic Institute, Blacksburg, Virginia, April 22, 1982. Abstract published in Va. J. Sci., 33(3), 158 (1982).

(16) R. E. Barker, Jr., D. Y. Chen, and W. S. Huang, "Ionic Transients in an Extended Chain Aromatic Hetero-Cyclic Polymer," 1982 Annual Report: Conference on Electrical Insulation and Dielectric Phenomena, IEEE - Electrical Insulation Society, Publication 82CH1773-1 Lib. Congr. No. 79-649806, pp. 102-107 (October 1982).

(17) R. E. Barker, Jr., "Overview of the Status of Experimental and Theoretical Research on the Electrical Conductivity of Extended Chain Aromatic Hetero-cyclic Polymers," U.S. Air Force (AFWAL/MLBC) meeting on: Transport Properties of Rigid Rod Polymers, Dayton, Ohio, February 9, 1983. Oral presentation.

(18) R. E. Barker, Jr., "Diffusion in Polymers: Theory and Experiment," Invited talk, Polymer Physics Seminar, National Bureau of Standards, Gaithersburg, Maryland, February 17, 1983.

(19)\* J. A. Hawk, D. Y. Chen, and R. E. Barker, Jr., "Studies of the Effects of Moisture Sorption on Electrical Conduction in Ion Doped Polymers," presented at the 61st Annual Meeting of the Virginia Academy of Science, May 18-20, 1983, George Mason University, Fairfax, Virginia. Abstract published in Va. J. Sci., 34(3), 181 (1983).

(20)\* C. C. Huang and R. E. Barker, Jr., "Transient Dielectric Properties of Polymer-Diluent Systems," presented at the 61st Annual Meeting of the Virginia Academy of Science, May 18-20, 1983, George Mason University, Fairfax, Virginia. Abstract published in Va. J. Sci., 34(3), 180 (1983).

(21)\* R. E. Barker, Jr., D. Y. Chen, J. A. Hawk, and C. C. Huang, "Extension of the Weak Electrolyte Model to Anisotropic Polymers," presented at the 1983 Annual Conference on Electrical Insulation and Dielectric Phenomena (Institute of Electrical and Electronics Engineers), Buck Inn, Buck Hill Falls, Pennsylvania, October 16-20, 1983.

B. Published Reprints and Abstracts

Published reprints and abstracts can be found on the following pages.

\* These were covered in part by AFOSR 82-0290.

# VIRGINIA JOURNAL OF SCIENCE

OFFICIAL PUBLICATION OF THE VIRGINIA ACADEMY OF SCIENCE

Vol. 31

No. 4

129

Winter 1980

TECHNIQUES FOR THE MEASUREMENT OF THE AXIAL ELECTRICAL CONDUCTIVITY OF POLYMER FIBERS. D. Y. Chen and R. E. Barker, Jr., Materials Science Dept., Univ. of Va., Charlottesville, VA. 22901.

Certain evidence indicates that an extended chain ("rod-like") polymer, such as a polybenzobisthiazole, will have a larger electrical conductivity along its chain direction than along other directions. Efforts to study electrical anisotropy in fibers and fibrilose films often encounter extreme difficulties when the level of conductivity is low. Many factors contribute to the difficulty, among them: the small cross-section of a fiber, electrostatic shielding, electrode contacts, etc. In this paper, a number of techniques for determining the anisotropic electrical properties are discussed. Furthermore there is an intrinsic importance in techniques capable of yielding values for the transport properties of small fibers.

# VIRGINIA JOURNAL OF SCIENCE

OFFICIAL PUBLICATION OF THE VIRGINIA ACADEMY OF SCIENCE

Vol. 31

No. 4

128

Winter 1980

## Materials Science

Fifty-Eighth Annual Meeting of the Virginia Academy of Science  
May 13-16, 1980, University of Virginia

PRELIMINARY ATTEMPTS TO DETERMINE THE AXIAL THERMAL CONDUCTIVITY OF SMALL POLYMER FIBERS. Larry J. Adams and R. E. Barker, Jr., Materials Science Dept., Univ. of Va. Charlottesville, Va. 22901.

Even under ideal circumstances certain difficulties may be encountered in measuring the true thermal conductivity perpendicular to the surface of a polymer film. The difficulties are greatly magnified when it is desired to determine the anisotropic conductivities in a small fiber or thin fibrillous film. However this is a frequently occurring situation and it would be valuable to have a technique capable of overcoming the formidable problems. Among other merits, such a technique would make it possible to determine the axial conductivities  $K_{||}$  of small amounts of newly synthesized fibrous materials. Such a technique also would have important theoretical implications with regard to the effect of fiber size relative to dominant phonon wavelength. For these and related reasons we are investigating methods that may make possible the determination of  $K_{||}$  and  $K_{\perp}$  for small fibers. (Funded by Airforce Office of Scientific research, Grant No. AFOSR-80-0014)



Classification  
No. 72.20

Abstract Submitted for the  
March 1981  
(Phoenix) Meeting of the American Physical Society

Division of High  
Polymer Physics

Current-Voltage Characteristics of Small Diameter Poly(p-phenylene benzobisthiazole) Fibers. D.Y. CHEN, and R.E. BARKER, JR., Dept. of Materials Science, U. of Virginia.\*--It is very difficult to measure I-V characteristics for very small insulating fibers although this type of information would frequently be useful in polymer science and in biophysics. This paper discusses our efforts to make such measurements on some 10 to 40  $\mu$ m diameter PBT fibers. Several electrode systems suitable for this kind of measurement will be discussed including some designed for use within a scanning electron microscope (SEM). The monomers for PBT and similar polymers tend to form nematic phase liquid crystals and this tendency is carried over into the polymeric solid state, leading to an extreme anisotropy of mechanical and electrical properties. In addition to developing techniques for making charge transport measurements on very small diameter polymer samples, the research has been concerned with the influence of the small size itself because the dominant phonon wavelength may be comparable to the diameter. The effect of temperature on the electrical conduction is also considered in this paper.

\*Supported by US Air Force Grant AFOSR 80-0014

# 1980 Annual Report

## *Conference on Electrical Insulation and Dielectric Phenomena*

prepared by the  
PROGRAM COMMITTEE  
of the  
CONFERENCE ON ELECTRICAL INSULATION  
AND DIELECTRIC PHENOMENA

ASSEMBLY OF ENGINEERING  
NATIONAL RESEARCH COUNCIL

Editors: Steven A. Boggs, Chathan M. Cooke, R. J. Densley,  
J. K. Nelson, D. Turnquist, James E. West, M. Zahn

NATIONAL ACADEMY PRESS  
WASHINGTON, D.C. OCT. 1980

The National Research Council was established by the National Academy of Sciences in 1916 to associate the broad community of science and technology with the Academy's purposes of furthering knowledge and of advising the federal government. The Council operates in accordance with general policies determined by the Academy under the authority of its Congressional charter of 1863, which establishes the Academy as a private, non-profit, self-governing membership corporation. The Council has become the principal operating agency of both the Academy of Sciences and the National Academy of Engineering in the conduct of their services to the government, the public, and the scientific and engineering communities. It is administered jointly by both Academies and the Institute of Medicine. The Academy of Engineering and the Institute of Medicine were established in 1964 and 1970, respectively, under the charter of the Academy of Sciences.

International Standard Book Number 0-309-03126-5

Library of Congress Catalog Card Number 79-649806

Available from:

National Academy Press  
2101 Constitution Avenue, N.W.  
Washington, D.C. 20418

Printed in the United States of America

## ABSTRACT

### PROBLEMS IN THE DETERMINATION OF ANISOTROPIC TRANSPORT PROPERTIES IN VERY THIN POLYMER FIBERS

by

R. E. Barker, Jr., D. Y. Chen, and L. J. Adams

Department of Materials Science  
University of Virginia  
Charlottesville, Virginia 22901


In a research program supported by the U.S. Air Force (AFOSR80-0014) the only form of samples currently available for study are thin fibers (5 to 20  $\mu\text{m}$  diameter) and fibrilose films of irregular thickness and relatively small area ( $\sim 1\text{ cm}^2$ ). The particular polymers involved (polybenzthiazoles: PBT) are stronger than steel along their fiber axis and have use temperatures above  $300^\circ\text{C}$  and are members of a class of materials referred to as "rod-like polymers" or "self-reinforcing composites." The monomers for such polymers are fairly rigid planar molecules which form nematic phase liquid crystals. This basic structure tends to be carried over into the polymeric form. Virtually nothing has been done in the way of systematic studies of transport properties in these polymers although their molecular structure suggests the results would be of great scientific interest. Furthermore there is an intrinsic importance in techniques capable of yielding values for the transport properties of small fibers. Such materials are anisotropic and, especially in the case of thermal conductivity, the transport properties may be influenced by the small sample size because the dominant phonon wavelength will be a significant fraction of the minimum dimension of the specimen. This paper discusses some of the problems involved in the measurement of electrical conductivity and thermal conductivity in thin fibers.

# PROBLEMS IN THE DETERMINATION OF ANISOTROPIC TRANSPORT PROPERTIES IN VERY THIN POLYMER FIBERS

R. E. Barker, Jr., D. Y. Chen, and L. J. Adams  
Materials Science Department  
University of Virginia  
Charlottesville, Virginia

## INTRODUCTION

The technological need often arises to know the conductivity of a thin fiber. There are numerous references in the literature to the conductivity of fibers but when one looks in detail at these references it is found that the measurements have been made on woven fabrics or mats of fibers.

In a research program supported by the U. S. Air Force (AFOSR-80-0014) the only form of samples currently available for study are thin fibers (5 to 20  $\mu\text{m}$  diameter) and fibrilose films of irregular thickness and relatively small area ( $\sim 1\text{ cm}^2$ ). The particular polymers involved (poly-p-phenylene benzobisthiazole ) or PBT, and related polymers) are stronger than steel along their fiber axis, have use temperatures above  $300^\circ\text{C}$  and are members of a class of materials referred to as "rod-like" or extended chain polymers.<sup>1-3</sup> The monomers for such polymers are fairly rigid planar molecules which form nematic phase liquid crystals. This basic structure tends to be carried over into the polymeric form. Virtually nothing has been done in the way of systematic studies of transport properties in these polymers although their molecular structure suggests the results would be of great scientific interest. Furthermore there is an intrinsic importance in techniques capable of yielding values for the transport properties of small fibers. Such materials are anisotropic and, especially in the case of thermal conductivity, the transport properties may be influenced by the small sample size because the dominant phonon wavelength will be a significant fraction of the minimum dimension of the specimen. This paper discusses some of the problems involved in the measurement of elec-

trical conductivity and thermal conductivity in thin fibers.

#### NATURE OF DIFFICULTIES

For both the electrical and thermal conductivity measurements the most serious problems are very similar and arise due to the very small cross-section of the fibers. Some typical problem areas are listed.

- Low total current or heat flux.
- Difficult manipulation and preparation of samples.
- Problems with contacts, anisotropy
- Thermometric devices disturb temperature.
- Unfeasible to use guarded electrodes or hot plates.
- Surface and volume conductivities mixed.

Numerical examples will illustrate the severity of the difficulties. A 20 $\mu$ m diameter fiber with a test dimension  $b = 100\mu$ m, an electrical conductivity  $\sigma = 10^{-14}$ S/m, and a potential drop of 100V, would have a current  $I = \pi r^2 \sigma V / b \approx 3 \times 10^{-18}$ A, to be contrasted with  $I \sim 10^{-11}$ A for a sample with a more typical area of 10 cm<sup>2</sup>. If the 20 $\mu$ m fiber has a thermal conductivity  $K \approx 300$ mW m<sup>-1</sup>K<sup>-1</sup> then the thermal power flux in a temperature gradient of 0.1K/mm will be  $Q = K \pi r^2 \nabla T \sim 10$ nW. By contrast, a 10 mil (254 $\mu$ m) diameter copper thermocouple lead, in the same gradient, would have a thermal flux of 2mW. This 10<sup>5</sup>-fold difference, coupled to a large difference in total heat capacities, means that the disturbance of the system measured by the measuring device is a serious problem. The various difficulties are compounded if the dependences of transport properties on pressure or mechanical stress are also sought.

#### EXPERIMENTAL APPROACHES

Many approaches have been considered. Some of the more feasible ones are listed below for the electrical measurements.

1. Evaporated electrodes with a very small gap (fibers and fibrilose films).
2. Bundles of fibers mounted in low melting metals.

3. Electrochemically formed "catwhisker" on a microtomed disc.
4. Doped polymers ( $I_2$ ,  $AsF_5$ , etc.) to increase  $\sigma$ .
5. Oriented polymer on surface of a long wire.
6. Partially delaminated mica sandwich (films).
7. Interdigitated electrode systems.
8. Scanning electron microscope used as a surface potential probe.

Some of these will be mentioned in more detail, particularly the SEM method.

Among the many methods considered for the measurement of thermal conduction are the following.

1. Symmetrical comparison bridges using bundles of fibers mounted in contact with thermocouples, thermistors, etc.
2. Use of small light bulb filament as a heat source.
3. Oriented polymer on the surface of a long resistance wire.
4. Modified Ingen-Hausz<sup>4</sup> method using Tempilstik markers or other temperature indicators.
5. Modified Angstrom<sup>5</sup> periodic temperature wave method.

Since it is desired to measure conductivity along the chain axis as well as transverse to it, we tried several electrode systems similar to those of Fig. 1. The fabrication of such samples was accomplished by using 20 $\mu$ m  $Al_2O_3$  fibers to shield the polymer fibers to produce the narrow gap during the metalizing process by evaporation. In some earlier attempts, small spiderwebs were wrapped around the PBT fibers but it was too difficult to remove them after metallization.

Another approach, to overcome the difficulty of the small area of the PBT fibers was to try to microtome the fibers into discs 0.1 $\mu$ m thick. This would then provide a current level about 1000 times larger than that of the example. This method has some serious problems. The fibers were first mounted in a resin which is soluble in benzene. A microtome was then used to cut off 1000<sup>2</sup> slices which were collected in a beaker of benzene. An electrode system similar to van Roggen's<sup>7</sup> was to be used and the discs were supposed to settle randomly so that some would be in the correct position for measurement. Unfortunately, the resin also precipitated on the electrodes and the solution damaged the electrodes.

An attempt was made to separate the PBT discs from the solution by an inhomogeneous electric field near the edge of a small capacitor. The separation was not effective, possibly because the dielectric constant of the PBT is too close to that of the benzene (2.27 at 25°C).

The force acting on a particle of size  $a$  and permittivity  $\epsilon_p$ , suspended in a liquid of permittivity  $\epsilon_L$  is<sup>7</sup>

$$F = 4\pi\epsilon_L a^2 \left( \frac{\epsilon_p - \epsilon_L}{\epsilon_p + 2\epsilon_L} \right) E_0 \cdot \nabla E.$$

The next effort will be to use very sharp tungsten probes, with a tip radius  $r_0$  less than 0.1  $\mu\text{m}$  (prepared by electrochemical etching in 1M-KOH), to try to collect the microtomed discs. The W-probes will also serve as "catwhiskers" for making electrical contact. Near the tip  $E_0 \sim V/r_0$  and  $\nabla E \sim -V/r_0^2$  so that  $F \sim 10^{-9} \text{N}$  (or about  $10^6$  times the weight) for a polymer sphere with  $a \sim 0.1 \mu\text{m}$ ,  $\epsilon_p/\epsilon_L \sim 1.1$ , and  $V = 10 \text{V}$ .

#### Electron-Microscope Technique For Measuring $\sigma$

In our search for ways to overcome the difficult problems imposed by the nature of the currently available PBT samples, we have conceived a way that looks promising. The central idea for this technique is to charge one end of a polymer fiber by scanning the SEM beam across it and then to use the decaying deflection of the beam to measure the decay of the surface charge as it leaks through the fiber to a conducting base in which the fiber is mounted. Figure 2 shows the arrangement of the sample in the SEM beam. The method is similar to the method of Watson, et al.<sup>8,9</sup> but uses only one electron beam. As a working hypothesis we are assuming that the deflection  $\xi$  will decay exponentially,  $\xi = \xi_{\text{max}} \exp(-t/\tau)$ , with a time constant  $\tau = \epsilon/\sigma \approx (\epsilon/\epsilon_0) \exp(+H^*/RT)$ , where  $\epsilon$  is the dielectric permittivity and  $H^*$  is the activation enthalpy for the conduction process. Later in the analysis of data obtained, we may need to use a space charge limited (SCL) decay process.<sup>10</sup>

As outlined in Fig. 2, electrons leave the electron gun at a potential  $-V$  and move toward a spot on the sample holder platform. A short polymer fiber protrudes a distance  $b$  out of a conducting base and is rotated into the beam to have its end charged and is then rotated so that its axis is perpendicular to the original path of the electrons. If the distance  $b$  is small compared with

the fiber radius  $r$ , the electric field perpendicular to the beam will be

$$E_x = q_s / 2\epsilon_0, \quad (1)$$

where  $q_s$  is the charge density on the end of the fiber. The change in momentum of an electron in the field will be given by

$$\Delta p_x = \int_0^t F_x \cdot dt \approx \int_0^t eE_x dt. \quad (2)$$

The effective interaction time for the force  $F$  is taken to be the transit time  $t \approx 2r/v_0$  of an electron moving past the end of the fiber. Thus

$$\Delta p_x \approx \int_0^{2r/v_0} (eq_s / 2\epsilon_0 v_0) dt \approx eq_s r / \epsilon_0 v_0. \quad (3)$$

The deflection angle  $\theta$  is given by

$$\theta = \tan^{-1} (\Delta p_x / p_0) \approx eq_s r / m\epsilon_0 v_0^2. \quad (4)$$

Or, since  $v_0^2 = 2Ve/m$ , Eq. (4) becomes  $\theta \approx q_s r / 2\epsilon_0 V$ . To bracket the postulated deflection we can take the other extreme model, namely the assumption that the charge  $Q = \pi r^2 q_s$  is concentrated in a region small compared with the interaction distance between the beam and the tip. This model is mathematically identical to Rutherford scattering by a nucleus of infinite mass.

The classical result for the scattering of a particle of mass  $m_1$  and charge  $q_1$  by one of mass  $m_2$  and charge  $q_2$  is<sup>11,12</sup>

$$\tan \frac{\theta}{2} = \frac{q_1 q_2}{(4\pi\epsilon_0)} \frac{m_1 + m_2}{m_1} \frac{1}{T_0 a} \quad (5)$$

where  $T_0 = \frac{1}{2} m_1 v_1^2 = Ve$  is the initial kinetic energy of the particle  $m_1$  in the laboratory coordinate system. The particle  $m_2$  is assumed to be initially at rest. The "impact parameter" (see Fig. 2) is denoted by  $a$ . In our case  $q_1 = \pi r^2 q_s$  and  $m_2/m_1 \gg 1$ . Thus

$$\theta = 2 \tan^{-1} \left\{ \frac{\pi r^2 q_s e}{(4\pi\epsilon_0) 2eVa} \right\} \approx 2 \tan^{-1} A. \quad (6)$$

For small angles,  $\tan^{-1} A \approx A - A^3/3$ , so that, as a first approximation,



$$\theta \approx 2\lambda = \pi r^2 q_s / (4\pi \epsilon_0) Va.$$

The ratio of the first approximations for the two models is

$$\frac{v \text{ (plane charge)}}{v \text{ (point charge)}} = \frac{rq_s/2\epsilon_0 V}{r^2 q_s/4\epsilon_0 Va} = 2 a/r. \quad (7)$$

In the original model,  $a$  was less than  $r$ , so that the ratio is near unity. The planar charge model is preferable for  $a \ll r$  and the point charge model for  $a \gg r$ . If it becomes necessary to worry about the statistical distribution of electrons over distance  $a$  from the fiber tip, the Rutherford scattering cross-section concept could be utilized.

#### METHODS FOR THERMAL CONDUCTIVITY K

In developing the ideas behind the methods considered, we came to what we now believe may be the most suitable approaches for determining  $K$  for small fibers. Paradoxically they are special adaptations of some of the oldest methods known, namely, the Ingen-Hausz<sup>14</sup> method and the Angstrom<sup>15,16</sup> technique.

#### Adaptations of the Ingen-Hausz Method

In this approach, we propose to avoid the problems introduced by thermocouples and the like, by using temperature sensitive marking pens (Tempilstiks, Tempil Division of Big Three Industries, Inc.). To keep the mathematical presentation in this section manageable, assume that  $K$  is constant. Consider a fiber of length  $L$ , heated to a temperature  $T_H$  at its left end ( $x=0$ ). Temperature will drop to a steady value  $T_L$  at the other end ( $x=L$ ) and heat is lost through the surface of the fiber. The cross-section is  $A$  and the perimeter of  $A$  is  $P$ . The heat transfer coefficient for this loss is  $h_p$ , such that the differential loss is given by  $h_p P(T-T_c)dx$ . Thus the differential equation for the fiber is

$$\rho c_p A \frac{\partial T}{\partial t} = KA \frac{\partial^2 T}{\partial x^2} - h_p P(T-T_c). \quad (8)$$

$T_c$  is the effective temperature of the environment of the fiber. After introducing  $\theta = T-T_c$  and rearranging we have

$$\frac{\partial^2 \theta}{\partial x^2} = \frac{1}{D} \frac{\partial \theta}{\partial t} + \frac{h_p P}{KA} \theta \quad (9)$$

(The dimensionless group  $h_p P / KA \equiv B$  is "Biot's number"). At steady state  $\partial\theta/\partial t = 0$  so  $(d^2\theta/dx^2) = B\theta$ . The boundary conditions are:

$$\theta(L) = \theta_L = (T_L - T_c) \text{ and } \theta(0) = \theta_H = (T_H - T_c). \quad (10)$$

Then by standard techniques one assumes a steady solution of the form

$$\theta(x) = A_1 e^{\alpha x} + A_2 e^{-\alpha x} \quad (11)$$

and finds by direct substitution in Eq. (9) that

$$\alpha = (h_p P / KA)^{1/2}, \quad A_1 = (\theta_L - \theta_H e^{-\alpha L}) / 2 \sinh(\alpha L),$$

and  $A_2 = -(\theta_L - \theta_H e^{+\alpha L}) / 2 \sinh(\alpha L)$ . If  $L \rightarrow \infty$  we get the Ingen-Hausz situation, with

$$A_1 = -e^{-2\alpha L} A_2 \text{ and } \theta(x) = \theta_H e^{-\alpha x} = \theta_H e^{-x/x_0}. \quad (12)$$

Thus Ingen-Hausz coated rods of several materials (a, b, ...) with wax, heated one end to a common temperature and then noted the position  $x_a, x_b, \dots$  at which the wax melted. Therefore

$$\alpha_a x_a = \alpha_b x_b = \dots \text{ or } \frac{h_a P_a}{K_a A_a} x_a = \frac{h_b P_b}{K_b A_b} x_b, \quad (13)$$

for similar dimensions and surface conditions ( $K_b/K_a = (x_b/x_a)$ ). Previous investigators have not used this technique<sup>11</sup> for fibers. To see if it is at all feasible we have extrapolated a semi-empirical approach outlined by Pitts and Sissom<sup>14</sup> to very small diameters, beyond the range of known data. The result suggests that the technique is feasible. By the semi-empirical approach, the heat exchange coefficient  $h_c$  is related through the Nusselt number  $Nu = 2h_c r / K_{\text{fluid}}$ , to a function of the Prandtl number  $Pr = (c_p \eta / K)_{\text{fluid}}$ , and the Grashof number  $Gr = (2r)^3 g \alpha \nu (T_{\text{surf}} - T_{\text{fluid}}) \nu^{-1}$  where  $\nu = \eta / \rho$  is the kinematic viscosity of the fluid (air). The volume expansivity of air is  $\alpha_v = 1/T$  which is taken as an average between  $T_s$  and  $T_f$ . For a 20  $\mu\text{m}$  fiber, with  $T_s - T_f = 127^\circ\text{C} - 27^\circ\text{C}$ , the graphs in Pitts and Sissom lead to  $Pr = 0.708$ ,  $Gr = 1.06 \times 10^{-5}$ , and  $Nu = 0.43$ . For air  $K_{\text{air}} = 0.026 \text{ Wm}^{-1} \text{ } ^\circ\text{C}^{-1}$  so that  $h_c \approx K_{\text{air}} Nu / 2r \approx 560 \text{ Wm}^{-2} \text{ } ^\circ\text{C}^{-1}$ , which is quite high, as one might expect for something with a large surface to volume ratio. It follows that we can

estimate the temperature profile because

$$\alpha = x_0^{-1} = (2h_c/Kr)^{1/2} \approx 10^3 \text{ m}^{-1} \quad (14)$$

where a value  $K \approx 1 \text{ W m}^{-1} \text{ }^\circ\text{C}^{-1}$  is assumed for the polymer. If  $T_H = 127^\circ\text{C}$  and a Tempilstik marker that melts at  $57^\circ\text{C}$  is used, then  $x_m$  (the demarcation point for melting) will be

$$x_m = x_0 \ln(\theta_H/\theta_m) = x_0 \ln[(T_H - T_e)] \approx 120 \mu\text{m}. \quad (15)$$

Although microscopic observation will be required the experiment appears feasible.

#### The Angstrom Method for Thermal Diffusivity

The Angstrom method is an ingenious periodic adaptation of similar principles. A disadvantage of transient or periodic methods is that the property directly available from the measurements is the thermal diffusivity  $D = K/\rho c_p$  rather than  $K$  itself, so that separate determinations of  $c_p$  and  $\rho$  are needed.

As a mathematical basis for this method, a time dependent solution is sought to the partial differential equation for heat flow (Eq. (9) of the previous section), subject to the periodic boundary condition

$$\theta(0, t) = \theta_H + \Omega \sin \omega t. \quad (16)$$

A proper solution must exhibit the same periodicity and drop off more or less exponentially with distance from the heated end. Also one suspects a wave like movement of the changes in temperature. By direct substitution in to Eq. (9) it may be shown that an appropriate solution (for the case  $B \approx 0$ ) is

$$\theta(x, t) = \theta_H - gx + \Omega e^{-ax} \sin(\omega t - kx). \quad (17)$$

The wavelength  $\lambda$  of the "temperature wave" is

$$\lambda = 2\pi/k = 2\pi(2K/\rho c_p \omega)^{1/2} \quad (18)$$

The speed is

$$v = \lambda\omega/2\pi = (2K\omega/\rho c_p)^{1/2}. \quad (19)$$

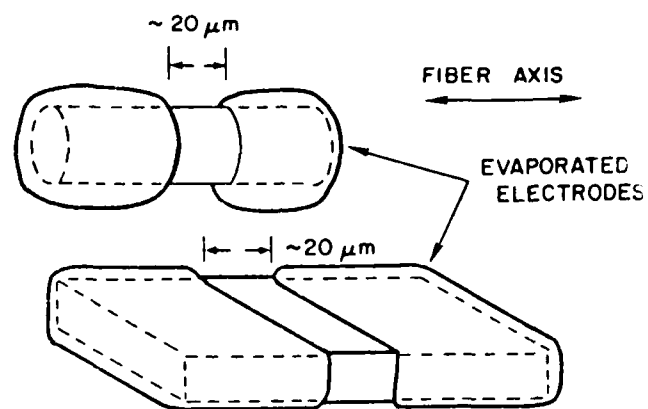
Thus

$$K = \rho c_p v^2/2\omega = \rho c_p \omega \lambda^2/8\pi^2, \quad (20)$$

so that by measuring either the speed or the wavelength of the temperature wave, one can obtain  $D = K/\rho c_p$ .

## REFERENCES

1. G. C. Berry, J. Polymer Science, Phys. Ed. 14, 451 (1976).
2. J. F. Wolfe, B. H. Loo, and F. E. Arnold, ACS-Polymer Prepr., 19 (2), 1 (1978).
3. J. F. Wolfe, B. H. Loo, and F. E. Arnold, ACS-Polymer Prepr., 20 (1) 82 (1979).
4. J. Ingen-Hausz, Jour. Phys. 68, 380 (1789).
5. A. J. Angstrom, Phil. Mag., 25, 130 (1863).
6. A. van Roggen, Phys. Rev. Letters 9, 368 (1962).
7. W. K. H. Panofsky and M. Phillips, Classical Electricity and Magnetism, Addison-Wesley Publishing Co., Inc., Cambridge, Mass., 1955, p. 77, 98.
8. P. K. Watson and T. M. Clancy, Rev. Sci. Instr., 36, 217 (1965).
9. P. K. Watson and J. M. Schneider, Ann. Rept. 1967 CEIDP, Nat. Acad. Sci. Publ. 1578, 95 (1968).  
\_\_\_\_\_, Ann. Rept. 1970 CEIDP, Nat. Acad. Sci. Publ. 1870, 125 (1971).
10. G. M. Sessler and H. von Seggern, Ann. Rept. 1979 CEIDP, Nat. Acad. Sci. Publ. 2933, 160 (1979).
11. A. E. Ruark and H. C. Urey, Atoms, Molecules, and Quanta, Dover Publications, NY, 1964, pp. 46-51, 106-109.
12. J. B. Marion, Classical Dynamics, Academic Press, NY (1970) 2nd Edition, p. 307.
13. W. E. Byerly, An Elementary Treatise on Fourier's Series, Dover Publications, Inc., NY, 1959, pp. 89-92.
14. D. R. Pitts and L. E. Sissom, Heat Transfer, Shaum's Outline Series, McGraw-Hill Book Co., NY, 1977, p. 74.



SAMPLES FOR AXIAL CONDUCTIVITIES

FIGURE 1

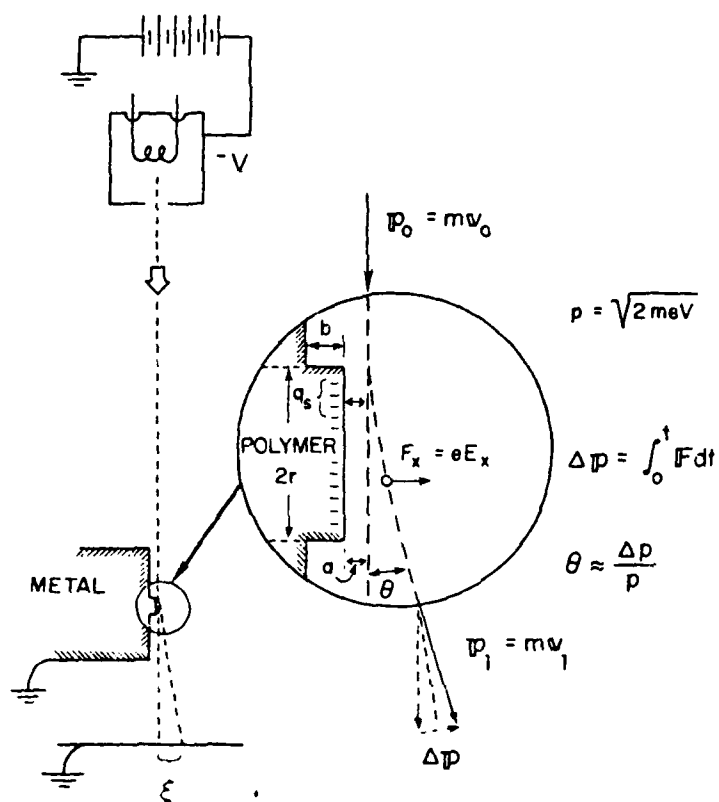


FIGURE 2  
Schematic of the principles involved in the use  
of the SEM to measure electrical conductivity.

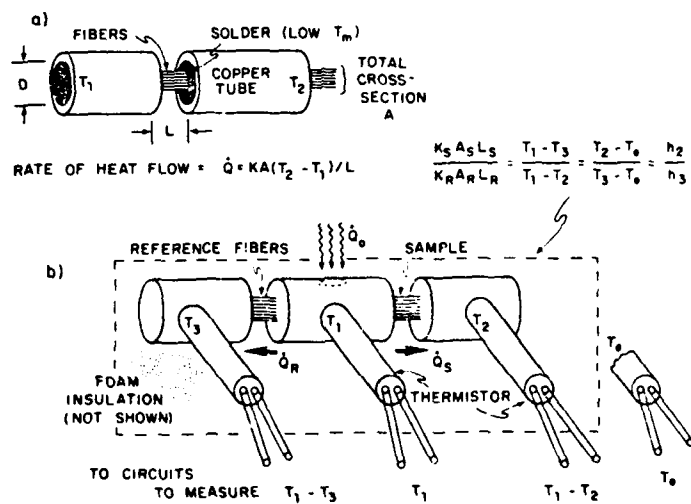


FIGURE 3 (a) Illustration of one of the ways to mount fiber samples.  
(b) Schematic of one of the comparison methods for measuring thermal conductivity.

Abstract of a paper presented at the North American Thermal Analysis Society, Symposium on Application of Thermal Analysis to the Electronics and Electrical Industries, Oct. 26-29, 1980, Boston, Mass.

THERMAL CONDUCTION IN POLYMERS AND ITS RELATION TO ELECTRICAL SYSTEMS.

R. E. Barker, Jr. and L. J. Adams, Dept. of Materials Science, University of Virginia, Charlottesville, VA 22901.

In this paper the reasons why the conduction of heat through polymers and across interfaces is important in electrical applications will be discussed, as will the relations between the mechanisms of heat transfer and polymer microstructure. A brief review of some of the problems and techniques of thermal conductivity measurements will be presented. The principles will be illustrated by reference to conductivity data vs. temperature, pressure, and structure for a number of representative polymers.



ELECTRICAL CONDUCTIVITY OF HIGHLY ANISOTROPIC FIBERS AND FILMS OF POLY(P-PHENYLENE BENZOBISTHIAZOLE). D. Y. Chen\* and R. E. Barker, Jr. Dept. of Materials Science, Univ. of Va., Charlottesville, Va. 22901.

Due to its molecular geometry poly(p-phenylene benzo-bisthiazole) tends to form an extended chain conformation. This tendency leads to an extreme anisotropy of mechanical and electrical properties. Experimental data, which will be discussed, reveal that the axial conductivity ( $\sigma_{||}$ ) is  $10^6$  times larger than the transverse conductivity ( $\sigma_{\perp}$ ). This large ratio along with the fact that the conduction is ohmic up to at least  $1.2 \times 10^5$  V/m, is thought to imply one dimensional electronic conductivity. The presence of the "as received" acid content of samples affects the value of electrical conductivities. After washing in ethyl alcohol and then drying, PBT tends toward a value of electrical conductivity which is about 1/5 of the value for an untreated sample. On the other hand a sample treated in a solution of ammonium hydroxide tends to increase its electrical conductivity to a much higher value. Thermal treatment (e.g. oven drying) also reduces electrical conductivities to lower values. In this paper some results will be discussed of special techniques which have been developed for measuring electrical conductivities of very small samples (10 to 40  $\mu$ m diameter for fibers). (Work supported by the U.S. Air Force Grant AFOSR-80-0014.)

*R. Edward Barker Jr.*

Development of Techniques to Study Vapor Diffusion and Solubility in Fibers and Films of Poly (P-Phenylene Benzobisthiazole), W. S. Huang and R. E. Barker, Jr., Materials Science Department, University of Virginia, Charlottesville, Virginia 22901

The study of the transport properties of polymers has added to the understanding of relations between macroscopic and microscopic properties. Little is known about transport properties in PPBT and related extended chain polymers, which should be interesting due to their anisotropic character. This work deals with the determination of diffusion coefficients  $D$  and sorption coefficients. It is part of a study that includes the determination of electrical and thermal conductivities of the same materials. PPBT samples are available only in limited quantities as fine fibers ( $\sim 20 \mu\text{m}$ -diameter) and thin narrow film, therefore we have focused attention on the development of sensitive techniques for such samples. Later, spectrophotometric and electron microscopic analytical techniques will be used, but up to the present time an apparatus based on a classical sorption balance with a sensitive quartz spring in a thermostated evacuable chamber has seemed the most suitable approach. Problems of interpreting the sorption balance data for anisotropic fibers with possible concentration dependencies of the pre-exponential factor  $D_0$  and the activation energy  $E_D$  will be discussed along with related matters. (Funded by U.S. Air Force - OSR-80-0014.)

TECHNIQUES FOR THE DETERMINATION OF THE THERMAL CONDUCTIVITY OF SMALL FIBERS AND FILMS. L. J. Adams and R. E. Barker, Jr., Dept. of Materials Science, Univ. of Va., Charlottesville, Va., 22903.

Recent years have seen intense interest in polymeric "one dimensional" extended chain conductors and semi-conductors such as polysulfur nitrite and polyacetylene. Materials of this type are expected to have interesting anisotropic thermal properties. Although it is not yet known whether their electrical conductivities are due to electrons or to ions, extended chain polymers such as poly-paraphenylene benzobisthiazole (PPBT) and polyparaphenylene terephthalamide (Kevlar) are expected, because of their high axial modulus  $Y_{||}$  to have an axial conductivity  $K_{||} \approx 0.33 C \Lambda (Y_p)^{1/2} \approx 1 - 10 \text{ W m}^{-1} \text{ K}^{-1}$  due to "lattice" vibrations.  $C \Lambda$  is the product of heat capacity and the phonon attenuation length. Transverse thermal conductivities of fiber forming materials are expected to be the usual values for insulating polymers, namely  $\approx 0.3 \text{ W m}^{-1} \text{ K}^{-1}$ . Efforts to develop techniques for the measurement of  $K_{||}$  and  $K_{\perp}$  for fibrilous materials will be discussed. For example, great difficulties in the determination of  $K_{||}$  result from the large heat exchange coefficient ( $h \approx 200 \text{ W m}^{-2} \text{ K}^{-1}$ ) between small fibers and thin surrounding space. Our most successful attempts to date have utilized small thin films for the determination of  $K_{\perp}$  followed by an adaptation of a method due to de Senarmont to determine the ratio of  $K_{\perp}/K_{||} = (b/a)^2$  on wax coated films exposed to a "point" heat source. The wax melts into an elliptical pattern  $2a \times 2b$ . The observed K-ratios are near 6 for PPBT. (Funded by U.S. Air Force - OSR-80-0014)

*L. J. Adams*



**1981 Annual Report  
Conference on Electrical Insulation  
and  
Dielectric Phenomena**

**October 26-28, 1981**

**Pocono Hershey Resort Motel  
Whitehaven, PA**

**Sponsored by the  
IEEE Electrical Insulation Society  
Library of Congress Catalog Card  
Number 79-649806**

**Available from  
IEEE Service Center  
Single Publication Sales Dept.  
445 Hoes Lane  
Piscataway, N.J. 08854**

Abstracting is permitted with credit to the source. Libraries are permitted to photocopy beyond the limits of U.S. copyright law for private use of patrons those articles in this volume that carry a code at the bottom of the first page, provided the per-copy fee indicated in the code is paid through the Copyright Clearance Center, P.O. Box 765, Schenectady, NY 12301. Instructors are permitted to photocopy isolated articles for noncommercial classroom use without fee. For other copying, reprint or republication permission, write to Director, Publishing Services, IEEE, 345 E. 47 St., New York, NY 10017. All rights reserved. Copyright© 1981 by The Institute of Electrical and Electronics Engineers, Inc. Printed in U.S.A.

# ELECTRICAL CONDUCTIVITY OF ANISOTROPIC POLY(PARAPHENYLENE-BENZOBISTHIAZOLE)

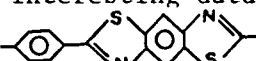
R. E. Barker, Jr. and D. Y. Chen  
Materials Science Department, University of Virginia  
Charlottesville, Virginia 22903

## INTRODUCTION

There is a great deal of scientific and technological interest in the electrical properties of (quasi-) one dimensional conductors (1,2). Most of the interest centers around polymers such as  $\{SN\}_n$ ,  $\{\text{C}_6\}_n$ ,

$\{\text{C}_6\text{S}\}_n$ , and  $\{\text{C}=\text{C}\}_n$ . The literature about these polymers suggests electronic mechanisms.

Previously (3,4) we discussed a number of serious problems in the determination of transport properties (such as electrical and thermal conductivities) of extremely small samples of highly anisotropic polymers. In the present paper we wish first to discuss some special techniques developed to overcome the problems of D.C.-conduction measurements on very small fibers and films and then we wish to discuss some interesting data

for an important extended chain polymer 

which we shall call PPBT. In contrast to the claims in the literature, for one-dimensional metallic type conduction for polyacetylene and other polymers like those mentioned above, PPBT possibly exhibits a mixed electronic and ionic conductivity which is influenced strongly by changes in relative humidity. There is some evidence that protons moving along or between chains contribute significantly to the observed current flow. The axial conductivity exceeds the transverse conductivity by a factor of  $10^6$ . The techniques developed have been applied to fibers less than 20  $\mu\text{m}$  in diameter and to 20  $\mu\text{m}$  thick films only 6  $\times$  6 mm square.

## EXPERIMENTAL TECHNIQUES

Materials

The PPBT samples were supplied by the Celanese Research Co. The monomers for PPBT and similar polymers tend to form nematic phase liquid crystals. This tendency is carried over into the polymeric solid state leading to an extended chain ("rigid rod") morphology and to an extreme anisotropy of mechanical and electrical properties (5,6). The only known practical solvents for PPBT are methane sulfonic acid (MSA) and polyphosphoric acid (PPA). The acids are usually removed by extensive washing in water or by treatment with  $\text{NH}_4\text{OH}$ . Electron and optical microscopy reveal that the presence of voids, interfiber interfaces, acid residues, etc. are for practical purposes almost unavoidable consequences of the synthesis methods and processing conditions. Clearly  $\sigma$  will be influenced by such variables. For example, the measurements reported herein are on samples with an appreciable volume fraction of voids, so the reported conductivities should set a lower limit for samples without voids. The values for  $\sigma$  also are for samples with the "as received" acid content, except for some ethyl alcohol-treated ones, (which systematically reduced the surface conductance by a factor 0.25 and the volume conductivity by a factor 0.4).

Instrumentation

The Keithley Model 642 Electrometer, with a sensitivity of  $10^{-17}$  A, has been essential to many of our measurements. Even so some special precautions have been necessary and special cells and techniques had to be developed. After trying many of the previously proposed (3,4) techniques we were finally successful in developing miniature cells that fit into a standard Hewlett-Packard (16008A) high resistance cell. Some of the over-all convenience, stability, and shielding features of the commercial cell are retained but now we can accommodate samples with only  $10^{-8}$  of the cross-sectional area ( $\sim 10^2 \text{ cm}^2$ ) normally needed. One (Fig. 1) of the types of miniature cells developed is a miniature guarded cell (MGC) for films about  $6 \text{ mm} \times 6 \text{ mm}$  and the other (Fig. 2) is a notched electrode system (NES) for fibers down to  $10 \text{ }\mu\text{m}$  in diameter. The MGC is compatible with the surface and volume conductance modes of the HP-16008A cell, so that for the small films we can

separate surface resistance  $\sigma_s$  and the transverse conductivity  $\sigma_1$ . The NES cell gives the axial conductance of a fiber, but to separate the surface and volume contributions indirect means must be used. For example, by assuming additivity of the surface and volume contributions it can be shown that the effective conductivity is  $\sigma_{eff} = \sigma_{vol} + (2/r)\sigma_{surf}$  for a cylindrical fiber of radius  $r$ , so that  $\sigma_{eff}$  vs.  $1/r$  should be linear. In the present research, the lack of availability of geometrically perfect, defect-free samples to give good statistical results led us to develop an alternative "notched electrode" technique which only requires a series of measurements (in principle just two) on the same fiber. The derivation of these techniques will be described in more detail in a subsequent paper. In summary, the second technique involves changing the effective length from  $L_1$  to  $L_2$  by adding to silver paste electrodes between measurement 1 and 2 of the effective conductivities  $\sigma_1$  and  $\sigma_2$ . The results are:

$$(\sigma_{11})_{vol} = [\sigma_1 - \sigma_2] [1 - (L_1/L_2)]^{-1}$$

$$(\sigma_{11})_{sur} = [1/2] [\sigma_2 - (L_1/L_2)\sigma_1] [1 - L_1/L_2]^{-1}$$

By carefully introducing notches of known depth (and filling them with electrode paste) these expressions can be further modified to improve the experimental resolution when the measured values of  $\sigma_1$  and  $\sigma_2$  would be too close for usable values of  $L_1$  and  $L_2$ .

Due to the nature of the samples, the H.P. Cell, and the Keithley Electrometer, a period of over 9 hours is needed to reach a quasi steady state for current measurements, as shown in Fig. 3 for a notched PPBT fiber.

## RESULTS

### Current vs. Voltage in a PPBT Notched Fiber

Since the quantitative characterization of non-ohmic behavior of the polymer would aid in understanding the conduction mechanism we made a series of measurements at different voltages (7). For a fiber (PPBT 28555-19-2) with an effective length of 200  $\mu\text{m}$ , the axial current was quite linear up to 0.12 MV/m (the highest field available on this sample because of a design feature of the Keithley 642 electrometer which

limits the maximum voltage that can be used). In future experiments still higher fields will be tried.

#### Temperature Dependence of the Electrical Conductivity

Within the ohmic region, the conductivity can be calculated from the relation  $\sigma = iL/AV$ . Due to imperfections in the samples, this should be a lower limit. For a given experiment  $L/AV$  was constant so that, as Fig. 4 illustrates for typical data, an Arrhenius relation,  $\sigma_{11} = (\sigma_{11})_0 \exp(E^*/RT)$ , describes the data well. There are differences in the parameters for PPBT fibers processed in different ways. At 22°C and about 40% RH.

The axial conductivity spread was from about  $10^{-9}$  to  $20 \times 10^{-9} \Omega^{-1} m^{-1}$  and  $E_{11}^*$  ranged from 8.8 to 9.9 kcal/mol ( $0.41 \pm 0.02$  eV).

#### Anisotropic Conductivities

Typical values of the various parameters for PPBT are listed below (with  $\sigma_{22} = \sigma_{\perp}$ )

R%	$\sigma_{11}(\Omega^{-1} m^{-1})$	$E_{11}^*$ (kcal/mol)	$\sigma_{22}(\Omega^{-1} m^{-1})$	$E_{22}^*$
0	$1 \times 10^{-10}$	9.9	$4.5 \times 10^{-16}$	20.7
40	$1.2 \times 10^{-9}$	8.8	$3.8 \times 10^{-15}$	kcal/mol

The surface conductivity of about  $10^{-16} \Omega^{-1}$  at 40% RH is sufficiently high that it doesn't create much of an error when unguarded axial measurements are made. The ratio  $\sigma_{11}/\sigma_{22}$  is about  $10^6$ , which is near the values found for some of the one dimensional electronic conductors. However, in the case of PPBT, as the typical result of Fig. 5 shows, moisture strongly influences  $\sigma$ . Such data we well described by an equation of the form

$\sigma_{11}(R) = \sigma_{11}(0) \exp(R/R_{11}) = \sigma_{11}(0) 10^{R/R_{11}'}^{\log e}$  where  $R$  is the % relative humidity in which the fibers are conditioned. It is significant that PPBT still exhibits a finite conductivity when  $R$  is vanishingly small. For the data shown,  $\sigma_{11}(0) \cong 10^{-10} \Omega^{-1} m^{-1}$  and  $R_{11}' \cong 36\%$ . These values vary somewhat for samples processed in different ways.  $E_{22}^*/E_{11}^* \sim 2$  is in accord with the idea that charge transfer is easiest along the chains.



## DISCUSSION AND CONCLUSION

The results for  $\sigma_{22}(R)$  were similar to those for  $\sigma_{11}(R)$  and have led us to develop a technique for determining the diffusion coefficient of water from the time dependent perturbation of the current when  $R$  is quickly changed from one steady value to another. This technique will be published elsewhere, as will a new modification of the Barker-Sharbaugh (7,8), weak-electrolyte theory for ionic conduction in moist polymers. The new theory relates  $\sigma_{11}$  and  $\sigma_{22}$  to the anisotropy of the dielectric constant in such a way that ionic conductivity is strongly implicated in PPBT. Protons are among the likely types of ionic charge carriers (9). In support of this we mention the observation of Thomas, Farris, and Hsu (10) that PPBT is easily protonated in MSA ( $\text{CH}_3\text{SO}_3\text{H}$ ).

$\text{PPBT} + n(\text{CH}_3\text{SO}_3\text{H}) \rightleftharpoons \text{H}_n(\text{PPBT})^{n+} + n\text{CAH}_3\text{SO}_3^-$ . Due to their high mobility, the protons from a relatively small amount of residual MSA could go a long way in providing the observed conductivity.

As Glasser has pointed out protonic conduction in solids is of special interest because some situations require quantum mechanical interpretation (9).

To our knowledge, the special techniques developed in this research, for measuring the axial and transverse electrical conductivities of PPBT fibers and films, are applicable to samples which are smaller than those of any techniques previously reported for low conductivity materials. For PPBT, the large ratio of axial to transverse conductivity ( $\sigma_{11}/\sigma_{22} \sim 10^6$ ) implies mainly one-dimensional electric conduction. This is thought to be consistent with the molecular geometry of the polymer which leads to an extended chain conformation. The extent to which electrons as well as ions are involved in the conduction process remains a subtle question which we hope to soon solve.

## ACKNOWLEDGEMENTS

We are glad to acknowledge support by a grant from the U.S. Air Force Office of Scientific Research (AFOSR-80-0014). We wish to thank Dr. E. C. Chenevey and Dr. J. R. Leal of the Celanese Research Company and Dr. J. F. Wolfe of SRI International for supplying PPBT.

samples and related information. We also wish to express our appreciation for very useful discussions with Drs. D. Bhanmik, G. C. Berry, S. L. Hsu, T. E. Helminiak, F. E. Karasz, K. R. Lawless, J. E. Mark, E. Soloski, E. L. Thomas, and D. R. Ulrich.

#### REFERENCES

- (1) J. C. W. Chien, G. E. Wnek, F. E. Karasz, and J. A. Hirsch, *Macromol.* 14, 479 (1981).
- (2) J. F. Rabolt, T. C. Clarke, K. K. Kanazawa, J. R. Reynolds, and G. B. Street, I.B.M. Research Lab., San Jose, Calif., *Jour. Chem. Soc. Chem. Commun.*, p. 348 (1980).
- (3) R. E. Barker, Jr., D. Y. Chen, and L. J. Adams, 1980 Ann. Rept. CEIDP, National Academy Press, ISBN 0-309-03126-5, p. 357 (Oct. 1980).
- (4) D. Y. Chen and R. E. Barker, Jr., *Bull. Am. Phys. Soc.* (Phoenix Meeting, March 19, 1981) 26, 434 (1981).
- (5) G. C. Berry, "Properties of Rigid Chain Polymers in Solution," in *Contemporary Topics in Polymer Science*, Vol. 2, E. M. Pearce and J. R. Schaefgen, (eds.) (Plenum Press, New York 1977) p. 55.
- (6) J. F. Wolfe, B. H. Loo, and F. E. Arnold, *ACS-Polymer Prepr.*, 20(1), 82 (1979).
- (7) R. E. Barker, Jr., *Pure and Appl. Chem.* 46, 157-170 (1976).
- (8) R. E. Barker, Jr., and A. H. Shaubargh, *J. Polymer Sci.* C10, 139 (1965).
- (9) L. Glasser, *Chem. Revs.* 75, 21 (1975).
- (10) E. L. Thomas, R. J. Farns, and S. L. Hsu, "Mechanical Properties vs. Morphology of Ordered Polymers" AFWAL-7R-00-4045 (May 1980).

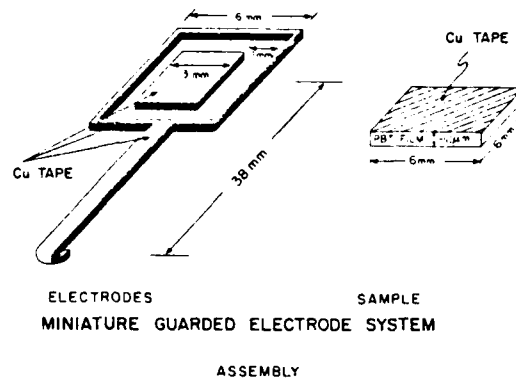
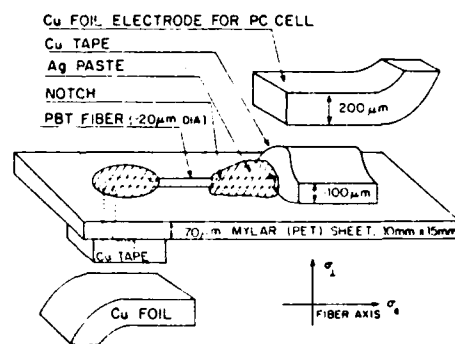


Fig. 1

# TECHNIQUE FOR MEASUREMENT OF $\sigma_{II}$ PARALLEL TO FIBER AXIS

## (a) ELECTRICAL CONTACTS (SCHEMATIC)



## (b) THE EQUIVALENT CIRCUIT

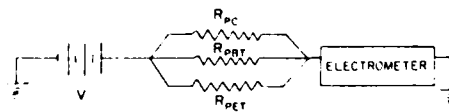


Fig. 2

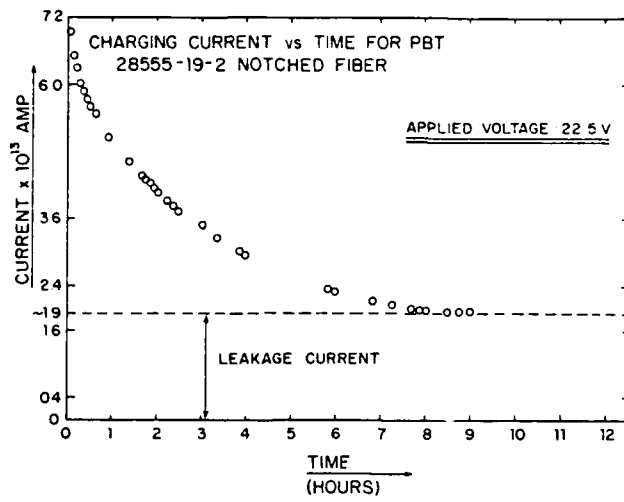


Fig. 3

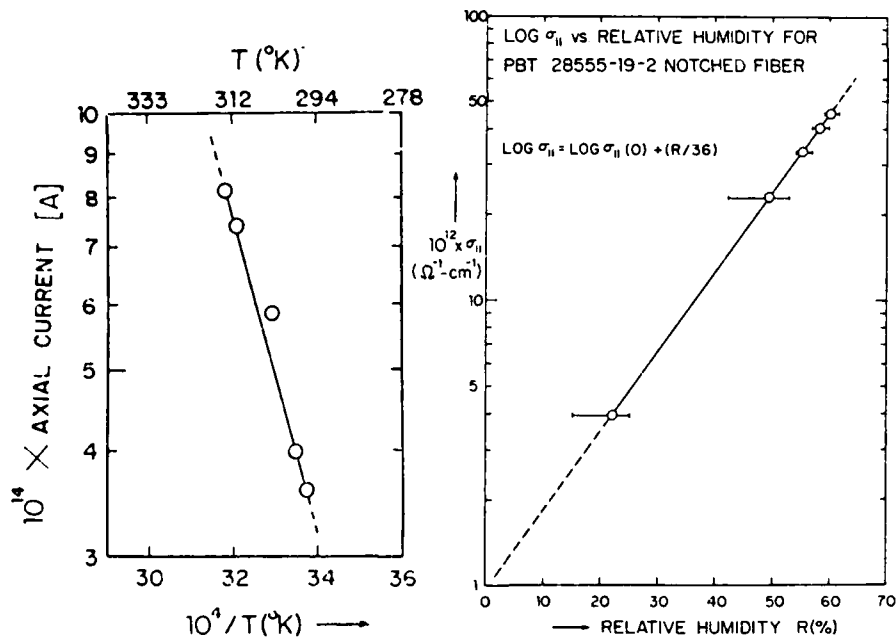


Fig. 4

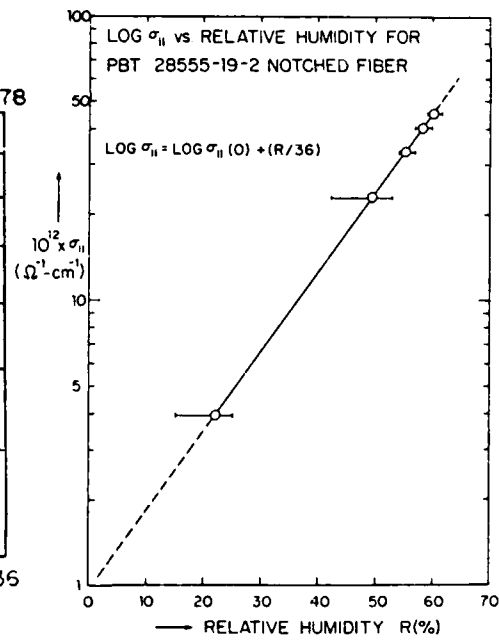


Fig. 5

# FIGURE CAPTIONS

Fig. 1 Schematic view of the miniature guarded electrode system. Copper tape (200  $\mu\text{m}$  thick) provides a convenient conducting contact with the top of the sample as shown in the sketch of the "assembly." The Lexan sandwich consists of 100 x 100 x 0.5 mm sheets through which copper foil contacts pass.

Fig. 2 (a) Schematic view of a notched electrode system for measurement of electrical conductivity ( $\sigma_{11}$ ) parallel to the fiber axis.  
(b) Equivalent circuit.

Fig. 3 Charging Current vs time for a notched PPBT fiber, a period of over 9 hours is needed to reach a quasi steady state for current measurements.

Fig. 4 Log  $\sigma_{11}$  vs relative humidity (R) for a notched PPBT (28555-19-2) fiber, the empirical equation for the data is shown.

Fig. 5 Axial Current ( $i_{11}$ ) vs  $\frac{10^4}{T}$  for a notched PPBT (28555-19-2) fiber. The data support an Arrhenius type relation. The activation energy  $E_{f1}^*$  corresponds to a gap energy of 0.76 eV ( $E_{\text{gap}} = 2E_{f1}^*$ ).

The Anisotropic Transport of Charged and Neutral Species in Extended Chain Polymers. R.E.BARKER, JR., D. Y-J. CHEN, and W-S. HUANG, U.of Va.\*--Most previous research on electrical conductivity  $\sigma$  and vapor diffusion  $D$  of polymers has been done on thin films of extruded or molded thermoplastics and elastomers. Although some studies have examined the effects of orientation the present study involves a very different type material, in samples much smaller than usual for studies of  $\sigma$  and  $D$ , Poly-p-phenylene benzobisthiazole (PPBT) samples subjected to a variety of treatments to modify the morphology were studied. The monomer is a nematic liquid crystal and the extended chain configuration exists in PPBT. The morphology dependent axial conductivity is given by  $\sigma_{11} = (\sigma_{11})_0 \exp(-E_{11}/RT)$ , with a similar expression for the transverse conductivity  $\sigma_{22}$ . For dry conditions,  $\sigma_{11}/\sigma_{22} \approx 10^{-9}/10^{-15}$  (ohm<sup>-1</sup> m<sup>-1</sup>) and  $E_{11}/E_{22} \approx 0.41/0.84$  (eV). An anisotropic version of the ionic conductivity model of Barker and Sharbaugh was developed and its main features checked by measuring  $\sigma_{11}$  and  $\sigma_{22}$  as functions of concentration of ionic compounds, such as LiCl, CaCl<sub>2</sub>, and LaCl<sub>3</sub>. Diffusion and sorption of H<sub>2</sub>O, benzene and ethanol also were measured to further understand the process of molecular mobility in PPBT.

\*Supported by US-AFOSR-80-0014A

# VIRGINIA JOURNAL OF SCIENCE

OFFICIAL PUBLICATION OF THE VIRGINIA ACADEMY OF SCIENCE

Vol. 33

No. 3

Fall 1982

158

## THE VIRGINIA JOURNAL OF SCIENCE

DUAL SORPTION MODEL FOR DIFFUSION IN POLY (p-PHENYLENE BENZOBISTHIAZOLE). Wu-Song Huang and R. E. Barker, Jr.  
Dept. of Materials Science, UVA, Charlottesville, VA 22903.

When combined with other techniques, the study of sorption (s) and diffusion (D) provides a valuable way to enhance the understanding of certain types of molecular interactions in polymeric systems. Measurements of s and D for PPBT, which is an extended chain (rigid rod) type polymer, give very different results depending on whether the observations were carried out in a vacuum chamber to which the diffusant ( $H_2O$ ) was subsequently admitted, or carried out in air on previously desiccated samples. It has been possible to resolve the differences by assuming a dual sorption model wherein the micro-voids sorb according to a Langmuir isotherm and the other portions of the polymer obey Henry's law. (This research was supported by US Air Force Grant 80-0014A).

## THE VIRGINIA JOURNAL OF SCIENCE

159

EVIDENCE FOR THE APPLICABILITY OF AN ANISOTROPIC VERSION OF THE WEAK-ELECTROLYTE THEORY TO IONIC CONDUCTIVITY IN EXTENDED CHAIN POLYMERS. D. Y. Chen\* and R. E. Barker, Jr. Dept. of Materials Science, Univ. of Va., Charlottesville, Va. 22901

Several years ago Barker and Sharbaugh demonstrated that the mathematical model for aqueous solutions of weak electrolytes could be adapted to provide a useful description of many of the observed phenomena in low conductivity systems such as organic liquids and polymers. Recent work involving a highly anisotropic (extended chain) polymer, poly-paraphenylene benzobisthiazole (PPBT), showed some persuasive evidence for the applicability of the weak-electrolyte theory. A mixed ionic and electronic conduction is proposed based on a detailed analysis of the data in view of the weak-electrolyte theory. The conclusion is that intrinsic and extrinsic ionic species are dissociated as a result of exposing PPBT samples to a conditioned humid environment. The experimentally observed transient phenomena which accompanied these dissociation processes will be discussed to further support the applicability of the weak-electrolyte theory.



**1982 Annual Report  
Conference on Electrical Insulation  
and  
Dielectric Phenomena**

**October 17-21, 1982**

**University of Massachusetts  
Amherst, MA**

**Sponsored by the  
IEEE Electrical Insulation Society**

**Library of Congress Catalog Card  
Number 79-649806**

**Available from  
IEEE Service Center  
Single Publication Sales Dept.  
445 Hoes Lane  
Piscataway, NJ 08854**

Abstracting is permitted with credit to the source. Libraries are permitted to photocopy beyond the limits of U.S. copyright law for private use of patrons those articles in this volume that carry a code at the bottom of the first page, provided the per-copy fee indicated in the code is paid through the Copyright Clearance Center, P.O. Box 765, Schenectady, NY 12301. Instructors are permitted to photocopy isolated articles for noncommercial classroom use without fee. For other copying, reprint or republication permission, write to Director, Publishing Services, IEEE, 345 E. 47 St., New York, NY 10017. All rights reserved. Copyright © 1982 by The Institute of Electrical and Electronics Engineers, Inc. Printed in U.S.A.




# IONIC TRANSIENTS IN AN EXTENDED CHAIN AROMATIC

## HETERO-CYCLIC POLYMER

R. E. Barker, Jr., D. Y. J. Chen, and W-S. Huang

Department of Materials Science  
University of Virginia  
Charlottesville, VA 22901

### INTRODUCTION

In an effort to better understand the process of charge transport in extended chain aromatic hetero-cyclic polymers we have made detailed studies of d.c. conduction in one such rigid rod polymer, viz. poly(p-phenylene benzobisthiazole) or PPBT . Two types of transient currents have been measured. One of these is the gradual decay of current over a long period of time in a PPBT sample exposed to a step function voltage. Typically the current  $I$  drops by about three orders of magnitude over a period of six hours and, when plotted on a log-log graph, exhibits a series of linear segments  $I \propto t^{-n}$ . Such measurements were made on samples doped with  $\text{LiCl}$ ,  $\text{NaCl}$ ,  $\text{CaCl}_2$ ,  $\text{LaCl}_3$ , etc. The other type of transient, measured for the same samples, resulted when the humidity was suddenly increased from dry conditions to some finite value on a specimen in a quasi-steady state of conduction. A large increase of relative current ( $\Delta I/I_{\text{min}}$ ) occurs, followed by a gradual decrease over a long period of time. Efforts to relate these effects to the nature of the conduction mechanisms and diffusion of water are discussed.

### EXPERIMENTAL SECTION

**Materials** Polyphenylene benzobisthiazole films about 6 mm wide and 20  $\mu\text{m}$  thick, and PPBT fibers of similar diameters were used. The PPBT was synthesized by Wolfe [1] and processed into fibers and films by the Celanese Research Company. The processing solvents were polyphosphoric acid (PPA) or methane sulfonic acid (MSA). Residual acids had been removed by extensive washing and treatment with  $\text{NH}_4\text{OH}$ . The polymer chains tend to be highly oriented in the final materials. Silver paste electrodes were used. They had to be applied with great care under a microscope.

Techniques and Apparatus Only limited quantities of very small fibers and films were available so that special techniques and cells had to be developed. The special cells have been described previously [2], they were designed to be accommodated as a cell within a cell using the Hewlett-Packard 16008A high resistance cell in conjunction with the essential item for the measurements, namely a very sensitive electrometer. The Keithley Model 642, with its sensitivity of  $10^{-17}$  A, served this function. The design of the cells allowed for the determination of the surface and volume components of the conductivity. [2] In some experiments, the PPBT samples were doped by soaking in salt solutions. When this was done, the samples were rinsed and blotted dry, to remove surface deposits, when taken from the soaking solution. Moisture sorption measurements were made by using a very sensitive (48  $\mu$ g/mm) quartz spring in an evacuable container. Spring deflections were measured with a stage micrometer microscope.

## RESULTS

Current-time Characteristics for Dry PPBT A plot of current  $I$  vs time  $t$  (as in ref. 2) makes it appear that there is a limiting current  $I_{\min}$  after about 8 hours at 24° C. However, as Stetter [3] has shown for polyethylene, the minimum current is only a convenient fiction. A  $\log I$  vs  $\log t$  plot, as in Fig. 1, is a better representation of the situation. The point is not that every detail of such an observation will be reproduced upon repetition of the experiment but that the tendency to get data which can be represented by sections of curve  $I \propto t^{-n}$  is a recurring theme.

Transient Currents Upon Exposure to Humid Air After a sufficient period, a convenient pseudo-asymptotic current,  $I_{\min}$ , is chosen and then the relative differential current,  $\Delta I/I_{\min} = (I - I_{\min})/I_{\min}$ , is plotted vs the square root of the time following the first instant of exposure of the dry sample to moist air while the voltage ( $\sim 22$  V) continues to be applied. A collection of such plots for salt doped samples is given in Fig. 2. It is seen that the type of salt and its concentration has a significant effect on the curves.

Water Sorption and Diffusion in PPBT Clearly the

time dependent uptake and redistribution of water in a polymer plays a crucial, usually dominant, role in the transient electrical behavior, therefore a direct determination of the sorption and diffusion coefficients was made for water in PPBT. An Arrhenius plot of  $D$  is shown in Fig. 3. The data are well described by  $D = (4.3 \times 10^{-6} \text{ cm}^2/\text{s}) \exp(-E_D/RT)$  where  $E_D = 6000 \text{ cal/mol} = 0.26 \text{ eV}$ . The sorption measurements from which the value of  $D$  was obtained were somewhat non-Fickian and exhibited a temperature dependent negative enthalpy of sorption (less water was sorbed at higher temperatures). Below 32° C  $\Delta H_S \approx -35 \text{ kcal/mol}$  ( $-1.52 \text{ eV}$ ) and above 32° it is about  $-7 \text{ kcal/mol}$  ( $-0.304 \text{ eV}$ ). At 26° C, and a water vapor partial pressure of 24 Torr, the relative sorption (water/polymer) is  $5.2 \times 10^{-3} \text{ g/g}$  (0.52 w/o) or about 1  $\text{H}_2\text{O}/11$ mers.

## DISCUSSION

The data reveal that there are two types of transients in these experiments: (a) the gradual long term decay, sectionally represented by  $I \propto t^{-n}$ , and (b) the relative increase in current  $\Delta I/I_{\min}$ , subsequent to exposure to moisture. It is believed that the first type transient can be explained in terms of Maxwell-Wagner interfacial polarization effects related to the complex internal morphology. Also influencing the current decay, we would expect some effects related to a random distribution of charge carrier trap depths, similar to cases described by Scher and Montroll [4].

A central motivation for the salt doping experiments was our hypothesis (to be discussed in detail elsewhere) that the Barker-Sharbaugh [5] weak electrolyte model for ionic conduction in isotropic organic liquids and polymers would apply with appropriate detailed modifications to highly anisotropic polymers. The resulting new model appears to be even more useful than the previous one, but though the evidence of Fig. 2 is related to the new hypothesis we are not herein defending it. Instead we merely point out that our motivation in plotting  $\Delta I/I_{\min}$  vs  $t^{1/2}$  was to try to relate the second type of transient conductivity data to the diffusion of water vapor. (It is fully realized that a proper treatment will involve an integration over the spacial concentration distribution.) The form of the data themselves suggests some molecular in-

terpretations. The initial sorption of water enhances conduction in the outer layer of the sample, causing the initial rapid rise in  $\Delta I$ , then subsequently the ion that can move most readily to do so, leading to peaks in  $\Delta I$ . Inflection or auxiliary peaks in  $\Delta I$  reflect ions that are more weakly bound, and finally we would expect a decrease in current as the ions become depleted from the bulk system and blocked at the electrode.

#### ACKNOWLEDGEMENT

The authors would like to express their acknowledgement to the support by a grant from the U.S. Air Force Office of Scientific Research (AFOSR-80-0014A). We wish to thank Dr. E. C. Chenevey and Dr. J. R. Leal of the Celanese Research Company for supplying PPBT samples and related information. We also wish to express our appreciation for very useful discussions with Drs. D. Bhaumik, S. L. Hsu, T. E. Helminiak, F. E. Karasz, K. R. Lawless, J. E. Mark, E. L. Thomas, and D. R. Ulrich.

#### REFERENCES

- [1] Wolfe, J. F., Loo, B. H., and Arnold, F. E., ACS-polymer preprint, vol. 19 (2), pp. 1-6, 1978.
- [2] Barker, Jr., R. E. and Chen, D. Y., 1981 Annual Report CEIDP, IEEE 79-649806, pp. 351-359, Oct. 1981.
- [3] Stetter, G., 1964 Annual Report CEIDP, National Academy of Science: Washington, D.C., pp. 21-24, 1964.
- [4] Schar, H. and Montroll, E. W., Physical Review B, Vol. 12, No. 6, pp. 2455-2477, 1975.
- [5] Barker, Jr., R. E. and Sharbaugh, A. H., J. Polym. Sci., Vol. C10, pp. 139-152, 1965.

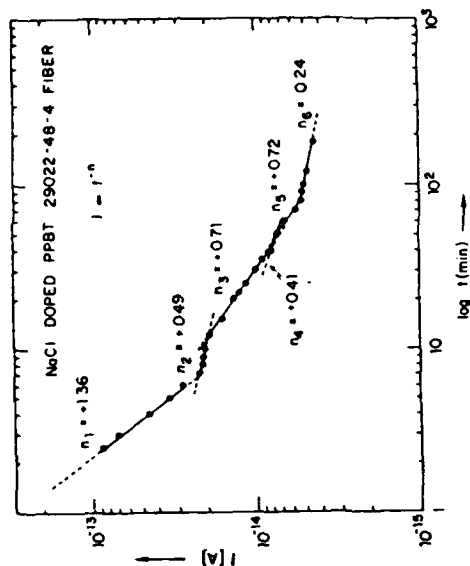


Figure 1: Transient Current vs Time for a NaCl doped PPBT fiber.

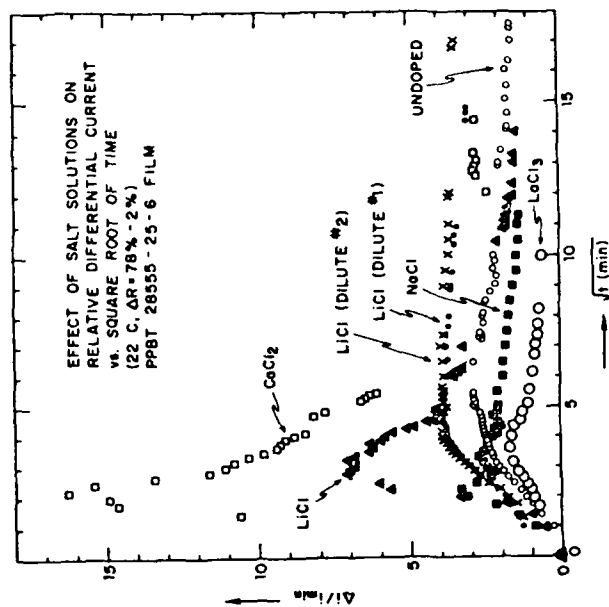


Figure 2:  $\Delta I/I_{\min}$  vs  $\sqrt{t}$  curves for salt doped PPBT samples.

# TEMPERATURE DEPENDENCE OF D WATER IN PPBT

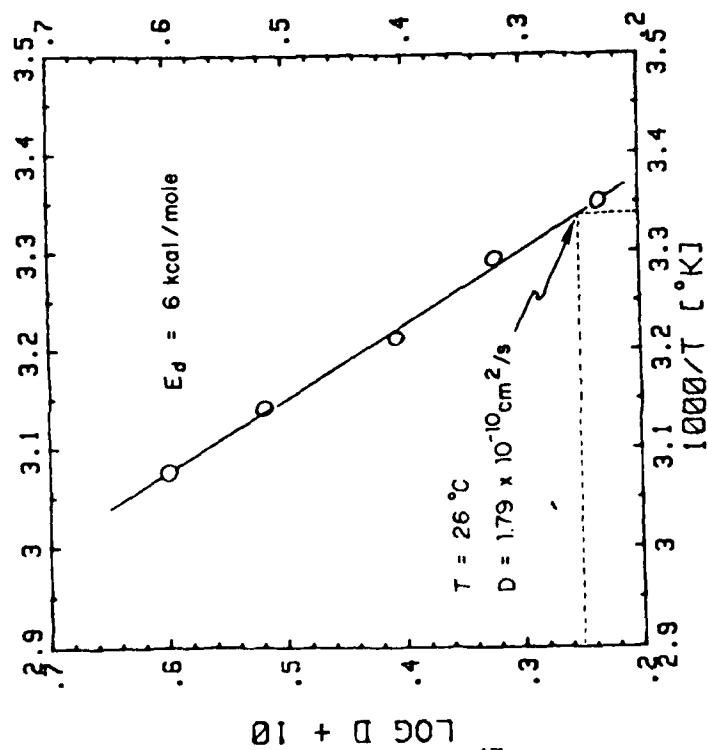


Figure 3: Temperature dependence of the coefficient D for water diffusion in PPBT.

# VIRGINIA JOURNAL OF SCIENCE

OFFICIAL PUBLICATION OF THE VIRGINIA ACADEMY OF SCIENCE

Vol. 34

No. 3

Fall 1983

178

THE VIRGINIA JOURNAL OF SCIENCE

STUDIES OF THE EFFECTS OF MOISTURE SORPTION ON ELECTRICAL CONDUCTION IN ION-DOPED POLYMERS. J. A. Hawk\*, D. Y. S. Chen\*, and R. E. Barker, Jr., Dept. of Mat. Sci., Univ. of Va., Charlottesville, Va. 22901. Previously Barker, Chen, and Huang have examined the process of charge transport in rigid rod polymers such as poly(p-phenylene benzobisthiazole), or PPBT, by measuring two types of transient currents. The PPBT is an extended chain aromatic hetero-cyclic polymer which exhibits both a gradual current decay over long periods of time, as well as large jumps in the relative current (i.e.,  $\Delta I/I_{min}$ ) when the PPBT sample is subjected to increases in relative humidity from essentially dry conditions. Experiments were conducted on PPBT samples doped with various solutions of  $LiCl$ ,  $NaCl$ ,  $CaCl_2$ ,  $LaCl_3$ , etc. In addition, undoped PPBT fibers were also tested, against which the doped results were compared. In the present work our goal has been to see if the transient current phenomena curve is distinguishably different for different types of polymers, or if there was something unique about the rigid rod polymers. Additional experiments have been performed on fibers of nylon 6,6 and polyethylene (PE) in both the doped and undoped form for a variety of experimental conditions. The most interesting general result is that each material appears to have its own characteristic type of  $\Delta I/I_{min}$  curve.

THE VIRGINIA JOURNAL OF SCIENCE

181

TRANSIENT DIELECTRIC PROPERTIES OF POLYMER-DILUENT SYSTEMS. C.-C. Huang\* and R. E. Barker, Jr., Dept. of Mat. Sci., Univ. of Va., Charlottesville, Va. 22901. Recent work by Chen and Barker has provided persuasive evidence that a useful extension of the "weak electrolyte" model (of Barker and Sharbaugh) to the case of anisotropic polymer systems is possible. In continuing our studies of this and other more general features of transport mechanisms in polymers, quantitative information was needed for the dielectric permittivity tensor ( $\epsilon_{ij}$ ) and for its variation with temperature, frequency, and the concentration of various diluents and dopants. The present work relates some of the experimental approaches undertaken with these goals in mind and in particular addresses the relevant fact that during diffusion of a diluent into a polymer, the system is inhomogeneous and the effective average dielectric properties ( $K'$ ,  $K''$ , or  $\tan \delta = K''/K'$ ) have a time dependence which is related to the diffusion coefficient. A combination of dielectric cells (including a liquid immersion cell) and bridge techniques have been applied to examine PMMA, PS, PTFE, and PPBT (poly(p-phenylene benzobisthiazole), in addition to a quartz standard.

## EXTENSION OF THE WEAK ELECTROLYTE MODEL TO ANISOTROPIC POLYMERS

R. E. Barker, Jr., D. Y. J. Chen, J. A. Hawk, and C. C. Huang

Department of Materials Science  
University of Virginia  
Charlottesville, Virginia 22901

A number of years ago Barker and Sharbaugh explored the nature of the relationship between electrical (ionic) conductivity  $\sigma$  and dielectric constant  $\epsilon$  for organic liquids and for solid polymers. Statistically, for the whole class of materials, and individually for systems in which it was possible to vary  $\epsilon$  by moisture sorption, it was found that an adaptation of the theory of weak electrolytes provided a useful model for correlating the observed ionic transport properties.

By its nature the original theory was based on a dissociable ion pair surrounded by an isotropic dielectric continuum. In recent attempts to gain insight into the mechanism of charge transport in highly anisotropic extended chain polymers it has been possible to make a major extension of the B-S model to the case of anisotropic polymers by utilizing ideas analogous to those in the Born solvation theory. The new model will be discussed in relation to some experimental data.

R. E. Barker, Jr.  
Department of Materials Science  
School of Engineering and Applied Science  
Thornton Hall  
University of Virginia  
Charlottesville, VA 22901  
(804) 924-6339 or 924-3264

### C. Summary of Results for Thermal Conductivity

Contrary to what is believed in some circles, the thermal conductivity  $K$  of polymers is a structure sensitive property, and important information can be obtained if  $K$  is measured with some care vs. temperature  $T$  and pressure  $p$  for a wide range of values and polymers, some truly remarkable differences appear. Due to the limited quantity and form of the available PPBT, it has not yet been possible to conduct as full of a range of experiments as might be desirable but nevertheless some interesting and useful results have been obtained. These results are also believed to have a semi-quantitative applicability to other extended chain polymers of similar structure.

A useful heuristic approach to thermal conductivity of solids is to consider

$$K \approx (1/3)C_V \rho \Lambda s \approx (1/3)C_V \rho \Lambda^2 / \tau \approx (1/3)C_V \rho s^2 \tau = (1/3)C_V \Lambda (Y \rho)^{1/2}$$

where  $C_V$  is the heat capacity,  $\rho$  is the density,  $\Lambda$  the effective phonon mean free path,  $s \approx \sqrt{(\text{modulus}/\text{density})} = \sqrt{(Y/\rho)}$  is the speed of sound, and  $\tau$  is the effective phonon relaxation time. Although the expression is over-simplified, it is apparent that important structural considerations are involved. There will be contributions over a spectrum of frequencies and  $\Lambda_\omega$  and  $\tau_\omega$  will be functions of frequency. The elastic properties parallel and perpendicular to the rod-axis, in concert with the transverse vibrational coupling, will lead to very anisotropic thermal conductivities. As Choy, Chen and Luk and also Meissner have shown, the ratio of axial to transverse thermal conductivity of oriented polyethylene varies strongly as a function of elongation ratio. In distinction to polymers such as PE, which can be put into an extended chain conformation only by special processing

techniques, and which will rearrange to other conformations at elevated temperatures, PPBT is synthesized from rod-like monomers which are nematic phase liquid crystals, therefore making extended chain arrangements and correspondingly high axial thermal conductivity much more likely and much more stable.

### 1. Techniques

Partly due to the nature of PPBT as a material and partly due to the limitations on the size, form, and perfection of the samples available, it has proved quite difficult to make the kinds of thermal conductivity measurements we wanted. Several of the techniques we proposed previously were attempted. However, due to the small diameters of the available fibers ( $\sim 20 \mu\text{m}$ ), along with the inherently large heat transfer coefficient ( $> 200 \text{ W/m}^2\text{°C}$ ) we have not yet been able to obtain the necessary resolution of thermal gradients and transients to make any of the mentioned techniques completely feasible for available PPBT fiber samples. The heat transfer coefficient is a measure of the convective heat loss from the fiber's surface to the surrounding air per unit surface area per unit degree Kelvin. Although the fibers have a small surface area and the heat loss rate is small, it is difficult to elevate the fiber's temperature due to the product of the large heat transfer coefficient and the large surface area to volume ratio which results in a very large heat loss per unit volume per unit difference in temperature between the fiber surface and the surrounding air.

Thus far the only successful techniques have employed PPBT films with a thickness of about  $20 \mu\text{m}$  and a width of about  $5 \text{ mm}$ . The molecular chains of the PPBT film are aligned in one direction in



the plane of the film. The tensor term for the thermal conductivity in the direction of the molecular chains is  $K_{11}$ . The tensor terms for the thermal conductivity transverse to the molecular chain,  $K_{22}$  and  $K_{33}$ , are assumed to be approximately equal due to the nematic liquid crystal ordering of PPBT.

Two techniques for anisotropic thermal conductivity determination of the PPBT film were used. The first technique uses a symmetrical sandwich cell to estimate thermal conductivity transverse to the molecular chain axis ( $K_{22}$ ). A heater is sandwiched between two identical samples and the temperature across each sample is determined by differential thermocouples. The total heat flux transversing both samples was estimated, accounting for heat losses from the heater through the thermocouples in the heater and through the Teflon shield surrounding the heater. Due to the small symmetrical cell diameter of about 5 mm, the cell had to be checked for accuracy with a sample of known thermal conductivity; Teflon was chosen. After accounting for heat losses, our values for thermal conductivity of Teflon were within the range of values from other workers.

The second successful technique, the de Senarmont method, estimated the ratio of the axial to transverse thermal conductivity ( $K_{11}/K_{22}$ ) by forming a molten ellipse on a very thinly wax coated PPBT film by touching the sample surface with a heated needle or by directing a circular laser beam onto the coated PPBT film. By measuring the lengths of major and minor axes, an estimate of the ratio ( $K_{11}/K_{22}$ ) is calculated. However, due to the unavailability of suitable samples, the de Senarmont technique was not checked with a

sample of known anisotropic thermal conductivity but our values of the ratios ( $K_{11}/K_{22}$ ) should be valid since the technique is comparative.

The basis and limitations of the de Senarmont technique can best be seen by considering a thermal energy flux balance. Thus the rate of energy storage per unit time in a unit volume is equal to the difference in energy flux across the unit volume plus the rate of thermal energy generation by sources in the unit volume. Thus if the specimen is a thin sheet of thickness  $\zeta$  which is heated at a small central hotspot of temperature  $T_0$  and  $r_0$ , and if the heat transfer rate per unit area to the surrounding air is  $h(x,y)\theta$ , where for present purposes the heat exchange coefficient  $h(x,y)$  is a constant, then

$$\rho C_p \frac{\partial \theta}{\partial t} = K_{11} \frac{\partial^2 \theta}{\partial x^2} + K_{22} \frac{\partial^2 \theta}{\partial y^2} - \frac{2h\theta}{\zeta} \quad (1)$$

for  $r > r_0 = x_0^2 + y_0^2$ , and  $\theta = T - T_e$ . This equation can be transformed by the relations

$$\xi = x/\sqrt{K_{11}}, \quad \eta = y/\sqrt{K_{22}} \quad (2)$$

Therefore, for steady state

$$\frac{\partial^2 \theta}{\partial^2 \xi} + \frac{\partial^2 \theta}{\partial \eta^2} - \frac{2h\theta}{\zeta} = 0 \quad (3)$$

In the case  $h=0$ , the isotherm in  $\xi$ - $\eta$  space will be circular  $\xi^2 + \eta^2 = r_\theta^2$  and the corresponding relation for  $x$ - $y$  space will be an ellipse

$$x^2/K_{11} + y^2/K_{22} = r_\theta^2 \quad (4)$$

The ratio of the semi-major and semi-minor axes is then

$$\frac{K_{11}}{K_{22}} = \left(\frac{a}{b}\right)^2 \quad (5)$$

When  $h \neq 0$ , it can be seen by symmetry that the isotherms are still circular in  $\xi-\eta$  space (and therefore ellipses in  $x-y$  space) but the simple relation of Equation (5) will be a lower limit estimate of  $K_{11}/K_{22}$ . Due to the heat exchange with the surrounding atmosphere by convection, one expects that  $K_{11}/K_{22} \geq (a/b)^2$  and if the effect of radiative transfer between the hot needle, and the surface is taken into account, the strength of the inequality will be increased. However, the results using the laser agreed with those for the needle rather well.

## 2. Experimental Results

For a typical sample film (As Cast or Heat Treated) with a wax coating of a specific melting temperature, approximately 15 trials were run. Three waxes of different melting temperatures (38°C, 69°C, and 118°C) provide the means for surveying a large range of temperature.

To minimize convective heat transfer from the heated needle to the sample and the convective heat loss from the heated sample, the needle and sample were placed in the bell jar of a Differential Thermal Analyzer (DTA) and evacuated to a pressure of about 10  $\mu\text{m}$  (Hg) by application of a rotary vacuum pump. To minimize convective thermal boundary overlap from the needle to the sample, the wax coated sample film was horizontal and the heated needle was vertical.

Some typical results for the de Senarmont technique are presented in Fig. 1. A line through the origin with a constant slope would correspond to an ideal situation. Each point is a separate experiment.

PPBT; AS CAST #28555-25-5 & 6

WAX MELTS AT 118°C

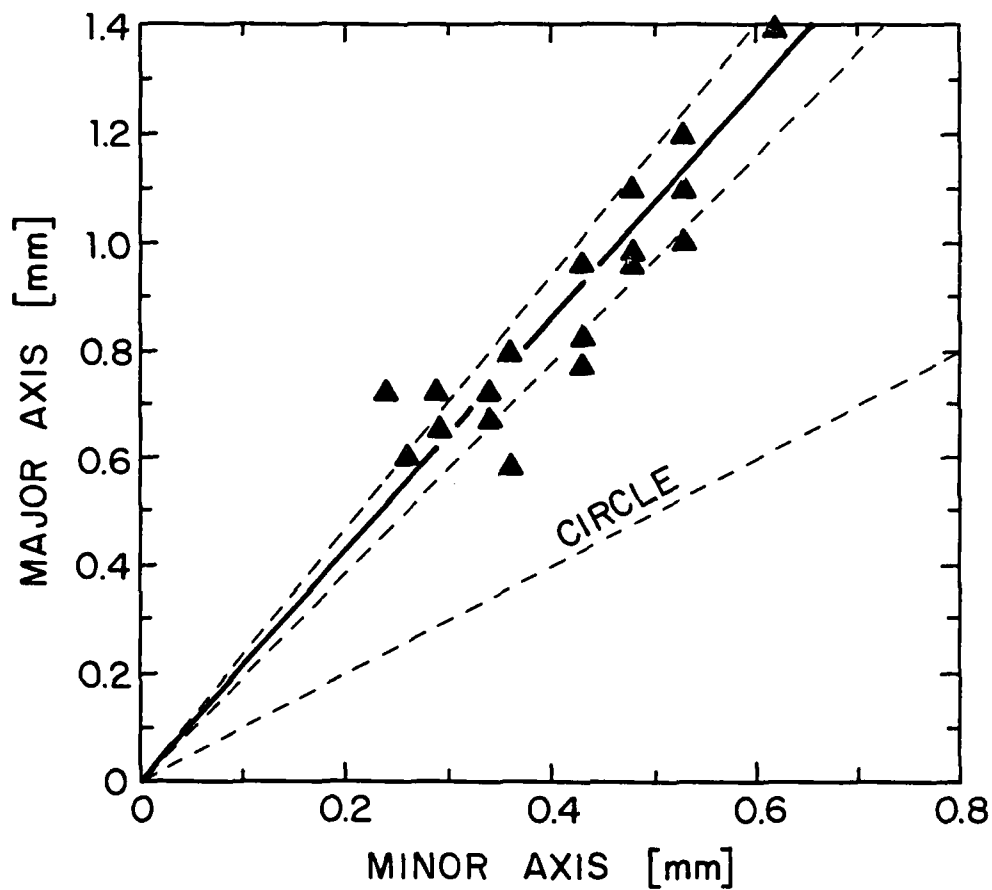


Figure 1. De Senarmont technique for "As Cast" PPBT  $T_m = 118^\circ\text{C}$ . The line marked "circle" would correspond to the isotropic case.

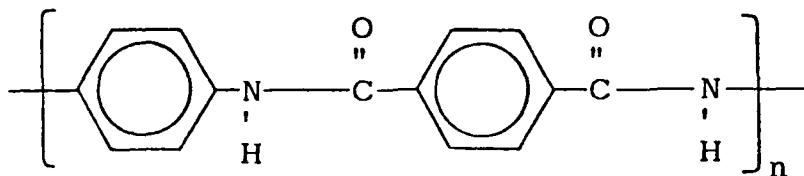
For such plots, as Fig. 1, for the major axis  $a$  vs. the minor axis  $b$ , a least-squares line through the origin rather than a displaced one has been used to fit the data. There did in fact appear to be a trend toward somewhat higher slopes with some curves having an intercept on the minor axis near  $b = 0.1$  or  $0.2$  mm. Thus the value of  $K_{11}/K_{22}$  based on the line through the origin established a lower limit for the ratio. Table 1 below summarizes the values of  $K_{11}/K_{22}$  and the standard deviations in parentheses of the experiments for three values of the melting point of the wax coating. We emphasize that these ratios are lower limits.

TABLE 1  
 $K_{11}/K_{22}$  AND (STANDARD DEVIATION OF  $K_{11}/K_{22}$ )

Type Sample	$T_m(\text{wax})=$	38°C	69°C	118°C
PPBT 28555-25-5-6 As cast		5.1 (0.6)	3.5 (0.4)	4.7 (0.3)
PPBT 28555-25-6 Heat treated at 450°C		4.2 (0.5)	3.7 (0.4)	4.4 (0.4)

The average of the values in this table is  $(K_{11}/K_{22}) \approx 4.3 \pm 0.6$  whereas the value of  $K_{11}/K_{22}$  based on the maximum slope of the  $a$  vs.  $b$  plots is about  $(4.6)^2 \approx 21$ . The most consistent data appear to be for the "as cast" sample of PPBT 28555-25-5 at a wax-melting temperature of 118°C. The most probable slope for the data is about 2.33 giving  $K_{11}/K_{22} \approx 5.4$ ; whereas the maximum slope that one can reasonably assign to the data gives  $K_{11}/K_{22} \approx 8.9$ . From the above discussion, we adopt a value  $K_{11}/K_{22} \approx 5$  until future experiments provide a more accurate estimate of the ratio.

It is of interest to compare these estimates for PPBT with some results for Kevlar (polyphenylene terephthalamide)



Although rather different in terms of the chemical constitution, Kevlar is very similar to PPBT in a functional way. Both polymers are extended chain polymers related to nematic phase monomers. By utilizing some data for the thermal conductivity across the layers and along the "warp" a composite consisting of a Kevlar-49 fabric in an epoxy matrix, we have utilized a fairly simple volume-fraction model to calculate  $K_{11}$  and  $K_{22}$  for Kevlar. The results of our estimates are listed below

$$K_1 = K_{\text{epoxy}} = 0.22 \text{ W/m}^\circ\text{C}$$

$$K_{11} \approx 1.65$$

$$K_{22} \approx 0.20$$

$$\frac{K_{11}}{K_{22}} = 8.3 \text{ (for Kevlar 49).}$$

Due to the use of fabric rather than oriented fibers the estimate for  $K_{11}$  may be too small. In general, the various values appear reasonable, as will be shown below.

Although this method of composites has some unresolved fundamental as well as practical problems it is still a very useful technique. Unfortunately we never had enough PPBT available to make use of the method.

### 3. Measurement of the Transverse Thermal Conductivity of PPBT

Using the symmetrical sandwich described earlier, the value of  $K_{22}$  for PPBT has been estimated. A problem that caused a lot of trouble was the irregularity of the PPBT surfaces, which made it difficult to separate the increase in thermal conductivity due to pressure from the increase in the overall heat exchange coefficient. At low pressure, the irregular surfaces of PPBT may allow an air space between the sample and the cell, leading to an apparent conductivity which is too small and also to an apparent rate of increase with pressure  $(dK/dp)_{app}$  which is too large. With these qualifications some values of  $K_{22}$  are given in Table 2.

TABLE 2  
APPARENT TRANSVERSE THERMAL CONDUCTIVITIES  $K_{22}$   
FOR PPBT #28555-25-5 (mW/m°C)

<u>P[bar]*</u>	<u>T[°C]</u>	<u>32°C</u>	<u>50°C</u>	<u>130°C</u>
1		~ 50	~ 60	~ 55
60		100	—	—
1440		200	260	—

\*Note: 1 bar = 0.1 MPa  $\approx$  1 atm.

Several interpretations are possible. For example, if the value at 1440 bar is presumed to be near the true conductivity of PPBT and the difference is taken as the conductivity of an air layer then (since  $K_{air} \approx 26$  mW/m°C) we calculate an effective series air layer between 4 and 6  $\mu$ m thick on each surface.

On the other hand, if we assume that the low conductivity at  $P \approx 1$  bar is due to the fact that the true contact area

is through surface asperities and is much smaller than the apparent geometrical area, then an application of Hertz's theory (for spherical contact points) suggests that  $K_{app}$  vs.  $p^{1/3}$  should be linear. A plot of this type is shown in Fig. 2. The data seem to increase at a slightly slower rate than  $p^{1/3}$ , but at present it is necessary to give the Hertz type theory serious consideration, especially in practical terms related to applications of PPBT where transverse heat exchange across solid interfaces is involved.

#### 4. Longitudinal Thermal Conductivity $K_{11}$

By combining the results of the de Senarmont method with those of the symmetrical cell technique we have  $K_{11}/K_{22}$  and  $K_{22}$  and can therefore calculate  $K_{11}$ . The magnitude is  $K_{11} \approx 5 \times 200 \text{ mW/m}^\circ\text{C} = 1 \text{ W/m}^\circ\text{C}$ . The true way in which  $K_{11}/K_{22}$  varies with pressure is not yet known. Our best estimate is that  $K_{22}$  is more sensitive to pressure changes than  $K_{11}$  is, because the effect of pressure on transverse interchain interactions is expected to be greater than its effect on longitudinal interchain interactions. The use of the values given in Tables 1 and 2 lead to smaller values for  $K_{11}$ . However, if it is assumed that imperfect thermal contacts due to sample irregularities limit the low pressure measurements then the value  $K_{11} \geq 1 \text{ W/m}^\circ\text{C}$  is a better estimate, and also appears more consistent with the values calculated for Kelvar.

#### D. Summary of Results for Vapor Diffusion and Solubility in PPBT

The sorption  $\psi$  and diffusion  $D$  of molecular species in extended chain polymers is very closely related to the processes involved in charge transfer and somewhat less directly connected with



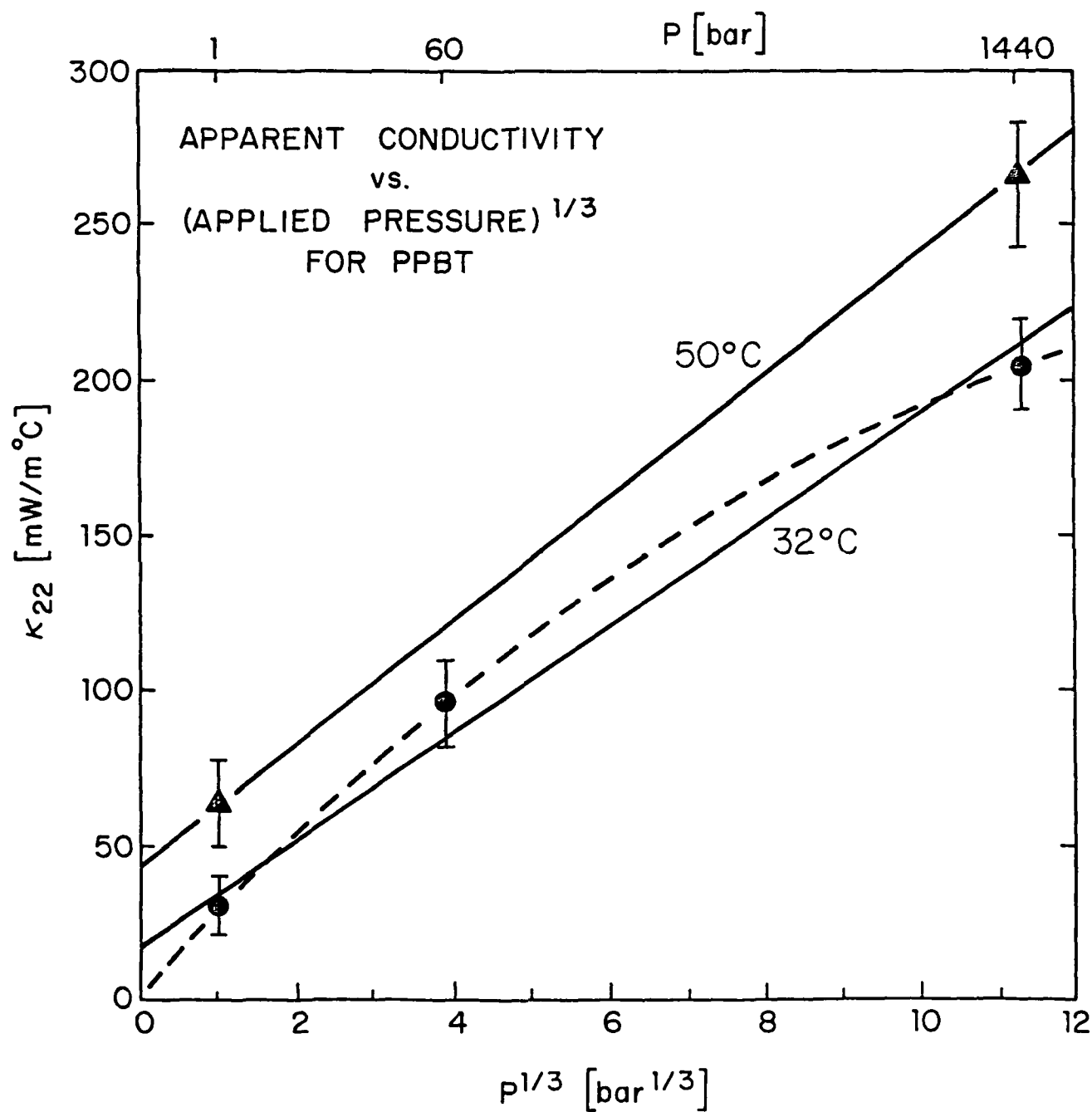


Figure 2. Apparent thermal conductivity of a film of PPBT vs. the cube root of the applied stress. The Hertz theory predicts a straight line.

thermal conductivity. The main technique utilized in  $D$  and  $\psi$  measurements during the funding period has been a classical one which is still among the best and most sensitive available. The source of vapor is connected through a system of valves to a thermostated evacuable chamber in which a small sample is suspended by a very sensitive quartz spring. The system was checked by measuring the sorption characteristics of polyethylene terephthalate (PET) for which reliable data were available in the literature. A second system used for some of the measurements utilized a Cahn electrobalance. Due to the limitations on the available amount of PPBT in the form of good quality films of uniform thickness, the PPBT experiments were done with samples of about 10 mg-mass and 20  $\mu\text{m}$ -thickness. The quartz spring for the PPBT sorption experiments was near the limit of what is commercially available, with a sensitivity of 47.5  $\mu\text{g}/\text{mm}$ . The deflection was measured with a stage microscope and the resulting sensitivity was about  $\pm 0.5 \mu\text{g}$ . It should be mentioned that although these experiments appear simple, a great deal of care must be exercised in their execution and interpretation. For example, due to the combination of small sample and low solubility, the differential thermal expansion of the quartz spring and the glass sample chamber sometimes had to be taken into account. Also due to the high sensitivity of the spring, provisions had to be made to avoid electrostatic effects in the chamber.

Due to its ubiquity and significant influence on so many other processes, it is important to know about the sorption and diffusion of  $\text{H}_2\text{O}$  in polymers such as PPBT. The nominal dimensions of the PPBT 28555-25-6 film were 52 mm x 6 mm x 0.02 mm (9.7 mg). After

outgassing in a vacuum for 48 hrs the uptake of moisture was measured at several temperatures.

The vapor pressure of the source was adjusted by controlling its temperature. The relative sorption of water in the polymer for a vapor pressure of 24 Torr is shown in Fig. 3 as a function of the square root of time. The sorption and desorption of water in PPBT is non-fickian. Similar behavior is noted, for example, in cellulose (Newns), keratin (King), and polyvinyl alcohol (Long and Thompson). It is seen, from a comparison of the sorption and desorption curves, that at 25°C, some of the water sorbed into the PPBT remains there upon desorption. The amount of residual water is  $1.02 \times 10^{-3}$  mg/mg at 25°C and 24 Torr or  $(N_w/N_{mer})_{resid.} \approx 1.51 \times 10^{-2}$  H<sub>2</sub>O/mer  $\approx (1/66)$  H<sub>2</sub>O/mer. By fitting the sorption curves with the well known solutions to the diffusion equation the data of Fig. 3 correspond to an average diffusion coefficient of  $2 \times 10^{-10}$  cm<sup>2</sup>/s. Measurements over a range of temperatures led to a diffusion coefficient, given by  $D = D_0 e^{-E_D/RT}$ , where for H<sub>2</sub>O,  $D_0 \approx 4.3 \times 10^{-6}$  cm<sup>2</sup>/s and  $E_D \approx 6$  kcal/mol = 0.26 eV  $\approx 25$  kJ/mol. This surprisingly small numerical value is quite similar to the estimates of Mark, Bhaumik and Welsh for the energy to rotate the benzobisthiazole group about the chain axis, suggesting a cooperative movement which allows the H<sub>2</sub>O molecule to squeeze between two chains. For benzene, similar measurements have been made and the results for PPBT are summarised below.

$$\begin{aligned}
 D(\text{H}_2\text{O}) &= 4.3 \times 10^{-6} \exp(-6000 \text{ cal mol}^{-1}/RT), & \text{cm}^2/\text{s} \\
 D(\text{Benzene}) &= 0.188 \exp(-12,000/RT), & \text{cm}^2/\text{s} \\
 \psi(\text{H}_2\text{O}, 26^\circ\text{C}) &= m_w/m_{\text{PPBT}} \approx 5.2 \times 10^{-3} \text{ g/g} \quad (p_w = 24 \text{ Torr}) \\
 \psi(\text{C}_6\text{H}_6, 24^\circ\text{C}) &= m_B/m_{\text{PPBT}} \approx 8.0 \times 10^{-3} \text{ g/g} \quad (p_B = 94 \text{ Torr}) \\
 \Delta H_{\text{sorption}} &\approx -30 \text{ kcal/mol for H}_2\text{O and } -23 \text{ kcal/mol for C}_6\text{H}_6.
 \end{aligned}$$

SORPTION AND DESORPTION  
CURVES OF H<sub>2</sub>O IN PPBT

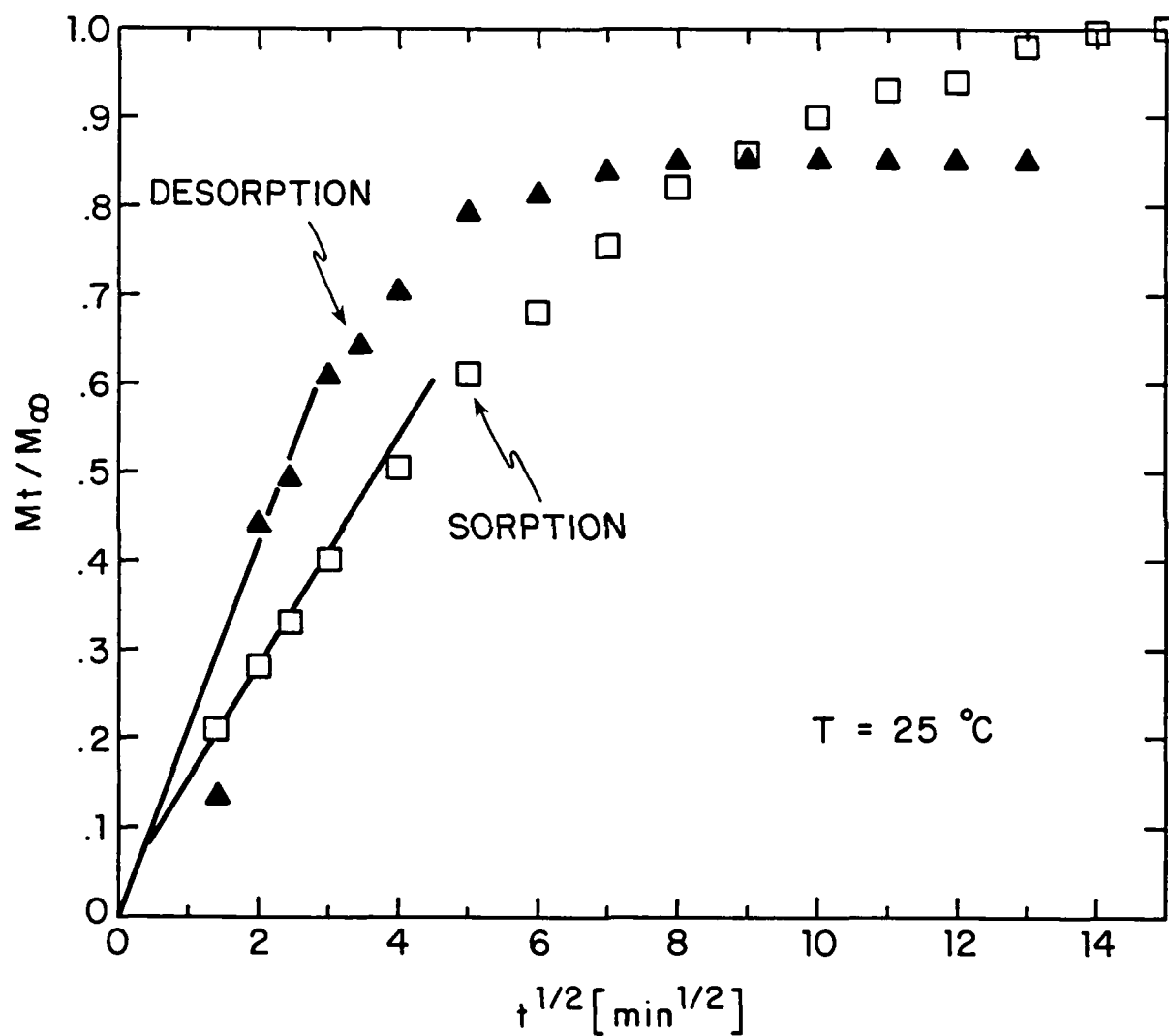
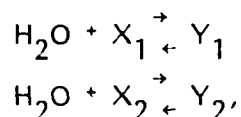


Figure 3. Relative sorption and desorption curves vs.  $t^{1/2}$  for water in PPBT films at  $25^\circ\text{C}$  (and  $p = 24 \pm 1.4$  Torr). The  $M_\infty$  value for the sorption process is used in both cases.

model proposed above for water, except that due to the larger size of the benzene molecule, that there needs to be a simultaneous cooperative interaction involving the rotation of two benzobisthiazole groups, thus giving  $E_D(C_6H_6) \approx 2E_D(H_2O)$ .

Measurements of the relative solubilities,  $\psi = (\text{mass diffusant})/(\text{mass of sample})$ , as a function of temperature have been made and the results are presented in Fig. 4, which is a Van't Hoff plot. There are two linear segments with an intersection near  $32^\circ\text{C}$  ( $10^3/T = 3.277$ ). The apparent enthalpies of solvation are  $\Delta H_S(T > 32^\circ\text{C}) \approx -7 \text{ kcal/mol}$  ( $-29.3 \text{ kJ/mol}$  or  $-0.304 \text{ eV}$ ) and  $\Delta H_S(T < 32^\circ\text{C}) \approx -35 \text{ kcal/mol}$  ( $-146 \text{ kJ/mol}$  or  $-1.52 \text{ eV}$ ). The negative enthalpies of sorption were slightly surprising (but not truly unusual). The negative sign reflects the fact that less of the diffusant will be sorbed at higher temperatures than at lower ones. In the case of  $H_2O$ ,  $\Delta H_S$  was variable over the experimental range of  $T$ .

One possibility, related to the two segments of the curve in Fig. 4, is that at least two different sorption processes are in equilibrium:



where  $Y_1$  and  $Y_2$  are complexes of  $H_2O$  and the entities  $X_1$  and  $X_2$  in the polymer. The question of whether  $X_1$  and/or  $X_2$  are intrinsic components of the chemical structure of the mer or whether they are due to impurities or structure imperfections can be addressed in part by calculating the mole fraction of  $H_2O$  sorbed. The ratio  $N_w/N_m$  of the number of water molecules per mer is given by

$$\frac{N_w}{N_m} = \frac{m_w}{m_m} \frac{M_m}{M_w} = \frac{266.34}{18.02} (m_w/m_m)$$

where  $M_m/M_w$  is the ratio of molecular weights of the mer to water and  $m_w/m_m$  is the ratio of the mass or sorbed water to the mass of mers (which, of course, is also the mass of polymer). Over the observed range of temperature (24°C to 52°C) the magnitude of  $m_w/m_m$  at  $P_v \approx 24$  Torr ranged from about  $10^{-3}$  to  $10^{-2}$ . The corresponding range of  $N_w/N_m$  is therefore 0.015 to 0.15 H<sub>2</sub>O/mer. For example, at  $T = 26^\circ\text{C}$ ,  $m_w/m_m \approx 6 \times 10^{-3}$  so that  $N_w/N_m \approx 0.09 \approx 1 \text{ H}_2\text{O}/11 \text{ mers}$ . At the hypothetical intersection of the -7 kcal/mol curve with the -35 kcal/mol curve ( $\sim 32^\circ\text{C}$ ) the ratio is  $N_w/N_m \approx 1/27$  (at  $P = 24$  Torr).

What these results appears to mean is that the observed sorption may be taking place on end groups, impurities, or imperfections in the structure. (It should be noted that this same statement could be made in reference to many other polymers, e.g., bisphenol-A polycarbonate.)

### III. PROFESSIONAL PERSONNEL AND INTERACTIONS

#### A. Professional Personnel

(1) Dr. R. E. Barker, Jr., Principal Investigator, Professor of Materials Science, University of Virginia.

(2) Dr. K. R. Lawless, Consultant on Microscopy and Structure, Professor and Chairman, Department of Materials Science.

(3) Dr. Daniel Y. Chen, Graduate Research Assistant (and Postdoctoral Fellow for three months), University of Virginia.

(4) Mr. Larry J. Adams, Graduate Research Assistant, University of Virginia.

(5) Mr. Wu-Song Huang, Graduate Research Assistant.

(6) Mr. Chin-Ching Huang\*, Graduate Research Assistant.

(7) Mr. Jeffrey A. Hawk\*, Graduate Research Assistant.

B. Interactions

Several trips have been made along with a number of advisory and consultative contacts with personnel of other laboratories working on programs supported by the U.S. Air Force. On January 26, 1979, R. E. Barker, Jr. and K. R. Lawless visited the laboratories of Dr. T. E. Helminiak and coworkers at AFML/MBP-WPAFB in Dayton. This visit provided a good orientation to the areas in the field of rod-like polymers of special importance to the Air Force. It also gave us an awareness of the special experimental facilities available there. On June 11, 1979, Barker attended a two-and-a-half day "Ordered Polymers Review" co-sponsored by WPAFB and AFOSR in Dayton. Other such conferences, held in Dayton on January 8, 1980 and September 22-24, 1980 were attended respectively by Barker and Daniel Chen, and by Barker and Lawrence Adams. Others of these well-organized Air Force conferences on ordered polymers were held in Dayton on October 21, 1981 and February 9, 1983. The contacts with Air Force scientists and with other grantees and invited visitors were good. All of these reviews were quite valuable in providing information and ideas applicable to the research on PPBT and related extended chain polymers.

On April 2-3, 1980, R. E. Barker, Jr. went to the University of Cincinnati to give a seminar on the transport properties of polymers

---

\*Messrs. C. C. Huang and Hawk were on AFOSR-80-0014 for a relatively short time.

and to discuss the research of Dr. James Mark and his research group, which has Air Force support. On July 24, 1980, Dr. T. E. Helminiak of WPAFB visited our laboratory at the University of Virginia.

Another trip was made on September 1-3, 1980 by Daniel Chen to visit the research groups of Dr. F. E. Karasz and Dr. E. L. Thomas to exchange research ideas and observe some experimental setups at the University of Massachusetts.

We also have been in contact with: (1) Dr. Jim Wolfe of Stanford Research Institute, who sent us some unprocessed PBT; (2) Dr. Guy Berry, who sent us a small PBT film; (3) Dr. Edward Soloski of the University of Dayton who provided us with a few micrograms of a crystalline model compound; (4) Dr. Edward Chenevey and coworkers at the Celanese Research Labs, who have provided us with fibers and films of PBT on several occasions. We have had numerous useful contacts with Dr. D. R. Ulrich of AFOSR, both on visits by Barker to Bolling AFB, and also on a visit of Dr. Ulrich to the University of Virginia, along with Dr. D. R. Wiff of the University of Dayton, and Dr. T. E. Helminiak.

Several other lectures were given at national meetings and these may be seen by referring to Section II.A.

#### IV. NEW DISCOVERIES AND INVENTIONS

Two of the most notable discoveries during the research were closely intertwined. These were the observation of the enormous asymmetry factor  $\sigma_{11}/\sigma_{22}$  of 100,000 for the ratio of electrical conductivities of PPBT at room temperature, and the discovery that a rationally based quasi-molecular anisotropic version of the weak



electrolyte model of Barker and Sharbaugh could be developed. The original model was a starting point for the new, much more detailed theory. The application of the theory to the data for the electrical conductivity dependence of PPBT on temperature, moisture content, dielectric constant tensor, and properties of the doping ions, is consistent with a predominantly ionic rather than electronic conduction process in PPBT.

We also succeeded in obtaining the activation energies of these two components of conductivity:  $E_{11}/E_{22} \approx (39 \text{ kJ/mol})/(82 \text{ kJ/mol}) = 0.41 \text{ eV}/0.85 \text{ eV} \approx 0.48$ . (Activation is easier along the chain.) Details of the conductivity experiments and of the new theory are given in Part II of this Final Report.

Although the short supply of samples of PPBT and other ordered polymers and the very limited sizes available were serious handicaps for most of the research goals, these factors did have the benefit of motivating some novel techniques appropriate to the measurement of transport properties in very small fibers and in narrow fibrillous films. For the case of electrical conductivity ( $\sigma$ ), this effort was met with considerable success and we now have not only  $\sigma$  data for PPBT under a number of conditions but also some new and hopefully broadly applicable techniques for conductivity measurements in general for fibers and narrow films. A patent application has been filed on our invention to make such measurements through the Patent Prosecution Office of the Judge Advocate General at Wright-Patterson AFB (Docket: S/N 06/528,309).

Another discovery which we hope will prove to be of significant usefulness in the future is the process we have termed DCDC (diffusion

controlled differential current). It is thought that this process is somewhat analogous to TSC (thermally stimulated currents) or TSD (thermally stimulated depolarization), the difference being that trapped charges or dipoles are released by the interaction with the polar diffusant (e.g.,  $H_2O$ ) instead of by thermal activation out of traps.

#### V. CONCLUDING REMARKS

The goal of this research has been to add to the store of fundamental knowledge about the Air Force's new high-strength, environmentally-stable, extended-chain polymers. Prior to the research initiated under Grant AFOSR-80-0014, there was an extensive deficiency in knowledge of transport phenomena in polymers such as poly-para-phenylene benzobisthiazole (PPBT). Our measurements and analyses of the electrical and thermal conductivities and of the solubility and diffusion of certain gases in PPBT have significantly increased the store of knowledge in these areas. We believe that the results demonstrate that a continuation of similar research on other ordered polymers as they become available (and especially as larger, better samples with a wider range of processing conditions become available) will provide a unified understanding of the three mentioned transport properties.

PART II

TECHNICAL NARRATIVE

## CONTENTS

	<u>Page</u>
 PART II TECHNICAL NARRATIVE	
Abstract .....	74
I. Introduction .....	76
II. Background .....	87
A. Overview .....	87
B. Transient Current .....	102
C. Charge Transfer Complexes .....	123
D. Ionic Dissociation and the "Weak Electro- lyte Model" .....	133
E. The "Local Structure Hypothesis" .....	139
III. Experimental Instrumentation and Techniques .....	144
A. The Experimental Instrumentation .....	146
B. The Auxiliary Measuring Cells .....	150
C. The Experimental Techniques .....	160
IV. Experimental Results and Discussion .....	171
A. Observation of Transient Phenomena .....	171
B. Field Dependence of Electrical Conductivity .....	179
C. Anisotropy .....	183
D. Thermal Activation of Electrical Conductivities .....	188
E. Effects of Additives and Processing on Electrical Conductivities .....	192
V. Weak Electrolyte Model (Ionic Conduction) .....	208
VI. I <sub>2</sub> Doping Experiments (Electronic Conduction) ..	217
VII. Future Research Possibilities and Applications .....	230
A. Electron-Microscopic Technique for Measuring $\sigma$ .....	230
B. Interdigitated Electrode System for Measuring $\sigma$ Due to Pressure .....	237
C. The "Catwhisker" Technique for High- Electric-Field Studies .....	241
D. Thermally Stimulated Current (TSC) Studies .....	241
E. A Possible Application -- The Indirect Method to Determine the Diffusion Coeffi- cient D of PPBT .....	245

## CONTENTS (Continued)

	<u>Page</u>
VIII. Conclusions .....	248
References .....	251
Appendix I .....	256
Appendix II .....	262
Appendix III .....	265
Appendix IV .....	271

## ABSTRACT

Surprisingly, in 1982, it remains difficult to unambiguously determine whether the observed level of electrical conductivity in a given polymer, under various conditions, is due to the motion of electrons or of ions. It is expected that much insight into the nature of the conduction process will be gained by choosing for study polymers that are highly anisotropic on the macroscopic as well as microscopic level. Extended-chain polymers such as poly-(paraphenylene benzobisthiazole), PPBT, represent unusual new types of materials for which very little is known about electrical and transport properties. Thus, PPBT was chosen as an appropriate material for detailed investigations of the electrical properties.

In this work, special techniques and instrumentation have been developed to measure electrical conductivities of small diameter PPBT fibers (10 $\mu$ m - 40 $\mu$ m) and small pieces of fibrillose PPBT films (6mm wide). A related technique has also been developed to distinguish between surface and bulk conductivities. It was experimentally found that a significant transient phenomenon which accompanied current measurements was due to the Maxwell-Wagner effect and intrinsic polymer defects. Near room temperature, the observed value of the ratio  $\sigma_{||}/\sigma_{\perp}$  is about  $10^6$ . This large value along with the fact that the conduction is ohmic up to at least  $1.2 \times 10^5$  V/m, is thought to imply one

dimensional electronic conductivity, although the effects of intrinsic ionic species are still present. In contrast, PPBT exhibits a mixed electronic and ionic conductivity which is strongly influenced by changes in relative humidity. The Barker-Sharbaugh "Weak electrolyte model" provided a theoretical tool to further rationalize the proposed mixed conduction mechanism. Both axial and transverse conductivities obey an Arrhenius type relation  $= \sigma_0 \exp (-E^*/RT)$  with  $E^*_{||}/E^*_{\perp} = 0.41/0.84$  (eV/eV).

Preliminary  $I_2$  doping experiments have shown that a charge transfer complex of  $I_2$ -PPBT is formed upon iodination. In sum, it may be said that the study of electrical properties of PPBT is a field rich in potential and cast important light on the whole matter of the nature of transport in PPBT.

## Chapter I

### INTRODUCTION

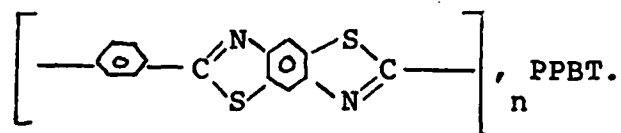
Conducting polymers, such as polythiazyl,  $\{SN\}_x$ , and polyacetylene,  $\{CH\}_x$ , have been investigated intensively in the last few years. The primary motivation for much of this activity has been the search for possible electronic applications. Although A.G. MacDiarmid, et al. of the University of Pennsylvania has successfully developed a light-weight plastic battery by using polyacetylene electrodes (1), substantial advances toward the goal of ultraminiaturization of electronic devices through the use of conducting polymers are still not obvious. Another impetus for the study of conducting polymers is the possibility of synthesizing superconducting polymers (2,3). The assumption, implicit or explicit, in the current literature is that any significant application of conducting polymers will depend on the electronic nature of the conduction process. Ionic (or electrolytic) conduction is most frequently not considered at all and when it is mentioned, it is often viewed as an uninteresting complication due to incomplete purification of the polymers which exhibit it. Of course polymers which are only ionic conductors will not likely be well suited to microelectronics application and it is important for this reason to know for a given polymer whether ionic or elec-



tronic conduction mechanisms dominate. Of greater significance, however, is whether the ionic conductivity is extrinsic or intrinsic and whether it can be used as a probe to obtain an improved understanding of molecular and microstructural processes within the polymer. Unfortunately, it still is often difficult to unambiguously distinguish the type of conducting mechanism of a specific polymer system. There is a controversy as to whether the conduction mechanism in certain specific polymers is ionic or electronic. While the charge carrier has been believed to be ions in some cases, a number of results supporting the electronic process have been extensively accumulated (4,5). Seanor (4) has reviewed the charge transfer in polymeric systems and concluded that electronic conductions exist in some polymers such as polyacrylonitrile and polyamides. However, a very large amount of further research remains to be done, and more work is needed in applying several proposed models, such as Barker's "local structure hypothesis" (6) and the "weak electrolyte model" (7-10), to specific polymer systems.

To conduct good experiments, the choice of an experimental material is crucial. Ideally, the experimental material should not only serve as a model material but also possesses potential for technological application. The material investigated is the U.S. Air Force's new high

strength, environmentally stable, extended chain polymers, poly-(paraphenylene benzobisthiazole),



Along the fiber axis PPBT is stronger than steel, has excellent thermal stability at temperatures above 300°C, and is a member of a class of materials referred to as extended-chain, "rod-like polymers" or "self-reinforcing composites." Some other extended chain polymers are poly-(paraphenylene benzoxazole), PPBO, and poly-(phenylene terephthalamide), PPTA (Kevlar). The monomers for such polymers are fairly rigid planar molecules which form nematic phase liquid crystals (11). This basic structure tends to be carried over into the polymeric solid state, leading to an extreme anisotropy of mechanical (12), optical, and electrical properties.

The anisotropy of electrical properties has been observed in many organic solids including polymers. For example, TTF (tetrathiofulvalene) and TCNQ (7,7,8,8-tetracyano-p-quinadimethane) form a quasi-one-dimensional solid which, at a comparatively low temperature of about 50°K, has an electrical conductivity along a ring stacking direction about the same as that of copper at room temperature (13). Figure 1 shows the herringbone pattern which is formed by the planes of stacked molecules in the salt (TTF)(TCNQ).

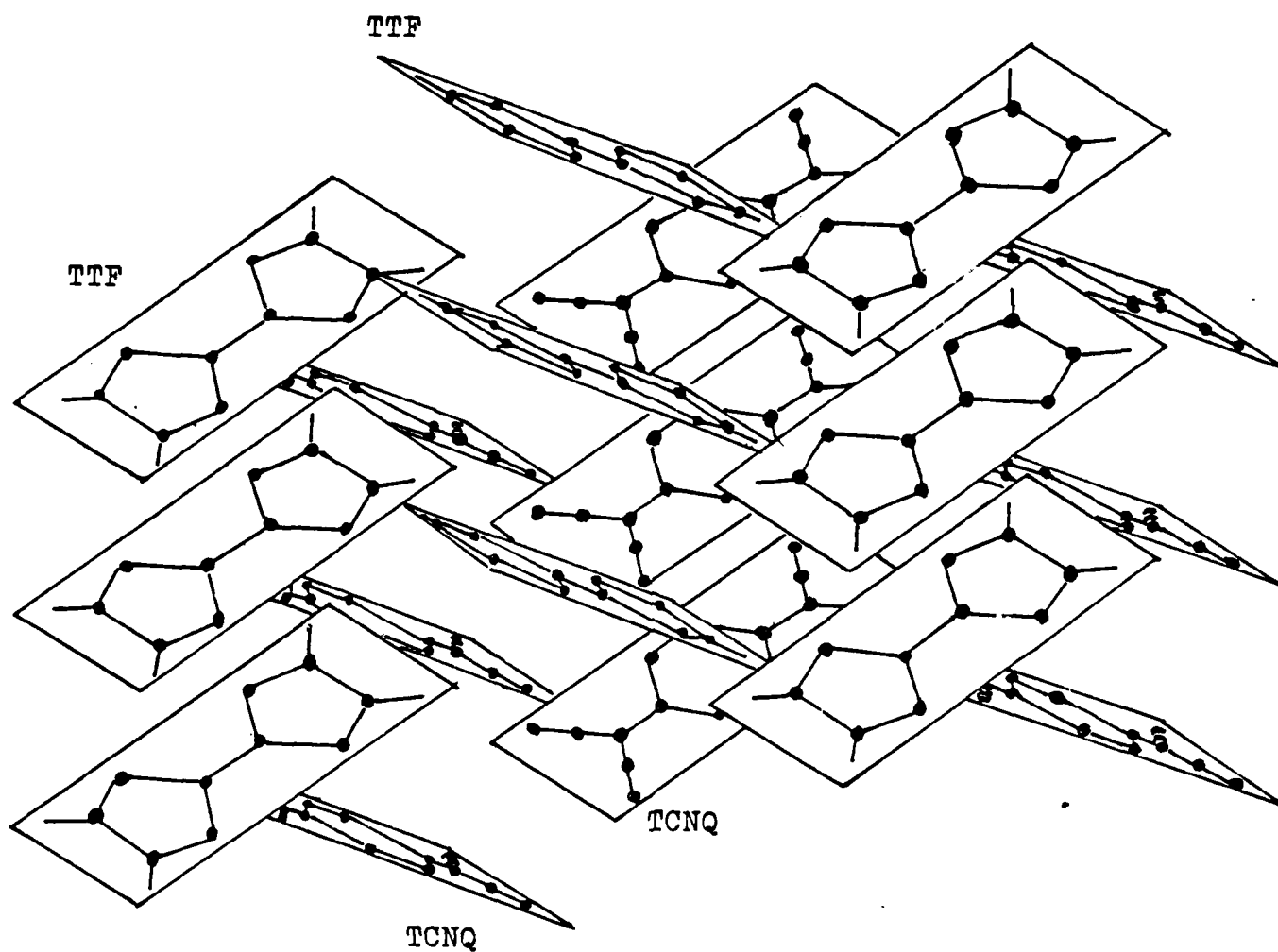


Fig. 1. "Herring bone" pattern in the salt (TTF)(TCNQ).

Within each stack the molecules are parallel to one another, but they are inclined to the axis of the stack. Orbitals that extended above and below the plane of each molecule overlap, giving rise to an electronic conduction band along the stacks. It has been found that on the average 0.59 of an electron per molecule is transferred from TTF to TCNQ, which creates a partially filled band in both molecules; as a result conduction takes place in both kinds of stack. In TCNQ the charge is carried by electrons and in TTF by holes, which represent the absence of electrons. The model compound of PPBO to which PPBT is analogous also has the herringbone structure (11), Fig. 2, which indicates that a similar anisotropic nature would exist in the Air Force's rigid-rod polymers. The anisotropy of electrical conduction has also been studied in nylon 66 (5,14). The anisotropy originates from three unique crystallographic features of nylon 66. These are: the chain direction, the plane parallel to the chain axis, and the plane containing the interchain hydrogen bonds (15). Therefore, the geometry of the chemical structure of PPBT should be carefully examined when the anisotropic nature is considered.

The PPBT samples were supplied by the Celanese Research Company. Due to the current processing condition, the only available PPBT samples were very small diameter fibers ( $\sim 20\mu\text{m}$  in diameter) and small quantities of a narrow film

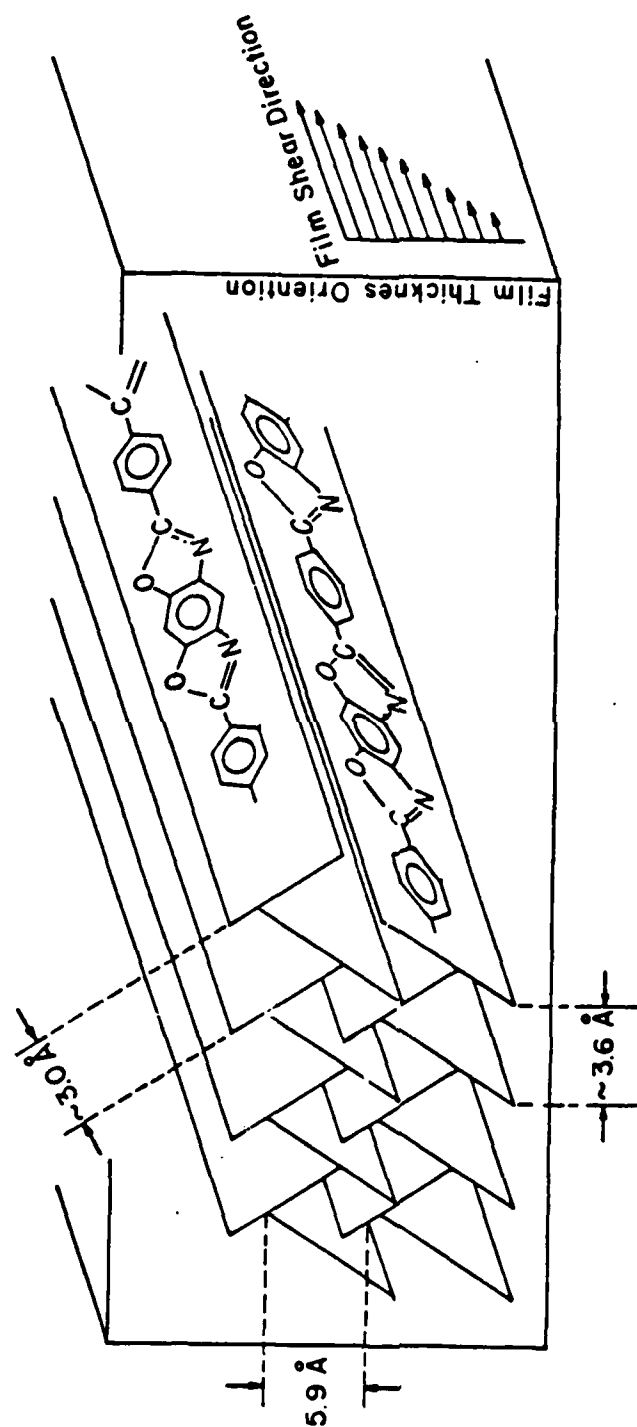


Fig. 2. "Herring bone" structure of poly-(paraphenylene benzoxazole).

( $\sim 6$ mm in width). Thus it was necessary to utilize measuring techniques orders of magnitude more sensitive than usually anticipated. Furthermore, the use of a conventional guarded cell (16) to separate surface current and volume current was not feasible for the small PPBT samples (Appendix I). The development of an appropriate instrumentation was also necessary. By the following example, the difficulties of the electrical conductivity measurements can be understood. For a typical measurement of the conductivity of a polymer, one might use a sample  $100\text{cm}^2$  in area and 0.1mm in thickness with a potential difference of 100V. Then, with a typical conductivity of  $10^{-16} \Omega^{-1}\text{-cm}^{-1}$ , the observed current would be:

$$I = \sigma AV/b \sim (10^{-16} \Omega^{-1}\text{-cm}^{-1})(100\text{cm}^2)(10^2\text{V})/(10^{-2}\text{cm}) \simeq 10^{-10} \text{ A}$$

For a very low conductivity material such as Teflon or mica, the observed current would be about three orders of magnitude smaller. For a fiber of 20  $\mu\text{m}$  diameter, with a conductivity  $\sigma = 10^{-16} \Omega^{-1}\text{-cm}^{-1}$ , and other values are given in the example, the observed current would be smaller by a factor to the area ratio  $\pi^2/A_0 = 3.14 \times 10^{-8}$ , that is, to a current of about  $3 \times 10^{-18} \text{ A}$  (or 20 electrons per second). The experimental techniques and instrumentation developed to measure electrical conductivities of PPBT samples will be

discussed in Chapter III.

The only known practical solvents for PPBT are methane sulfonic acid (MSA) and polyphosphoric acid (PPA). One of these acids are used in the fiber or film making process. The acids are usually removed by extensive washing in water or by treatment with  $\text{NH}_4\text{OH}$ . Electron and optical microscopy reveal the presence of voids, interfiber interfaces, acid residues, etc. (12,17) which are for practical purposes almost unavoidable consequences of the synthesis methods and processing conditions. Clearly  $\sigma$  will be influenced by such variables. For example, the measurements reported hereafter are on samples with an appreciable volume fraction of voids, so the reported conductivities should set a lower limit for samples without voids. The values for  $\sigma$  are also for samples with the "as received" acid content, except for some samples treated with ethyl alcohol, ammonium hydroxide, and salt solutions (e.g. Sodium Chloride, Lithium Chloride, Calcium Chloride, and Lanthanum Chloride). As a summary, the main factors leading to experimental difficulties were the following ones:

1. low total current,
2. difficult sample manipulation,
3. problems with electrical contacts,
4. the anisotropy itself,
5. infeasibility of conventional guarded electrodes,
6. mixed surface and volume conductivities,

7. variable diameter along a fiber, Table 1, (12),
8. fiber defects (e.g. voids), Table 2, (12),
9. unknown sample impurities,
10. residual acids, i.e. MSA and PPA, and
11. limitation of the maximum voltage across the electrometer.

The measurement of d.c. conductivities of PPBT samples in terms of transient phenomena, anisotropy, moisture content, thermal activation, impurities (or additives), and processing history will be discussed in Chapter IV in light of the known structure of PPBT and of established theoretical models. In addition to these data, an ohmic condition region for PPBT will also be mentioned.

The fundamental problem of this research is concerned with the species of charge carriers (ions or electrons) and the source of ionic charge carriers. The evidence in detail for the ionic conduction in PPBT samples will be presented in Chapter V through the analysis of the Barker-Sharbaugh "weak electrolyte model." The possibility of electronic conduction in PPBT samples and its implications will be discussed in Chapter VI.

Chapter VII will focus on certain special applications and future research possibilities for PPBT. Several preliminary attempts at measuring  $\sigma$  for PPBT will be briefly discussed in Appendix I.



Table 1: DEFECTS IN PPBT-27554-#

Fiber #	Linear Number Density (Defects/mm)		
	Internal Voids	Erupted Voids	Circumferential Bands*
6-2	0.5	15	14
6-3	0.6	15	7
9-1	0.4	<1	7
9-3	1.1	<1	26
9-5	0.2	<1	1
9-6	0	4	8
9-7	0.1	5	9
9-10	0.7	7	9
9-11	0.8	3	5

\* The existence of Circumferential Bands in PPBT fibers are an unique characteristic which forms a bamboo outlook in SEM micrographs.

TABLE 2: FIBER DIAMETER AND STANDARD DEVIATION

<u>PPBT Fiber</u>	<u>Diameter (<math>\mu\text{m}</math>)</u>	<u>S.D. (<math>\mu\text{m}</math>)</u>
27554 - 6-1	39.6	4.70
- 6-2	23.1	1.60
- 6-3	25.0	1.05
- 9-1	25.1	0.65
- 9-3	23.2	0.54
- 9-6	25.8	0.86
- 9-7	22.5	0.98
- 9-10	23.1	1.11
- 9-11	26.1	1.30

## Chapter II

## Background

A. Overview

## (i) Definition:

Electrical conductivity is a property of matter that has an enormous range of values, Table 3. The unit of measurement is the mho per centimeter ( $\Omega^{-1}\text{cm}^{-1}$ ), which is the reciprocal of the ohm centimeter. "Mho" was coined by Lord Kelvin as the backward spelling of "ohm", the unit named for Georg Simon Ohm. A new name for the mho is the Siemens  $100\text{S/m} = 1 \text{ mho/cm} = 1 \Omega^{-1}\text{cm}^{-1}$ . The best insulators, such as Teflon and polystyrene, have conductivities of about  $10^{-18} \Omega^{-1}\text{cm}^{-1}$ ; the best room-temperature conductors, copper and silver, approach  $10^6 \Omega^{-1}\text{cm}^{-1}$ . Several linear-chain materials, such as (TTF)(TCNQ) and  $(\text{SN})_x$ , have conductivities (measured at room temperature along the favorable axis) that range from a hundred to a few thousand  $\Omega^{-1}\text{cm}^{-1}$ .

## (ii) Electronic conduction and ionic conduction:

TABLE 3: THE LIST OF FOR VARIOUS MATERIALS\*

Classification <sup>+</sup>	Material	$\sigma$ (mho cm <sup>-1</sup> )
A	Teflon	$10^{-18}$
	Polystyrene	$10^{-18}$
	Quartz	$10^{-17}$
	PPBT(I)	$10^{-17}$
	Nylon	$10^{-14}$
	DNA	$10^{-12}$
B	Diamond	$10^{-12}$
	PPBT(II)	$10^{-11}$
	Dyes	$10^{-11}$
	Polyacetylene	$10^{-9}$
	Water	$5 \times 10^{-8}$
C	Si	$10^{-4}$
	Ge	$10^{-2}$
D	(TTF) (TCNQ)	$7 \times 10^2$
	$\{SN\}_x$	$2 \times 10^3$
	pt	$10^5$
E	Cu	$10^6$
	Ag	$10^6$
F	Pb (at 1.4°K)	superconducting
	Nb <sub>3</sub> Sn (at 18.05°K)	superconducting
	V <sub>3</sub> Si (at 17.1°K)	superconducting
	TiCo (at 3.44°K)	superconducting

\*  $100 \sigma(\text{sm}^{-1}) = \sigma(\text{mho cm}^{-1})$

+ The span is enormous, over 24 orders of magnitude (omitting the superconductors) Class A represent excellent insulators and very poor conductors.

The conductivity of a solid is usually determined by its electronic structure. The distribution of the electrons in the vicinity of an atom is described by a system of orbitals, each of which has a characteristic shape and size. In a highly conductive solid, orbitals of adjacent atoms or molecules overlap, so that electrons can readily move from site to site through the structure. Anisotropic conductors are materials in which there is a greater overlapping of orbitals along one axis than others. In the PPBT system, theoretical studies on its electronic structure have been reported by Mark et al. of the research group at the University of Cincinnati (18). Bauhmik used the extended Hückle technique (EHT) to find the wavefunction of electrons. Theoretical calculations based on the EHT have indicated an energy gap in PPBT of about 1.73 eV along the axial direction. It was assumed that electronic conduction is the only contribution. When electrons are tightly bound to the individual atoms or molecules of the solids, as in most polymeric materials, it is often easier for conduction to occur by the motion of the ions. The flow of charge then follows a slightly modified version of the kinetics involved in the diffusion of the ions. Thus, the energy gap calculated from the thermal activation energy, i.e.  $E_{\text{gap}} = 2E_{\text{activation}}$ , will be quite different from 1.73eV. Eyring's (19) rate process model will now be

used to examine the behavior of an ionic conductor.

For a simple ionic solid composed of atomic ions in the absence of an external electric field, the diffusing ion would move either by exchange with an adjacent vacancy or by being excited to an interstitial position from which activated diffusion becomes easier. In the first case, the number of ions adjacent to vacancies is  $N \exp(-E_F/KT)$ , where  $N$  is the total number of ions of the given type and  $E_F$  is the formation energy of a vacancy. In the alternative case, the number of ions occupying an interstitial site is  $N \exp(-E_I/KT)$ , where  $E_I$  is the formation energy of an interstitial-vacancy pair. For a general diffusion mechanism, the number of ions in sites from which motion is possible is:

$$n = N \exp(-E^*/KT). \quad (1)$$

If the activation barrier for the jump itself is  $E^*$  and the frequency of vibration is  $\nu$ , the number of jumps  $\Gamma$  per second for each of the  $n$  potential diffusive centers in the absence of an applied field is  $\nu \exp(-E^*/KT)$ . As indicated in Fig. 3, the effect of an applied field  $\epsilon$  on a positive ion  $e$  is to lower the activation barrier in the direction of the field of  $e\epsilon l/2$ , where  $l$  is the characteristic diffusion distance, and to raise the barrier in the

AD-A162 765

STUDY OF TRANSPORT PROPERTIES AND STRUCTURE OF  
EXTENDED-CHAIN POLYMERS (U) VIRGINIA UNIV  
CHARLOTTESVILLE DEPT OF MATERIALS SCIENCE

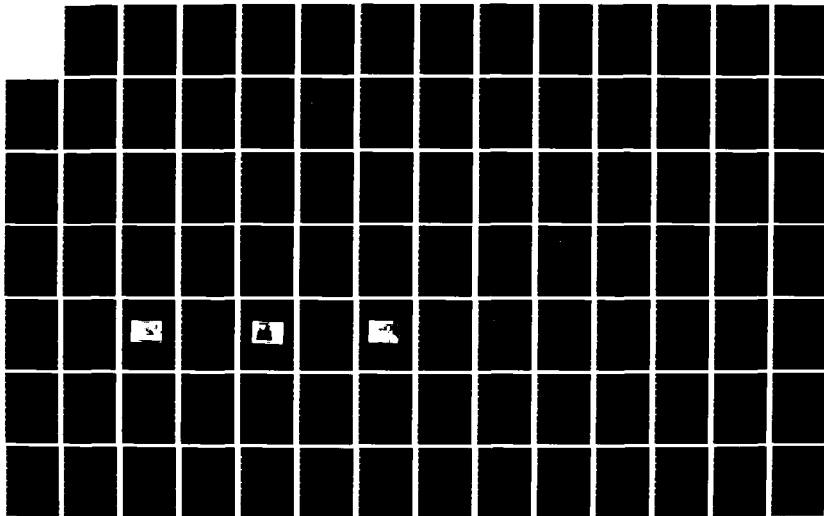
2/3

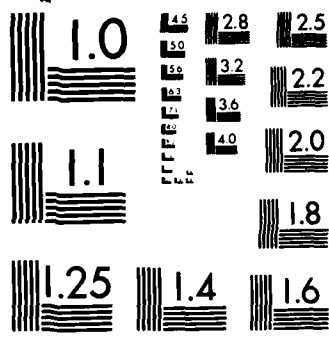
UNCLASSIFIED

R E BARKER ET AL SEP 85

F/G 11/9

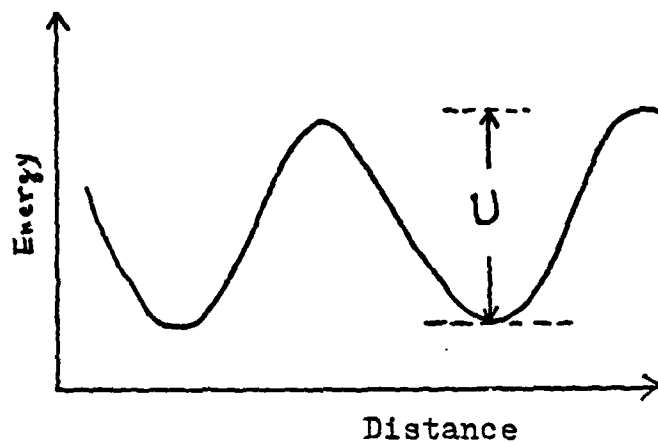
NL



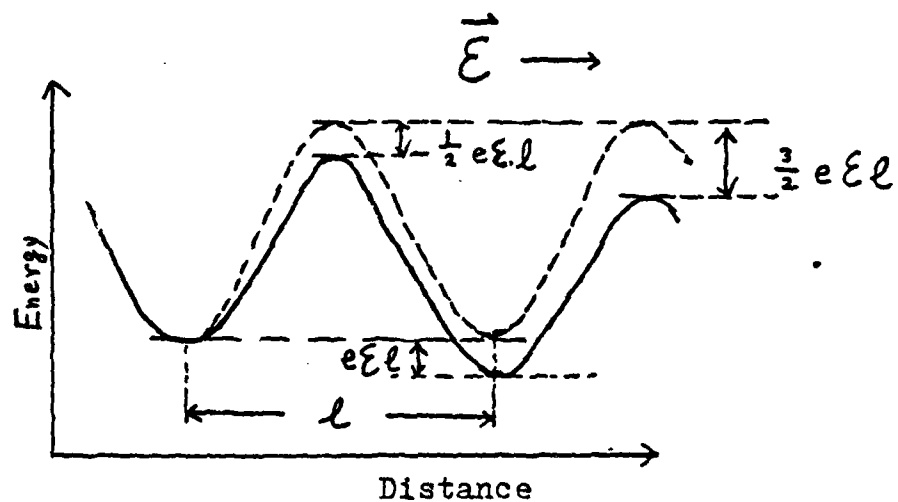


MICROCOPY RESOLUTION TEST CHART  
NATIONAL BUREAU OF STANDARDS-1963-A





(a). In the absence of  $\vec{\mathcal{E}}$ .



(b). In the presence of  $\vec{\mathcal{E}}$ .

Fig. 3. Activation barrier to ionic diffusion.

opposite direction by the same amount. Thus, for a positive ion the net number of jumps  $\bar{\nu}$  per second in the direction of the field is:

$$\begin{aligned}\bar{\nu} &= \bar{\nu}_+ - \bar{\nu}_- = N e^{-(E/KT)} \left\{ \nu \exp[-(E^* - \frac{ze\epsilon l}{2})/KT] \right. \\ &\quad \left. - \nu \exp[-(E^* + \frac{ze\epsilon l}{2})/KT] \right\} \\ &= 2N \nu \exp(-\frac{E+E^*}{KT}) \sinh(\frac{ze\epsilon l}{2KT}).\end{aligned}\quad (2)$$

The current density  $j$  is the product of the charge  $ze$  per ion, the distance per jump  $l$ , and the jump rate  $\bar{\nu}$  (per unit volume):

$$j = 2N \nu z e l \exp(-\frac{E+E^*}{KT}) \sinh(\frac{ze\epsilon l}{2KT}). \quad (3)$$

In Eq. (3), it is assumed that the energy function has a minimum which is symmetrically placed between the maxima. Barker and Thomas (8) have worked out a similar expression for the asymmetrical case in which they introduced an asymmetry parameter defined as the ratio of trough-to-peak forward jump distance to the total jump distance. This parameter was used to modify Eq. (3). Therefore, the current at any value of  $\epsilon$  (and hence the conductivity) will increase with increasing temperature. Fig. 4 and Fig. 5 (20) show the temperature dependence of the d.c. conductivity for PVC, PMMA, etc. In these figures, thermal

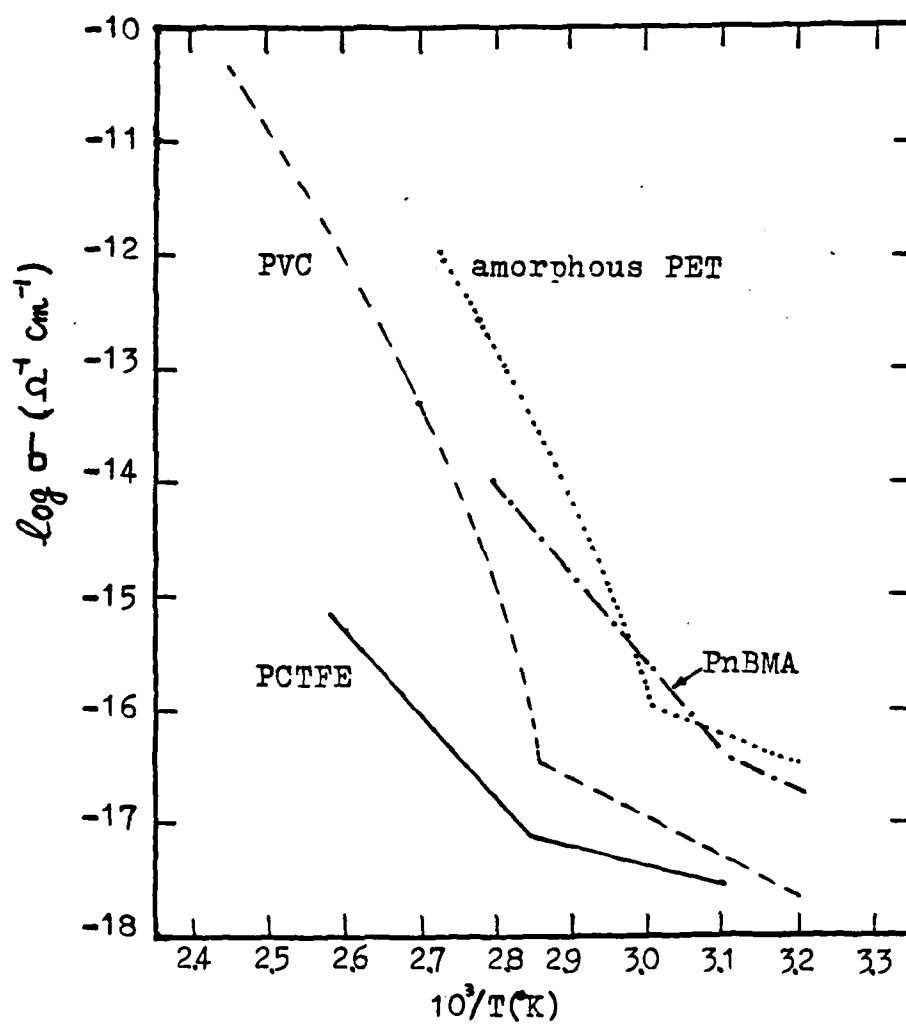


Fig. 4.  $\log \sigma$  vs.  $10^3/T$  for PCTFE, PVC, PnBMA, and amorphous PET.

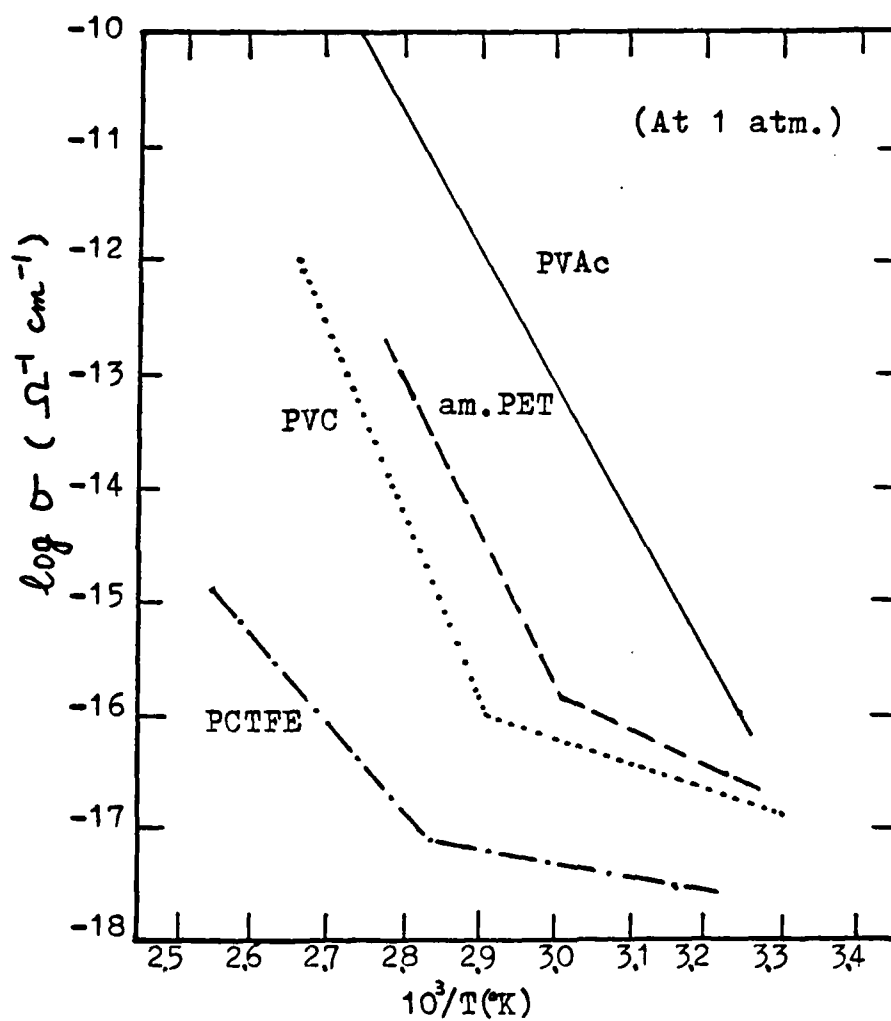


Fig. 5.  $\log \sigma$  vs.  $10^3/T$  for PCTFE, PVC, amorphous PET, and PVAc.

activation energies were calculated from the slopes of straight lines below and above glass transition temperatures ( $T_g$ ), respectively.

In addition to the temperature dependence, the pressure dependence also reveals some important features of the conduction mechanism for a given polymer. When it is subjected to external pressure, a given material will undergo a compression, the microscopic effect of which is the shortening of the intermolecular distances. Thus, electrical conductivity due to electronic processes will increase due to the larger overlapping region of electronic orbitals, but it will be diminished if due to ionic movement. (See Figure 6).

(iii) Ohmic conduction and non-ohmic conduction:

If Ohm's law applies to the conducting medium, then, at any given point outside a source

$$\vec{j} = \sigma \vec{E}, \quad (4)$$

where  $\sigma$  is the conductivity of the medium, expressed in mhos/meter, at that point. This is Ohm's law, wherein the current density  $j$  is expressed as  $j = I/A$ , where  $I$  is the total current passing through the medium,  $A$  is the

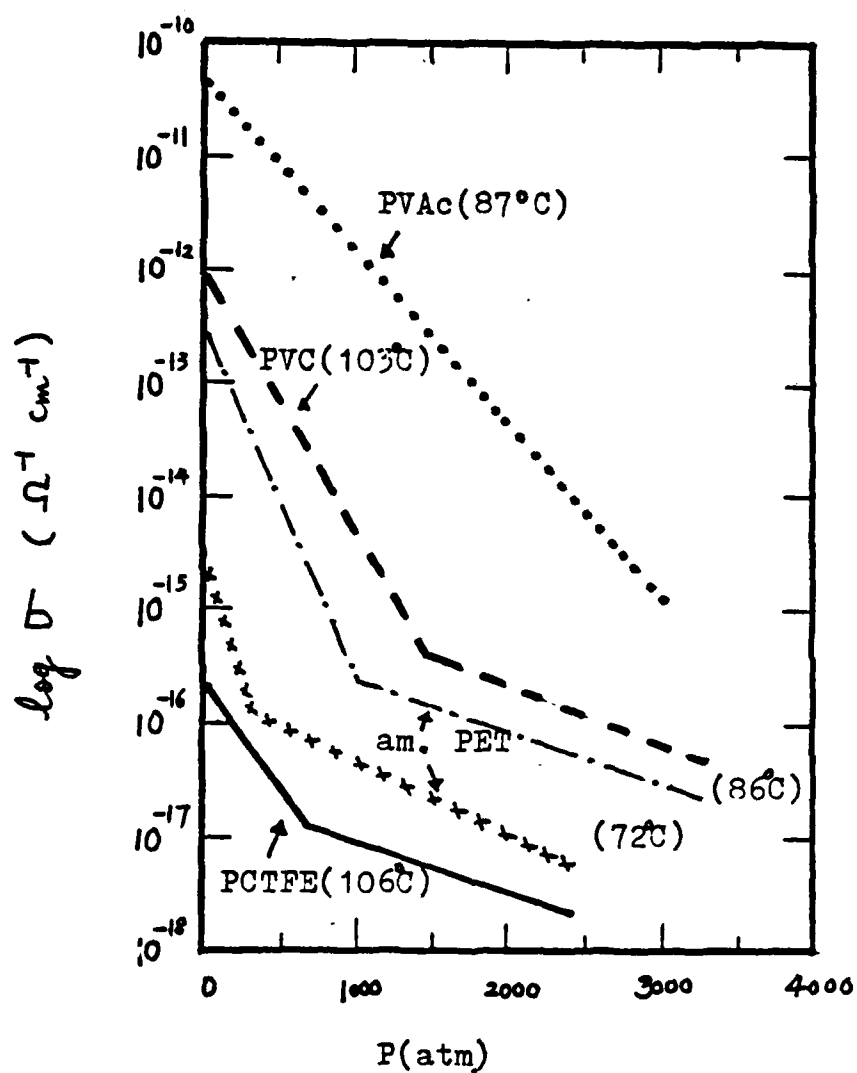


Fig. 6.  $\log \sigma$  vs.  $P$  for the polymers of Fig. 5.

effective area for current flow,  $\epsilon$  is equivalent to  $V/b$ ,  $V$  is the applied voltage, and  $b$  is the effective distance between two electrodes. Ohm's law can be further written as:

$$\sigma = Ib/VA. \quad (5).$$

For an anisotropic material,  $\sigma$  is no longer a constant through the conducting medium. Instead, it is a tensor, i.e.

$$\underline{\sigma} = \begin{pmatrix} \sigma_{11} & \sigma_{12} & \sigma_{13} \\ \sigma_{21} & \sigma_{22} & \sigma_{23} \\ \sigma_{31} & \sigma_{32} & \sigma_{33} \end{pmatrix}$$

It is customary to designate  $\sigma_{11}$  as the axial conductivity and  $\sigma_{22}$  (and  $\sigma_{33}$ ) as the transverse conductivity because they are the most interesting components. In the case of high external electric fields, the conduction process eventually will become non-ohmic. In the electronic conduction case, under high applied voltage, the space charge in the vicinity of the electrodes might cause the sample to be non-ohmic. The equations describing space-charge-limited currents were derived by Mott and Gurney (1940) (22) on the basis that:

- (a) The electrode is injecting in the sense that it can supply all the charge carriers which the solid can transport and that there are no potential barriers at the electrode/insulator interface, i.e.,

$$n(0) = \infty \text{ and } \epsilon(0) = 0.$$

- (b) The current flowing through the sample is independent of the position in the sample, i.e.

$$j = qn(x)\mu\epsilon(x) \neq f(x), \quad (6)$$

where  $x$  is the distance from the injecting electrode,  $n(x)$  is the number concentration of charge carriers at the distance  $x$ ,  $\epsilon(x)$  is the field at that point, and  $\mu(\text{cm}^2/\text{V-sec})$  is the drift mobility.

- (c) Poisson's equation is obeyed, i.e.,

$$qn(x) = e [d\epsilon(x)/dx], \quad (7)$$

where  $e$  is the electrical inductive capacity of the medium.



- (d) The integral of field strength  $\epsilon(x)$  across the sample is the applied voltage  $V$ , i.e.,

$$\int_0^1 \epsilon(x) dx = V. \quad (8)$$

Substituting  $qn(x)$  from Equation (7) into Equation (6) gives:

$$j = e\mu\epsilon(x) [d\epsilon(x)/dx] = \left(\frac{e\mu}{2}\right) d[\epsilon(x)]^2/dx. \quad (9)$$

Integration of Equation (9) and substitution into Equation (8) yields:

$$V = \int_0^1 (2j/e\mu)^{1/2} x^{1/2} dx,$$

which upon integration gives:

$$j = 9e\mu V^2/8l^3. \quad (10)$$

This is known as Child's law for the trap-free insulator. Figure 7 shows schematic I-V curves for space-charge limited currents (22). In the case of ionic conduction, as can be seen from Equation (3), if the applied field  $\epsilon$  is small, then  $\sinh\left(\frac{ze\epsilon l}{2KT}\right) \approx \frac{ze\epsilon l}{2KT}$  and the conduction is ohmic. As the applied field increases to sufficiently high values, non-ohmic behavior will become significant (Fig. 8) (23).

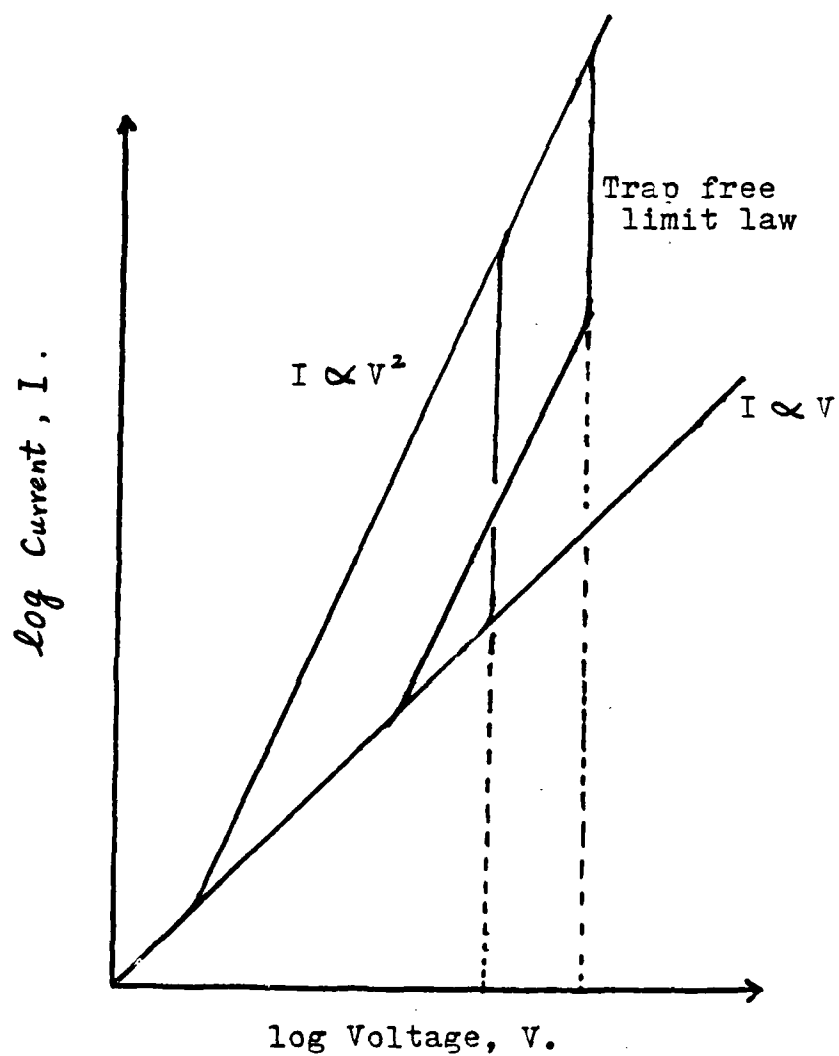


Fig. 7. Schematic I:V curves for space-charge-limited currents.

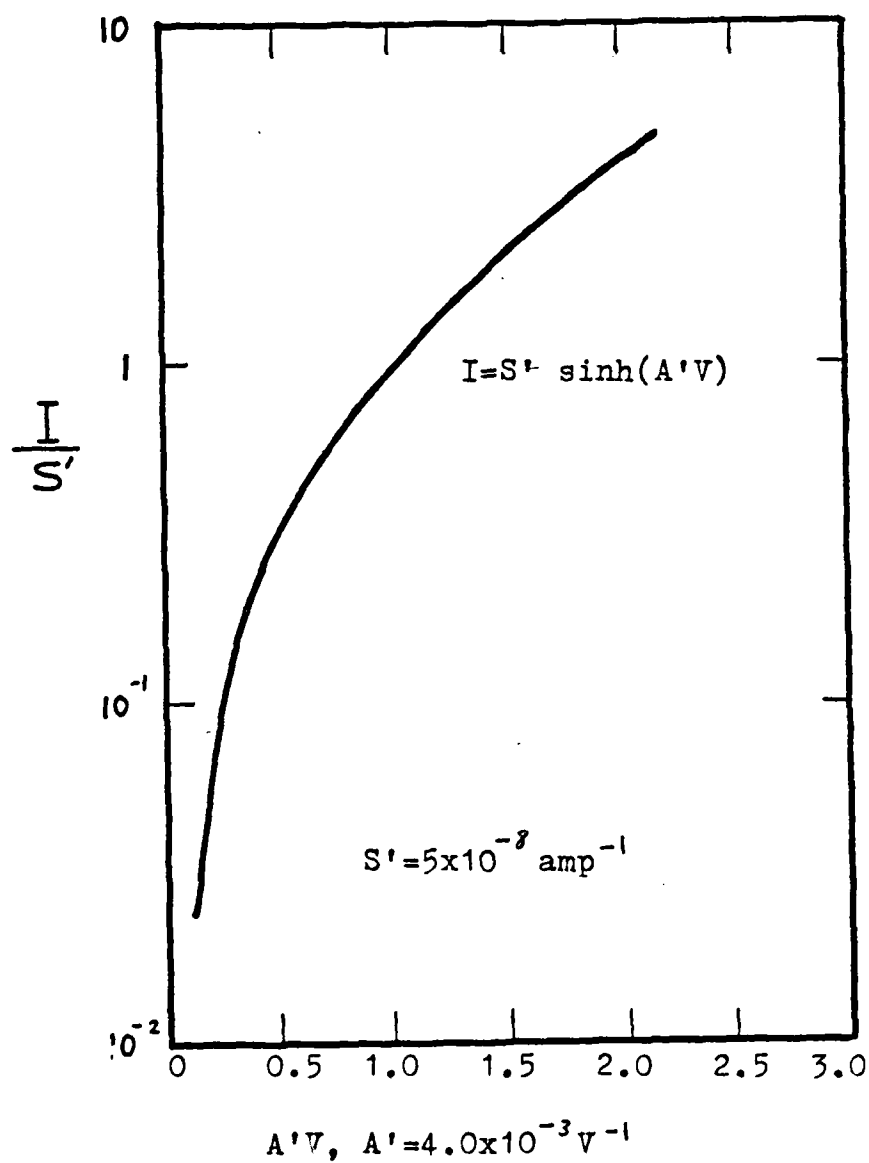


Fig. 8. Hyperbolic sine relationship between current and voltage for poly(ethylene terephthalate) films.

## B. Transient Current

When an electric field is applied to a dielectric, the field interacts with the bound and free charges causing their motion. The motion of charge manifests itself as a current flow in the external circuit. Generally, this current depends on the time elapsed after the application of voltage to the electrodes. Usually, it falls off at first (where the effect is sometimes termed polarization, absorption or anomalous charging current) and then it may become steady (and is called the leakage current), See Fig. 9 (24). This effect has been known for more than one hundred years and many explanations of the observed behavior in different dielectric materials have been given (25-28). At low fields, in general, the following processes may take place (29):

- (1) charging of the geometrical vacuum capacitance;
- (2) fast polarization processes, e.g. resonance and some type of dipole orientation polarization;
- (3) slow types of dipole relaxation polarization;
- (4) flow of conduction current caused by the motion of charges injected from the electrodes, or generated by thermal ionization of impurities or of the dielectric itself, or produced by photoionization or high-energy radiation ionization;

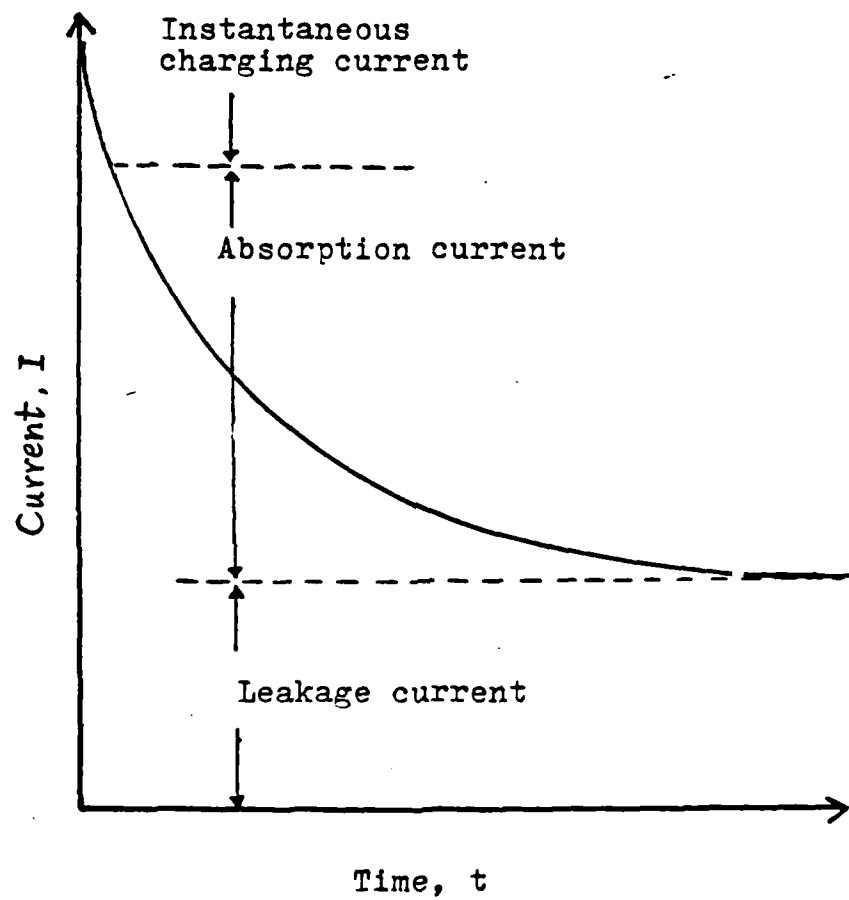


Fig. 9. Schematic  $I$  vs.  $t$  curve.

- (5) relaxation polarization of the Maxwell-Wagner type caused by micro- or macro- heterogeneities of a continuous or discrete nature;
- (6) electrode polarization due to complete or partial electrode blocking;
- (7) trapping of charge carriers in the bulk of the dielectric.

The time constant of currents corresponding to the first two processes is so short that these currents are not detected when the time dependence of the current is measured. At room temperature, the typical time variations of effective conductivities calculated from (a) the charging current and (b) the discharging current from PMMA (polymethylmethacrylate), a representative of the polar polymers, as well as for PS (polystyrene), a representative of the so-called non-polar polymers, are shown in Fig. 10 (29). In general, these are decay functions, which can usually be approximated over several decades of time by a power law:

$$\sigma(t) = \sigma(t_0) (t/t_0)^{-n}. \quad (11)$$

Usually a reference time  $t_0$  of one second is chosen, and then

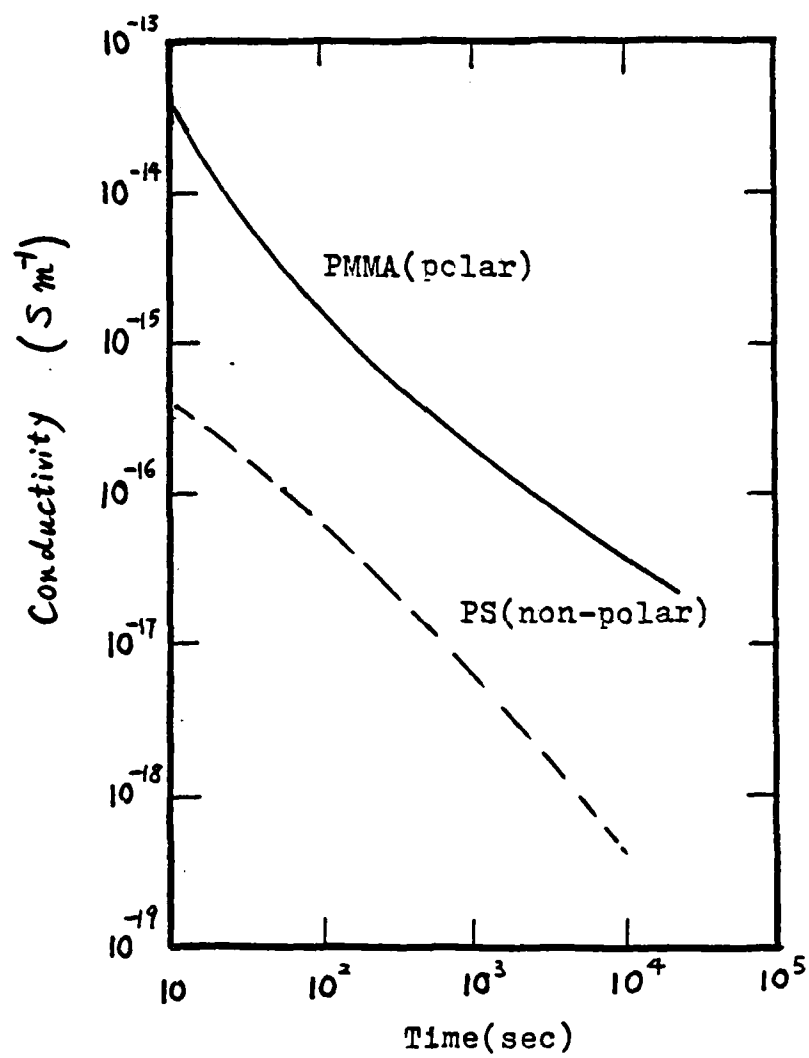


Fig. 10. Time dependence of effective conductivity for PMMA and PS.

$$\sigma(t) = \sigma_0 t^{-n} \quad (12)$$

from which it follows that  $\sigma_0$  is numerically equal to the conductivity one second after voltage application.

Although leakage current is relatively constant with time, absorption current may diminish slowly to zero for minutes or even hours (23). For example, it has been found that even after six hours (Fig. 11) of current measurement in a PPBT 28555-19-2 fiber at room temperature, the steady state is not achieved. The steady-state current usually is ascribed to the conductivity of the dielectric. G. Stetter (26) has observed that the curve of  $\log I$  vs.  $\log t$  for polyethylene showed that the asymptotic current is only a convenient fiction. There are several models to explain these transient phenomena.

(i) Free-volume model (27, 30):

An amorphous or molten polymer is a conglomeration of poorly packed interlacing chains and the extra empty space caused by this random molecular arrangement is called the "free volume" which essentially consists of all the holes in the matrix. When sufficient thermal energy is present in the system, the vibrations can cause a segment to jump into a hole by cooperative bond rotation, e.g. Crankshaft motion, Fig. 12, and a series of serpentine jumps will enable the complete polymer chain eventually to



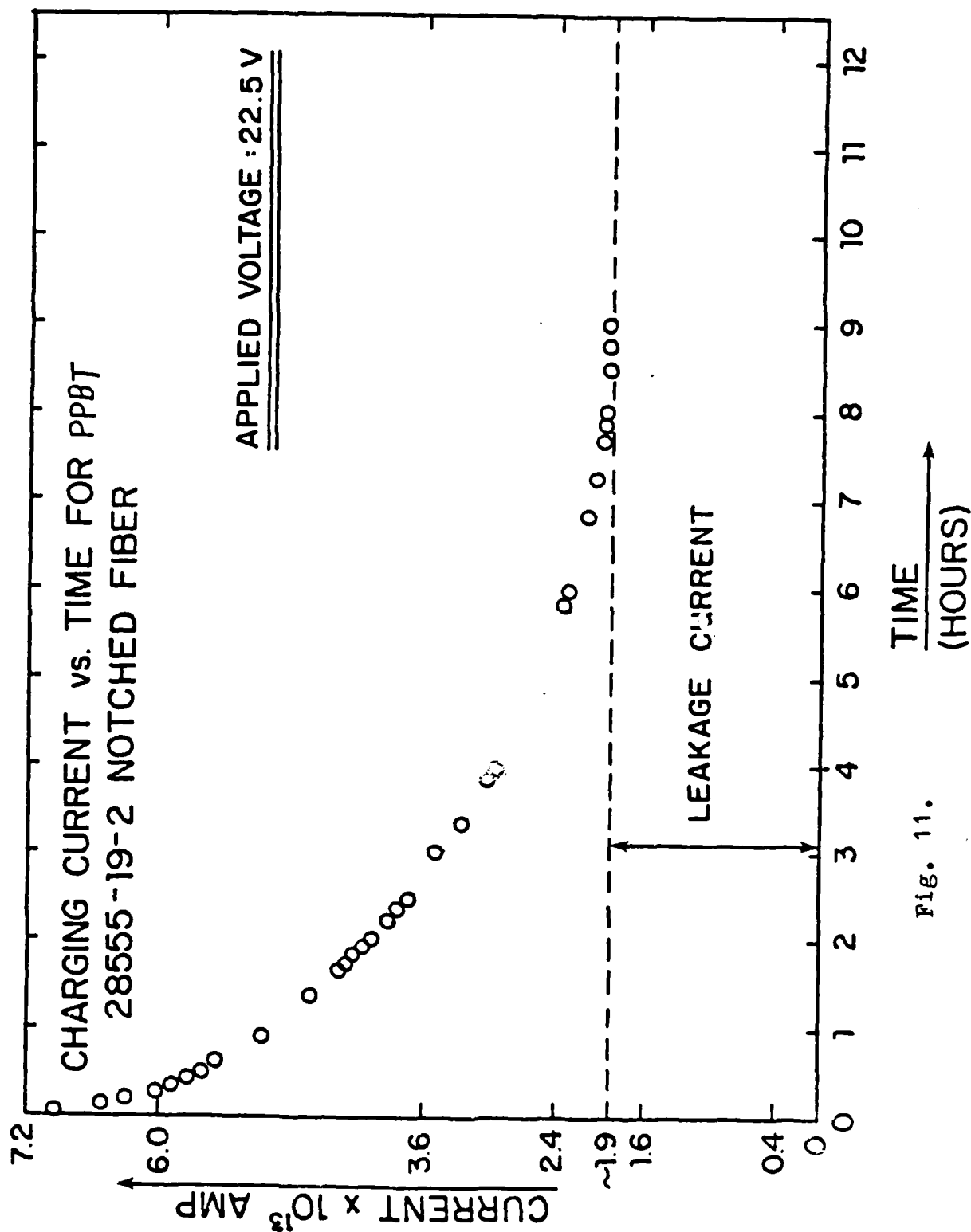


Fig. 11.

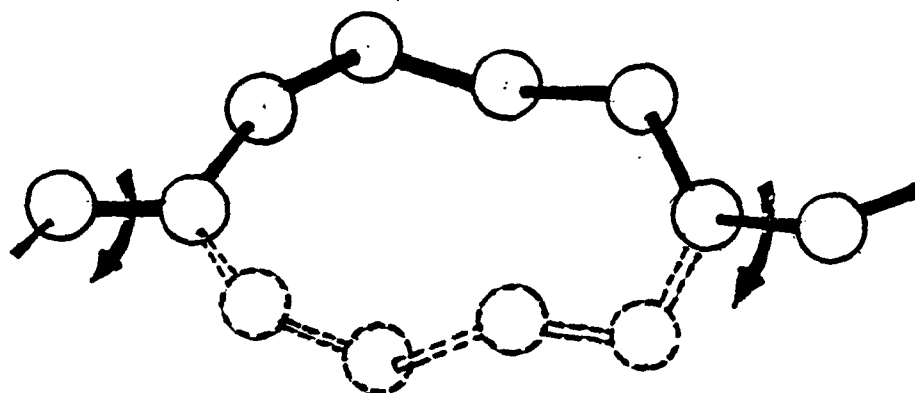


Fig. 12. Crankshaft motion in a polymer chain.

change its position. Heating will cause a polymer sample to expand, thereby creating more room on the average for movement of each kinetic unit, and the application of a stress in a particular direction will encourage flow by reducing the activation barrier for segmental motion in the direction of the stress. The segmental transposition involving six carbon atoms is called crankshaft motion and is believed to require an activation energy of about 25 KJ/mol (31). Although the current view of segmental motion has been modified somewhat, the overall effect is similar. Currently, on the basis of computer simulation and fluorescence spectroscopy (32), it is believed that, instead of a crankshaft motion, a given bond rotates with the distortion of neighboring bonds and that the distortion relaxes quickly by an opposite rotation two bonds away. Since viscosity and the electrical resistivity associated with ion movements depend upon temperature in a similar way (i.e. Arrhenius behavior), La Mantia extended this temperature-dependence analogy to the transient behavior through an analysis of a free-volume model.

The dependence of viscosity upon temperature in terms of free volume has often been written as (33):

$$\eta = \eta_0 \exp \left( \frac{1}{f} - \frac{1}{f_0} \right) \quad (13).$$

where the free volume fraction,  $f$ , is considered to vary linearly with temperature at temperature near  $T_g$  (the glass transition temperature) or near  $T_0$  (the reference temperature):

$$f = f_0 + \Delta\alpha(T - T_0), \quad (14)$$

where  $\Delta\alpha$  is the difference in the thermal expansion coefficient at temperature above and below  $T_0$ . In equation (13),  $\eta_0$  is the viscosity corresponding to the free volume fraction  $f_0$ . An equation similar to equation (13) was proposed for electrical resistivity ( $\rho$ ):

$$\rho = \rho_0 \exp \left( \frac{1}{f} - \frac{1}{f_0} \right). \quad (15)$$

Similar relationships have been found in PMMA, PS, and an unsaturated polyester by T. Miyamoto and K. Shibayama, Fig. 13 (34).

According to modified Walden's rule, (35) the ratio  $\eta/\rho^m$  is independent of temperature, or equivalently, the activation energy for the two processes is the same. In the field of polymers rheology, the application of a tensile stress to a polymeric corresponds to a temperature increase (36). In particular, the assumption has been made that the free volume changes, not only because of changes in temperature, but also as a consequence of the applied

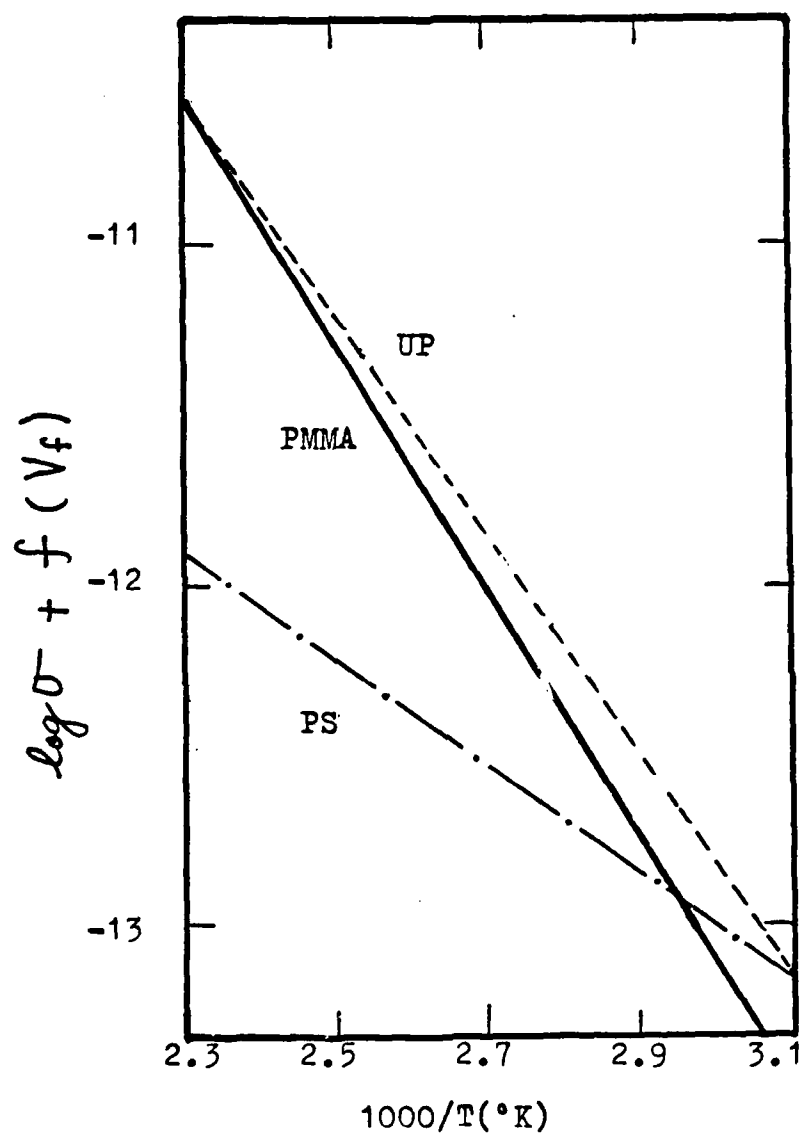


Fig. 13.  $\log \sigma + f(V_f)$  vs.  $1000/T$  for PS, PMMA, and unsaturated polyester(UP), where  $f(V_f)$  is a function of free volume  $V_f$ .

stress through the stored elastic energy. It is proposed that a similar approach can be used to explain the dependence of current upon the application of voltage. La Mantia used the following model shown in Fig. 14 where a capacitor C and a second resistor R' are added in parallel to the steady state resistor R. Such a model accounts for the current decay which is typical of "real" dielectrics even in the linear range (37).

The equation used to describe the circuit in Fig. 14 is:

$$I = \frac{V}{R} + \frac{V}{R'} \exp \left( -\frac{t}{R'C} \right) \quad (16)$$

where V is voltage and t is time (30). By defining the relaxation time,  $\tau$ , as  $\tau = R'C$ , equation (16) may be rewritten as:

$$j = \frac{\epsilon}{\rho} + \frac{\epsilon}{\rho'} \exp \left( -\frac{t}{\tau} \right) \quad (17)$$

where j is current density and  $\epsilon$  is electric field.

Theoretical predictions based on Equation (17) were in good agreement with experimental data, Fig. 15 (27).

(ii) Random-walk model (28):

This model was first proposed for transient photoconducting current, but it is also applicable to insulating materials. The central idea of this model is to

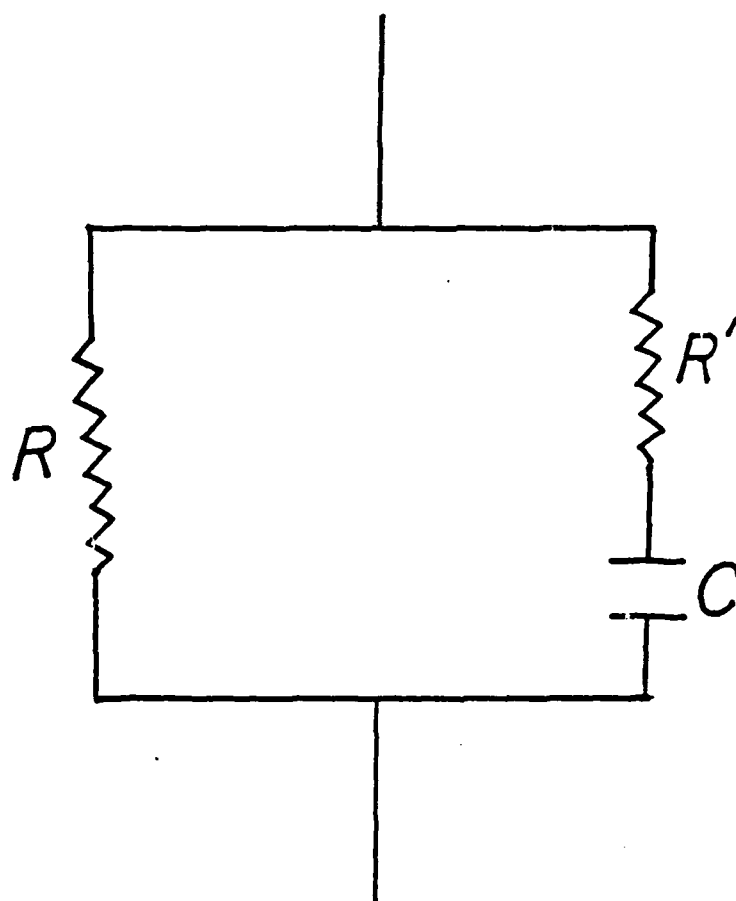


Fig. 14. Circuit used for modeling materials.

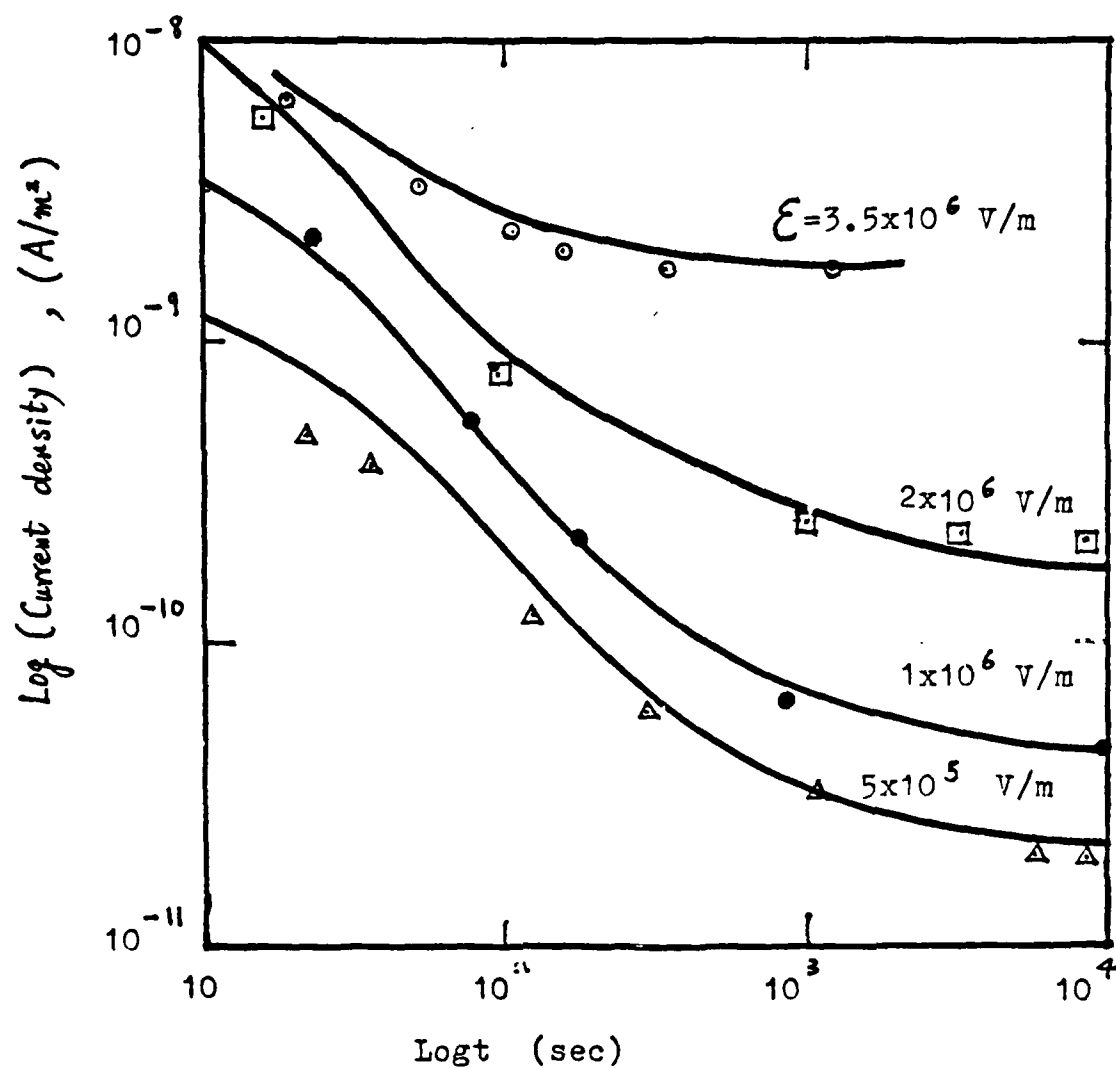


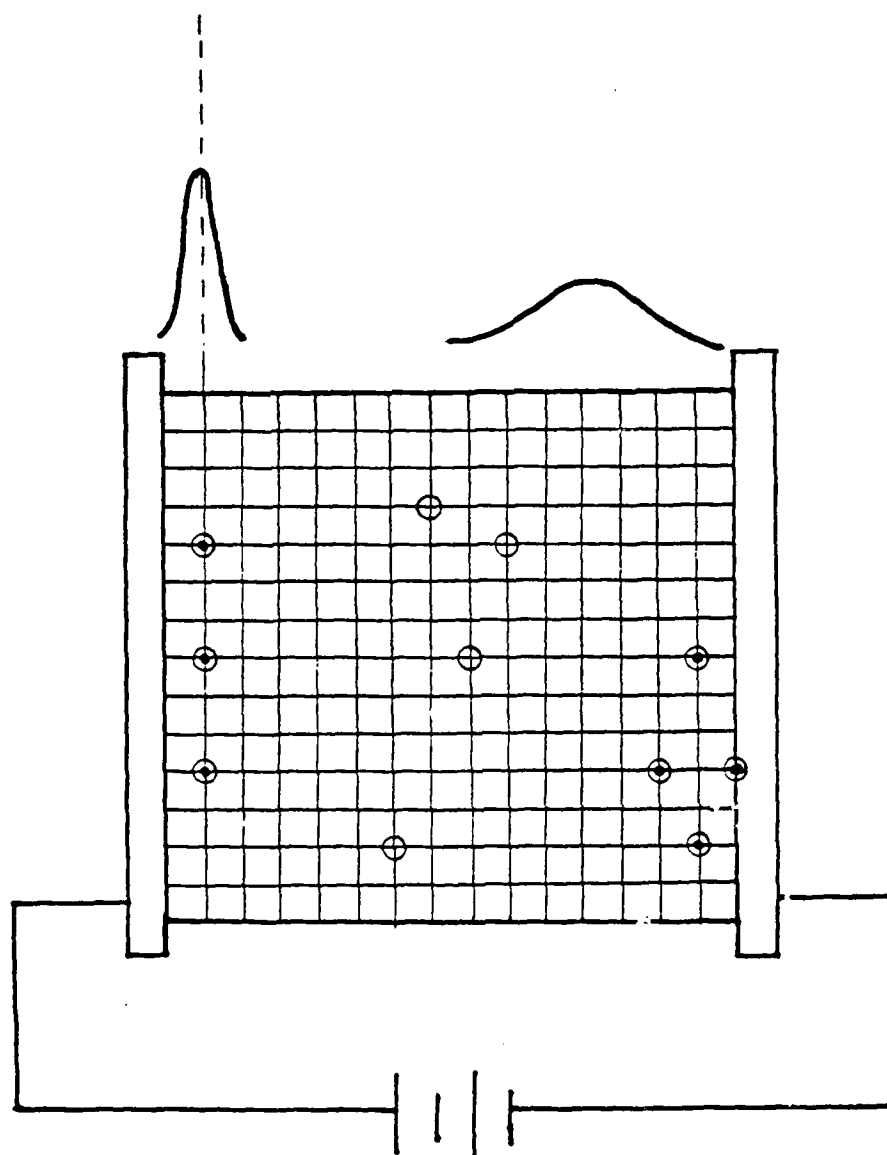
Fig. 15. Current density versus time for different values of the imposed electric field. Points are experimental data, curves are theoretical predictions.



consider an amorphous insulating material to be a network of localized sites for electrons and holes, Fig. 16 (28). The tool used in this model is a hopping-time distribution function  $\Psi(t)$  (Appendix II). In an amorphous material there is a dispersion in the separation distances between nearest-neighbor localized sites available for hopping carriers and a dispersion in the potential barriers between these sites. Both of these variables strongly affect the hopping time, the time between a carrier arrival on successive sites. Hence, the distribution of these hopping times,  $\Psi(t)$ , would have a long tail. Scher and Montroll proposed tails of the form

$$\Psi(t) \approx \text{constant} \times t^{-(1+\alpha)}, \quad 0 < \alpha < 1. \quad (18)$$

indicating an extremely large hopping-time dispersion. The contrast between Eq. (18) and Classical Gaussian propagation,  $\Psi(t) \approx e^{-\lambda t}$ , which is characteristic of a system with a single transition rate  $\lambda$ , is that when the inverse-power tail of Eq. (18) applies, a considerable fraction of the carriers remain at the point of their formation for a long time. Those carriers whose local environment, at their initial point, permits their immediate motion (fast hops) will sooner or later find themselves immobilized at some site (long hops), thus reducing their contribution to the current, until they



BIASED OR ASYMMETRIC RANDOM WALK

Fig. 16. Schematic diagram for the random-walk model of transient photoconductivity. The carriers (•) are injected as a narrow distribution at  $t=0$  in the localized sites (o).

escape.

In an infinite sample, the decrease in velocity of the mean carrier in the Scher-Montroll propagation packets implies a continuous reduction of the current. The current variation derivable from Eq. (18) is:

$$\begin{aligned} I(t) &\approx \text{constant} \times t^{-(1-\alpha)}, & t < t_T, \\ I(t) &\approx \text{constant} \times t^{-(1+\alpha)}, & t \gg t_T, \end{aligned} \quad (19)$$

with  $0 < \alpha < 1$  where  $t_T$  is the transit time. The model predicts that plots of  $\log I$  as a function of  $\log t$ , will exhibit a sum of slopes at times  $t/t_T < 1$  and at times  $t/t_T \gg 1$  given by  $-[(1+\alpha) + (1-\alpha)] = -2$ . In Fig. 17, the data obtained for a number of inorganic  $\text{As}_2\text{Se}_3$  films indicate that such a relationship is maintained with  $\alpha = 0.45$ , while Fig. 18 shows that for organic amorphous TNF - PVK (Trinitrofluorenone and polyvinylcarbazole),  $\alpha = 0.80$  (28).

As mentioned before, a  $\log I$  vs.  $\log t$  plot will more accurately describe the so-called experimental asymptotic conduction current than a linear plot of  $I$  vs.  $t$ . The nature of the carrier transport is also easier to interpret on these plots. As an illustration, Fig. 19 (28) demonstrates how misleading would be an  $I$ - $t$  plot when used to determine an asymptotic current (or steady-state current).

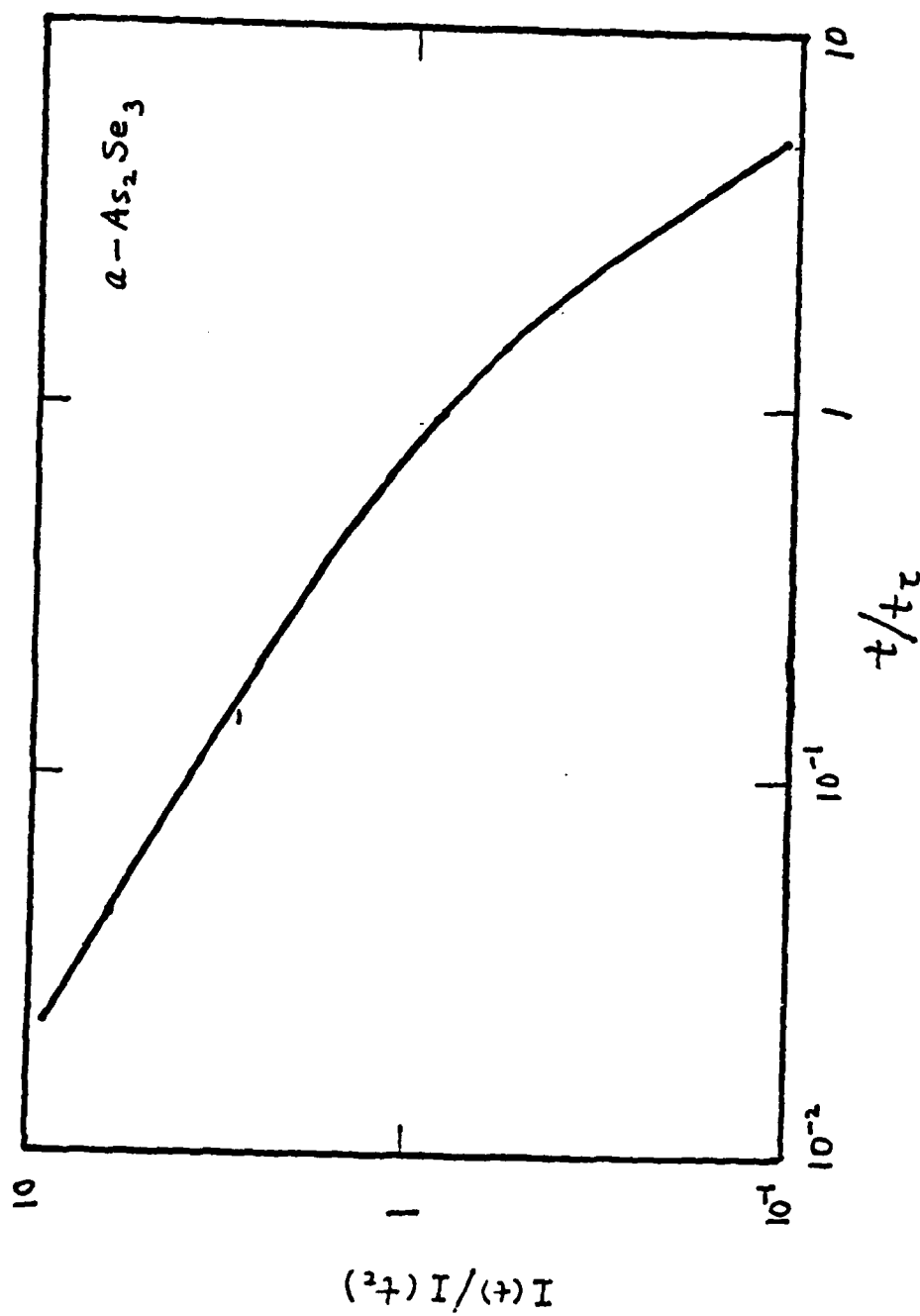


Fig. 17. A logI-logt plot for  $\alpha\text{-As}_2\text{Se}_3$ .

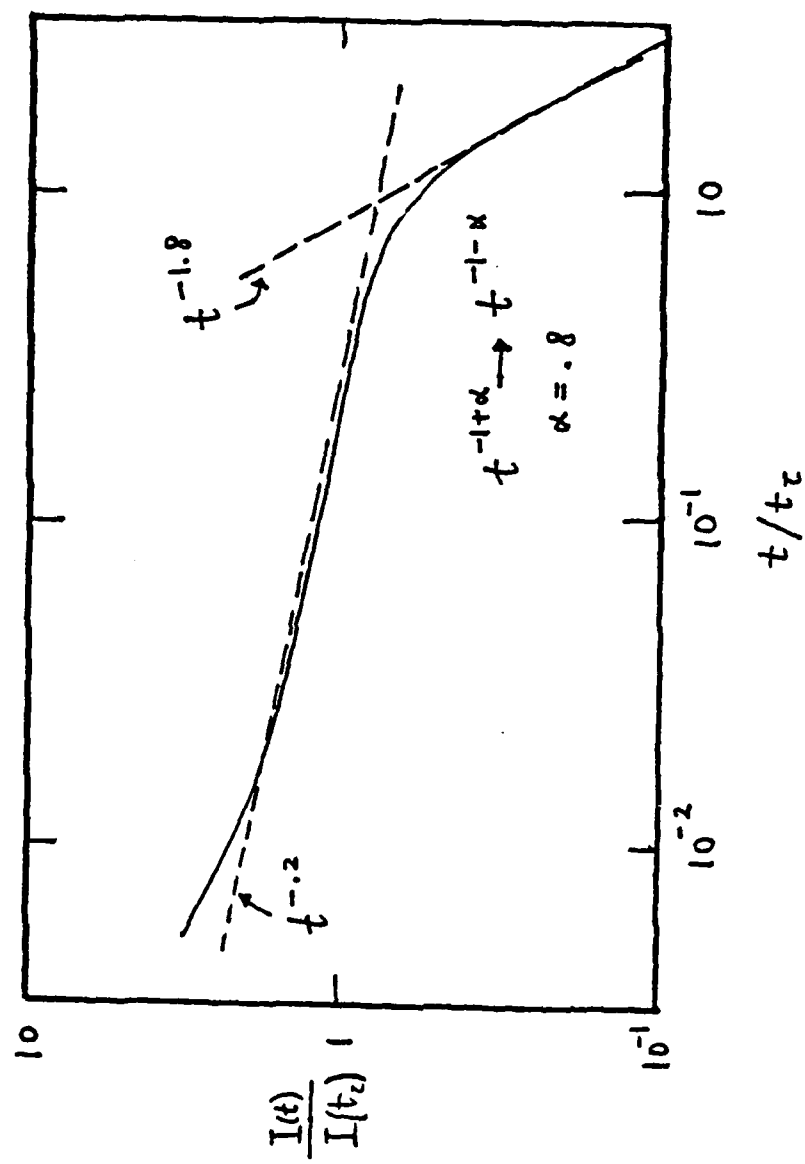


Fig. 18. A logI-logt for 1:1 TNF-PVK measured by Gill and taken from reference (28).

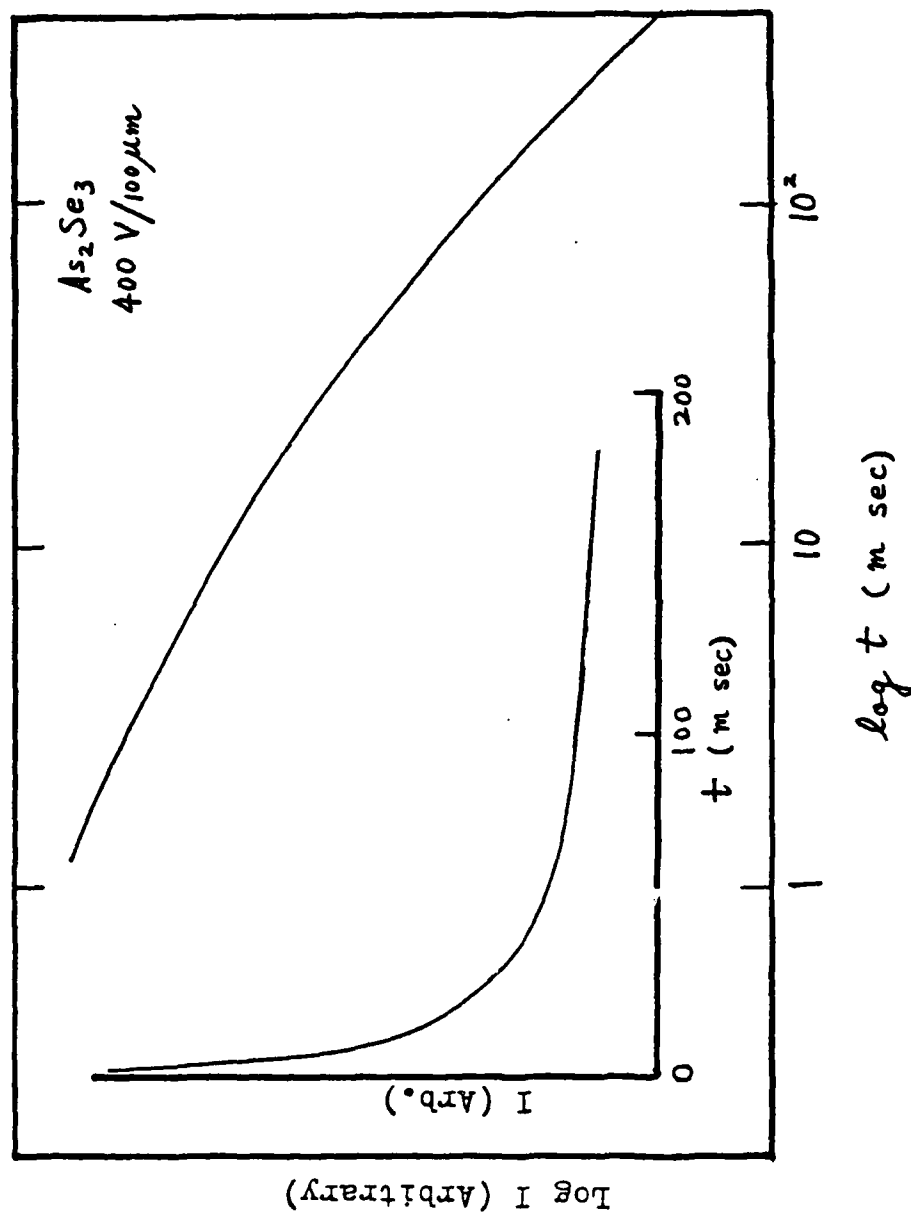


Fig. 19. Trace of an electronically produced logI-logt plot for  $\text{As}_2\text{Se}_3$  measured by Pfister(28).

## (iii) Maxwell-Wagner model (29):

The Maxwell-Wagner model for two-layer dielectrics may be used to describe the dynamics of the process in the simple case of totally blocking electrodes; a uniform layer adjacent to each electrode has a zero conductivity, permittivity  $\epsilon$  and combined thickness  $b_e$  which is usually much smaller than the overall thickness of the dielectric  $b$  with the bulk properties  $\epsilon$  and  $\sigma$ , Fig. 20. The effective conductivity calculated from the measured current should be given by:

$$\sigma_{\text{eff}} = \sigma \exp \left( -\frac{\sigma}{\epsilon \epsilon_0} \frac{b \epsilon}{b_e} t \right) \quad (29). \quad (20)$$

This means that the initial value of the effective conductivity is equal to the bulk conductivity of the dielectric, and then it drops exponentially with a time constant  $\tau = (\epsilon \epsilon_0 / \sigma) (b / b_e)$ . After a long time when the current flow has virtually ceased, the whole of the applied voltage appears across the blocking layers, leading to an apparent or effective permittivity given by  $\epsilon_{\text{eff}} = \epsilon (b / b_e)$ . Since  $b \gg b_e$  the apparent permittivity is much greater than the real permittivity of the bulk material. When an experiment seems to yield an extremely large permittivity, this may really be strong evidence for electrode polarization. The time dependence of effective conductivity in a cured and post-cured epoxy resin due to such type of polarization has

$$b_e \equiv b_o - b$$

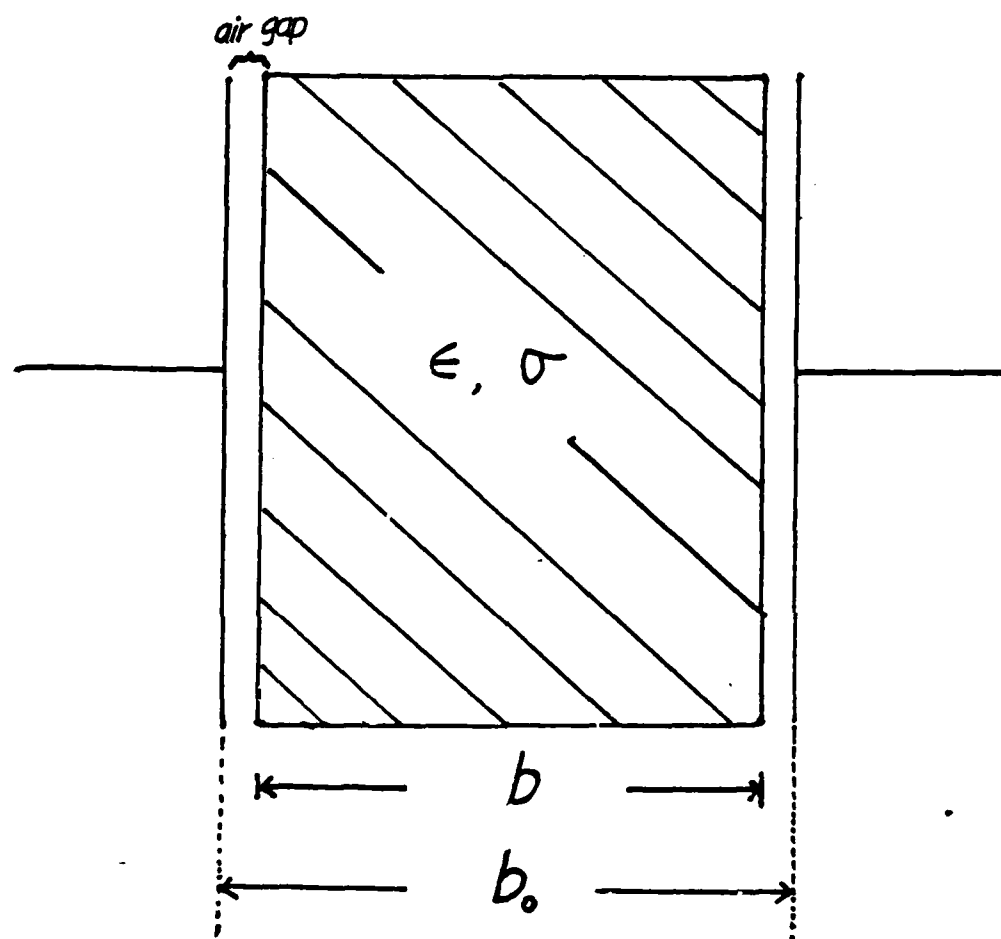


Fig. 20. Contactless electrodes, the air gaps can be thought as zero conductivity layers.



been observed by Adamec (1972), (Fig. 21) (29). The appearance of steady-state currents in the figure indicates that electrodes are only partially blocking, otherwise the currents will drop to zero when the electrodes are fully blocking.

In the case of polyethylene, G. Stetter (26) has observed that a second decrease of transient current occurred in the presence of a high electric field or high temperature. The second decrease of the transient current is caused by the build-up of space charge and thus a decrease of the effective field strength throughout the sample.

### C. Charge Transfer Complexes

It must be pointed out that one of the primary thrusts in the area of organic semiconductors is to create fused-ring, planar-network semiconductors from polymers. Usually, ring-containing linear polymers are heated to create the networks. An example of the mechanism proposed for one such reaction is shown in Fig. 22 (38). Clearly, such materials will, in general, conduct better than linear chain polymers due to the lack of need for interchain transfers.

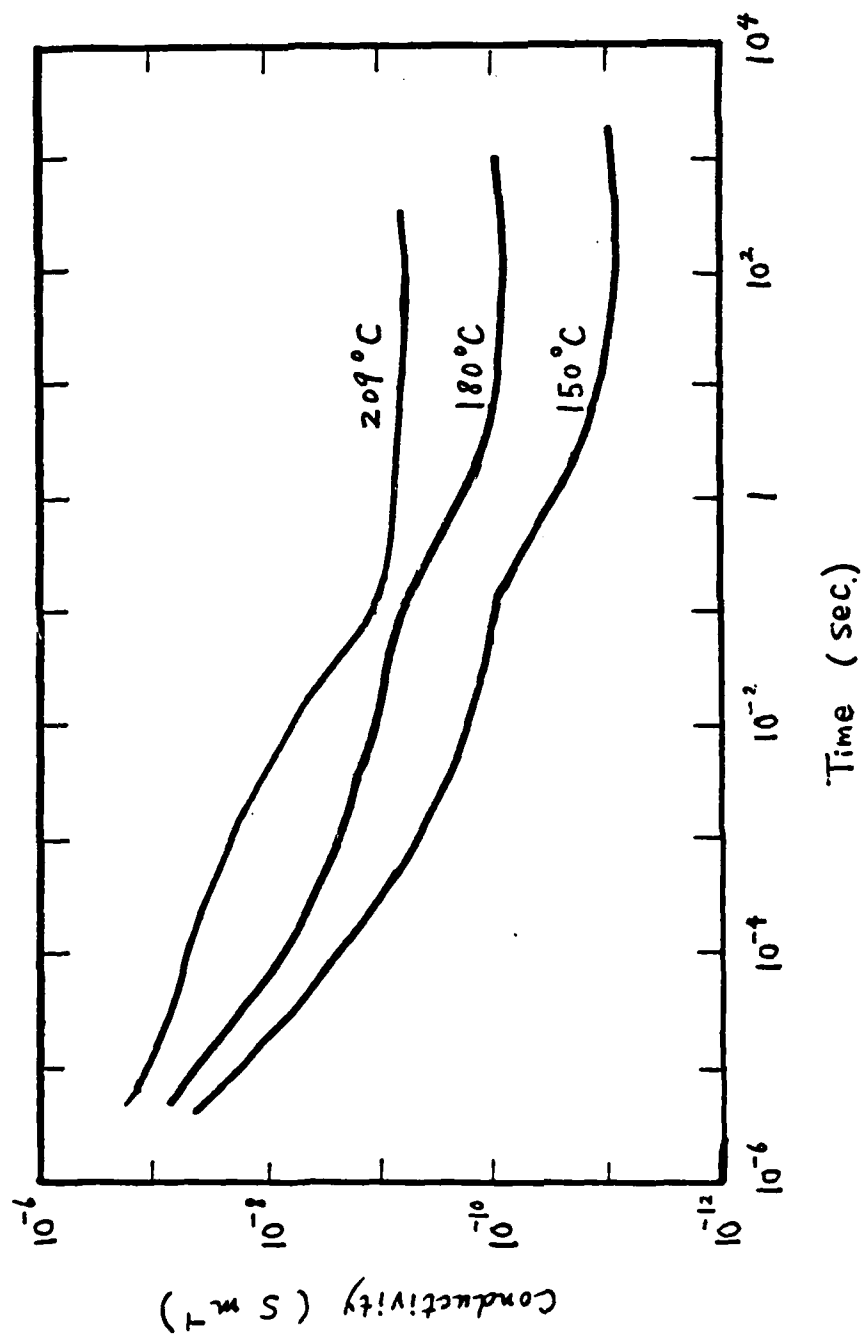


Fig. 21. Conductivity vs. time for an epoxynovolac resin at different temperatures.

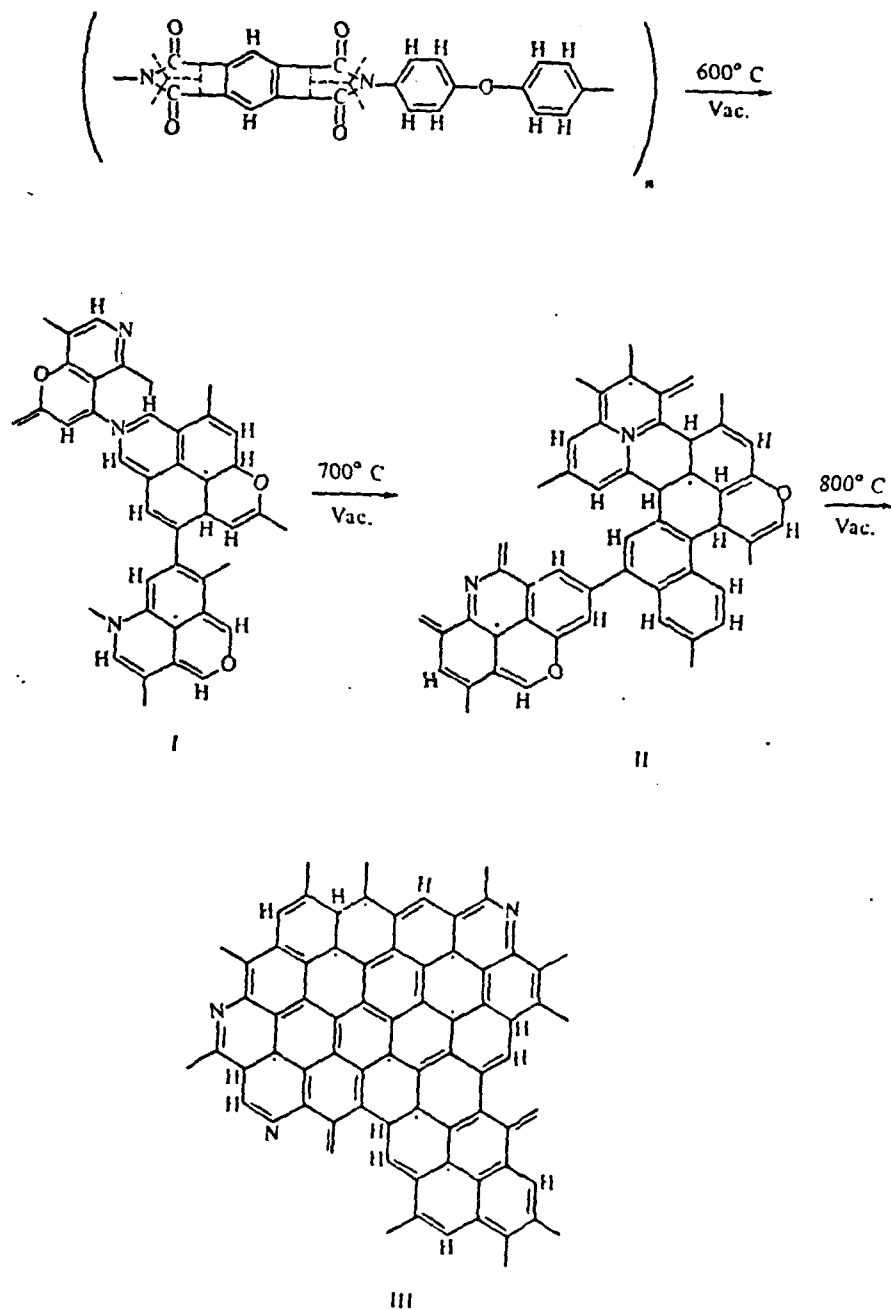


Fig. 22. Steps in pyrolysis of a polymer.

Other means of enhancing the conductivity of polymeric systems are by forming charge-transfer complexes, using transfer agents, such as metal atoms and halogens, and by incorporating these agents into the linear molecule.

"Charge-transfer complex" is the name which is given to the molecular compound formed between an electron-donating molecule D and an electron-accepting molecule A as a result of the partial or complete transfer of an electron from D to A. The new compound may be represented as  $[D^{\delta+} A^{\delta-}]$ , where the value of  $\delta$  is indicative of the strength of the interaction. The charge-transfer interaction is stronger than Van der Waal's interactions but is weaker than normal ionic or covalent bonding unless the electron transfer is complete (22). The electron transfer invariably results in the appearance of new, broad, structureless absorption bands in the visible or ultraviolet spectrum and is often accompanied by perturbation of the absorption bands of the parent molecule (39). Solutions of electron donors (D) and acceptors (A) exhibit absorptions not associated with either individual molecule. Mulliken (22) proposed that the absorptions involve an electron transfer from D to A, as expressed by:



Here  $h\nu_{CT}$  is the charge-transfer (CT) excitation energy, and the CT band is explicitly associated with the molecular complex formed between a D and an A molecule. Frequently, properties such as the electrical conductivity and absorption coefficient are noticeably anisotropic (22). In addition to the formation of ground-state charge transfer complexes, it is also possible to form excited-state charge-transfer complexes.

Mulliken's treatment also provides another relatively simple classification on the basis of the orbitals involved in charge-transfer complexes formation. The orbitals which can be involved are:

- (1) The  $\pi$  orbitals of either A and D both must be aromatic systems;
- (2) The  $\pi$  orbitals of either A or D and the orbitals of either molecule; one must be aromatic and the other must contain one or more heteroatoms.
- (3)  $\sigma$  orbitals of both A and D.

Examples of these molecules are given in Table 4 (22). It should be noted that some molecules have both  $\sigma$  and  $\pi$  orbitals in which case either or both may be involved in complex formation. The type of interaction and the

TABLE 4: ELECTRICAL PROPERTIES OF DONOR/ACCEPTOR COMPLEXES\*

	Donor (D)	Acceptor (A)	$I_g$ (eV) <sup>†</sup>	$E_a$ (eV) <sup>†</sup>	$\sigma$ (25 C) <sup>‡</sup>
Weak complexes	Anthracene	Trinitrobenzene	7.40	0.700	$1.7 \times 10^{-18}$
	Pyrene	Trinitrobenzene	7.55	0.700	$1 \times 10^{-20}$
Intermediate complexes	Anthracene	TCNE <sup>§</sup>	7.40	1.800	$9 \times 10^{-11}$
	Pyrene	TCNE	7.55	1.800	$2 \times 10^{-16}$
	Pyrene	Chloranil	7.55	1.370	$10^{-11}$
	N,N-dimethyl aniline	Chloranil	7.14	1.357	$10^{-10}$
	p-Phenylene diamine	Chloranil	7.20	1.357	$10^{-7}$
Strong complexes	Pyrene	Iodine	7.55	1.700	$1.25 \times 10^{-2}$
	Perylene	Iodine	7.22	1.700	$10^{-1}$

\* Extremely lengthy tables of electrical properties of monomeric charge transfer complexes included in Gutmann and Lyons (1967) and Katon (1968).

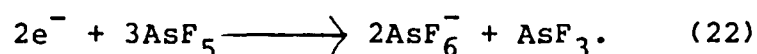
† Briegleb (1964) and references therein.

‡ Gutmann and Lyons references therein.

§ TCNE = tetracyanoethylene.

stereochemistry of the complex each affect the electrical properties.

According to the criteria, iodine ( $I_2$ ) and arsenic pentafluoride ( $AsF_5$ ) are often used as charge-transfer agents. R.H. Baughman (40) at Allied Chemical and G.B. Street (40,41) et al. at IBM (San Jose, California) reported their work on  $AsF_5$  doped poly - (p-phenylene sulfide), PPS. The undoped PPS is presumed to be nonplanar as represented in Fig. 23. After being doped with  $AsF_5$ , the formation of charge-transfer complexes caused phenylene groups in PPS to rotate. This phenylene rotation is said to enhance the degree of coplanarity which in turn increases the overlapping of  $\pi$  orbitals so that electrons can become delocalized. The following mechanism was proposed by the IBM group (41):



A similar mechanism has been proposed for  $AsF_5$ -doping of  $\{CH\}_x$ , but the group at the University of Pennsylvania disagreed. The Pennsylvania group proposed an interesting alternative picture of charge-transfer at low doping levels, involving polymer excitations called "solitons". These solitons are kinks moving along the polymer chain, separating two domains, to the left and right of the kink,

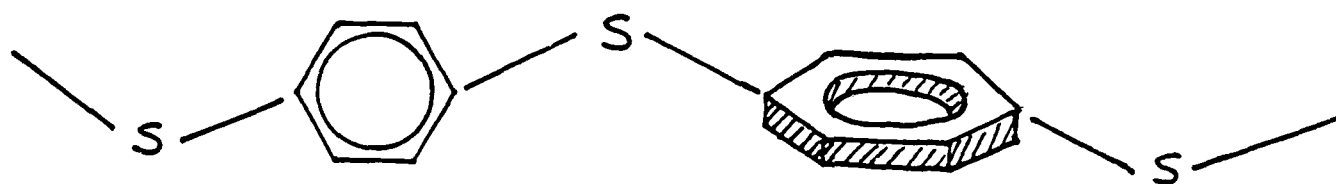


Fig. 23. In poly-(p-phenylene sulfide), adjacent phenylene groups are normal to each other.



whose single-double bond alternation patterns are out of phase with one another (see Fig. 24). Su, Schrieffer, and Heeger have calculated that at low doping levels it is energetically more economical for the carrier to bind to a soliton kink than to enter the conduction (or valence) band. They believe that charged solitons may be the primary conduction mechanism in lightly doped organic polymers. Their belief in this picture is strengthened by the observation of an enhanced infrared absorption peak in  $\{CH\}_x$  corresponding to a 0.1 eV transition, a value consistent with the soliton calculation. But Bredas, Chance, and Silbey (43) have suggested that the final decision is not yet settled and that polaron calculations also give numerical values in reasonable agreement with the absorption data. Experiments involving  $I_2$  doping have been reported by many scientists (40, 41). Benzene ring-containing polymers have been chosen as experimental samples mainly because of the spectroscopic fact which reveals that  $I_2$  will incorporate with benzene ring to form a charge-transfer complex. In this formation, an electron from  $\odot$  will transfer to the empty d-orbital of  $I_2$  molecule. In the presence of an external electric field or light, these transferring electrons are thought to be more readily available for conduction somewhat like an n-type semiconductor or photoconductor.

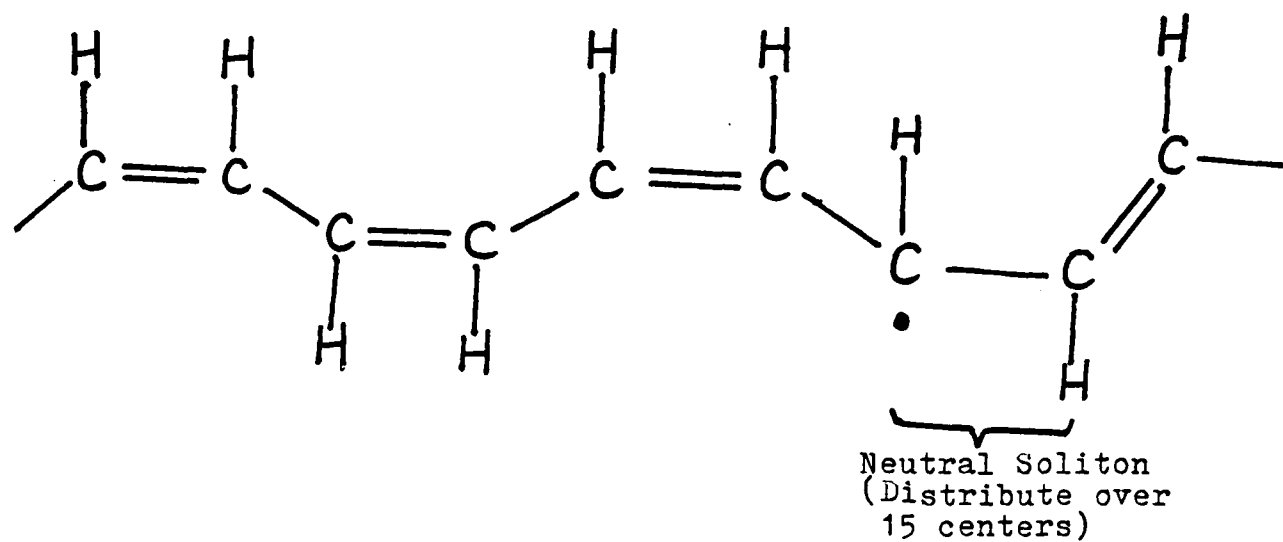


Fig. 24. Schematic diagram for a neutral soliton in polyacetylene.

Most charge-transfer complexes polymers are electronically conducting. A striking exception has been found by the research group at the GTE Laboratory (Waltham, Mass.) (44). They observed that the d.c. conductivity of iodinated polyphenylacetylene (PPA) is predominantly ionic.

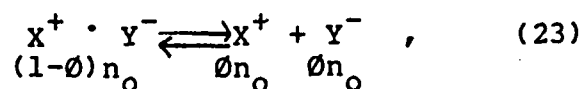
D. Ionic Dissociation and the "Weak Electrolyte Model"  
(7-10):

The fact is well known that the presence of moisture can increase the observed level of conductivity by as much as 6 decades in some cases. Barker and Sharbaugh (9,10) have explored the nature of the relationship between conductivity and dielectric constant for a long list of organic liquids for which measurements of both parameters on the same sample were available. Statistically there was a definite trend and by making suitable adaptations of the theory for weak electrolytes an equation was obtained to describe it.

Generally, ionic conduction in a polymer occurs when ionizable groups present as part of the macromolecule, or as impurities, dissociate and thus provide a dynamic equilibrium of mobile ions. The essential ideas of the work by Sharbaugh and Barker (10) are that water modifies the conductivity by (1) partial dissociation to mobile ions, and (2) by increasing the effective dielectric constant of the system, thus enhancing dissociation of

ionically bound groups present within the polymer. Based on these ideas and the Nernst-Thompson rule\*, the "Weak electrolyte model" was proposed.

Considering the equilibrium dissociation of  $n_0$  salt molecules per unit volume into  $\phi n_0$  ion-pairs per unit volume it follows that:



where the symbols underneath represent concentrations of the corresponding reactants and products. The dissociation constant  $K$  is given by<sup>§</sup>:

$$K = [x^+][y^-]/[x^+ \cdot y^-] = \gamma^2 \phi^2 n_0 / (1-\phi), \quad (24)$$

where  $[ ]$  denotes activity,  $\gamma^2$  is the product  $\gamma_+ \gamma_-$  of activity coefficients, and  $\phi$  is the fractional dissociation.  $K$  also is given by:

$$K = K_1 e^{-\Delta G/kT} \approx K_0 e^{-U'/kT}, \quad (25)$$

\* The Nernst-Thompson rule: A solvent of high dielectric constant  $K$  favors dissociation by reducing electrostatic attraction between ion pairs, and conversely for low  $K$  solvents.

§ Since  $n_0$  has dimensions molecules/vol. rather than moles/liter,  $K$  in Eqs. (24) and (25) does not have the usual chemical units, e.g. for acetic acid at 25°C,  $K_{\text{chem.}} = 1.8 \times 10^{-5} \left( \frac{\text{mol}}{\text{L}} \right)$  but  $K = 1.08 \times 10^{-2} \left( \frac{\text{molecules}}{\text{m}^3} \right)$ .

where  $\Delta G$  is the Gibbs' potential which is assumed to consist of an energy term  $U'$  associate with the work to separate ion pairs in dielectric medium plus terms involving the entropy and constant energies. Also assume that:

$$U' = U'_0/K' \quad (26).$$

In principle, we could combine Eq. (24), (25), and (26) to obtain  $\phi = \phi(U'_0, K')$ . A nontrivial assumption that  $K' = K'_{\text{local}} = K'_{\text{microscopic}} < 15$  will greatly simplify the analysis, for then  $\phi$  in the denominator of Eq. (24). can be neglected so that:

$$\gamma \phi \approx (K/n_0)^{1/2}. \quad (27)$$

In terms of ion concentrations  $n_i$  and mobilities  $\mu_i$ , the conductivity is:

$$\sigma = \sum_i n_i \mu_i e = \phi_i n_i^0 \mu_i e, \quad (28)$$

or, if only one kind of ion pair is involved,

$$\sigma \approx \phi n_0 e (\mu_+ + \mu_-). \quad (29)$$

Using Eqs. (29) and (27)

$$\begin{aligned}\sigma &\approx \gamma^{-1} (K n_o)^{\frac{1}{2}} (\mu_+ + \mu_-) e \\ &\approx \gamma^{-1} (K_o n_o)^{\frac{1}{2}} \exp(-U_o'/2K'kT) (\mu_+ + \mu_-) e. \quad (30)\end{aligned}$$

$$\begin{aligned}\log \sigma &= \log[\gamma^{-1} K_o^{\frac{1}{2}}] + \frac{1}{2} \log n_o \\ &\quad + \log [(\mu_+ + \mu_-) e] - [U_o'/4.605 kT] (1/K'). \quad (31)\end{aligned}$$

Several interesting features of the model emerge: (1)  $\sigma$  is not proportional to  $n_o$ , rather  $\sigma \propto n_o^{\frac{1}{2}}$ , (2)  $\log \sigma$  is a linear function of  $1/K'T$  and the slope is proportional to  $U_o'$ .

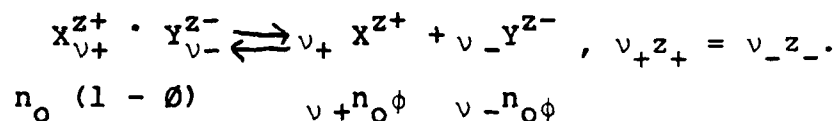
Even if a polymer contained no ionic species, conduction would be possible if moisture were sorbed since the water itself could dissociate:  $H_2O \rightleftharpoons H^+ + OH^-$ . If  $n_w = [H_2O]$ ,  $n_1 = [H^+]$ , and  $n_2 = [OH^-]$ , and the dissociation constant is  $K_w = n_1^2 / n_w$ , then by repetition of the steps leading to Eq. (30),

$$\sigma = 2(K_w n_w)^{\frac{1}{2}} \bar{\mu} e = 2\bar{\mu} e (n_w K_w^o)^{\frac{1}{2}} \exp(-U_w/2K'RT) \quad (32)$$

where  $\bar{\mu} = (\mu_1 + \mu_2)/2$  and  $(U_w/K')$  is the energy barrier for dissociation. In the initial stages of sorption by diffusion,  $n_w \propto t^{\frac{1}{2}}$ , consequently, a test of Eq. (32) would be to find  $\sigma \propto t^{\frac{1}{4}}$  during early stages of sorption. This of course neglects complications due to spatial distribution of the water, and the fact that equilibrium has not been

reached.

Most of the possible ionic contaminants (in the parts per million range) of polymers would be expected to be 1:1 type electrolyte. There are, however, a number of common multivalent ions which might occur, e.g.,  $Mg^{+2}$ ,  $Ca^{+2}$ ,  $Ba^{+2}$ ,  $Cu^{+2}$ ,  $SO_4^{-2}$ , and  $CO_3^{-2}$ . Thus, it is of interest to consider a more general form of the mass action relation than that corresponding to symmetrical salts, e.g.



As shown previously, if  $v_+ = v_- = 1$  and  $z_+ + z_- = 1$ , we obtain the equilibrium coefficient  $K_{1:1} = \gamma^2 \psi^2 n_o / (1 - \phi)$ , Eq. (24). In the approximation  $\psi \ll 1$ , the result is:

$$\sigma_{1:1} \approx \gamma^{-1} (K_{1:1}^o n_o) \exp(-U'_o / 2K'kT) (\mu_+ + \mu_-) e \quad (33)$$

where  $U'_o$  is the effective energy to separate ions in a vacuum,  $\mu_+$ , and  $\mu_-$  are ionic mobilities ( $cm^2/V\text{-sec}$ ), and  $K_{1:1}^o$  is the equilibrium constant of the reference state, i.e.,  $K_{1:1} = K_{1:1}^o e^{-\Delta G/RT}$ . From the more general mass action law of Eq. (33) we obtain:

$$K_{z+:z-} = a \pi \phi^{(v_+ + v_-)} n_o^{(v_+ + v_- - 1)} \quad (34)$$

where  $a_{\pi} = \gamma^{v+} \cdot \gamma^{v-} / \gamma_0$  and the approximation  $\phi \ll 1$  is used. For a single type of ion pair, the conductivity is:

$$\sigma = e\phi n_0(v+\mu+z+ + v-\mu-z-), \quad |z_{\pm}| = z_{\pm} \quad (35)$$

or, on solving Eq. (34) for  $\Psi$  and dropping the  $z_+ : z_-$  subscript

$$\Psi = (K/a_{\pi})^{1/(v+ + v-)} n_0^{-(v+ + v- - 1)/(v+ + v-)} \quad (36)$$

so that

$$\ln \sigma \approx [\ln(n_0) + \ln(K^0 a_{\pi})] / (v+ + v-) + \ln[(v+\mu+z+ + v-\mu-z-)] / (v+ + v-) - \Delta G/kT. \quad (37)$$

Before an explicit expression for  $\sigma$  is obtained, we must specify the Gibbs function for the equilibrium association. It would not be unreasonable to again assume the approximation  $\Delta G \approx U'_0/K'$ , but to obtain more generality, a semiempirical relation which was obtained by Magnusson (45) should be used. Thus,

$$\Delta G = \frac{z_+ z_- e^2}{K' S} \left[ 1 + K' \exp\left(\frac{-2S}{z_+^{1/2} z_-^{1/2} a_0}\right) \right] + B_M \quad (38)$$

where  $a_0 = 0.529\text{\AA}$  (the Bohr radius),  $S$  = the sum of ionic radii,  $B_M$  can be considered to contain energy and entropy terms, and where a symmetrical dependence on the valence



numbers  $z_{\pm}$  is inferred.

In measurements of  $\sigma$  versus  $T$  the data were interpreted via the relation:

$$\sigma = \sigma_0 e^{-E^*/kT}. \quad (39)$$

Thus,

$$E^* = [(z_+ z_- e^2 / SK') + B_M] / (v_+ + v_-) \quad (40)$$

Similarly, in  $\sigma$  versus  $K'$  determinations (8), Eq. (33) was used to obtain  $U'_0$  by plotting  $\log \sigma$  vs  $1/K'$ . Hence,  $U'_0$  and  $B_M$  can be expressed as:

$$U'_0 = 2z_+ z_- e^2 K' / K'_{\text{eff}} (v_+ + v_-) S, \quad (41)$$

$$\text{and } B_M = [E^* - (U'_0 / 2K')] (v_+ + v_-) \quad (42)$$

where  $K'_{\text{eff}} = K' / [1 + K' \exp(-2S / |z_+ z_-|^{1/2} a_0)]$ .

#### E. The "Local Structure Hypothesis"

Figure 25 (6) is a schematic view of ions in a polymer. The local structure hypothesis can be "visualized" through this figure. In a polymer, a given ion not only is very much influenced by the various structural features of the

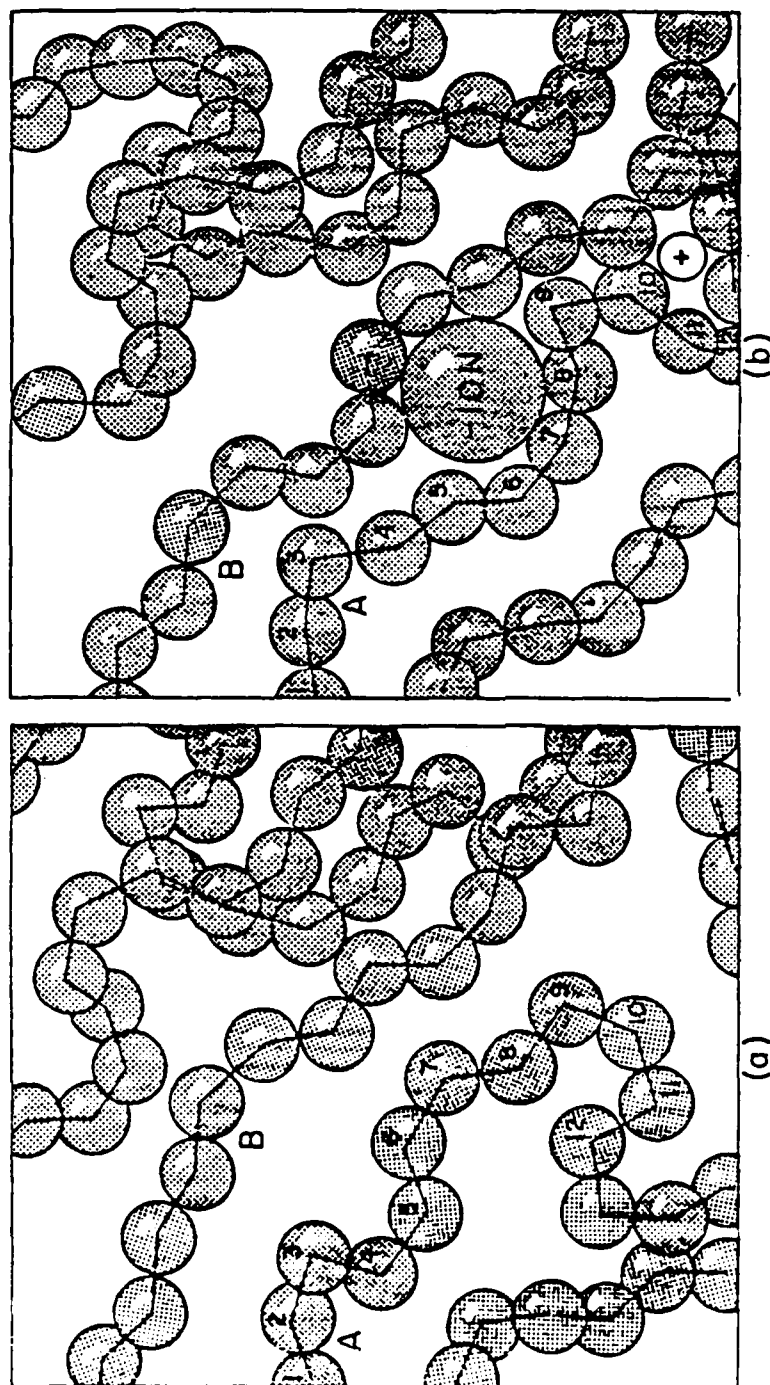


FIG 25. SCHEMATIC REPRESENTATION OF A NONCRYSTALLINE POLYMER (a) WITHOUT AND (b) WITH "INTERSTITIAL" IONS, FEWER AVAILABLE CONFIGURATIONS FOR CHAINS A & B IN (b).

polymer, it also modifies them in its own local neighborhood and therefore probes what may be a temporarily atypical part of the polymer. For example, Barker and Thomas (7) have presented evidence that, in the case of cellulose 2.5 acetate of bulk modulus  $B$ , the value of the glass transition temperatures determined by conductivity measurements depend upon the types of conducting ions. The shift in  $T_g'$  was found to be predictable from the well known statistical mechanical relation,

$$\langle (V - V_o)^2 \rangle_{\text{avg}} = kTV_o/B, \quad (43)$$

for the fluctuation of the volume  $V$  of a fixed number of particles about the mean  $V_o$ , and an additional stipulation that an effective ionic interaction volume,  $mW_1$ , should be subtracted from the instantaneous volume  $V$  of the group of molecular units participating in a unit diffusional process (i.e. the cooperative motion that must occur for the ion to move to a site outside of the group). The physical interpretation is that the ion reduces the local free volume and this raises the local  $T_g$ . For an ideal crystal, impurities will introduce disorder and thus cause a lowering of the melting point, but for a glassy polymer which already has a large amount of disorder, an ion can produce an increase in the local order and thus an increase in  $T_g'$ . It must be emphasized that for the cases

discussed, the ions occupy a small volume fraction of the total sample and thus they will not produce a significant change in  $T_g$  as measured dilatometrically or mechanically. The equation of Barker and Thomas (7) for the change in  $T_g'$  is a quadratic in ion volume  $W_i$ , i.e.

$$\Delta T_g' = -2am\delta \cdot w_i + am^2 W_i^2 \quad (44)$$

$\delta$  is a measure of free volume,  $a$  is determined by the bulk modulus of the polymer and the size of activated molecular cluster about the ion, and  $m$  is a measure of the ion's interaction size relative to its geometric size.

According to this local structure hypothesis, it will be expected to interact with the interfaces between crystalline and amorphous regions. Crystalline regions will have a slightly different dielectric constant  $K_c$  than that  $K_a$  of the amorphous regions. A simple model will now be developed to predict the interaction. A consequence of the model is that the interaction provides attractive trapping forces such that thermal detrapping might give current pulses at reasonably well defined temperatures.

Consider that a point close enough to an ion in a polymer, then inhomogeneities will be noticeable to a hypothetical observer on the ion. Perhaps the simplest case is to consider a planar inhomogeneity which is

analogous to close range interaction with a polymer crystallite and assume that the ion is in the non-crystalline part of the sample. Based on these assumptions and from electrostatic theory, a characteristic release temperature ( $T_r$ ) of ions from such interfacial "traps" can be derived as the following:

$$T_r \approx QQ'/16k\pi\epsilon_0 k_a r_i f, \quad (45)$$

where  $Q$  is the charge of the ion,  $Q'$  is the corresponding image charge of  $Q$ ,  $r_i$  is the ion's radius, and  $f$  is a geometrical factor which represents departure of the interfacial region from an ideal mathematical plane.  $T_r$  might range from more than  $400^\circ\text{K}$  for small multivalent ions in a low dielectric constant polymer to less than  $30^\circ\text{K}$  for large monovalent ions in a polymer of high dielectric constant. It appears that some considerations should be given to these ideas in the analysis of data obtained by the methods of thermally stimulated currents, thermodepolarization, etc.

### Chapter III

#### Experimental Instrumentation and Techniques

The effective conductivity  $\sigma$  is obtained by measuring the effective potential drop  $V$  and the current  $I$  flowing through a specimen of the material and then using the dimensions  $A$  and  $b$  to calculate  $\sigma$  from equation (5):

$$\sigma = \frac{Ib}{VA} \quad (5)$$

Hence the dependence of either the number of carriers or the carrier mobility upon the potential will be shown implicitly by the functionality of  $\sigma$  as defined above.

A typical experimental system consists of the following components:

- a. the sample;
- b. the sample holder;
- c. a source of electrical potential which is stable and variable over a wide range of voltage;
- d. a current detector, which is a high impedance electrometer or feedback operational amplifier (to avoid significant difficulties, the impedance of the detector should be greater than that of the sample being measured);
- e. a chamber for control of the ambient atmosphere is also desirable since the electrical properties of most polymers are sensitive to moisture and sometimes to oxygen.

In high-resistance circuits, electrical noise must be reduced to a minimum. This is accomplished by using coaxial cable, metal shielding, and common ground loops (46-47). The electrodes are usually formed by evaporating a metal such as gold or aluminum onto appropriate portions of the surface. Alternatively, graphite pastes, silver pastes, conductive cements, or paints can be used. Care must be taken when using conductive preparations containing organic solvents since the surface of the polymer to be measured can easily be altered and residual solvents may cause some plasticization of the sample.

To measure an ultralow current accurately, extreme care should be taken and a measuring device must be very cautiously chosen. Methods of measuring high resistances accurately and possible measurement errors are mentioned in Appendix III. According to these technical considerations, experience from previous attempts (see Appendix I), and difficulties due to the nature of PPBT samples (See Chapter I). A Keithley 642 electrometer and a Hewlett-Packard 16008A Resistivity cell were chosen as an appropriate experimental instrumentation. In addition to the instrumentation, auxiliary measuring cells and new experimental techniques to separate volume conductivity and surface conductivity of both PPBT film and fiber have been developed. All of these will be discussed in detail in the following sections.

## A The Experimental Instrumentation

### (i) Keithley model 642 electrometer (48):

The design of a portable, solid-state instrument such as Keithley model 642 electrometer shown in Fig. 26 embodies the concepts and techniques to make measurements of ultralow current and ultrahigh impedance. Basically, an electrometer is a refined direct-current multimeter. It can be used for virtually any task normally performed by a conventional multimeter. But its input characteristics, permit it to perform measurements of voltage, current, resistance, and charge far beyond the realm of the conventional multimeter.

An electrometer's input resistance is very high, typically above  $10^{14}$  ohms and sometimes as high as  $10^{16} \Omega$ . Offset current at the input is typically  $5 \times 10^{-14}$  ampere or lower. These characteristics allow voltage measurements that cause only an extremely small amount of circuit loading. Electrometers are capable of monitoring current levels down to the theoretical limits imposed by the level of the input offset current: The Keithley 642's most sensitive current scale reads 200 femtoamperes full-scale. Full-scale charge readings on the instrument's 4 1/2-digit display go from  $10^{-10}$  to  $10^{-12}$  coulomb; currents below  $10^{-15}$  A are generally best measured using the charge



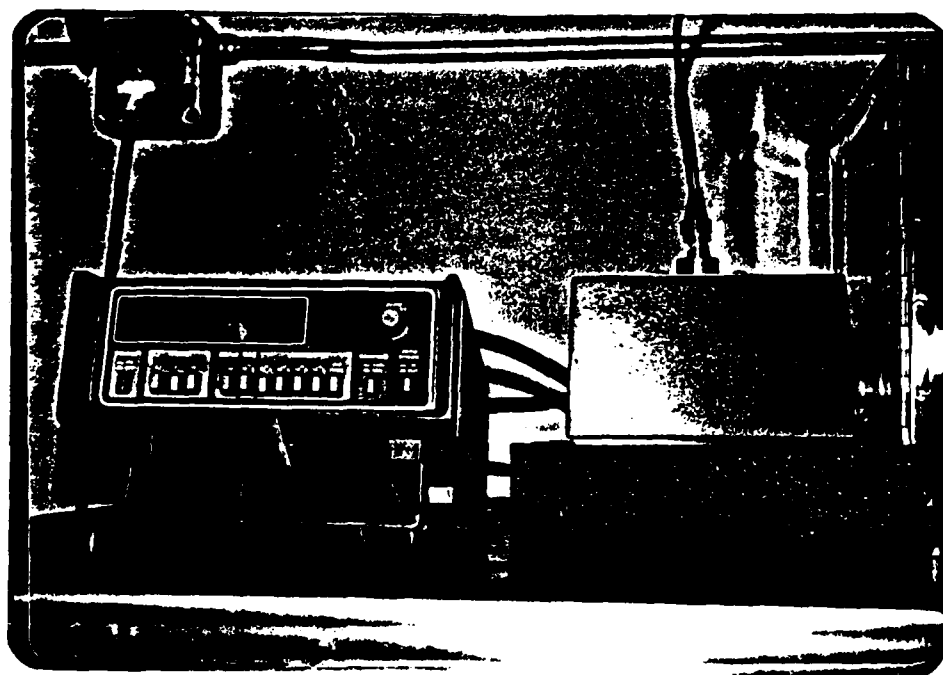


Fig. 26. Keithley model 642 electrometer.

function and a strip-chart recorder to monitor the analog output. In this way, resolutions of  $10^{-17}$  A can be achieved. Its high input resistance and low current offset also enable the electrometer to measure resistances from ordinary levels up to extremely high values.

In simplified form (See Fig. 27), the Keithley model 642 electrometer is divided into a measurement mainframe (on the right in Fig. 26) and a remote head (on the left in Fig. 26). A command from the mainframe configures the head for current, charge, or voltage measurements at a specified level. The Keithley 642 has a unique feature that all components whose performance would be affected by dust, moisture, or other contaminants are sealed inside of the remote head. The only exception is the sapphire-insulated input connector which is protected by the input slide cover. Thus, extreme caution of avoiding contact between the sapphire-insulated input connector and anything which might contaminate it should be kept in mind at all times.

(ii) Hewlett-Packard 16008A resistivity cell (24):

The HP model 16008A resistivity cell (See Fig. 28) is designed to be used for resistivity testing of insulation materials in "sheet" form. Surface and volume resistivity are readily measurable by clamping a sample in the cell between the guarded electrode and the large electrode.

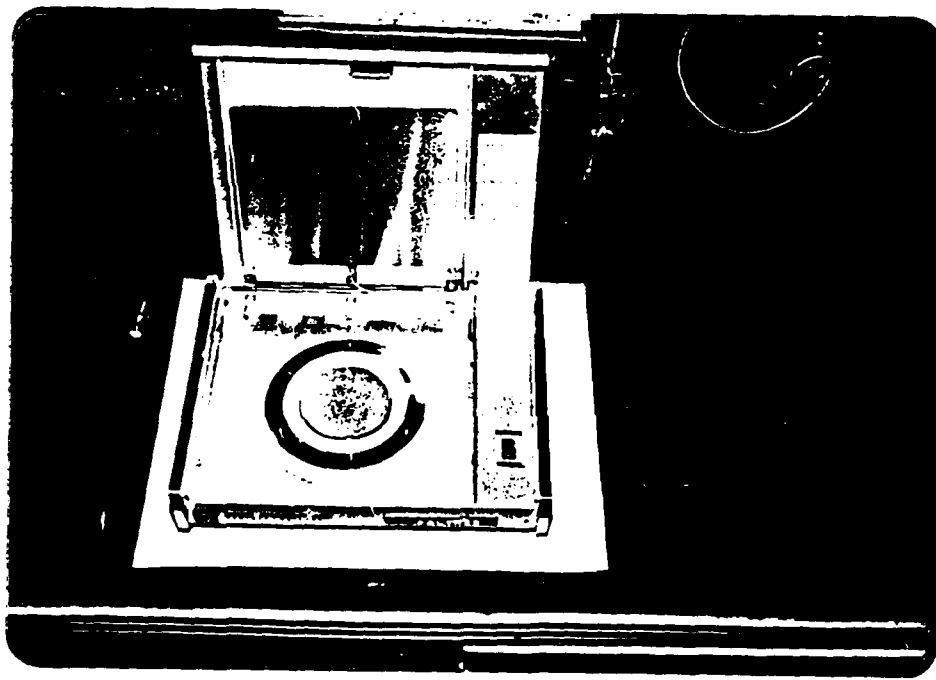


Fig. 28. Hewlett-Packard 16008A resistivity cell.

Cell conduction utilizes a conductivity plastic electrode for uniform contact without the inconvenience of liquid mercury. Samples to be measured should be less than 7mm thick and greater than 100mm in width (or diameter). For surface measurement applications, the voltage is applied to one side of sample sheet through guard ring and center electrode. For volume measurements, a test voltage is applied to both sides of sheet samples through the upper and center electrodes. A guard ring provides normal guarding in volume resistivity measurements.

As mentioned before, the resistivity of solid insulating materials is especially affected by ambient temperature and relative humidity. Before measurement, moisture pretreatment is normally required. The moisture pretreatment can be done by conditioning samples in a controlled environment test chamber for a specific time. In the present system, a desiccant chamber was used to control the ambient conditions of the HP resistivity cell (See Fig. 29).

#### B The Auxiliary Measuring Cells

Due to the design of the HP resistivity cell, available PPBT samples did not meet the size and shape requirements. Therefore, it has been necessary to develop auxiliary measuring cells and special techniques of sample preparation. The developments are listed below:

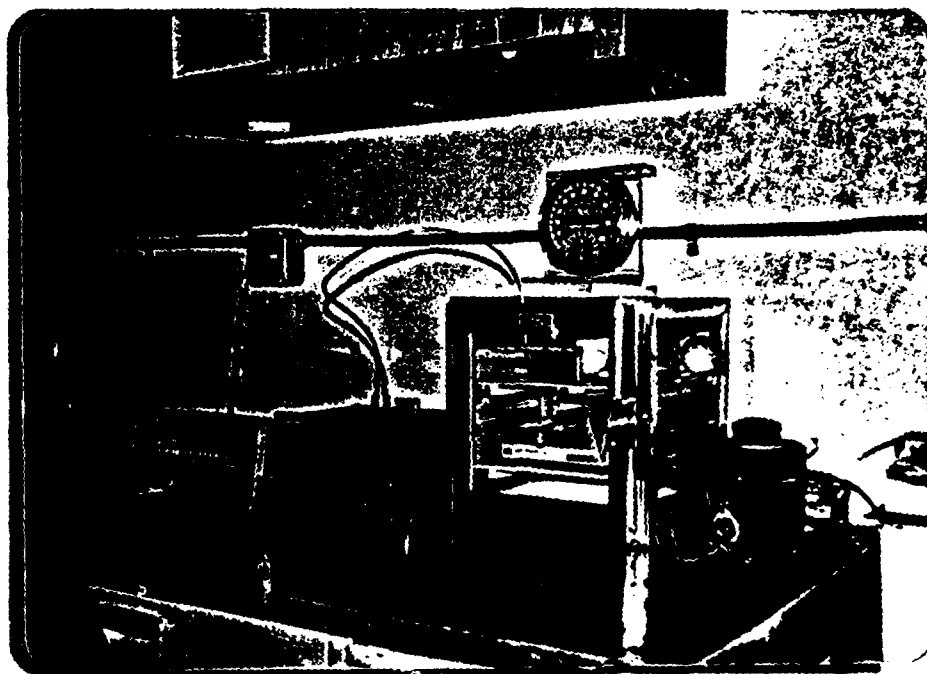


Fig. 29. Experimental setup.

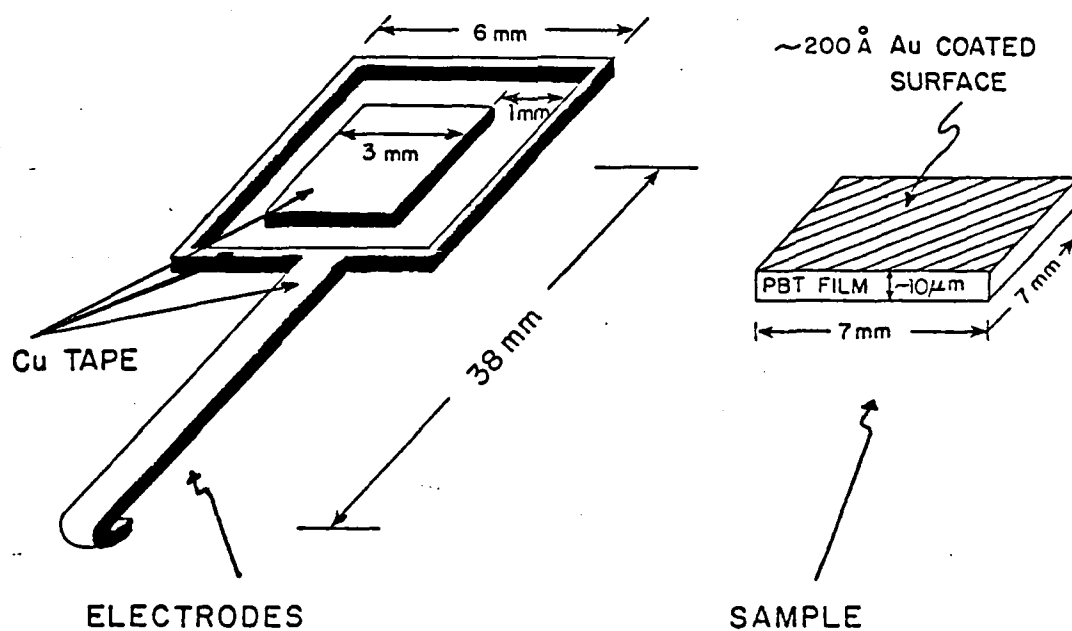
(i) The Miniature Guarded Cell (MGC):

In order to measure transverse conductivity from a PPBT film surface, a miniature guarded cell, utilizing polycarbonate (PC) films, was designed to fit into the HP cell. Figure 30 shows the schematic views of the MGC which consists of two PC (or Lexan) films as holders for the top and bottom electrodes. A miniature guarded electrode system was attached to the bottom PC film. 3M-conductive tape<sup>R</sup> was used to provide a conducting pathway connected to the HP cell's electrodes.

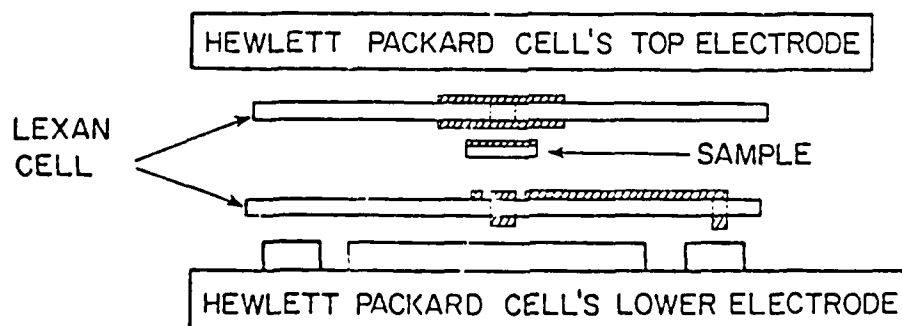
Before using the MGC to conduct conductivity measurements, the calibrations of the device must be considered. The first calibration was to check the accuracy of the instrumentation, i.e. the Keithley 642 electrometer and the HP 16008A cell. By using a 10 cm diameter PC film as a standard sample, its electrical conductivity measured by using the instrumentation was about  $1.3 \times 10^{-16} \Omega^{-1}\text{-cm}^{-1}$  which is very close to the tabulated value,  $\sim 10^{-16} \Omega^{-1}\text{-cm}^{-1}$  (49). Then a 10 cm diameter polyethylene terephthalate (PET or Mylar) film was used as another standard sample, the electrical conductivity of Mylar was measured to be about  $10^{-17} \Omega^{-1}\text{-cm}^{-1}$  which is also close to the tabulated value,  $\sim 10^{-17} \Omega^{-1}\text{-cm}^{-1}$  (49). Thus, the calibration of the instrumentation was established.

# TECHNIQUE FOR MEASUREMENT OF $\sigma_{\perp}$ PERPENDICULAR TO FIBER AXIS

## (a) MINATURE GUARDED ELECTRODE SYSTEM



## (b) ASSEMBLY



## (c) EQUIVALENT CIRCUIT

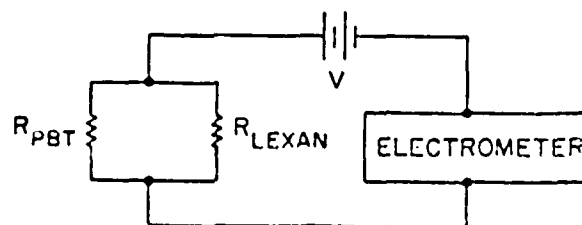


Fig. 30.

The second calibration was to measure the resistance of the MGC. This resistance will be used as the correction parameter for electrical conductivity measurements using the MGC. Two measurements were performed. In the first measurement, a smaller piece of Mylar film (1 cm x 1 cm x 70  $\mu$ m) was used as the sample to be measured by using the MGC. The resistance of the MGC can be calculated through the analysis of the equivalent circuit in Fig. 31. Since the electrical conductivity of Mylar is known, the resistance of the smaller piece of Mylar film can be calculated by using the equation:

$$R = \frac{b}{\sigma A}, \quad (46)$$

and  $R_{\text{Mylar}} \approx 7 \times 10^{14} \Omega$ . Then, the resistance of the MGC was obtained from the following derivation:

$$\begin{aligned} \therefore \frac{1}{R_{\text{Mylar}}} + \frac{1}{R_{\text{MGC}}} &= \frac{1}{R_{\text{Experimental}}}, \\ \therefore V \left( \frac{1}{R_{\text{Mylar}}} + \frac{1}{R_{\text{MGC}}} \right) &= \frac{V}{R_{\text{Exp.}}} = I_{\text{Exp.}}, \\ \Rightarrow R_{\text{MGC}} &= \frac{V}{I_{\text{Exp}} - I_{\text{Mylar}}}, \quad (47) \end{aligned}$$

where  $I_{\text{Mylar}} = \frac{V}{R_{\text{Mylar}}}$  is the current through the Mylar, without the MG cell. In the second measurement, the Mylar sample was replaced by a smaller PC film (1 cm x 1 cm x 0.5 mm). Then, the  $R_{\text{MGC}}$  obtained this way was



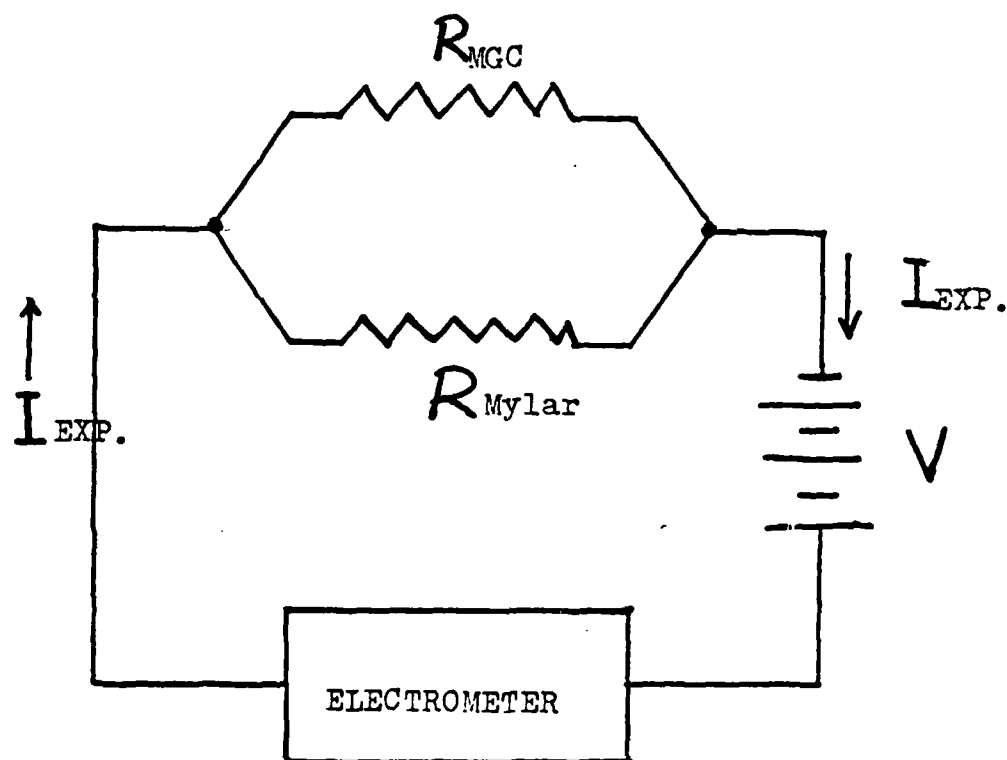


Fig. 31. Equivalent circuit for a Mylar film in the MGC.

$$R_{MGC} = \frac{V}{I_{Exp} - I_{PC}}, \quad (48)$$

$$\text{where } I_{PC} = \frac{V}{R_{PC}} \quad \text{and } R_{PC} = \frac{b_{PC}}{\sigma_{PC} A_{PC}} \approx 3.85 \times 10^{14} \Omega.$$

Values of  $R_{MGC}$  from both measurements were comparable.

Thus, an average value was obtained, i.e.  $R_{MGC} = 7.5 \times 10^{15} \Omega$ .

When a PPBT film is placed inside the MGC, the transverse electrical conductivity of the PPBT film can be measured and expressed as:

$$(\sigma_{\perp})_{PPBT} = \frac{I_{PPBT} b}{AV} \quad \text{with}$$

$$I_{PPBT} = I_{Exp} - \frac{V}{R_{MGC}} = I_{Exp} - I_{MGC}. \quad (49)$$

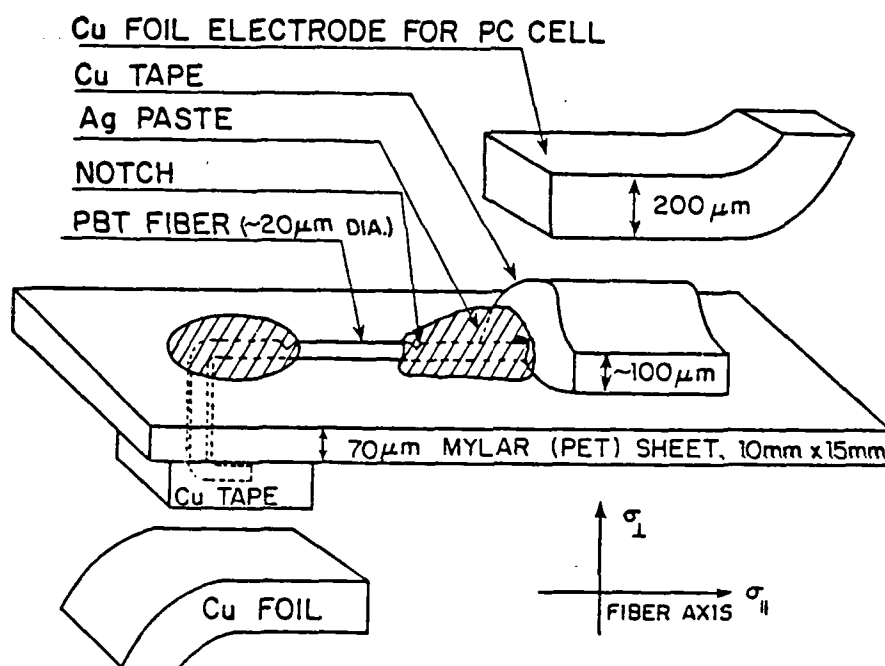
(See Fig. 30 (c) for the equivalent circuit and note that the analysis is similar to the derivation of  $R_{MGC}$ .)

#### (ii) The Notched Electrode System (NES):

The notched electrode system was designed mainly for the measurement of the axial conductivity of small fibers. The general features of the experimental arrangement are shown schematically in Fig. 32. Fiber samples were mounted as indicated on a Mylar film. One end of the fiber was threaded through a hole on the Mylar film and copper tape (3M conductive tape) was used to hold both ends of the PPBT fiber on the Mylar film. Two notches were made on the PPBT

# TECHNIQUE FOR MEASUREMENT OF $\sigma_{II}$ PARALLEL TO FIBER AXIS

## (a) ELECTRICAL CONTACTS (SCHEMATIC)



## (b) THE EQUIVALENT CIRCUIT

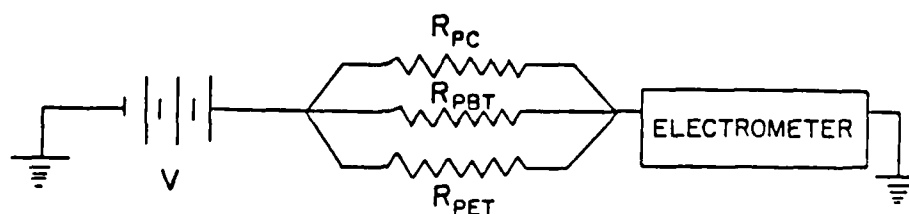


Fig. 32.

fiber by using a very sharp surgical blade under a microscope. PELCO Colloidal Silver paste was applied to the notched regions for the purpose of allowing the electrical current to flow along the fiber axis inside the fiber instead of only on the fiber surface. From Fig. 32(b), the apparent axial conductivity (volume and surface conductivities combined) can be expressed as:

$$(\sigma_{||})_{PPBT} = \frac{I_{PPBT}}{AV} l, \quad (50)$$

where  $l$  is the length of the gap between 2 notches and

$$I_{PPBT} = I_{Exp} - \left( \frac{V}{R_{Mylar}} + \frac{V}{R_{MGC}} \right) = I_{Exp} - I_{Mylar} - I_{MGC}. \quad (51)$$

Note: the technique to separate surface conductivity and volume conductivity of the PPBT fiber will be discussed in section (C) of this Chapter.

(iii) The Alternative Cell (AC):

It is important to determine the activation energy of conduction by measuring the temperature dependence of electrical conductivity. It is also very likely that the HP cell may be damaged when heat is applied to the sample. An alternative cell (See Fig. 33) was designed to prevent the problem. In Fig. 33 (a) and (b), a Teflon base was used to support Cu electrodes and a 22.5 volts battery was placed inside an aluminum box which was grounded to provide elec-

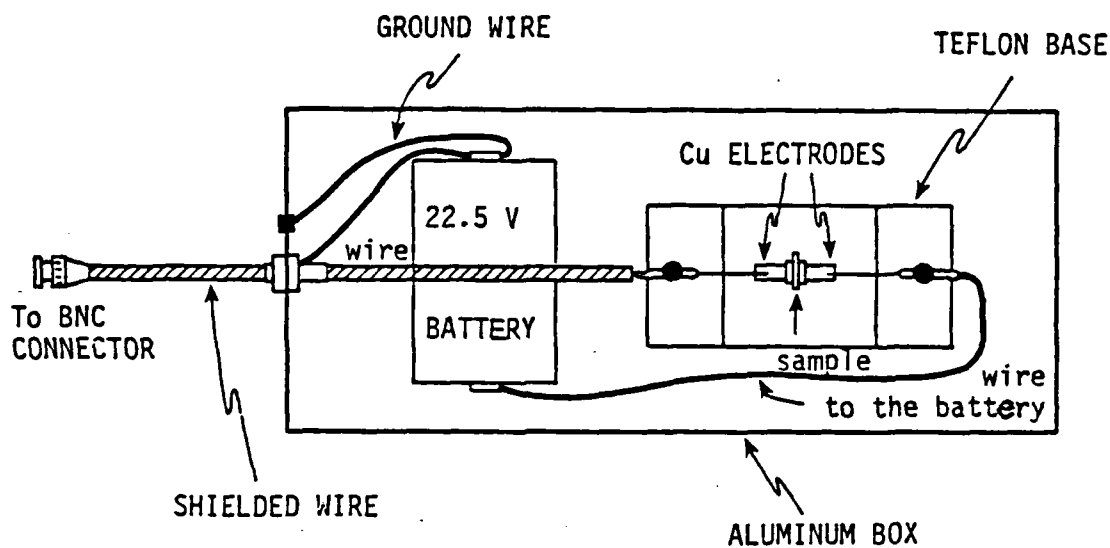
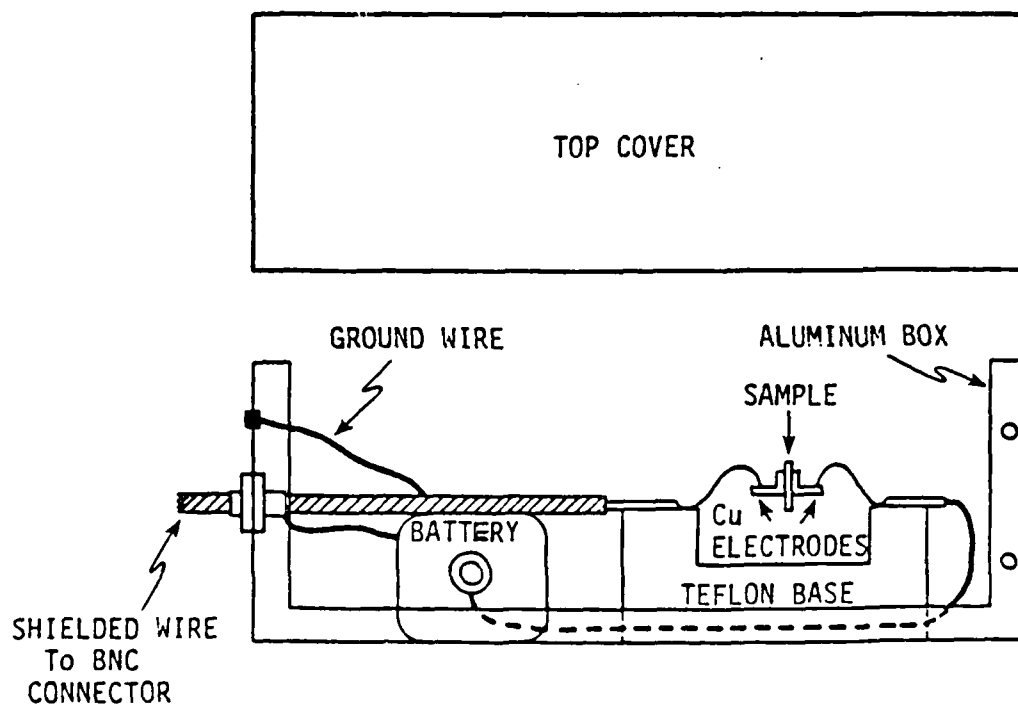
a) TOP VIEWb) SIDE VIEW

Figure 33. The Alternative Cell.

trostatic shielding for the electrode system.

It is necessary to know the current contribution from the Teflon base, as it was used as a component of the alternate cell. Figure 34 shows that in the presence of a PPBT sample, the current contribution from the cell can be neglected after 1 hour of measurement. This cell is unguarded, but experimental data revealed that, to a certain extent, surface current can be neglected. The experimental data are listed below:

$$\frac{\left(\frac{I_{\text{surf}}}{I_{\text{Exp}}}\right)_{\text{Fiber}}}{\sim 4\%} \quad \frac{\left(\frac{I_{\text{surf}}}{I_{\text{Exp}}}\right)_{\text{Film}}}{\sim 3\%}$$

Although these contributions were surprisingly small, they are in accord with the morphology of PPBT samples. The presence of erupted voids on PPBT's surface (12) restricts the flow of sample current.

### C. The Experimental Techniques

Because of the sensitive nature of the measurements, the operation procedures will be outlined in considerable detail.

- (i) General operation procedures (48):

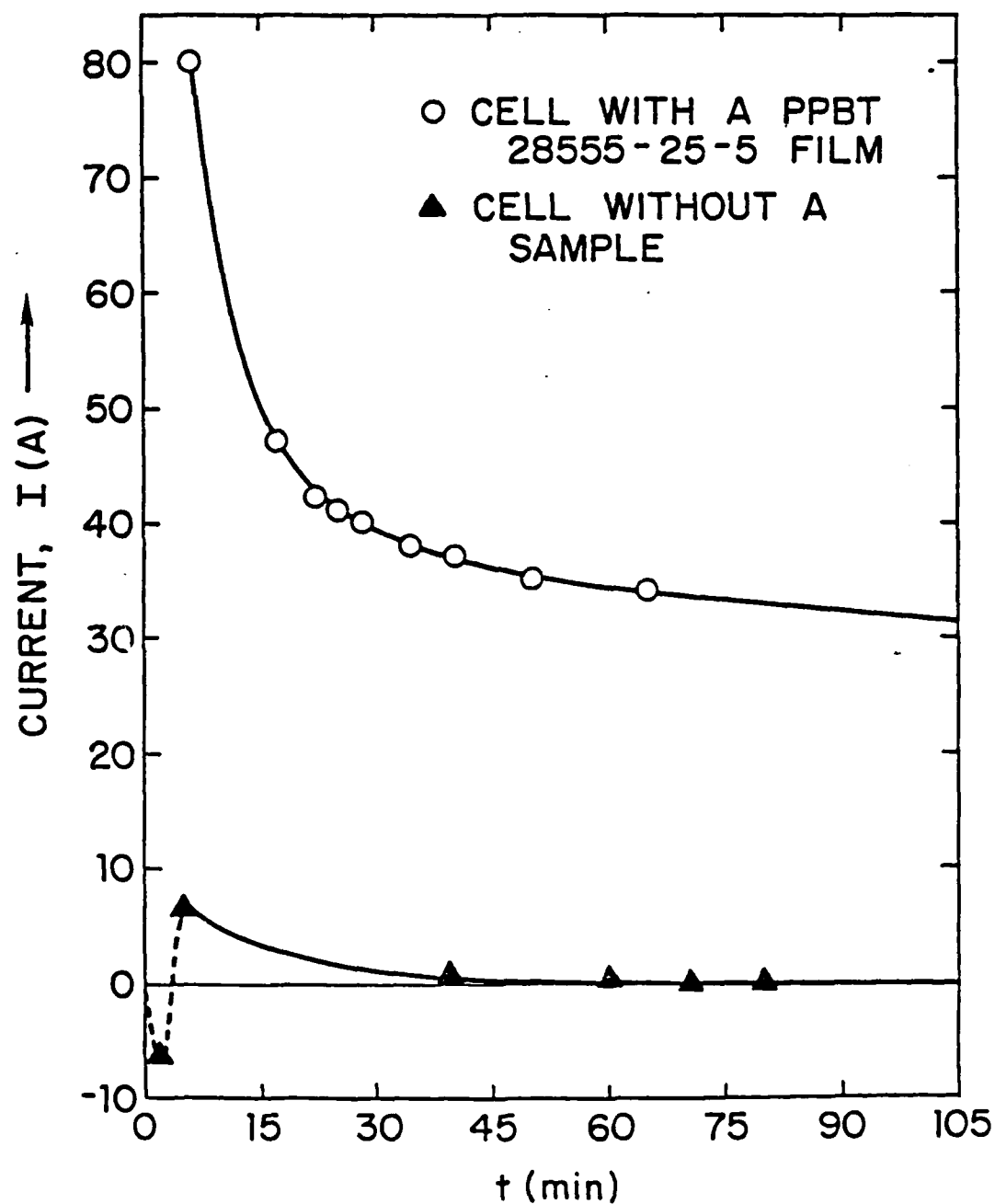


Fig. 34. Curves of  $I$ - $t$  for the Alternative Cell with and without a PPBT sample.

- a. First the Keithley 642's mainframe and the remote head are connected as instructed in the operation manual;
- b. Next the HP 16008A cell (or the alternative cell) is connected as in Fig. 34 to the remote head of the Keithley 642 (See Fig. 35);
- c. It then is important to push the "Zero check" button of the Keithley 642 electrometer;
- d. After the zero check, one can turn on the power.
- e. Choose the function mode for the measurement (the "Current Mode" was usually used in this research);
- f. Choose the range of the sensitivity for the measurement;
- g. Place a sample (either a PPBT film or a fiber sample prepared as described before) in the Miniature Guarded Cell;
- h. Put the MGC into the HP 16008A cell;
- i. Set "Volume" or "Surface" mode on the HP cell;
- j. Close the HP Cell's cover and release the "Zero Check" button;
- k. Allow a settling time (for PPBT usually over 6 hours) for the measurement because of the transient phenomena (See Chapter II);
- l. After the digital display is steady, (i.e., conduction current has settled), take data ( $I_{Exp}$  vs.  $t$ );



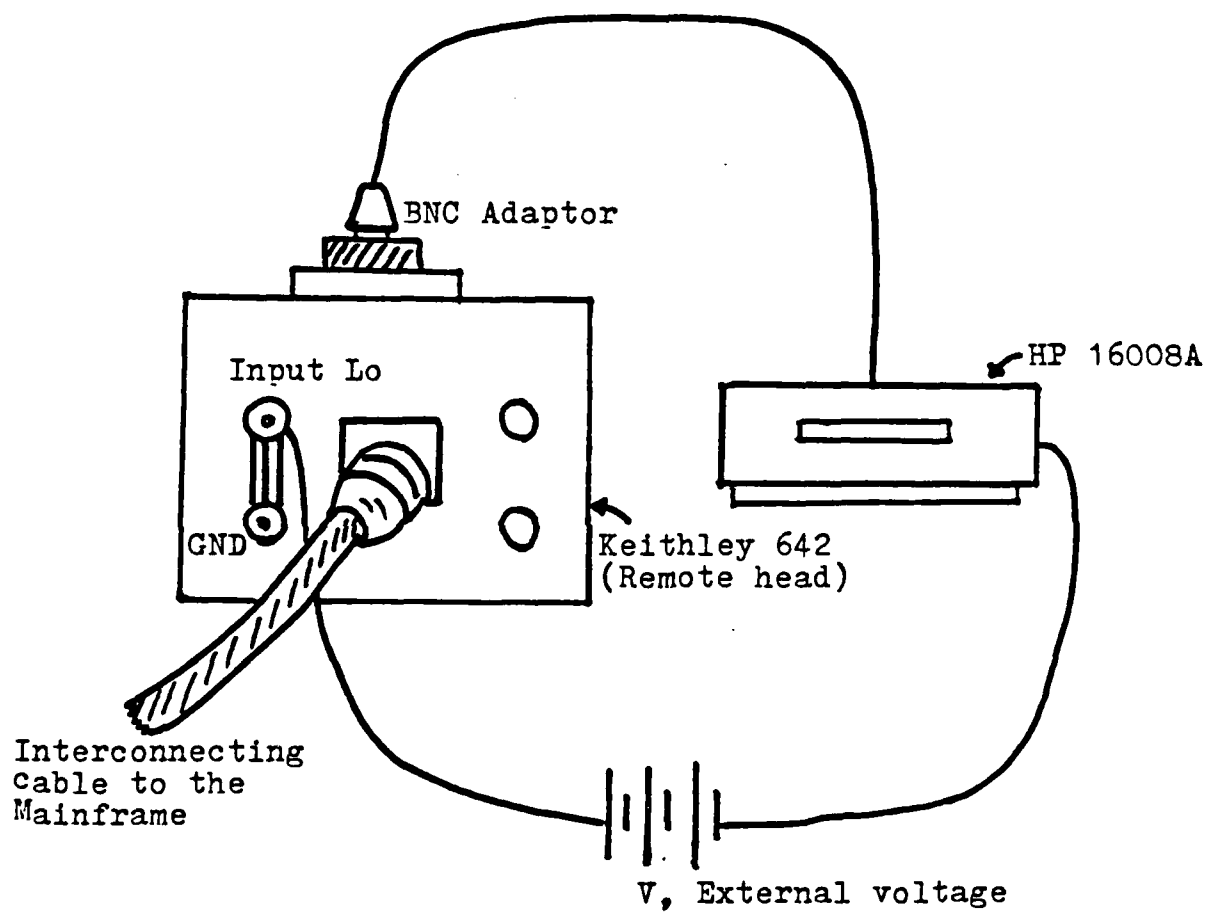


Fig. 35. Experimental configuration.

- m. Use the values of  $I_{Exp}$  in Eq. (49) or Eq. (51) to calculate effective conductivities  $(\sigma_{\perp})_{PPBT}$  or  $(\sigma_{||})_{PPBT}$ .

- (ii) Special technique developed to separate volume and surface conductivity from apparent conductivity:

In principle,  $\sigma_{vol.}$  and  $\sigma_{surf.}$  of a fiber can be determined by measuring a series of fibers with various radii,  $r_1$ ,  $r_2$ , etc. Figure 36 shows the experimental technique and data analysis. By assuming additivity of the surface and volume contributions, from Fig. 36(a), it can be shown that:

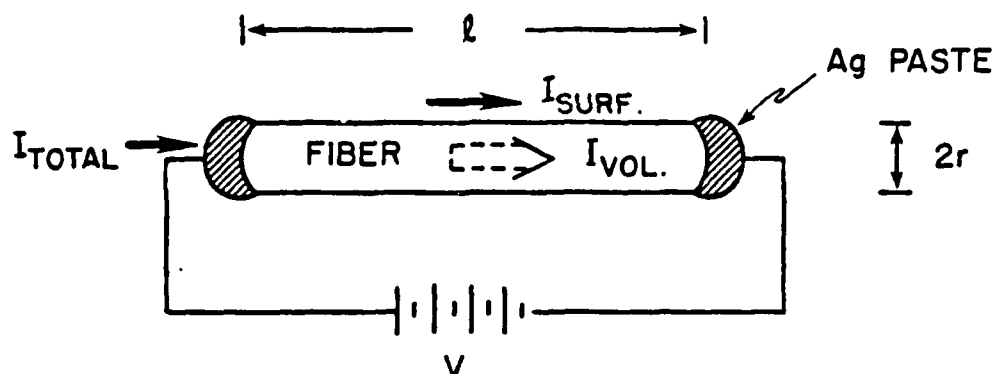
$$I_{Total} = I_{surf.} + I_{vol.}, \quad (52)$$

and

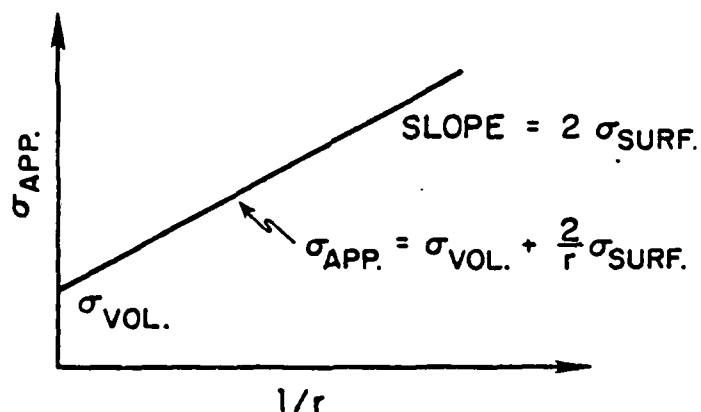
$$\sigma_{Apparent} = \sigma_{vol.} + \frac{(2)\sigma'_{surf.}}{r} \quad (53)$$

where  $\sigma'_{surf.}$  has units  $\text{ohm}^{-1}$  or  $(\text{ohms per square})^{-1}$ , and  $\sigma_{vol.}$  has units  $\text{ohm}^{-1}\text{cm}^{-1}$ . Thus, the plot of  $\sigma_{App.}$  versus  $1/r$  should be linear as suggested schematically in Fig. 36(b). In the present research, the lack of availability of geometrically perfect, defect-free samples (See Chapter

## (a) EXPERIMENTAL TECHNIQUE



## (b) DATA ANALYSIS



## (c) ADVANTAGES &amp; DISADVANTAGES

- |   |  |
|---|--|
| <ul style="list-style-type: none"> <li>• SIMPLE IN CONCEPT</li> <li>• INDIVIDUAL MEASUREMENTS EASY</li> </ul> | <ul style="list-style-type: none"> <li>• NEED MANY DATA POINTS</li> <li>• VERY UNIFORM DIAMETER SAMPLES NEEDED</li> <li>• NEED HIGHLY REPRODUCIBLE CONTROLLED ENVIRONMENT</li> </ul> |
|---|--|

Fig. 36. Theoretical technique to separate  $\sigma_{vol}$  and  $\sigma_{surf}$ .

1) to give good statistical results motivated the development of a special technique.

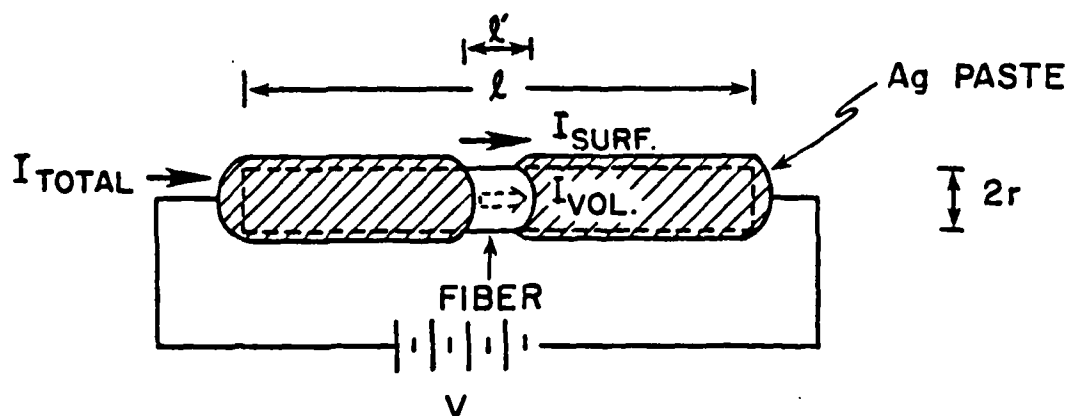
The special technique only requires two measurements on the same fiber is shown in Fig. 37. The first measurement has an effective length  $l$  between two electrodes. The second measurement has an effective length  $l'$  which is changed from  $l$  by advancing the silver paste electrodes. Thus,  $(\sigma_{vol.})_{ll}$  and  $(\sigma_{surf.})_{ll}$  can be calculated by solving the following simultaneous equations:

$$\sigma_{App.}(l) = (\sigma_{vol.})_{ll} + (2/r)(\sigma_{surf.})_{ll}, \quad (54)$$

and

$$\sigma_{App.}(l') = (l'/l)(\sigma_{vol.})_{ll} + (2/r)(\sigma_{surf.})_{ll}. \quad (55)$$

An equivalent-circuit model (see Fig. 38) was proposed to rationalize this special technique. In Fig. 38(a), a number of resistors in parallel, connect two electrodes; this situation is analogous to the nature of a PPBT fiber which is composed of a multitude of individual fibrils. The reduction of length between electrodes brought about by advancing the silver paste is viewed as being analogous to the partial shorting of  $R_s$  to give  $R_s'$  in Fig. 38(b). Thus, in this model, only the surface resistance is changed.



1st MEASUREMENT,

$$\sigma_{APP}(l) = (\sigma_{VOL.})_{||} + \frac{2}{r} (\sigma_{SURF.})_{||}$$

2nd MEASUREMENT,

$$\sigma_{APP}(l') = \left(\frac{l'}{l}\right) (\sigma_{VOL.})_{||} + \frac{2}{r} (\sigma_{SURF.})_{||}$$

IF

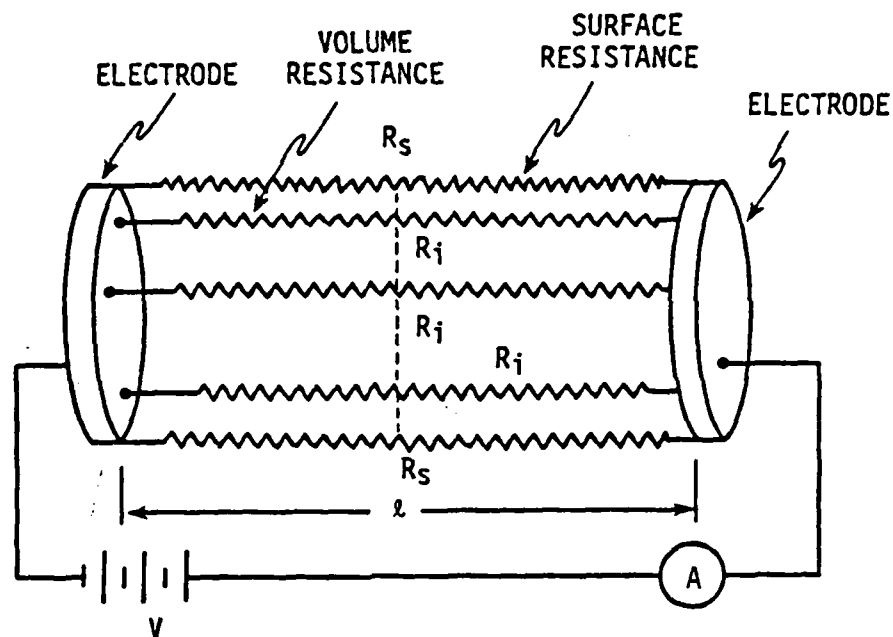
$$(\sigma_{VOL.})_{||} \gg (\sigma_{VOL.})_{\perp} \quad , \quad (\sigma_{SURF.})_{||} \gg (\sigma_{SURF.})_{\perp} \quad ,$$

AND  $\sigma_{APP}(l)$  &  $\sigma_{APP}(l')$  ARE KNOWN,

THEN  $(\sigma_{SURF.})_{||}$  AND  $(\sigma_{VOL.})_{||}$  CAN BE CALCULATED.

Fig. 37. Special technique to separate  $\sigma_{vol}$  and  $\sigma_{surf}$ .

a)



b)

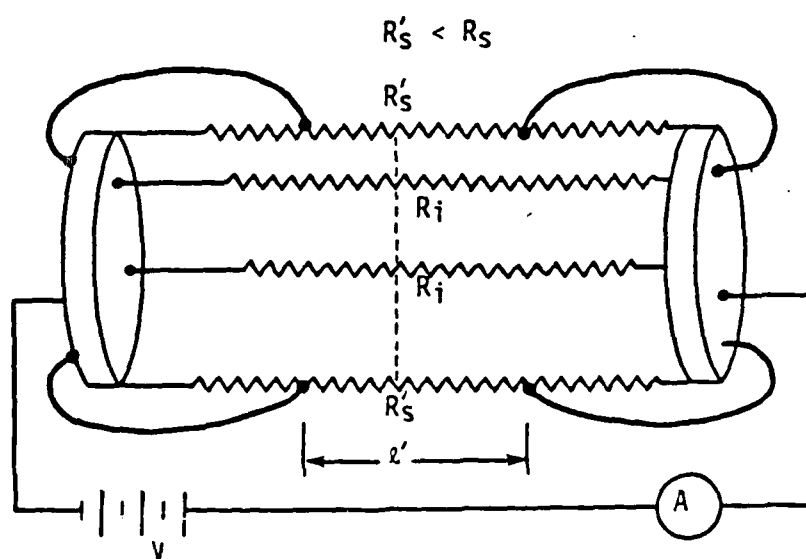


Figure 38. Equivalent-Circuit Model for the Special Technique.

This technique can be further modified by carefully introducing notches of known depth (and filling them with silver paste) to improve the experimental resolution when the measured values of  $\sigma_{\text{App.}}(l)$  and  $\sigma_{\text{App.}}(l')$  would be too close to provide reliable values. The corresponding model is shown in Fig. 39 and the equation for  $\sigma_{\text{App.}}(l')$  can be expressed as:

$$\sigma_{\text{App}}(l') = \left[ \left( \frac{l'}{l} \right) + \left( 1 - \frac{l'}{l} \right) \left( \frac{A_N}{\pi r^2} \right) \right] (\sigma_{\text{vol}})_{||} + \frac{2}{l} (\sigma_{\text{surf.}})_{||}, \quad (56)$$

where  $A_N$  is the cross-sectional area of the notches and  $\pi r^2$  is the cross-sectioned area of the fiber.

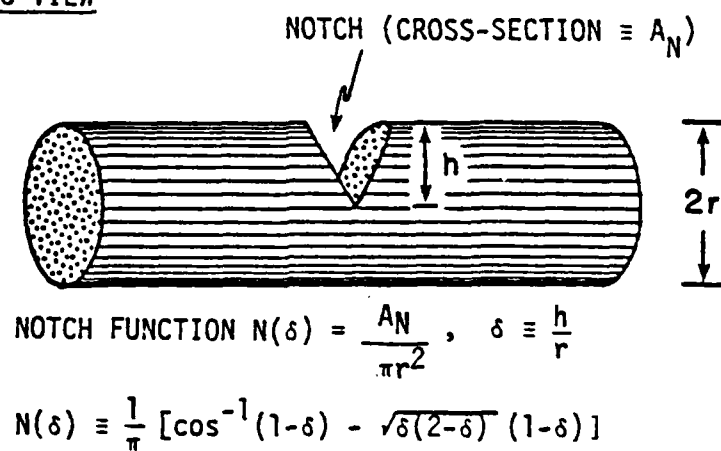
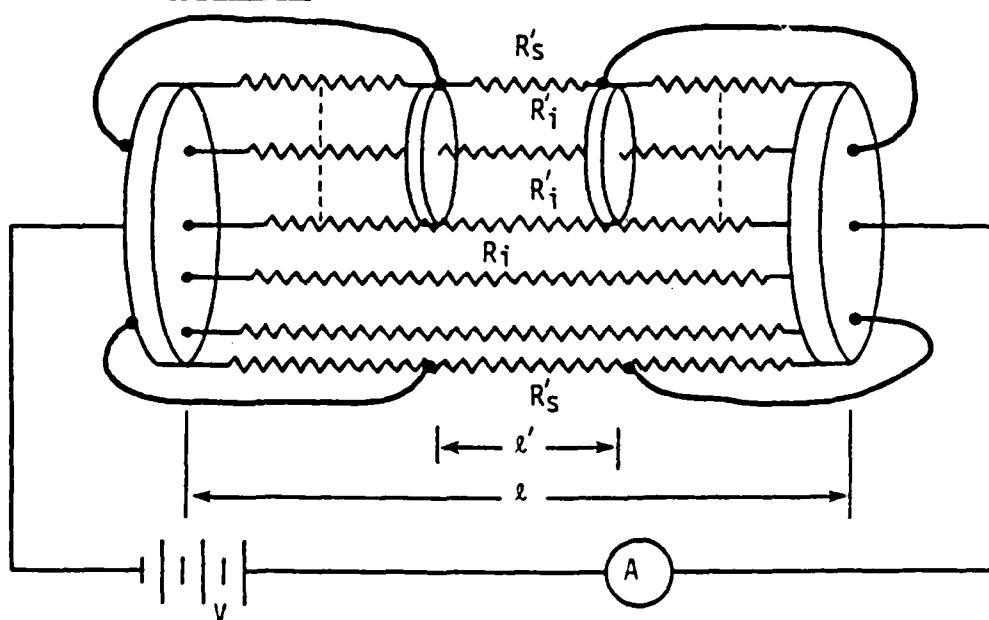
a) SCHEMATIC VIEWb) EQUIVALENT CIRCUIT

Figure 39. Notched — Fiber Technique. Applicable only to highly anisotropic fibers with  $\sigma_{11} \gg \sigma_{12}$ .



## Chapter IV

### Experimental Results and Discussion

#### A. Observation of transient phenomena

As mentioned previously, more than 6 hours usually is needed to obtain the so-called experimental asymptotic value of conduction current for PPBT samples. It was observed that different  $\log I$  vs  $\log t$  plots were obtained for different PPBT samples. Figure 40 shows  $\log I$ - $\log t$  curves for a notched PPBT (28555-19-2) fiber and a PPBT film (as "cast" 28555-25-6), respectively. In these logarithmic plots, it is observed that only after a sufficiently long measuring period, is the determination of the asymptotic conduction current reliable.

Microscopic examinations, even at low magnification, have revealed that PPBT samples are inhomogeneous, both on the surface (erupted voids) and in the interior (microvoids) (12,17). Thomas et al. (17) reported that typical voids are about  $49 \text{ \AA}$  in the fiber direction by  $35 \text{ \AA}$  at right angles. Another influence of microvoids also has been observed by W-S Huang in diffusion experiments (50). Thus, it is appropriate to apply the Maxwell-Wagner model (see Chapter II) to interpret the transient phenomena in PPBT. From an experimental point of view, the effective electrical conductivity is determined by factors such as the degree of surface roughness, the permittivity of PPBT

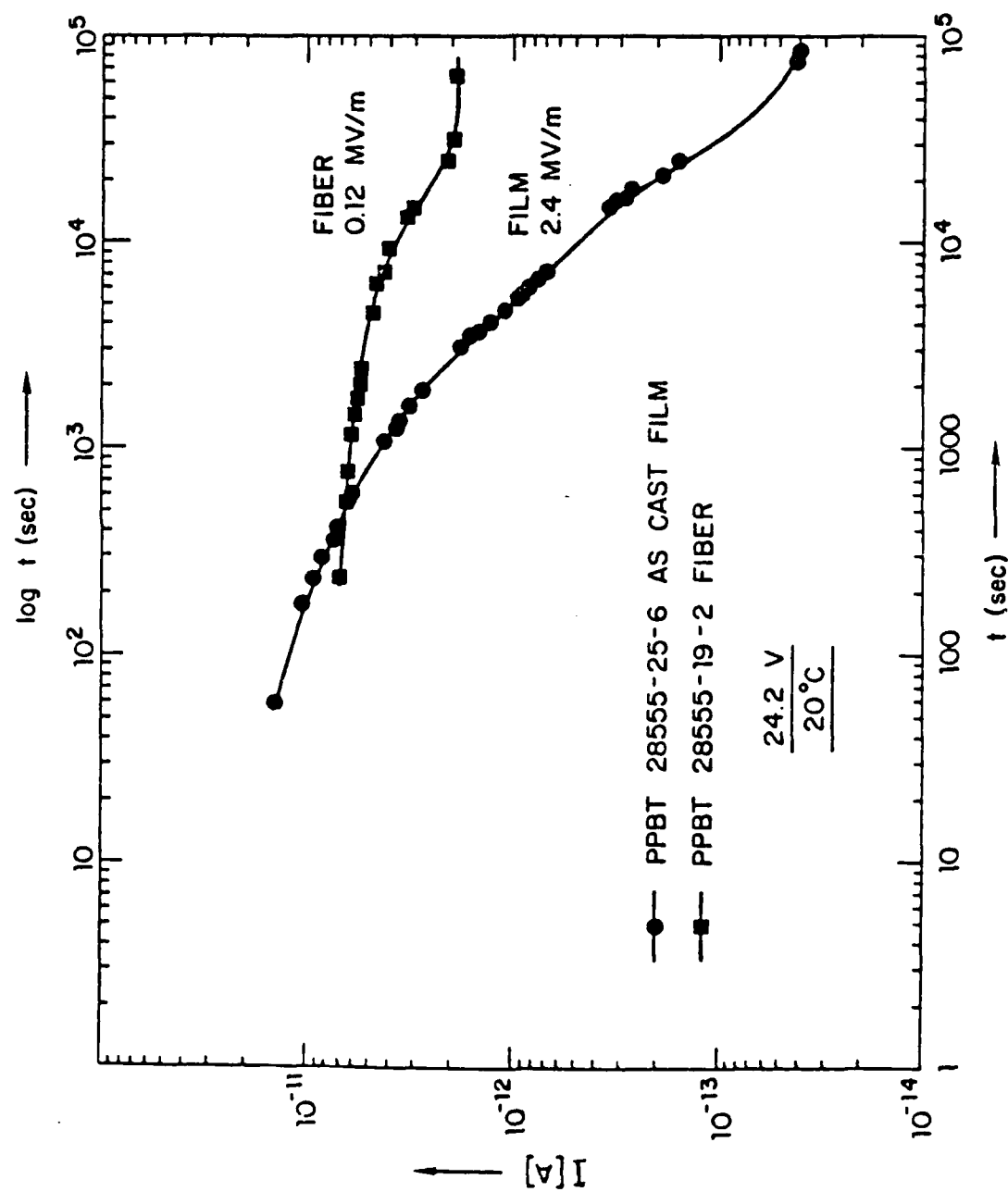


Fig. 40. Transient current vs. time for PPBT samples.

samples, and the permittivity of the air gap between the electrodes and the PPBT sample. Equation (20) summarizes their relationship as:

$$\sigma_{\text{eff.}} = \sigma \exp\left(-\frac{\sigma}{\epsilon\epsilon_0} \frac{be}{b} t\right). \quad (20)$$

Accordingly, the initial value of effective conductivity is equal to the bulk conductivity of PPBT samples, but thereafter an exponential decrease is expected, with a time constant

$$\tau = \left(\frac{\epsilon\epsilon_0}{\sigma}\right) \left(\frac{b}{b_e}\right). \quad (57)$$

Since  $b_e \ll b$  and  $\sigma$  is very small,  $\tau$  will be very large. This partly explains the long transient period for current measurements.

Measurements on other samples with different treatments may be interpreted with other models such as ionically blocking processes and trapping processes. Figures 41, 42, and 43 are for iodine doped, lithium chloride doped, and sodium chloride doped PPBT samples, respectively. Ionic blocking process can well explain behavior of salt solutions (e.g. LiCl, LaCl<sub>3</sub>, etc.) treated samples. Due to the presence of moisture, salt molecules may be dissociated and move to block electrodes. Apparently, the ionic blocking process is time-dependent. This dissociation process and related aspects will be fully discussed in the next Chapter through the analysis of the "Weak

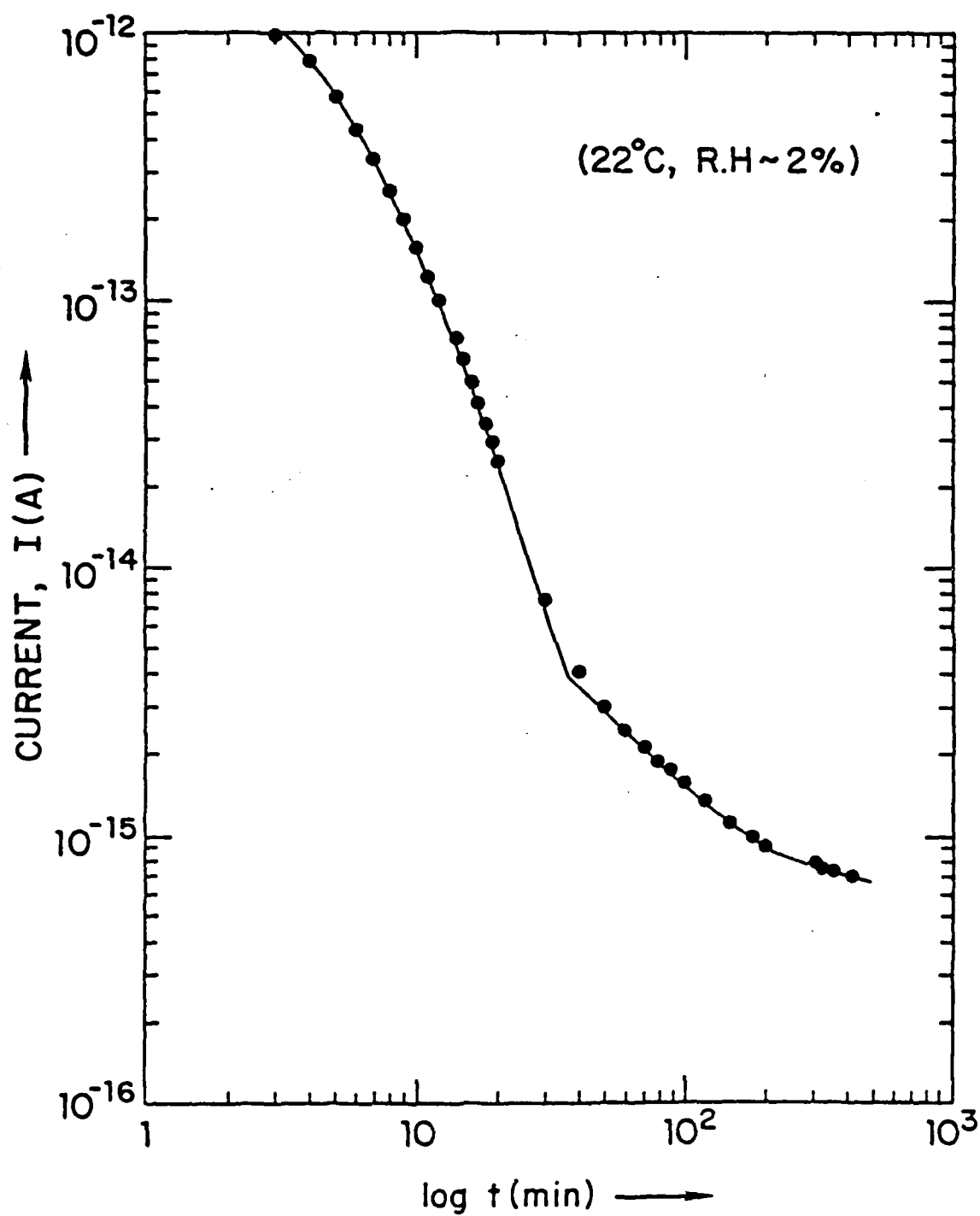


Fig. 41. Transient current vs. time for the  $I_2$  doped PPBT 28555-25-6 film.

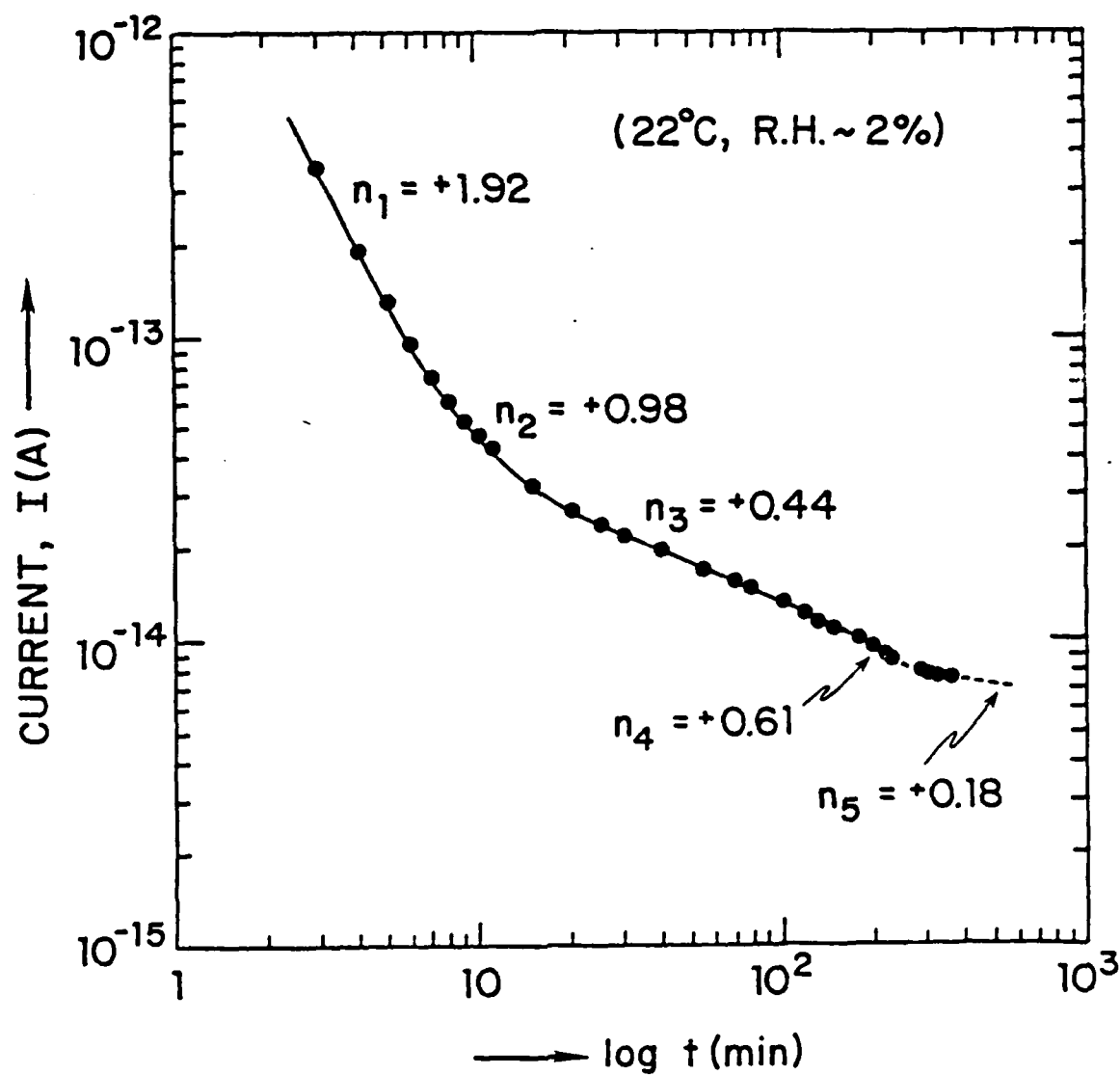


Fig. 42. Transient current vs. time for the LiCl doped PPBT 29022-43-4 fiber.

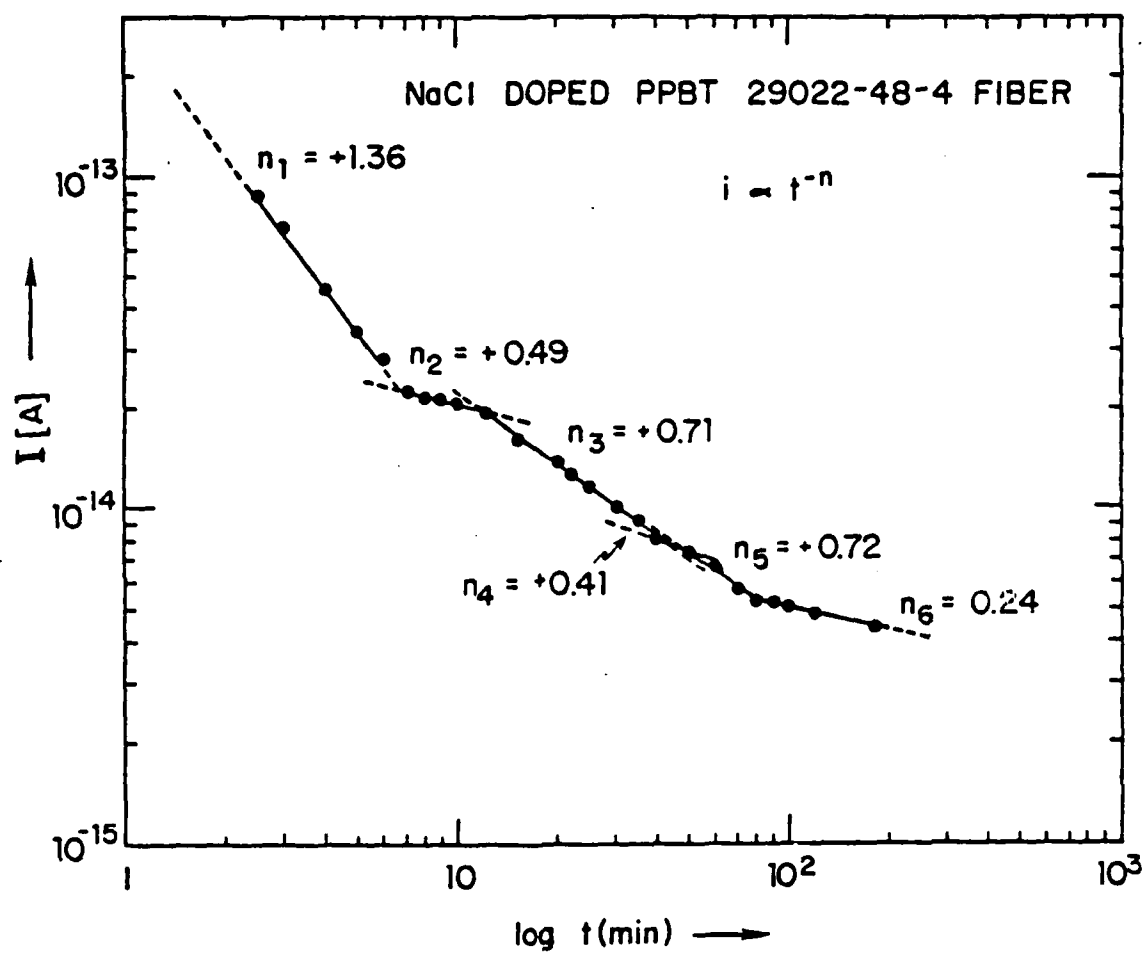


Fig. 43. Transient current vs. time for the NaCl doped PPBT 29022-48-4 fiber.

electrolyte model".

A typical microvoid inside a PPBT sample is shaped somewhat like a football (12,17) and can serve as a trapping site for charge carriers. Generally, in polymers, trapping can occur at particular molecular sites and at chain folds. Consider, for example, the motion of a charge carrier along a randomly oriented polymer chain as shown in Fig. 44. If there is an easy path of motion in which the charge carrier can move, then it will move along until it reaches the point B at which the chain is no longer aligned with the electric field. At this point, it will not have any momentum in directions perpendicular to the electric field nor can momentum perpendicular to field be supplied by any other source than the random fluctuation of thermal energy. A charge carrier cannot be accelerated around the bend to point C because there is no component of electric field in this direction. Therefore, point B is effectively a localized state. The charge carrier will stop there, the medium around it will polarize, and considerable thermal energy will be required to excite it out of the potential well into the next chain at D. If this is the case, it is quite possible that the depth of the potential well will be a time-dependent function related to the rotational or vibrational modes of the polymer (22). A central question whose answer must wait dielectric measurements, is: how much time will be required for the local polarization about a trapped charge carrier to form? Therefore, the observed

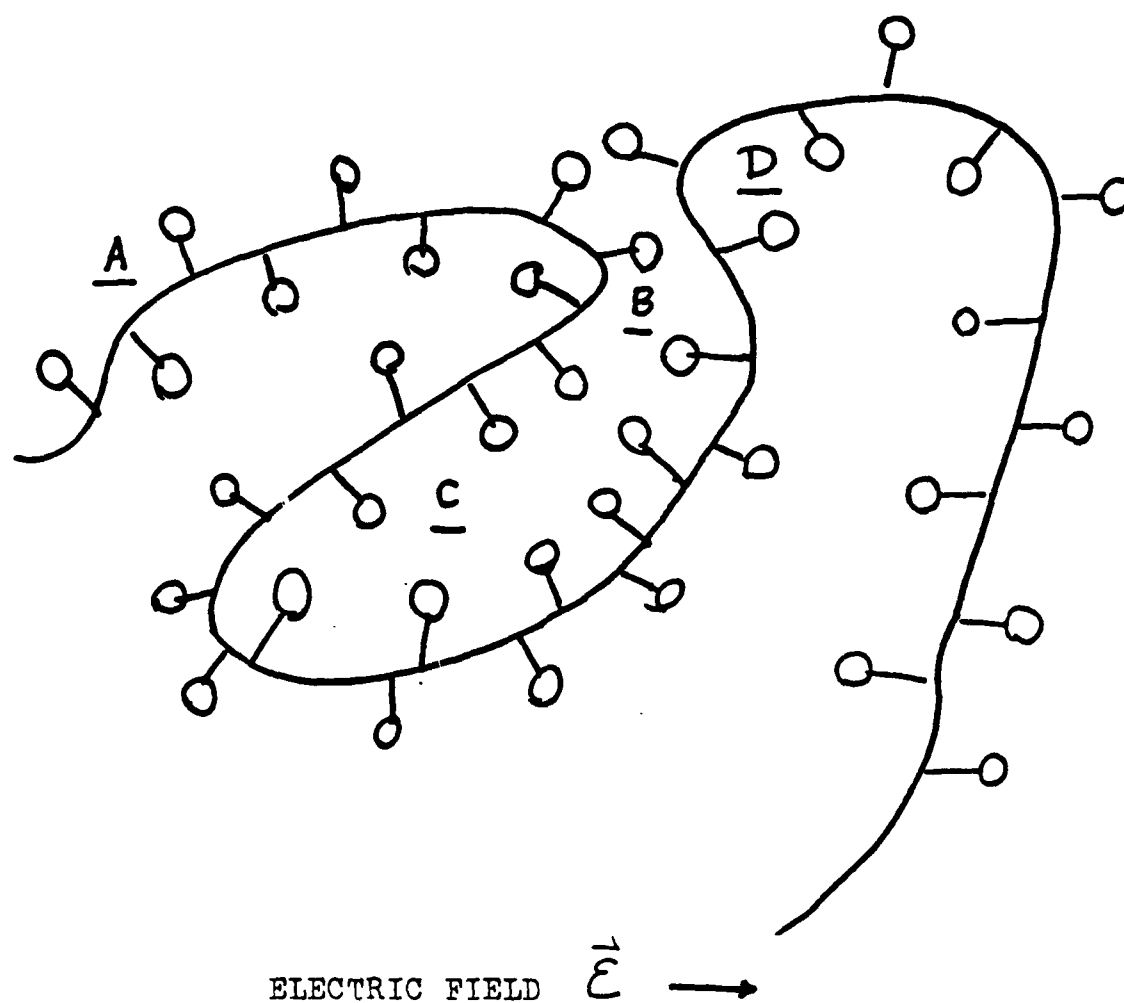


Fig. 44. Randomly oriented polymer chain.



transient phenomena probably have some contribution from the presence of microvoids in PPBT samples.

#### B. Field dependence of electrical conductivity

Under high applied voltage, the space charge in the vicinity of the electrodes might cause samples to be non-ohmic. The quantitative characterization of non-ohmic behavior of the polymer would aid in understanding the conduction mechanism. Because of a design feature, the Keithley 642 electrometer limits the maximum applied voltage that can be used to about 30 volts. For a notched fiber (PPBT 28555-19-2) with an effective length of  $200\mu\text{m}$ , the axial current was quite linear up to  $0.12\text{ MV/m}$  (the highest field available), Fig. 45. This meant that at least there was an ohmic region for PPBT samples. If the field can be made high enough to give non-ohmic behavior then it will be possible to deduce useful information about the nature of the charge carriers (6). Figures 46 and 47 are typical models which can be used for the identification of both non-ohmic electronic and ionic conductions, respectively. For example, in electronic conductor, the Poole-Frenkel effect is the consequence of a strong applied electric field enhancing the de-trapping of electrons within a semiconductor or insulator. In the case of ionic conduction, for example, the Stern-Eyring rate-theory model, non-ohmic processes have been discussed in Chapter II.

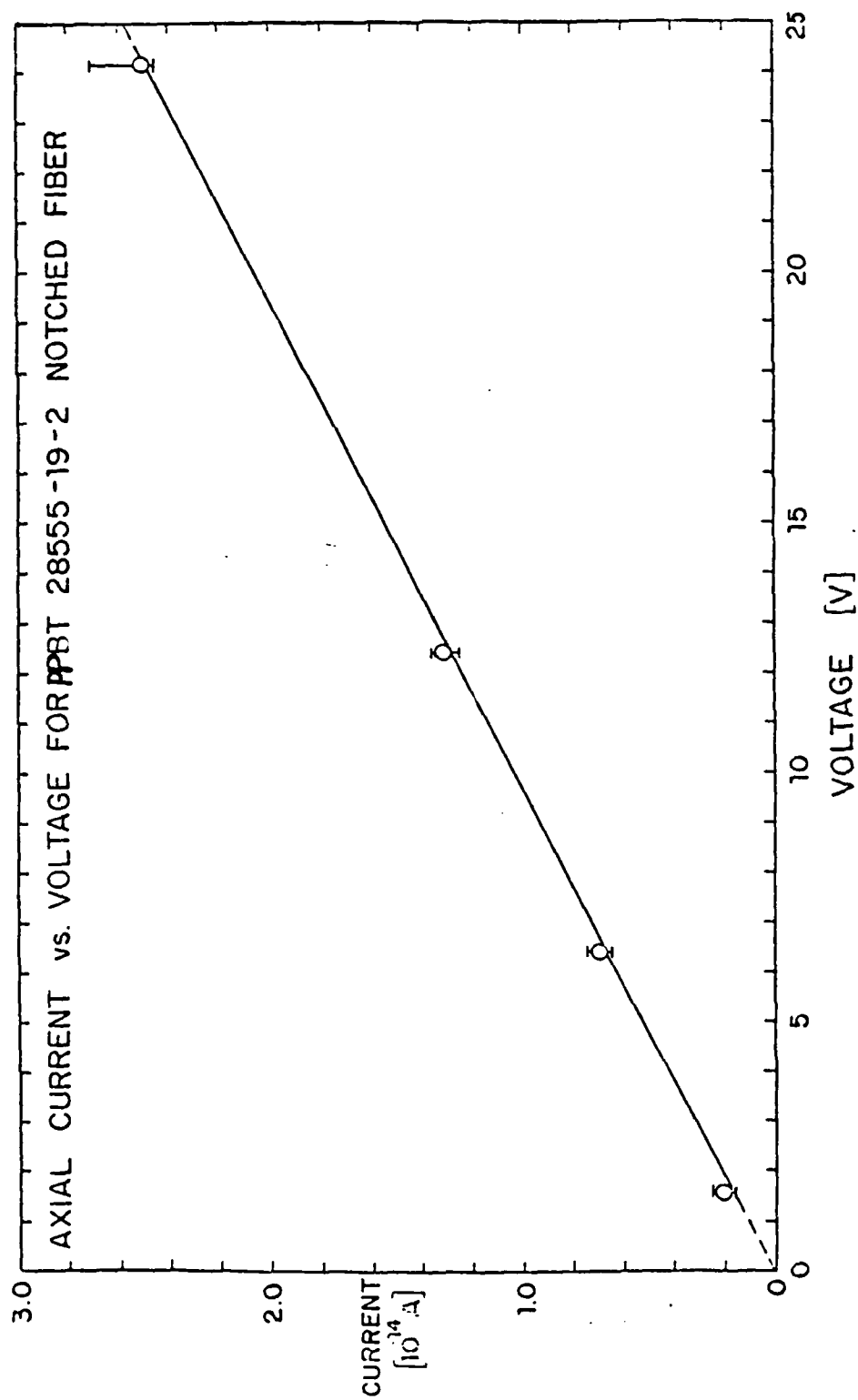


Fig. 45.

## NON-OHMIC ELECTRONIC PROCESSES


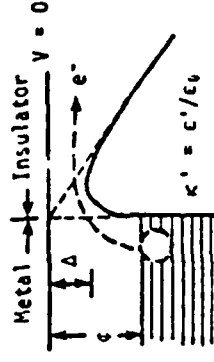

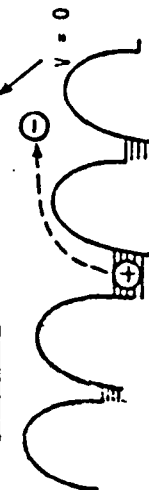
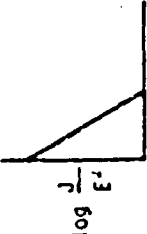
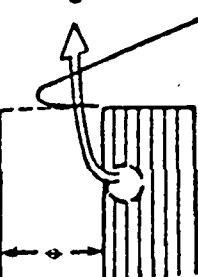
Name of Effect and Usual Test Plot	Descriptive Equations	Physical Interpretation
Schottky- (Richardson) Emission 	$\frac{J}{E} = \frac{A_R T^2}{E} \exp \left[ \frac{B_S E^{1/2} - \phi}{kT} \right]$ $A_R = 1.2(10^6 \text{ A/m}^2)$ $B_S/k = 0.44/\sqrt{kT}$	 Field Assisted Hopping over Image Barrier at Cathode
Poole-Frenkel Effect 	$\frac{J}{E} = A_R T^2 E^{-1} \exp \left[ \frac{B_P E^{1/2} - \phi}{kT} \right]$ $A_R = 1.2(10^6 \text{ A/m}^2)$ $B_P/k = 0.88/\sqrt{kT}$ $B_P = 2B_S$	 Field Assisted Electron-Hole Separation within Bulk of Sample
Fowler-Nordheim Emission 	$\frac{J}{E} = 1.54(10^{-6}) \frac{E}{\phi} \exp \frac{-6.8}{(10^{-9})} \frac{\phi^{3/2}}{E}$ (No Explicit Dependence on Temperature)	 Quantum Tunneling through Image Barrier

Fig. 46.

## NON-IONIC IONIC PROCESSES


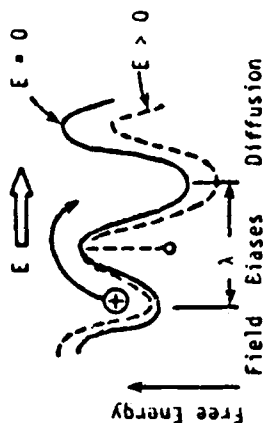
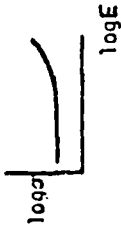
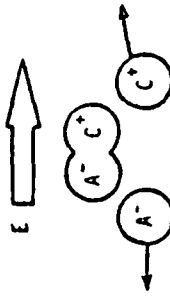
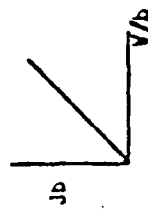
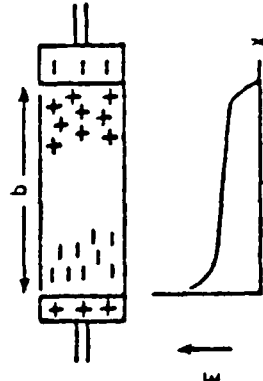
Name of Effect and Typical Test Plot	Descriptive Equations	Physical Interpretation
Modified Stern-Eyring Rate Theory 	$\sigma = \frac{J}{E} = n u q$ $u = \frac{D q}{k T} \left[ \frac{e^{\Delta W} - e^{-(n-1)W}}{W} \right]$ $W = E q \lambda / k T$	 <p>Free Energy</p> <p>Field Eases Diffusion</p> <p><math>E = 0</math></p> <p><math>E &gt; 0</math></p> <p><math>\lambda</math></p>
Onsager Theory 	$\frac{\sigma(E)}{\sigma(0)} = \left\{ \frac{-2iJ_1(if)}{f} \right\}^{1/2}$ $f = 88.1 T \sqrt{E/\kappa}$ $E \text{ in [V/m]}$	 <p>Field Tends to Separate Ions before They Recombine, Dissociation Enhanced</p>
Space-Charge-Limited Conduction 	$\text{If } v = uE, \frac{J}{E} = \frac{9}{8} \epsilon_0 u \frac{V}{b^2}$ $\text{If } v = \sqrt{\frac{2eV}{m}}, \frac{J}{E} = \frac{4}{9} \epsilon_0 \left( \frac{2e}{m} \right)^{1/2} \frac{V^{1/2}}{b}$	 <p>Separated Ion Clouds Perturb Field</p>

Fig. 47.

### C. Anisotropy

Within the ohmic region, the conductivity can be calculated from Eq. (5),  $\sigma = Ib/VA$ . Due to imperfections in the samples, this should be a lower limit. At a temperature of 22°C and at 0% relative humidity ( $R \sim 0\%$ ), the order of magnitude of axial conductivity  $\sigma_{||}$  is  $10^{-12} \Omega^{-1} \text{cm}^{-1}$  and that of transverse conductivity  $\sigma_{\perp}$  is  $10^{-18} \Omega^{-1} \text{cm}^{-1}$ . Their ratio is  $(\sigma_{||}/\sigma_{\perp}) \approx 10^6$ . Actually,  $(\sigma_{||}/\sigma_{\perp})$  is a function of temperature. At temperature of 505°C, which is above the decomposition temperature of PPBT (51),  $(\sigma_{||}/\sigma_{\perp})$  equals to unity. In the absence of other considerations, this large ratio implies that PPBT might be a one-dimensional electronic conductor such as Tetracyanoplatimate with a ratio of  $10^5$ . This is thought to be consistent with the molecular geometry of the polymer which leads to an extended chain conformation. If PPBT is an electronic semiconductor in this sense, then it is likely that compression by a large hydrostatic pressure would reduce the band gap and greatly increase  $\sigma$ . Whether a sample could resist stress without fracture is a moot question.

Two monoclinic unit cells have been proposed to relate to the anisotropic properties of PPE by Thomas et al. of the research group at the University of Massachusetts (12). Figures 48 and 49 are the schematic arrangements of PPBT in

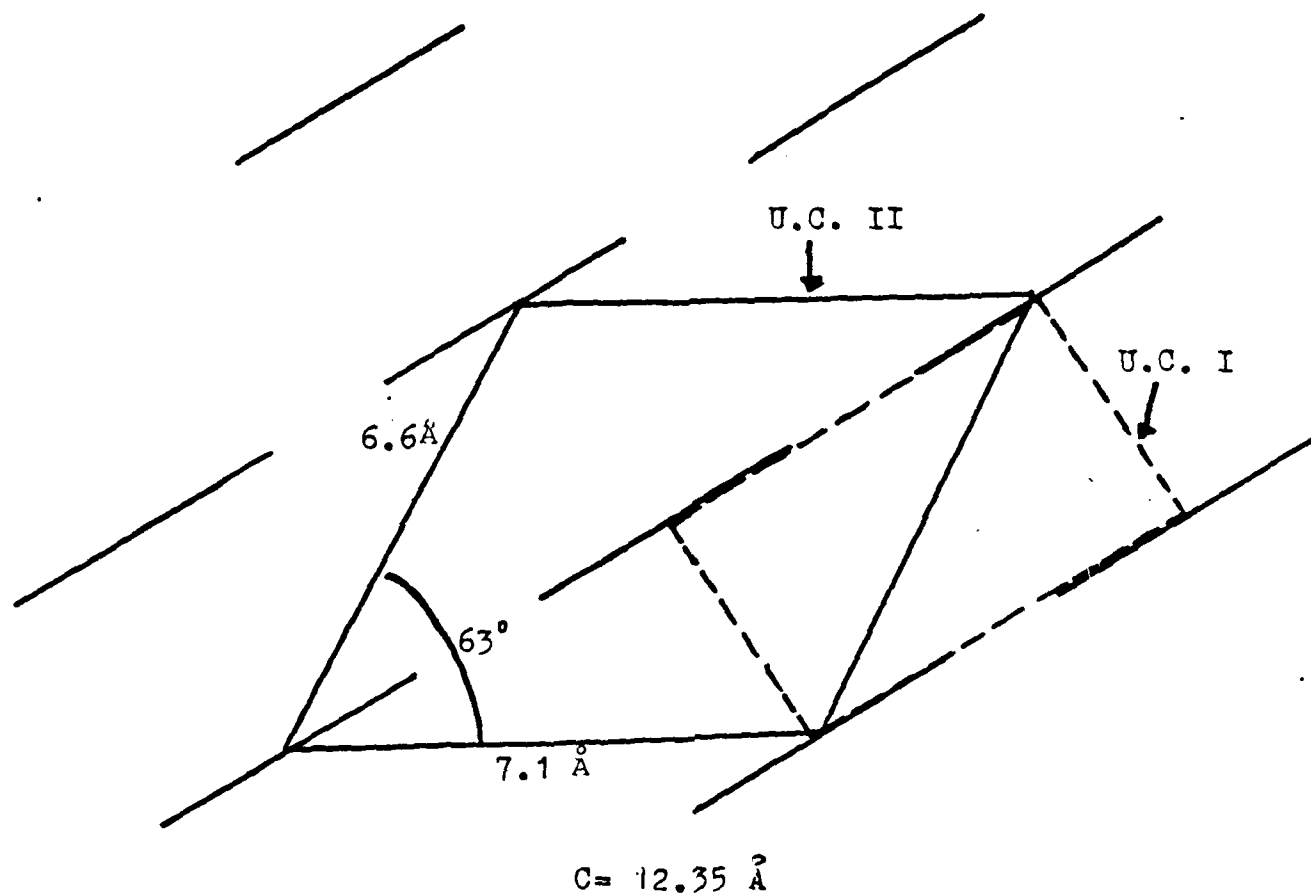


Fig. 48. Possible unit cells of the PPBT crystal structure (projection down the  $\underline{c}$  axis).

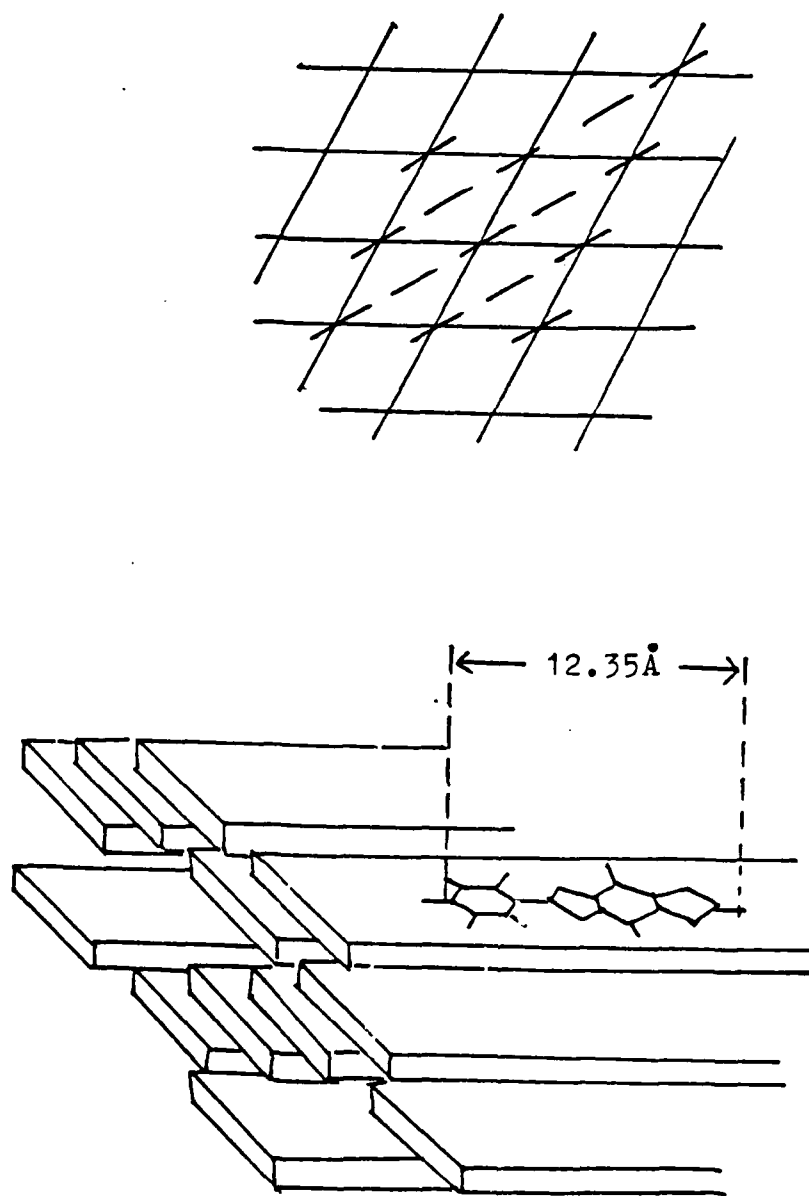


Fig. 49. Schematic of the proposed arrangement of PPBT molecules in a crystallite.

its crystal structure. The dimensions of these proposed unit cells are listed below:

Monoclinic Cell I

Monoclinic Cell II

$$a' = 5.83 \text{ \AA}$$

$$a = 7.10 \text{ \AA}$$

$$b' = 3.54 \text{ \AA}$$

$$b = 6.65 \text{ \AA}$$

$$c' = 12.35 \text{ \AA}$$

$$c = 12.35 \text{ \AA}$$

$$\gamma = 96^\circ$$

$$\gamma = 63^\circ$$

$$z = 1$$

$$z = 2$$

Unit cell I corresponds to a very simple arrangement of parallel sheets whereas Unit Cell II would allow more possibilities. Both unit cells have the same calculated density of  $1.69 \text{ g/cm}^3$ , which matches the observed density of approximately  $1.6 \text{ g/cm}^3$  for a fiber without macroscopic voids. From the data above, the charge mobility  $\mu$  can be approximately estimated in both axial and transverse directions.

The mobility is the magnitude of the drift velocity (v) of charge carriers per unit electric field:

$$\mu = \frac{|v|}{E}. \quad (58)$$

The mobility is defined to be positive for both electrons and holes, although their drift velocities are opposite. If in terms of electrical conductivity  $\sigma$  and the assumption of a single type of mobile charge carrier, Eq. (58) can be rewritten as:



AD-A162 765

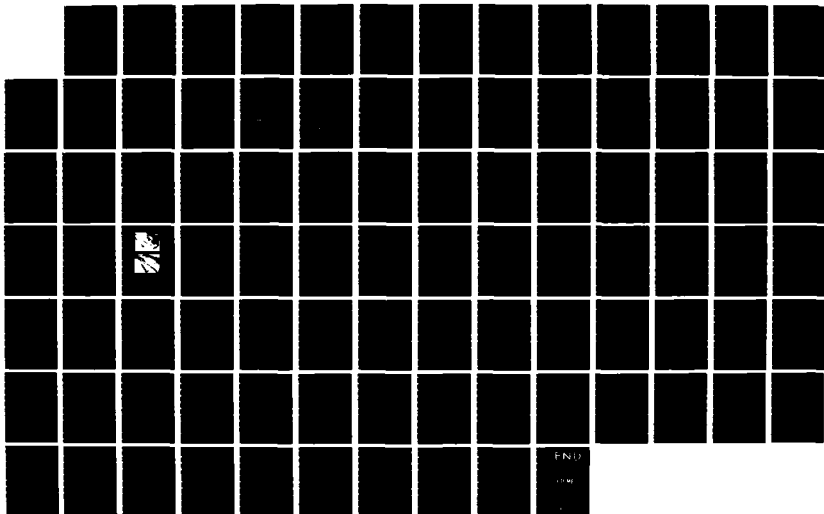
STUDY OF TRANSPORT PROPERTIES AND STRUCTURE OF  
EXTENDED-CHAIN POLYMERS (U) VIRGINIA UNIV  
CHARLOTTESVILLE DEPT OF MATERIALS SCIENCE  
R E BARKER ET AL SEP 85

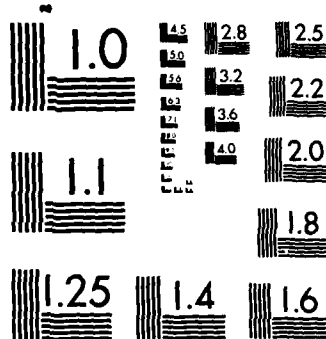
3/3

UNCLASSIFIED

F/G 11/9

NL





MICROCOPY RESOLUTION TEST CHART  
NATIONAL BUREAU OF STANDARDS-1963-A

$$\mu = \frac{\sigma}{nq}, \quad (59)$$

where  $n$  is the concentration of charge carriers and  $q$  is the charge per carrier. Now, assume that one electron per PPBT monomer involved in the conduction process, then  $n$  will be equal to the reciprocal of the volume of a PPBT monomer, i.e.  $n = 1/V_{\text{PPBT}}$ , and  $q = e = 1.60 \times 10^{-19}$  Coulomb. If the Unit Cell I is chosen to be the unit cell in this case, then

$$\begin{aligned} V_{\text{PPBT}} = V_{\text{Unit Cell}} &= [(5.83\text{\AA} \times 3.54\text{\AA}) \sin 96^\circ] \times 12.35\text{\AA} \\ &\approx 253.49(\text{\AA})^3 \approx 2.53 \times 10^{-22} \text{ cm}^3. \end{aligned}$$

Thus,  $n = 1/V_{\text{PPBT}} \approx 3.95 \times 10^{21} \text{ cm}^{-3}$ , and  $nq \approx 6.32 \times 10^2 \text{ C/cm}^3$ . The order of magnitude of the product of  $nq$  for PPBT is thus  $10^3 \text{ cm}^{-3} \text{ C}$ . At room temperature,  $\sigma_{||} \sim 10^{-12} \Omega^{-1} \text{ cm}^{-1}$  and  $\sigma_{\perp} \sim 10^{-18} \Omega^{-1} \text{ cm}^{-1}$ , therefore, from Eq. (59),  $\mu_{||}$  and  $\mu_{\perp}$  can be estimated as the following:

$$\begin{aligned} \mu_{||} &= \frac{\sigma_{||}}{nq} \sim 10^{-12} (\Omega^{-1} \text{ cm}^{-1}) / 10^3 (\text{cm}^{-3} \text{ C}) \\ &\sim 10^{-15} (\text{cm}^2/\text{V-sec}), \end{aligned}$$

$$\text{and } \mu_{\perp} = \frac{\sigma_{\perp}}{nq} \sim 10^{-18} (\Omega^{-1} \text{ cm}^{-1}) / 10^3 (\text{cm}^{-3} \text{ C})$$

$$\sim 10^{-21} (\text{cm}^2/\text{V-sec}).$$

These values are very small compared to the electron mobility in metallic copper ( $35 \text{ cm}^2/\text{volt-sec}$  at room temperature) (52). Even compared to the mobilities of general polymers,  $\mu \sim (10^{-4}-10^{-11}) \text{ cm}^2/\text{volt-sec}$ ; these values are still very small. It now appears that the estimate of  $n$  was much too large. A technique should be developed to measure mobilities directly for better understanding of conduction mechanisms. For example, Kaura and Nath (53) used a surface-charge decay technique to determine mobilities of pure and iodine doped polyvinylidene fluoride ( $\text{PVF}_2$ ). Their estimates were  $\mu_{\text{pure PVF}_2} \sim 8 \times 10^{-11} \text{ cm}^2/\text{V-sec}$ , and  $\mu_{\text{iodinated PVF}_2} \sim 10^{-8} \text{ cm}^2/\text{V-sec}$ . In this regard it is instructive to consider the Nernst-Einstein-Towensen relation

$$\mu kT = qD$$

between ionic mobility and diffusion coefficient. At  $300^\circ\text{K}$ ,  $\mu \approx 40D$  if  $q = e$ . Thus for example, if  $D = 10^{-10} \text{ cm}^2/\text{S}$  we obtain  $\mu \approx 4 \times 10^{-8} \text{ cm}^2/\text{V-S}$ .

#### D. Thermal activation of electrical conductivities

By measuring currents passing through PPBT samples at various temperatures,  $\log I$  vs.  $10^3/T$  curves were obtained with typical results as indicated in Figures 50 and 51. Since Eq. (5) was used to calculate  $\sigma$ , for a given experiment,  $b/VA$  was constant so that the same relationship

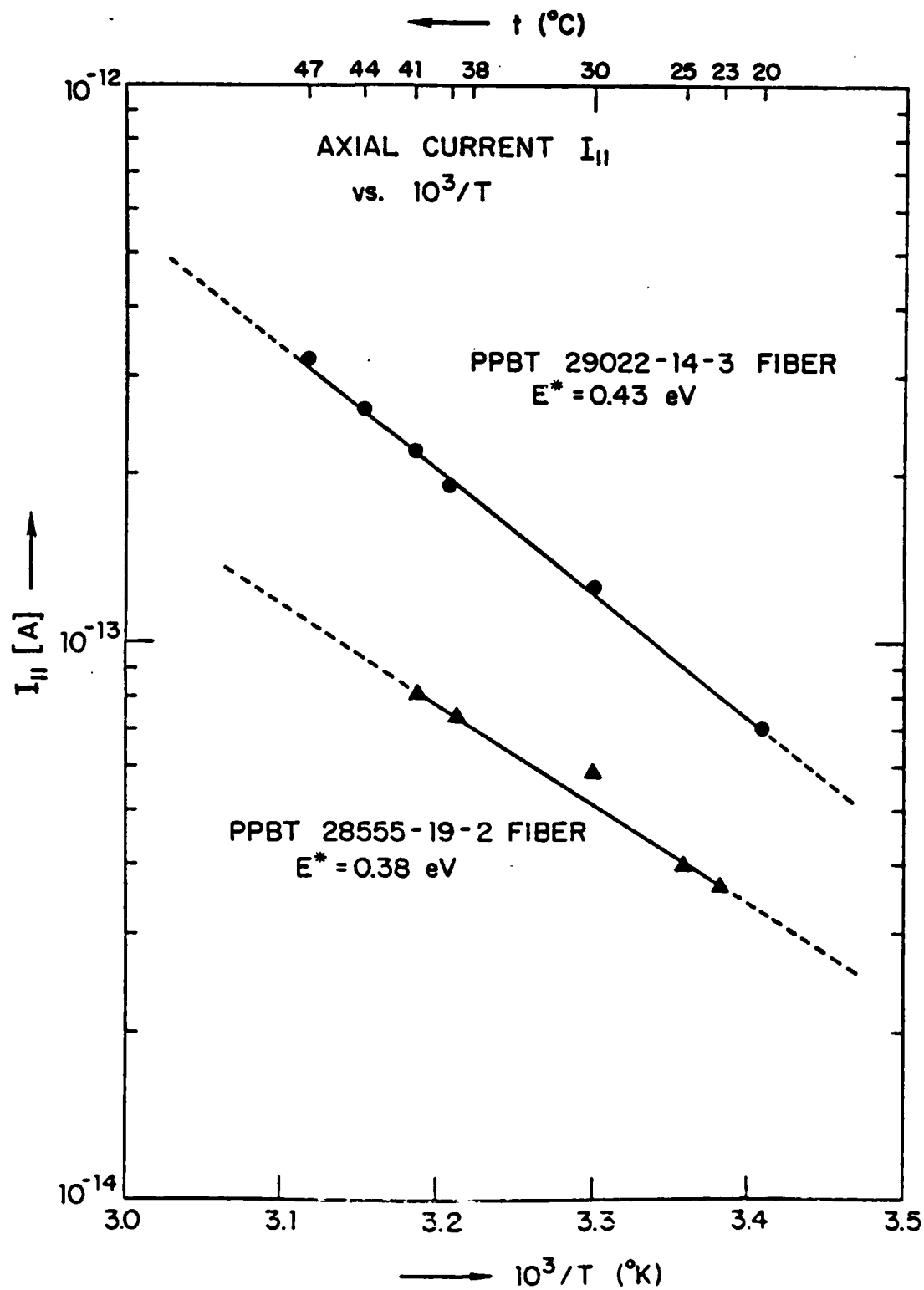


Fig. 50. Axial current vs.  $10^3/T$  for PPBT fibers.

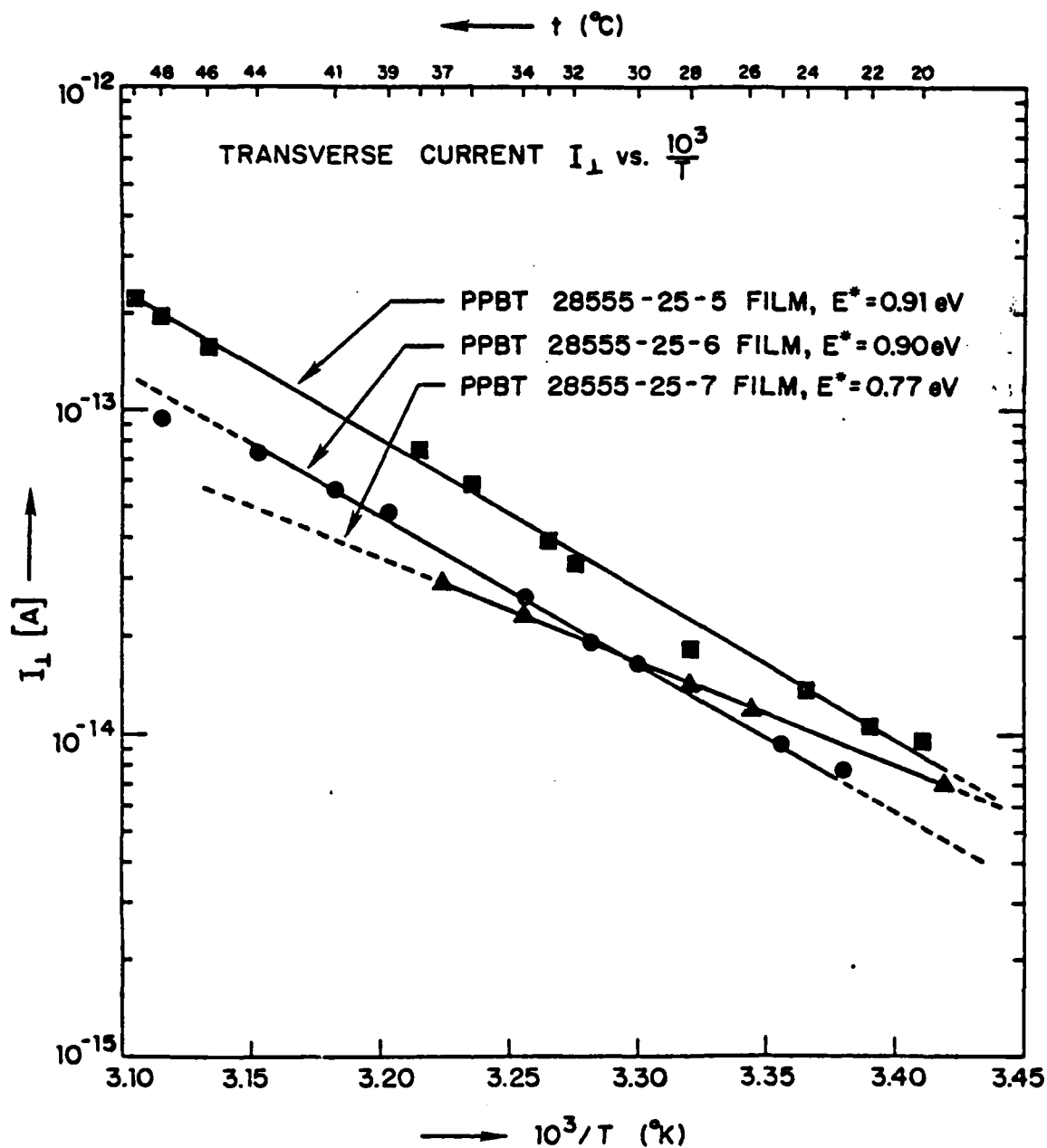


Fig. 51. Transverse current vs.  $10^3/T$  for PPBT films.

between I and T would be applicable to  $\sigma$  and T. Thus, the relation

$$\sigma = \sigma_0 \exp(-E^*/RT) \quad (60)$$

is maintained, where  $\sigma_0$  is the value of  $\sigma$  extrapolated to  $1/T = 0^\circ\text{K}^{-1}$  and R is the gas constant. Typical ranges of the values of  $E_{||}^*$  and  $E_{\perp}^*$  for PPBT samples are listed below (at R.H.  $\sim 0\%$ ).

$E_{  }^*$	$E_{\perp}^*$
<u>8.8 <math>\sim</math> 9.9 kcal/mol</u>	<u>18 <math>\sim</math> 21 kcal/mol</u>
or (0.38 $\sim$ 0.43 eV)	(or 0.77 $\sim$ 0.91 eV)

The differences in parameters for PPBT samples are thought to be due to different processing histories. The ratio of  $(E_{\perp}^*/E_{||}^*) \sim 2$  is in accord with the idea that charge transfer is easiest along the chains, i.e. the barrier for charge transfer between fibers is greater than the barrier for interchain charge movement.

In conjunction with the response to humidity, these thermal activated processes indicate that PPBT should be an ionic conducting material (15). On the other hand, the extreme anisotropy implies that PPBT might be an electronic conductor. Thus, a tentative conclusion that the conduction mechanism in PPBT is a mixture of ionic and electronic conduction was made. Further experimental data and theoretical ideas to support this conclusion will be discussed in Chapter V and Chapter VI. In terms of an energy gap interpretation,  $E_{\text{gap}} = 2E^*$  so that  $(E_{||})_{\text{gap}}$  is about 0.80

eV which is less than half of the theoretical value calculated by Bauhmik (18),  $E_{||,gap} = 1.73$  eV (see Chapter II). This is of little surprise because Bauhmik has assumed that electronic conduction was the only conduction mechanism in PPBT.

#### E. Effects of additives and processing on electrical conductivities

As in the case of inorganic semiconductors and insulators, the question of whether or not spurious impurities can overwhelm and effectively mask the intrinsic behavior becomes important in these conductivity investigations. It is reasonable to speculate on the same situation for PPBT because of the presence of residual acids (methane sulfonic acid or polyphoric acid) and other species (such as water molecules). Thus, additives either used to neutralize residual acids or to serve as extrinsic impurities are going to affect the electrical conductivity. The processing history of PPBT samples is also a factor which affects the electrical conductivity of PPBT. All of these effects are discussed below.

##### (i) Effects due to moisture content

Figures 52 and 53 show that linear relationships between  $\log \sigma$  and  $R$  are maintained for both axial and



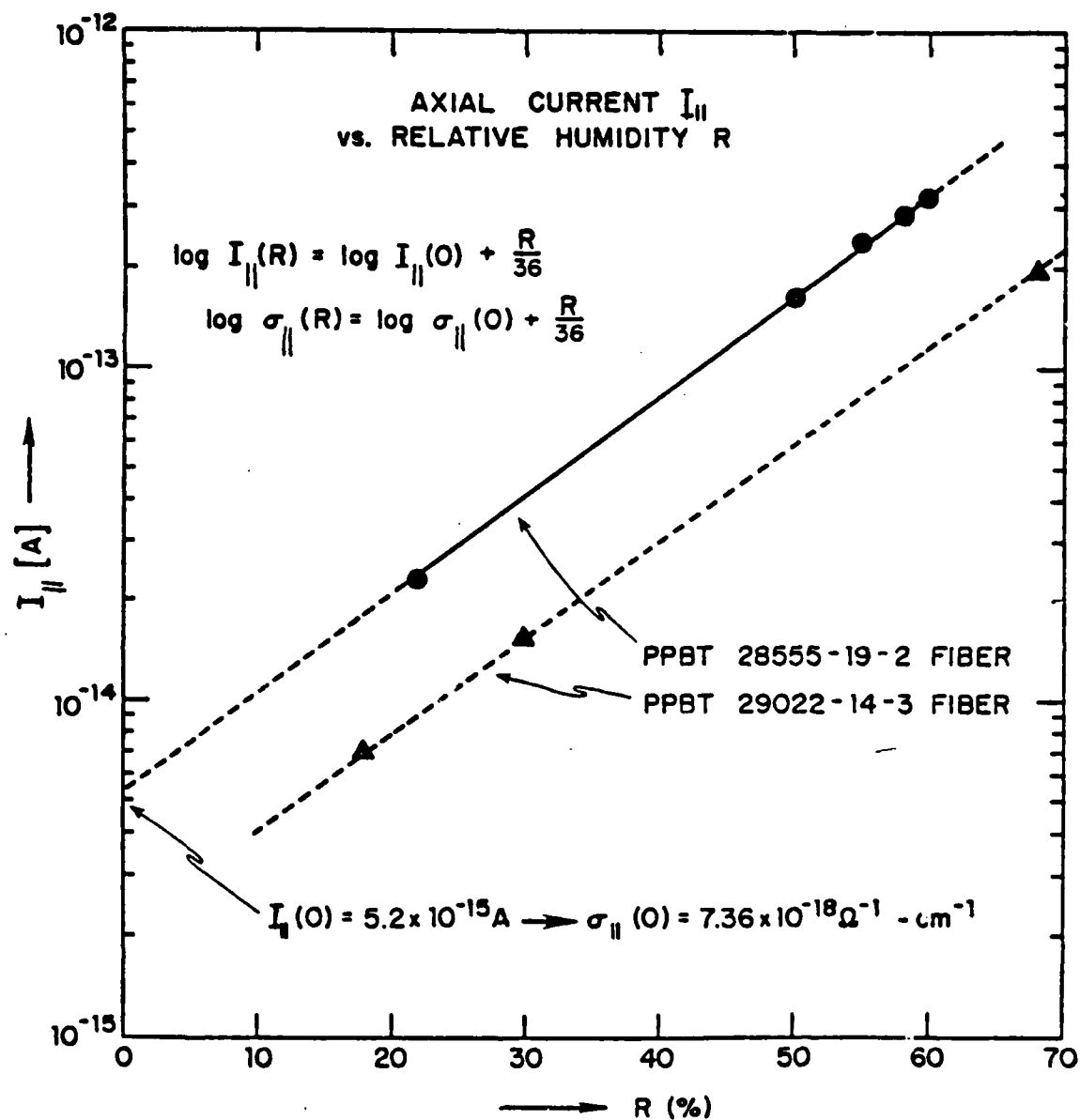


Fig. 52. Axial current vs. relative humidity for PPBT fibers.

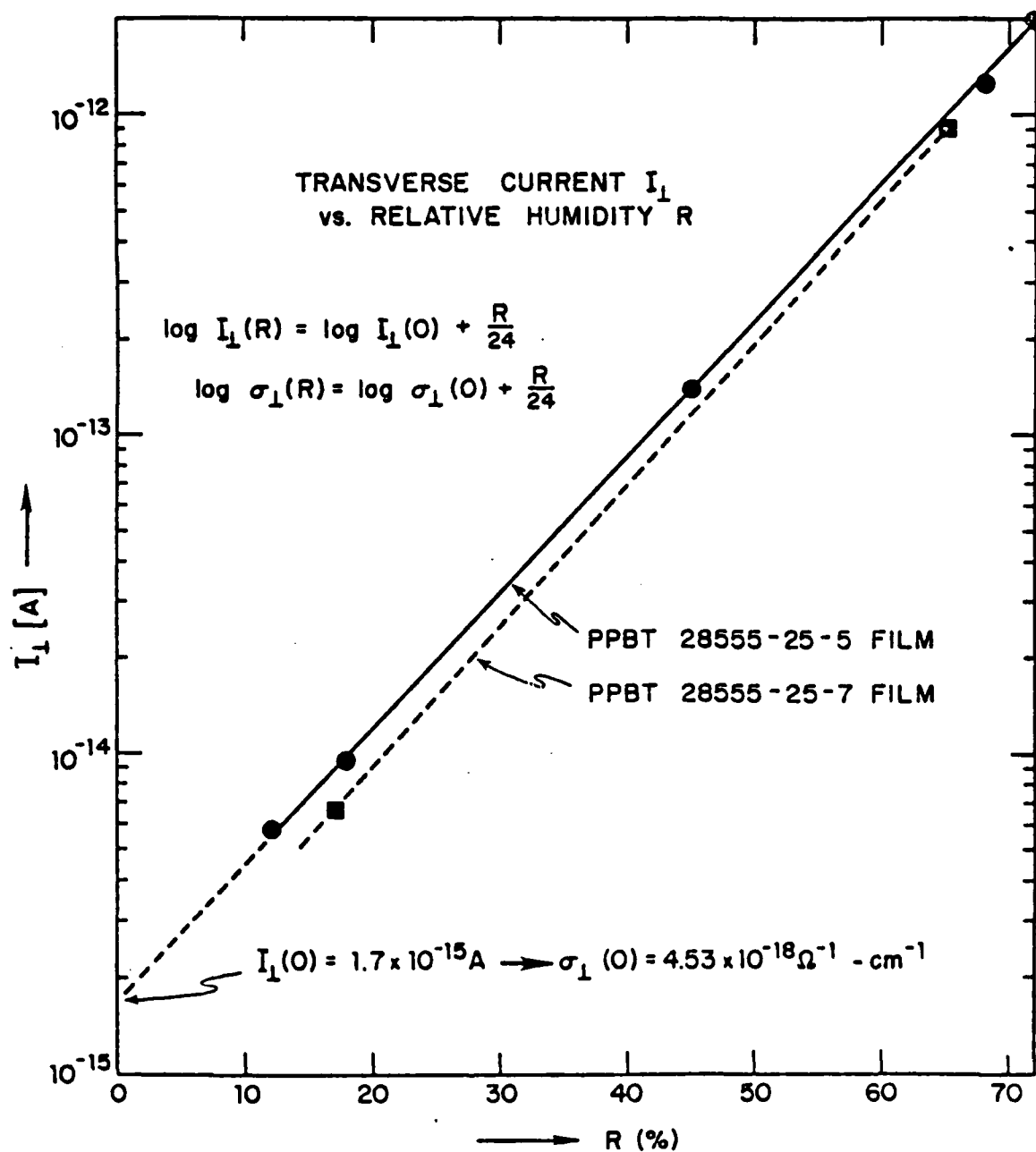


Fig. 53. Transverse current vs. relative humidity for PPBT films.

transverse directions, where  $R$  is the relative humidity (%). Two empirical equations,

$$\log \sigma_{||}(R) = \log \sigma_{||}(O) + R/36, \quad (61)$$

and

$$\log \sigma_{\perp}(R) = \log \sigma_{\perp}(O) + R/24, \quad (62)$$

were deduced from the experimental data. In the transverse case, the rate of change of  $\sigma_{\perp}$  due to the change of  $R$  is faster than that in the axial case, i.e.  $1/24 > 1/36$ . Although this fact does not appear to be usual, the data obtained are of great importance for the analysis using the "weak electrolyte model".

- (ii) Effects due to dopants used to neutralize residual acids:

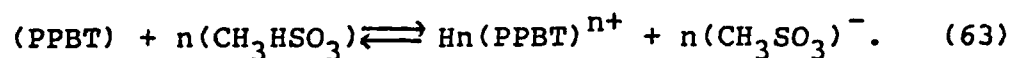
The PPBT samples were processed from methane sulfonic acid (MSA) or polyphoric acid (PPA) solutions. Although they were extensively washed with water, possible effects caused by the residue of these acids needed to be investigated. Ammonium hydroxide (Fisher A 669  $\text{NH}_4\text{OH}$ ) solution was used as the neutralization agent to neutralize the residual acids (54). Table 5 lists experimental results for both  $\text{NH}_4\text{OH}$  treated and untreated PPBT samples. The  $\text{NH}_4\text{OH}$  treated samples were immersed in the  $\text{NH}_4\text{OH}$  solution for different soaking periods and then air dried for

TABLE 5: PPBT 28555-25-6 HEAT TREATED AT 475°C FILM  
(NH<sub>4</sub>OH Solution Treated)

Time of Treatment	Time of Air Dry	$\sigma_{\perp}$
10 min.	24 hours	*
	40 hours	$1.54 \times 10^{-16} \Omega^{-1} \text{-cm}^{-1}$
	72 hours	$5.71 \times 10^{-17} \Omega^{-1} \text{-cm}^{-1}$
20 min.	2 hours	*
	24 hours	$1.83 \times 10^{-16} \Omega^{-1} \text{-cm}^{-1}$
	72 hours	$5.66 \times 10^{-17} \Omega^{-1} \text{-cm}^{-1}$
30 min.	12 hours	*
	60 hours	$2.6 \times 10^{-17} \Omega^{-1} \text{-cm}^{-1}$
	72 hours	$2.7 \times 10^{-17} \Omega^{-1} \text{-cm}^{-1}$
40 min.	60 hours	*
	72 hours	$5.4 \times 10^{-17} \Omega^{-1} \text{-cm}^{-1}$
1 hour	80 hours	$5.8 \times 10^{-17} \Omega^{-1} \text{-cm}^{-1}$

\* No data available because of the long settling period  
(over 24 hours).

various drying periods. After 72 hours of air drying (at 22°C and 40% RH), every treated sample had the same  $\sigma$  as that of an untreated sample. This fact led to the conclusion that the amount of residual acids in our "as received" samples was very small (virtually negligible) so that the electrical conductivity would not be affected. Otherwise the  $\sigma$  of a treated sample should be lower because residual acids (especially MSA) were going to protonate PPBT by the following reaction process (12):



The protonation products would strongly affect electrical conductivity measurements.

Absorbed  $\text{NH}_4\text{OH}$  evaporated during drying process and the corresponding  $\sigma$  gradually decreased. Further experimental data were used to support the conclusion that the quantity of residual acids was very small. An  $\text{NH}_4\text{OH}$  solution treated PPBT sample was placed in an oven at 120°C for an hour. The measured  $\sigma$  of this sample was the same as that of an untreated sample at 0%R, Table 6. During the oven drying process,  $\text{NH}_4\text{OH}$  was decomposed into  $\text{NH}_3$  gas and  $\text{H}_2\text{O}$  vapor at 120°C, i.e.



TABLE 6:  $\text{NH}_4\text{OH}$  SOLUTION TREATED SAMPLES\* Fisher A669  $\text{NH}_4\text{OH}$  Solution

[II] PPBT 28555-25-6 as Cast Film

Type of Treatment	$\sigma_{\perp}$	<u>Treated</u> Untreated
Untreated (40% R.H.)	$4.3 \times 10^{-17} \Omega^{-1}\text{-cm}^{-1}$	
Oven Dry (2 hours) at $120^{\circ}\text{C}$	$5.9 \times 10^{-18} \Omega^{-1}\text{-cm}^{-1}$	0.14
$\text{NH}_4\text{OH}$ Treated Over- night then oven dried at $120^{\circ}\text{C}$ for 2 hours	$5.5 \times 10^{-18} \Omega^{-1}\text{-cm}^{-1}$	0.13

[III] PPBT 28555-25-6 Heat Treated at  $475^{\circ}\text{C}$  Film

Type of Treatment	$\sigma_{\perp}$	<u>Treated</u> Untreated
Untreated (40% R.H.)	$6.0 \times 10^{-17} \Omega^{-1}\text{-cm}^{-1}$	
Oven Dried	$4.3 \times 10^{-18} \Omega^{-1}\text{-cm}^{-1}$	0.07
$\text{NH}_4\text{OH}$ Treated Then Oven Dried	$3.6 \times 10^{-18} \Omega^{-1}\text{-cm}^{-1}$	0.06

The sample treated by this procedure can be thought of as an untreated sample exposed to a 0% relative humidity environment. This further confirms that the presence of residual acids is negligible.

(iii) Effects due to ethyl alcohol treatment:

Several PPBT fibers and a film were immersed in  $C_2H_5OH$  at  $22^\circ C$  for one minute and then air dried for five minutes. The conductivities before the alcohol treatment ranged from  $4.3 \times 10^{-17} \Omega^{-1} cm^{-1}$  to  $2.3 \times 10^{-10} \Omega^{-1} cm^{-1}$  at  $22^\circ C$  and 40% R.H. After the treatment, with a good correlation, the conductivities were reduced by a factor of 1/4. [For the film  $\sigma_{vol}(treated)/\sigma_{vol}(untreated) = 0.4$  and  $\sigma_{surf}(treated)/\sigma_{surf}(untreated) = 0.25$ ], Table 7. A probable explanation for this phenomenon is that ethyl alcohol extracted water molecules and other ionic impurities out of PPBT samples. Hence the electrical conductivities turned out to be smaller, i.e. 1/4 of  $\sigma$  (untreated). Acetone was found to have the same effect.

(iv) Effects due to the treatment with salt solutions

From the experiments on the effects of moisture and ethyl alcohol treatments, the existence of an intrinsic dissociable ionic species in PPBT can be inferred. Thus, it is interesting to see what happens if aqueous solutions

TABLE 7:  
COMPARISON OF CONDUCTIVITY BEFORE AND AFTER WASHING SAMPLES WITH ETHYL ALCOHOL

PPBT Samples	Conductivities		
	Untreated ( $\Omega^{-1}\text{Cm}^{-1}$ )	Ethyl Alcohol Treated ( $\Omega^{-1}\text{Cm}^{-1}$ )	
28555-19-2	Fiber	5.28 x 10 <sup>-11</sup>	1.31 x 10 <sup>-11</sup>
29022-14-3	Fiber	1.17 x 10 <sup>-11</sup>	2.22 x 10 <sup>-12</sup>
27554-48-6	Fiber	2.03 x 10 <sup>-11</sup>	4.97 x 10 <sup>-12</sup>
27554-48-13	Fiber	2.33 x 10 <sup>-10</sup>	5.80 x 10 <sup>-11</sup>
28555-25-6	Film	4.30 x 10 <sup>-17</sup>	1.70 x 10 <sup>-17</sup>



of salts such as  $\text{LiCl}$ , and  $\text{CaCl}_2$  and  $\text{LaCl}_3$  are used to dope extrinsic ionic species into PPBT samples. Three experimental steps were performed: (1) the minimum-current-measurement, (2) the diffusion-controlled-current-measurement, and (3) the electrode-blocking-measurement step.

Typically, PPBT samples used for these experiments were immersed in salt solutions overnight and then put inside an evacuated desiccant jar to dry out the water. A conduction current was measured from this dried sample at  $\sim 0\%$  relative humidity environment (actually  $< 2\%$  on the hygrometer). The whole process corresponding to the minimum-current-measurement step was under dry conditions, i.e.  $R \sim 0\%$ . Thus, the quasi-limiting current measured this way can reasonably be considered as a minimum current.

After obtaining the minimum current  $I_{\min}$ , the PPBT sample was placed in an environment with  $R > 0\%$  to examine effects due to water diffusion. By plotting  $\Delta I/I_{\min}$  versus  $\sqrt{t}$ , where  $t$  is the time (minutes) elapsed during water diffusion and  $\Delta I$  is the differential current,  $(I - I_{\min})$ , the difference between current at time  $t$  and the minimum current, a set of curves was obtained for various PPBT samples with different salt solution treatments. Figures 54, 55, and 56 are plots for this type of experiment. The rising portions of the curves show the effect due to water diffusion. The water molecules which diffuse in tend to dissociate doped salt molecules into ions and thus enhance the conduction current toward a maximum value. This step,

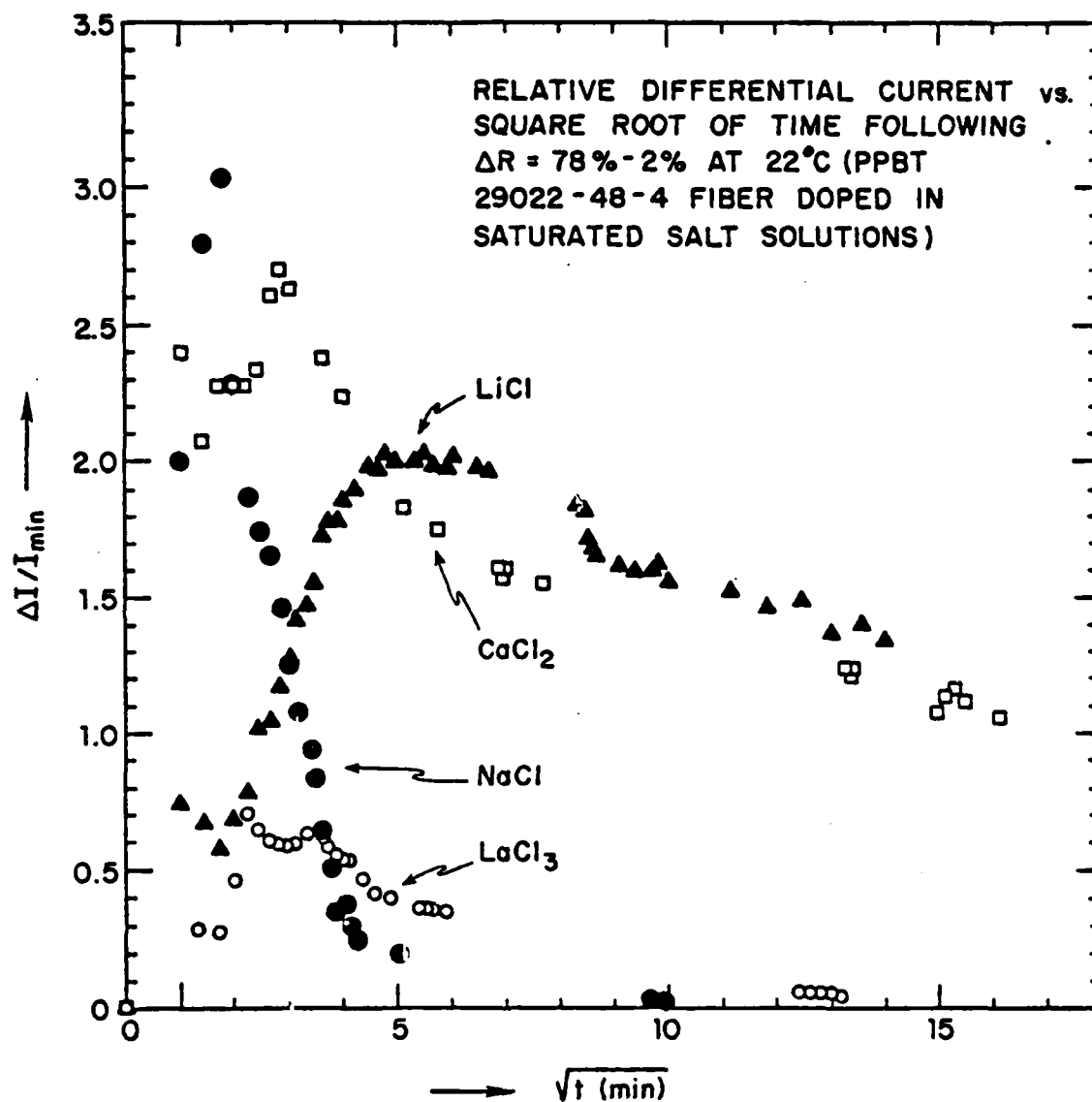


Fig. 54.  $\Delta I/I_{\min}$  vs.  $\sqrt{t}$  curves for PPBT 29022-48-4 fiber treated with various saturated salt solutions.

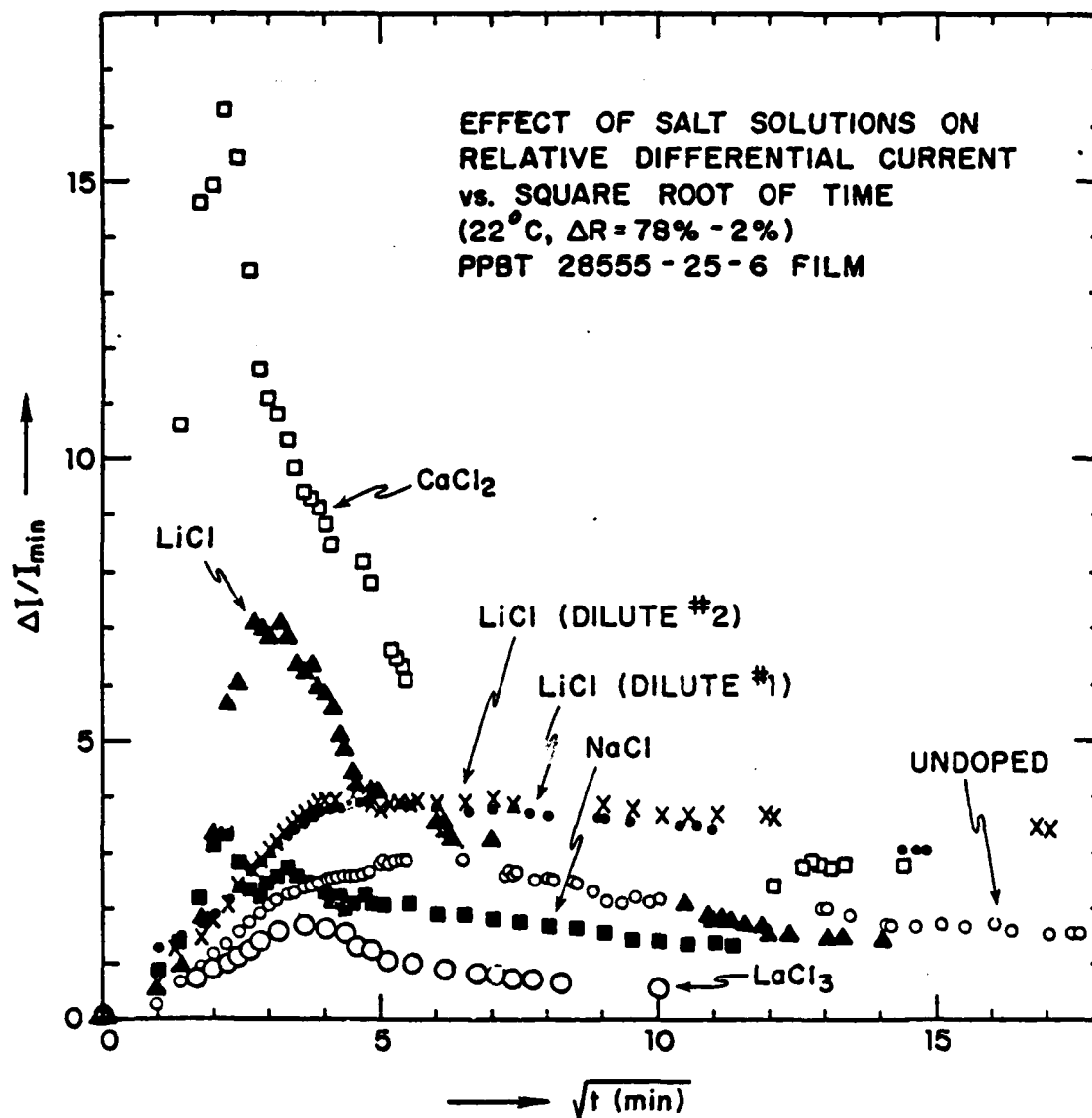


Fig. 55.  $\Delta I/I_{min}$  vs.  $\sqrt{t}$  curves for PPBT 28555-25-6 film treated with various salt solutions.

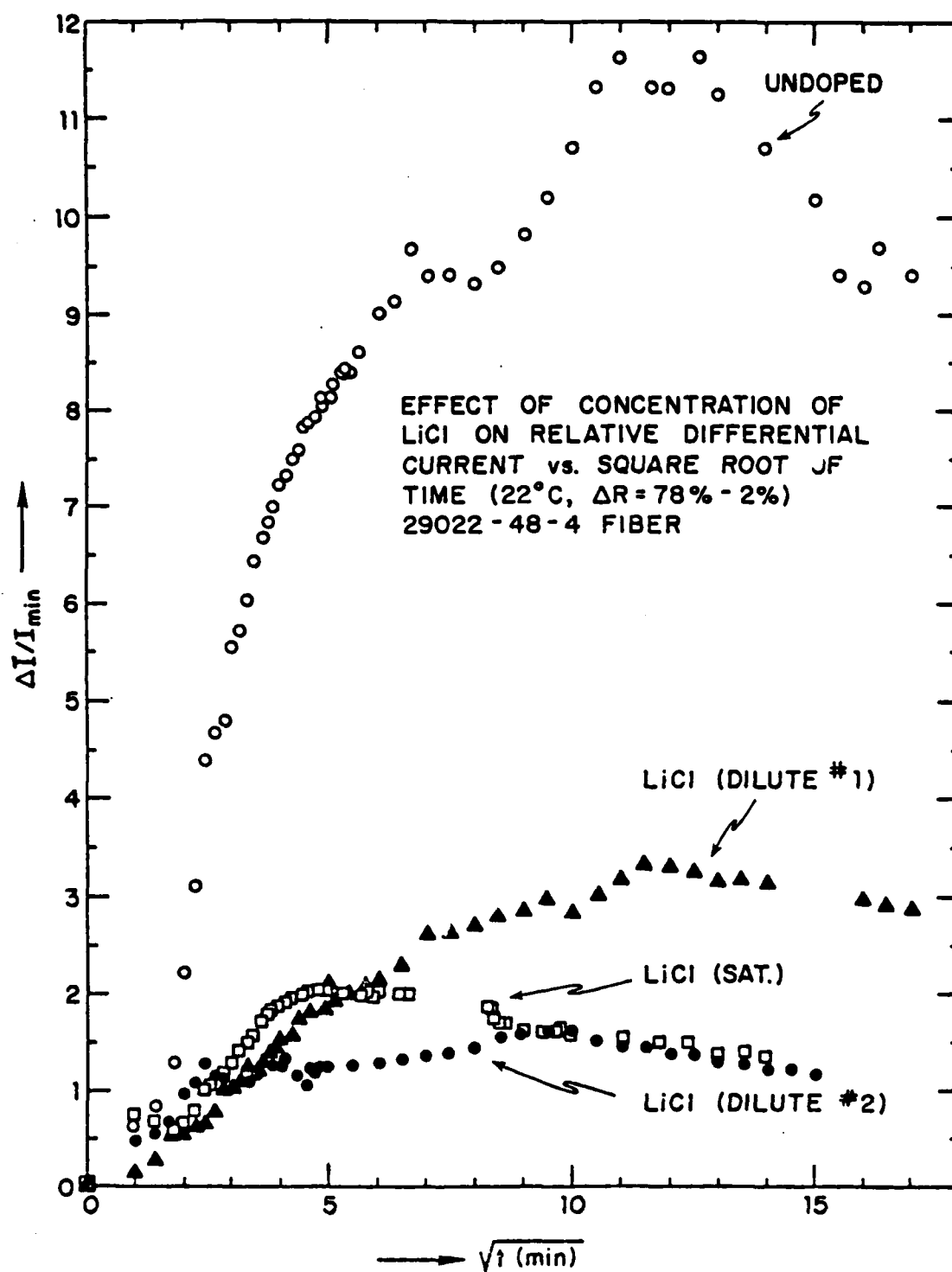


Fig. 56. Effect of concentration of LiCl on  $\Delta I/I_{\min}$  vs.  $\sqrt{t}$  for PPBT 29022-48-4 fiber.

which was referred to as the diffusion-controlled-current-measurement is analogous to a general diffusion process. After reaching the maximum value of current, the curve began to drop and continued to do so for a long time. This was the final step of the experiment. The main cause for the current decrease is the blocking process due to the interference with the movement of ions near electrodes during the application of an electric field. As this process goes on, the number of conducting ions available in the sample decreases and both electrodes are gradually blocked.

(v) Effects due to processing history

From the previous experiments, it has been shown that to our surprise there was no significant difference in the electrical conductivity of PPBT whether processed from MSA or PPA. For example, PPBT 29022-48-3 fiber with  $\sigma_{||,vol}^{(0)} \approx 7.8 \times 10^{-13} \Omega^{-1} \text{cm}^{-1}$  was processed from PPA solution, and PPBT 28555-19-2 fiber with  $\sigma_{||,vol}^{(0)} \approx 7.4 \times 10^{-13} \Omega^{-1} \text{cm}^{-1}$  was processed from MSA solution.

Another processing factor was the thermal history of the PPBT samples. The experimental result has shown that electrical conductivities were quite similar for both heat treated sample and untreated sample. For example, at 22°C and 40% relative humidity, PPBT 28555-25-6 film with  $\sigma_{\perp,vol}$  (untreated  $\approx 4.0 \times 10^{-17} \Omega^{-1} \text{cm}^{-1}$  and  $\sigma_{\perp,vol}$  (heat treated at

475°C)  $\approx 6.0 \times 10^{-17} \Omega^{-1} \text{cm}^{-1}$ . Therefore, processing history which is known to have a substantial effect on mechanical properties of PPBT (see Table 8)(55) but appears to have only a small effect on electrical conductivity of PPBT. It should be mentioned that the trend (toward higher  $\sigma$  after heat treatment) is what one would expect of electronic conduction but probably not for ionic (except perhaps protonic).

TABLE 8 (51): MECHANICAL PROPERTIES VS. PROCESSING HISTORY<sup>a</sup>

Processing Condition		Modulus (g/den)	Strength (g/den)
PPBT/MSA	As spun	350-1200	3-12
	Heat set	1000-2100	11-18
PPB/PPA	As spun	400- 600	4- 8
	Heat set	600-2100	6-20

<sup>a</sup> 1 g/den =  $1.41 \times 10^8$  N/M<sup>2</sup> for PPBT.

## Chapter V

## Weak Electrolyte Model (Ionic Conduction)

The experimental data presented in the preceeding chapter indicate that PPBT possibly conducts by both ionic and electronic transport processes. To rationalize this tentative conclusion, the Barker-Sharbaugh "Weak electrolyte model" is used.

Ionic impurities (tentatively assumed to be of the 1:1 type) in PPBT samples are presumed to become partially dissociated when moisture is introduced into a sample. To a first approximation, the dissociation energy is  $U_0 = (e^2/s) \approx 166 \text{ kcal/mol}$ , with  $s \approx 2\text{\AA}$  (56). But as the moisture content in a polymer changes, the effective dielectric constant  $K$  also changes. Due to this fact, an effective dissociation energy  $U'$  is defined as:

$$U' \equiv U_0/K. \quad (65)$$

Thus, Eq. (39) and Eq. (40) can be combined to obtain

$$\begin{aligned} \sigma &= \sigma_0 \exp\left[-\frac{1}{2kT} \left(\frac{U_0}{K} + B_M\right)\right] \\ \text{or,} \quad &= \sigma_0 \exp\left[-\frac{1}{2kT} (U' + B_M)\right]. \end{aligned} \quad (66)$$

Analogous to sorption experiments, moisture uptake should have an upper limit for a given material. The moisture uptake ( $\Delta m$ ) can be related to relative humidity



(R) as:

$$\Delta m = m_0 (1 - e^{-\alpha_m R}), \quad (67)$$

where  $m_0$  is the mass of the polymer which sorbed moisture and  $\alpha_m$  is a material parameter. The dependence of dielectric constant  $K$  can also be expressed in terms of  $R$  as:

$$K(R) = K(0) \exp(\alpha_K R), \quad \alpha_K \neq \alpha_m. \quad (68)$$

Figure 57 depicts schematic plots for  $\Delta m/m_0$  vs  $R$  and  $\epsilon(R)$  vs.  $R$ . Usually,  $\Delta m/m_0$  is quite small in polymeric materials. Hence, Eq. (67) can be approximated as:

$$\begin{aligned} \frac{\Delta m}{m_0} &= 1 - \exp(-\alpha_m R) \\ &\approx \alpha_m R - (\alpha_m R)^2/2 + \dots \quad (69) \end{aligned}$$

Similarly,

$$K(R) \approx K(0) (1 + \alpha_K R) + (\alpha_K R)^2/2 \quad (70)$$

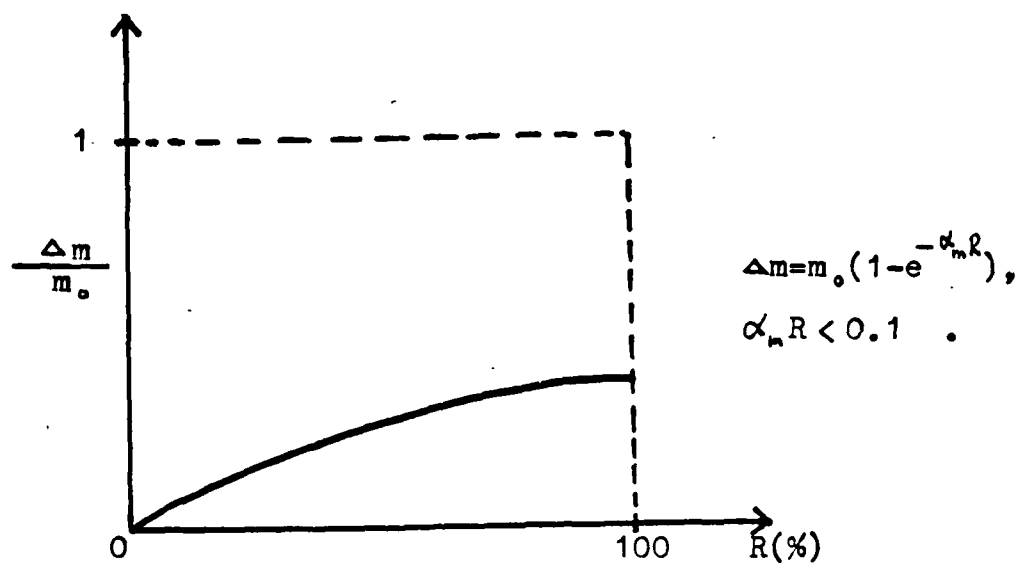
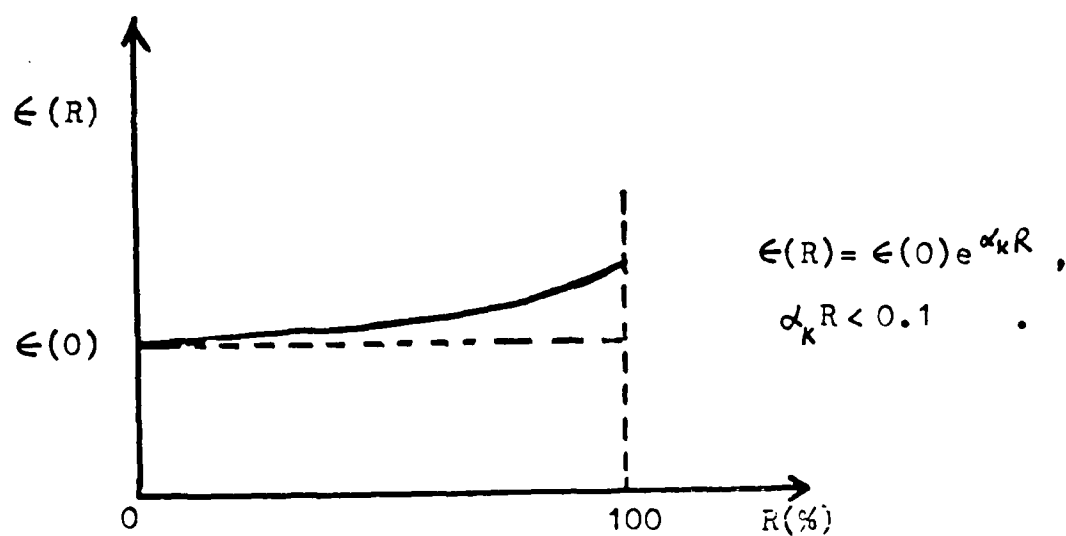
or, if only the first power terms are retained:

$$K(R) \approx K(0) (1 + \frac{\alpha_K}{\alpha_m} \frac{\Delta m}{m_0}). \quad (71)$$

Equation (66) can be rewritten as:

$$\sigma(R) = \sigma_0 \exp. \left\{ -\frac{1}{2kT} \left[ \frac{U_0}{K(0)} (1 - \sigma_K R) + B_M \right] \right\} \quad (72)$$

or,

(a)  $\Delta m/m_0$  vs.  $R$ (b)  $\epsilon(R)$  vs.  $R$ Fig. 57. Schematic curves for  $\Delta m/m_0$  and  $\epsilon(R)$  vs.  $R$ .

$$\ln \sigma(R) = \ln \sigma_o - \frac{1}{2kT} \left[ \frac{U_o}{K(O)} + B_M \right] + \left[ \frac{\alpha_K U_o}{2kTK(O)} \right] R. \quad (73)$$

By a comparison of Eq. (73) to Eqs. (61) and (62), the following relationship was obtained:

$$\ln \sigma(O) \equiv \ln \sigma_o - \frac{1}{2kT} \left[ \frac{U_o}{K(O)} + B_M \right], \quad (74)$$

and

$$\left[ \frac{\alpha_K U_o}{2kTK(O)} \right] = A_T, \quad (75)$$

where  $A_T$  is a dimensionless parameter which is constant at a given temperature  $T$ . Experimental results for  $A_T$  for axial and transverse measurements at 20°C are:

$$\left[ \frac{\alpha_K U_o}{2kTK(O)} \right]_{||} = (A_T)_{||} = \frac{2.303}{36} = 6.397 \times 10^{-2}, \quad (76)$$

and

$$\left[ \frac{\alpha_K U_o}{2kTK(O)} \right]_{\perp} = (A_T)_{\perp} = \frac{2.303}{24} = 9.596 \times 10^{-2}. \quad (77)$$

The ratio  $(A_T)_{\perp}/(A_T)_{||}$  gives

$$\frac{\alpha_{K\perp}}{K_{\perp}(O)} \frac{K_{||}(O)}{\alpha_{K||}} = 1.5.$$

$$\frac{K_{||}(O)}{K_{\perp}(O)} = 1.5 \frac{\alpha_{K||}}{\alpha_{K\perp}}. \quad (78)$$

Thus it may be inferred that the parameter  $\alpha_K$  which was introduced in Eq. (70), as though scalar properties

were involved, in fact plays a crucial role in the conversion of the originally scalar theory into a tensor form. Where as there appears to be no easy way to interpret the  $\alpha_m$  of Eq. (69) in any way except a scalar, although it can be viewed as a sum of coefficients  $\alpha_m = \sum_j (\alpha_m^j)$  for water absorbed into different types of sites, it does appear that  $\alpha_K$  may be interpreted to have components  $\alpha_{||}$  and  $\alpha_{\perp}$ , to represent the different ways that  $K_{||}$  and  $K_{\perp}$  respond to changes in moisture sorption. Basically, this is the reason why the rate of change of  $\alpha_{\perp}$  due to the change of R is faster than that of  $\alpha_{||}$  case.

There are neither experimentally measured values nor theoretically calculated values available for both  $K_{||}(0)$  and  $K_{\perp}(0)$ . But from several related sources (12, 20, 56, 60), the isotropic dielectric constant  $K_{iso}(0)$  of PPBT can be estimated to the  $K_{iso}(0) \approx 3.0$ . The details of this estimation are given in Appendix IV.

Since there are two transverse directions and one axial direction,  $K_{iso}(0)$  is the average of 2  $K_{\perp}(0)$  and 1  $K_{||}(0)$ , i.e.

$$\bar{K} = K_{iso}(0) = 1/3 [K_{||}(0) + 2K_{\perp}(0)]. \quad (79)$$

By solving the simultaneous equations of Eqs. (78) and (79),  $K_{||}(0)$  and  $K_{\perp}(0)$  were found to be:  $K_{||}(0) \approx 9\bar{K}q/(3q + 4)$  and  $K_{\perp}(0) \approx 6\bar{K}/(3q + 4)$  where  $q = \alpha_{||}/\alpha_{\perp}$ . Values calculated for a range of q-values are given in Table 9.

TABLE 9: PRINCIPAL DIELECTRIC CONSTANT VALUES

$$\text{VS } q = \alpha_{||} / \alpha_{\perp}$$

$q = \frac{\alpha_{  }}{\alpha_{\perp}}$	$K_{  }(0) = \left( \frac{27q}{3q+4} \right)$	$K_{\perp}(0) = \left( \frac{18}{3q+4} \right)$	$10^3 \alpha_{  }$	$10^3 \alpha_{\perp}$
0.5	2.456	3.273	1.10	2.20
1	3.857	2.571	1.73	1.73
2	5.400	1.800	2.42	1.21

In this Table, K is assumed to be 3.

Furthermore, it is interesting that the formation of the theory allows one to calculate  $K_{||}(0)$ ,  $K_{\perp}(0)$ ,  $\alpha_{||}$ , and  $\alpha_{\perp}$  if only  $\bar{K}$  and  $q$  are known. For example,  $A_{||}$  and  $A_{\perp}$  are obtained from the experimental slopes of  $\log \sigma$  vs  $R$  plots and then Eq. (76) gives:

$$\alpha_{||} = \left( \frac{2kT}{U_0} \right) A_{||} K_{||}(0) \quad (76)$$

so, at 20°C, if a value  $s = 2\text{\AA}$  is used for the spacing between monovalent charges then  $U_0 = 166 \text{ kcal/mol}$  (694 kJ/mol) and

$$\begin{aligned} \alpha_{||} &= \left[ \frac{2(1.986 \text{ cal mol}^{-1} \text{K}^{-1})(293 \text{ K})(6.397 \times 10^{-2})}{166 \times 10^3 \text{ cal/mol}} \right] K_{||}(0) \\ &= 4.48 \times 10^{-14} K_{||}(0) \end{aligned}$$

For the perpendicular component the corresponding result is  $\alpha_{\perp} = 6.73 \times 10^{-4} K_{\perp}(0)$ . Table 9 gives some of the values that result when  $\bar{K} = 3$  and for various values of  $q$ . A more complete vindication of the theory must await a detailed determination of the dielectric constants  $K_{||}$  and  $K_{\perp}$  vs.  $R$ . Wu-Song Huang's (50) estimate of  $\alpha_m (\sim 5.23 \times 10^{-23})$  already is available but  $K_{||} \simeq K_{||}(0) [1 + \alpha_K R]$  has not been measured yet.\*

---

\*If the ionic species are not of 1:1 type, then  $U_0$  might be greater than 166 kcal/mol. The greater  $U_0$  will lead to a smaller  $\alpha_K$  value. It is possible that  $\bar{K} = K_{iso}(0)$  has been over-estimated.

Values of  $(B_M)_\perp$  and  $(B_M)_\parallel$  could be calculated from Eq. (74) by using known values of  $K_\perp(O)$ ,  $K_\parallel(O)$ ,  $(\sigma_o)_\perp$ ,  $(\sigma_o)_\parallel$ ,  $\sigma_\perp(O)$ ,  $\sigma_\parallel(O)$ , and  $U_o$ . For purposes of illustration, the value  $q = 1$  will be assumed in the calculation of the  $B_M$ -values. From Fig. 52 and Fig. 53,  $\sigma_\parallel(O) = 7.36 \times 10^{-13} \Omega^{-1} \text{cm}^{-1}$ , and  $\sigma_\perp(O) = 4.53 \times 10^{-18} \Omega^{-1} \text{cm}^{-1}$ , and from Fig. 50 and Fig. 51,

$$(\sigma_o)_\parallel = 1.5 \times 10^{-4} \Omega^{-1} \text{cm}^{-1},$$

and

$$(\sigma_o)_\perp = 9.79 \times 10^{-2} \Omega^{-1} \text{cm}^{-1}.$$

Thus, at  $T = 20^\circ\text{C}$ ,  $(B_M)_\perp = -19.90 \text{ kcal/mol}$ , and  $(B_M)_\parallel = -20.17 \text{ kcal/mol}$  were calculated from Eq. (74). These two  $B_M$  values are very close which is consistent with the original symmetrical consideration of the  $B_M$  term. Therefore, the "Weak electrolyte model" is at the very least quite useful and self-consistent for representing the conductivity data for PPBT.

The conduction mechanism of PPBT can be inferred by the analysis of Eq. (74). Since

$$\ln \sigma(O) = \ln \sigma_o - \frac{1}{2kT} \left[ \frac{U_o}{K(O)} + B_M \right], \quad (74)$$

therefore,

$$\ln \left[ \frac{\sigma_{||}(O)}{\sigma_{\perp}(O)} \right] = \ln \left[ \frac{(\sigma_o)_{||}}{(\sigma_o)_{\perp}} \right] + \frac{1}{2kT} \left\{ U_o \left[ \frac{1}{K'_{\perp}(o)} - \frac{1}{K'_{||}(o)} \right] - \Delta B_M \right\} \quad (80)$$

where  $\Delta B_M = (B_M)_{||} - (B_M)_{\perp}$ . The first term on the right-hand side of Eq. (80),  $\ln [(\sigma_o)_{||}/(\sigma_o)_{\perp}]$ , will be interpreted as an electronic contribution because of the very dry conditions of the sample and because of its anisotropic nature, while the second term,  $1/2kT \{U_o [1/K'_{\perp}(O) - 1/K'_{||}(O)] - \Delta B_M\}$ , represents an ionic contribution term because it is consistent with ionic dissociation processes. According to Eq. (61) and (62), as  $R > 0$ , the ionic conduction processes will be predominant. But for a very dry state (i.e.,  $R \sim 0$ ), the electronic conduction process should play an important role. Further discussion about the electronic conduction nature of PPBT will be described in Chapter VI. In summary, the proposed conduction mechanism of PPBT is a mixture of both electronic and ionic conduction processes.



## Chapter VI

 $I_2$  Doping Experiments (Electronic Conduction)

On the basis of the analysis in terms of the "Weak electrolyte model", it appears that a certain level of electronic conduction exists in PPBT. To further pursue this hypothesis,  $I_2$  doping experiments were performed to investigate the formation of charge transfer complexes.

Two doping techniques, vapor-phase doping and solution-phase doping, were used in this investigation. In the vapor-phase doping, a vacuum system (see Figure 58) was constructed in which PPBT samples could be outgassed at elevated temperatures and then exposed to  $I_2$  vapor. In the solution-phase doping, PPBT samples were immersed in  $I_2$ /acetone solution at least for overnight. Upon iodination, the original reddish brown PPBT sample turned a shiny black, typical of charge-transfer complex formation. Due to the nature of PPBT samples, there is only a little spectroscopic information of charge transfer complexes. Figure 59 is the  $I_2$ -PPBT spectrum obtained with the aid of Prof. A.S. Brill with the Cary 14 spectrometer in the Physics Department of the University of Virginia. The figure shows that there is an absorption band between 500nm and 700nm for an iodinated PPBT 28555-25-6 film. Compared to the visible spectra of  $I_2$  vapor (61), Fig. (60), there is a shift of the absorption peak at 520nm to 570nm which is good experimental evidence that a charge transfer complex

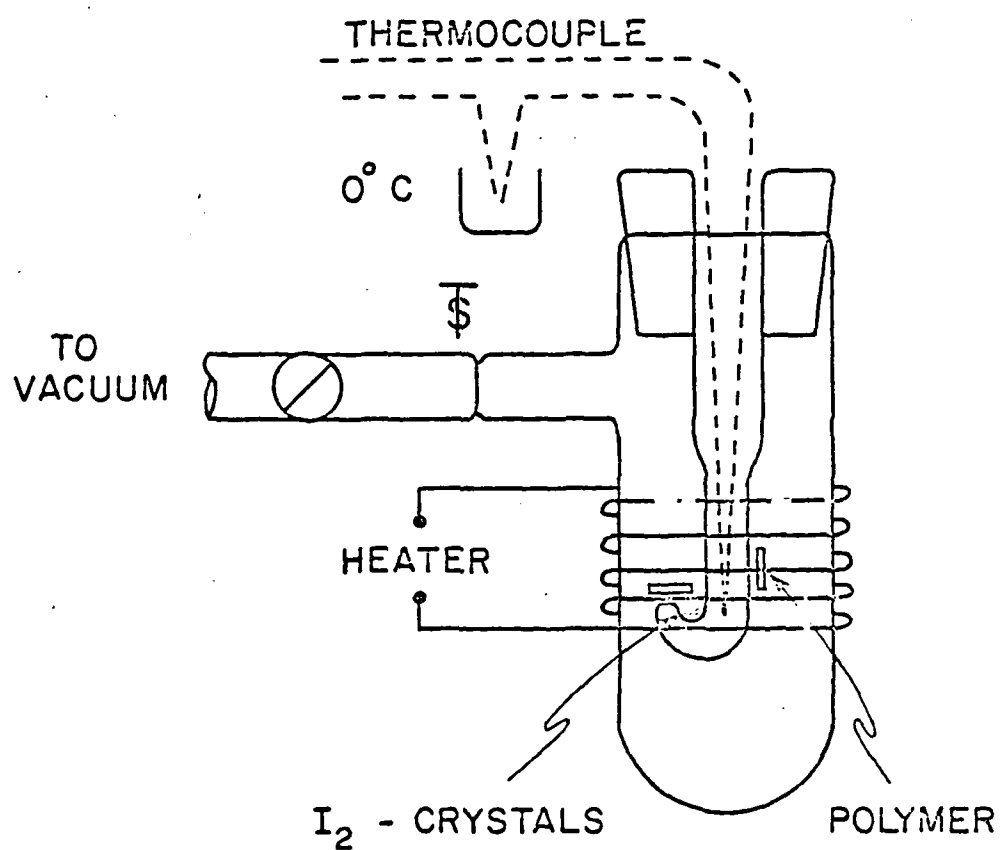


Fig. 58. APPARATUS FOR DOPING  
POLYMER SAMPLES

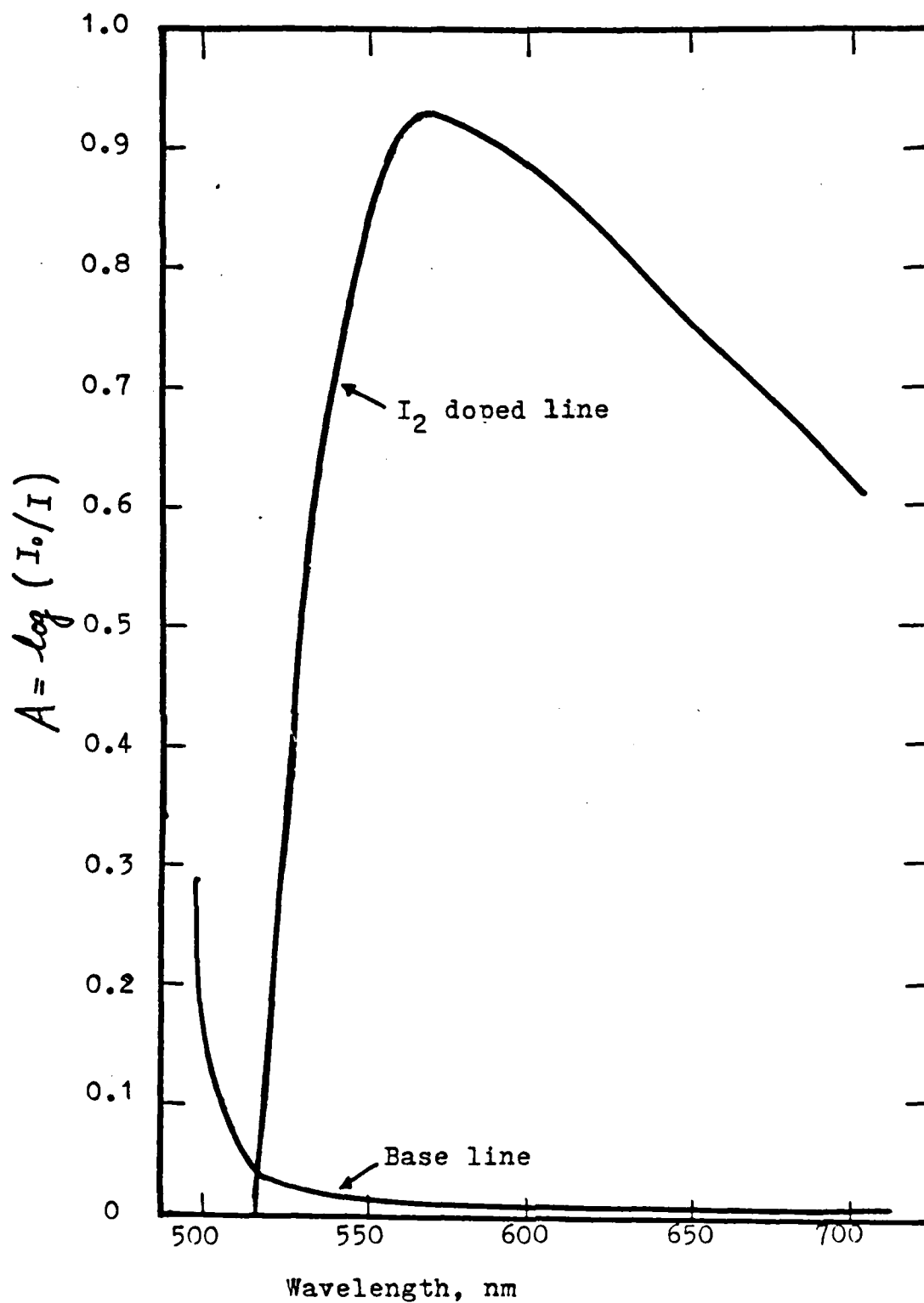


Fig. 59. Cary 14 spetrum for  $I_2$  doped PPBT 28555-25-6 film.

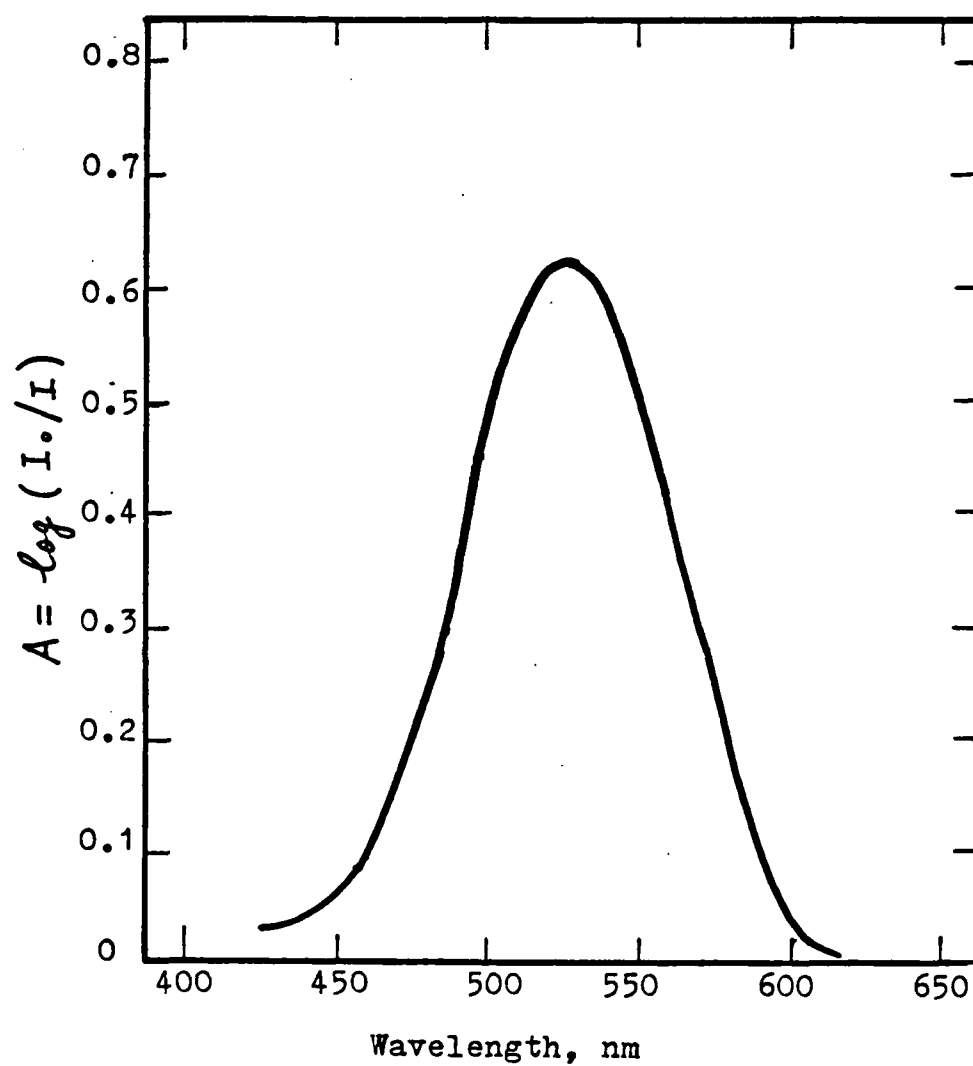


Fig. 60. From Liebhaufsky(61),  $10 \log(I_0/I)$  for  $16 \mu\text{mole/l}$  of  $\text{I}_2$  vapor in air at  $25^\circ\text{C}$ .

has possibly formed. According to this experimental evidence, Professor Brill (62) also predicted the formation of charge transfer complex from  $I_2$  doping. But for further spectroscopic confirmation, he suggested that PPBT samples should be synthesized in better form to accomodate the needs of the spectroscopic investigation. The reasons for this suggestion are based on the operational requirement for the Cary 14. The disadvantages of currently available PPBT samples for spectroscopy are:

- (1) PPBT samples are not sufficiently transparent;
- (2) The surface of PPBT is very rough;
- (3) The spectrometer, i.e. Cary 14, can just barely detect the "edge" of the whole spectrum;
- (4) Even a 20  $\mu$ m-thick PPBT sample is still too thick for the spectroscopic investigation and the thickness is somewhat irregular.

As mentioned in Chapter II, either or both of the aromatic rings in PPBT could presumably transfer an electron to an unoccupied energy level of the  $I_2$  molecule, resulting in an ionic bonding between  $I_2^-$  and the positively charged ring. Due to the tenuous attachment of the electrons, it is likely that they might move more readily in an electric field, especially in the presence of light, thus making the PPBT: $I_2$  complex somewhat like an n-type semiconductor or photoconductor. To support this idea, several measurements on iodinated PPBT samples have been

conducted. Figure 61 is the  $\log I$ - $\log t$  plot for a 1.05M ( $I_2$ /acetone) doped and an undoped PPBT (29022-48-4) fiber. It can be seen that the iodinated sample has a higher current at any time than that of the undoped sample. This transient phenomenon perhaps is due to the Maxwell-Wagner effect mentioned before. The concentration dependence on  $\sigma$  due to iodination is shown in Fig. 62. In this figure, the ratio ( $\sigma_{\text{iodinated}}/\sigma_{\text{undoped}}$ ) was used as the ordinate and the concentration  $C$  (M) and also the molar fraction  $C'$  (N) of  $I_2$ /acetone solution were used as the abscissa.

From Fig. 62, two implications can be readily made. First, the anisotropic nature is preserved, i.e. the increase of  $\sigma$  in the axial direction is faster than that in the transverse direction. This anisotropy is in good agreement with that diffusion process in PPBT should be anisotropic. Second, the enhancement rate of  $\sigma$  due to iodination is relatively slow compared to that of the well-known conducting polymer, polyacetylene, doped with  $AsF_5$ , Fig. 63, or the  $I_2$  doped polyphenylacetylene,  $\text{tC} = \text{C} - \text{C}_6\text{H}_4 -$ , Fig. 64, (44). This implies that only a small fraction of PPBT is involved in the formation of charge transfer complexes. In other words, there is only a very thin surface layer of a PPBT sample iodinated to form charge transfer complexes. Thus, a study of  $I_2$  diffusion in PPBT will be crucial to the understanding of this experiment. The study of  $I_2$  diffusion in PPBT should include the technique of subjecting an iodinated PPBT sample to a vacuum

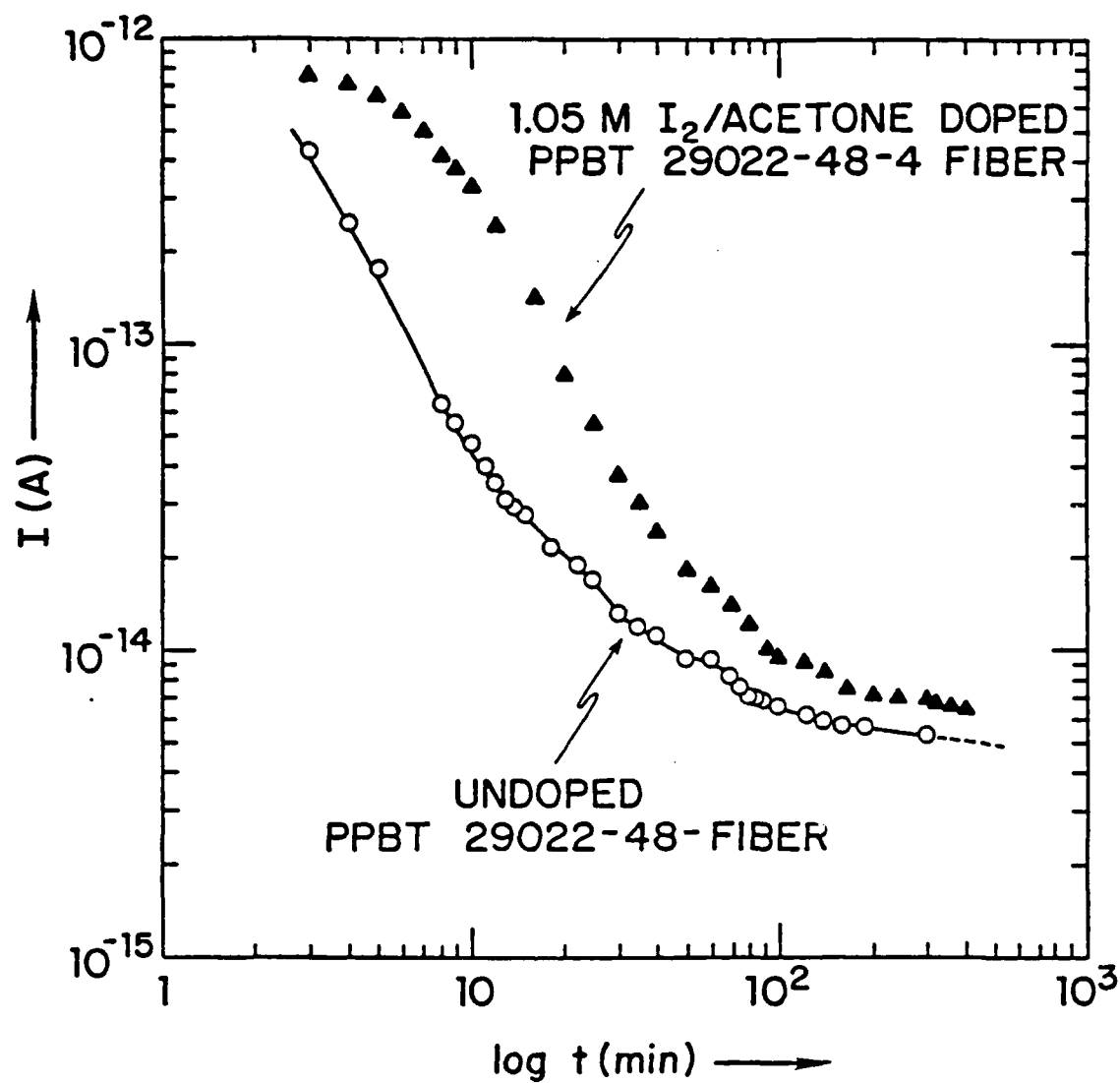


Fig. 61. Effect of iodination on transient currents.

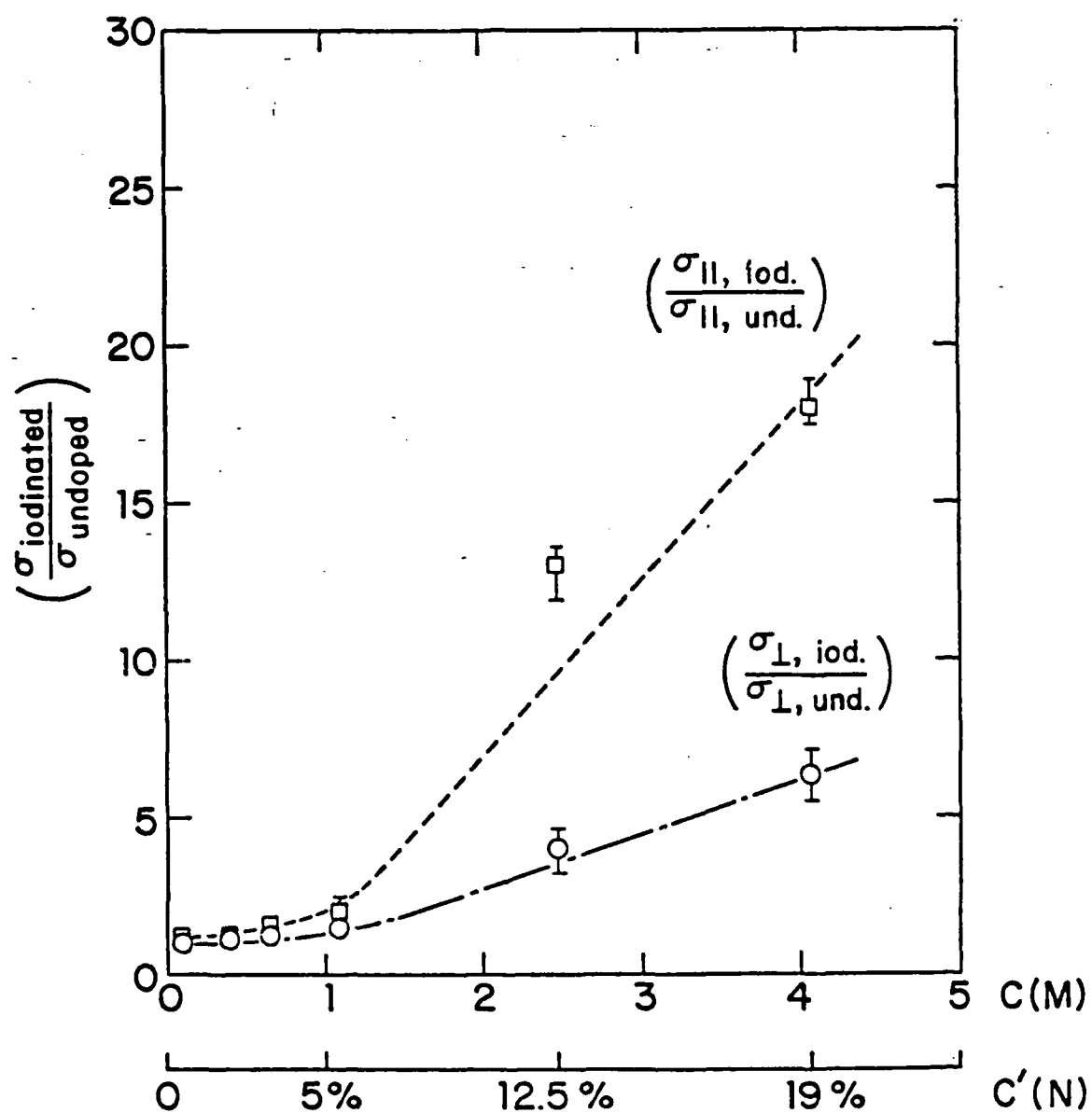


Fig. 62. Effect of iodination on  $\sigma$ .



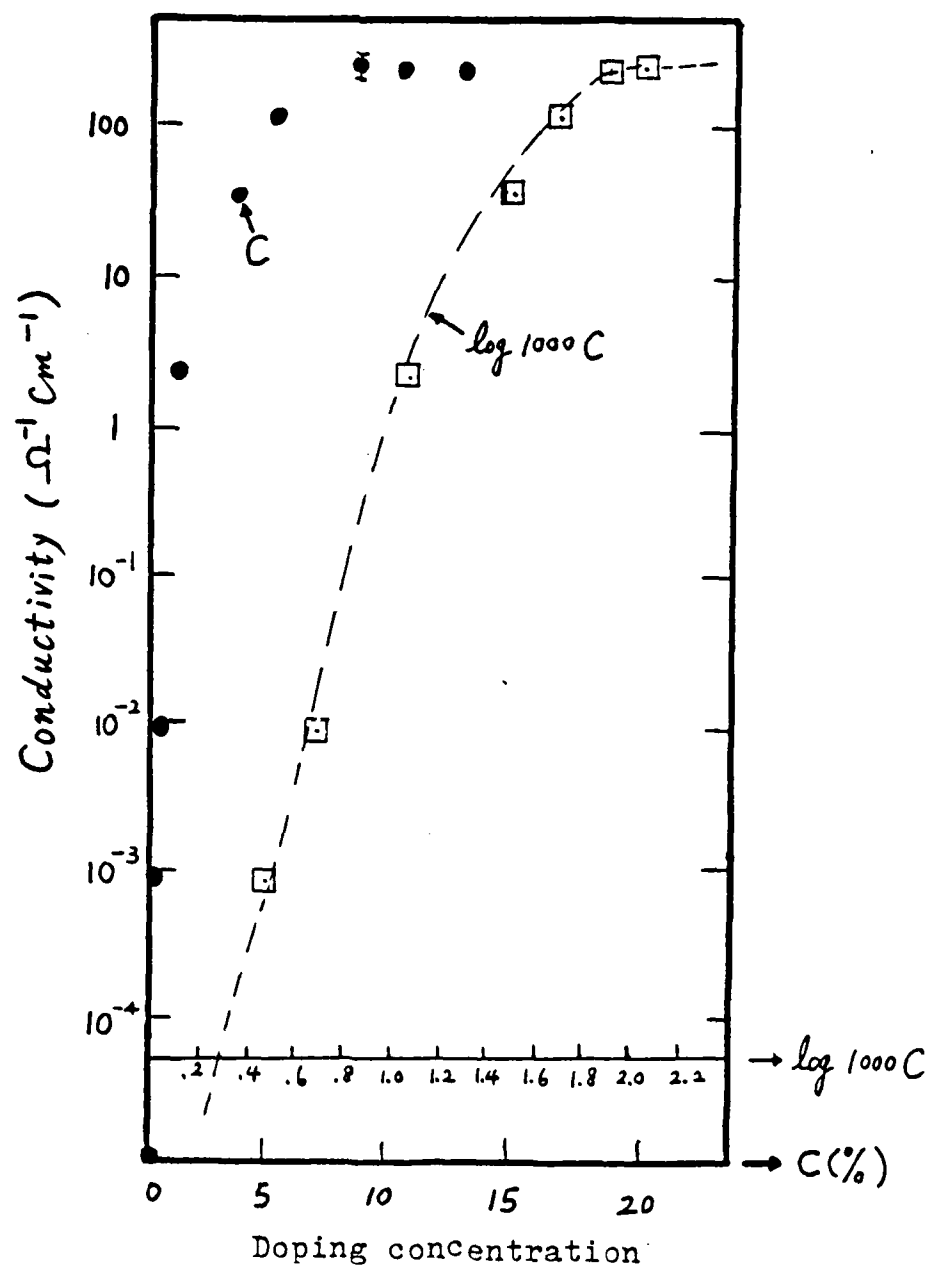


Fig. 63. Electrical conductivity of trans-polyacetylene film as a function of the doping concentration of  $\text{AsF}_5$  in molar percent.

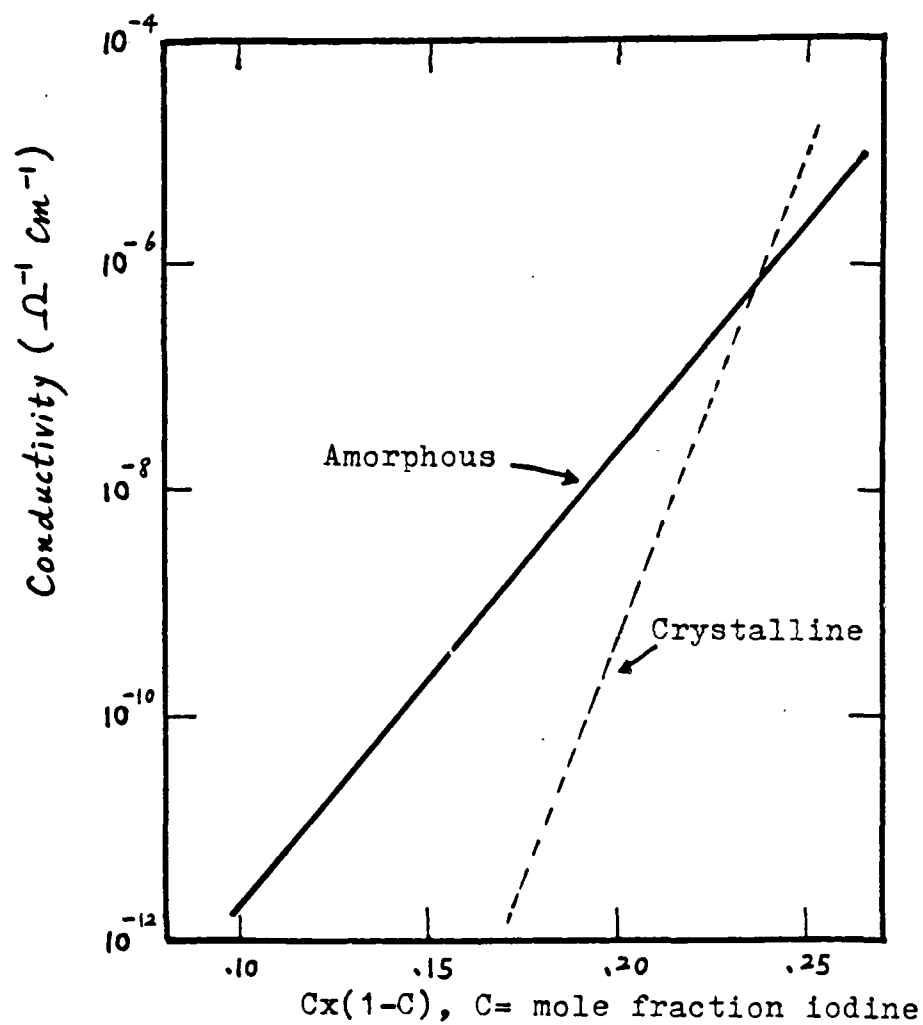


Fig. 64. Concentration dependence of conductivity for amorphous and crystalline cis-PPA.

and observing the iodine loss as a function of time. Hopefully, the penetration depth of  $I_2$  in PPBT samples can be deduced from this proposed diffusion study.

Two common problems accompany an  $I_2$  doping experiment: the surface contamination of  $I_2$  and the structural damage caused by  $I_2$ . The contamination problem is a source of scientific controversy. For example, the IBM San Jose group fears that non-uniformities at low doping levels produced by vapor-phase doping can confuse the interpretation of  $\langle CH \rangle_x$  data in the semiconducting region. McDiamid (63) countered by noting that his group had found samples lightly doped by gas-phase doping to exhibit properties identical to electro-chemically doped films. McDiamid concluded that the dopant is not, as some have suggested, confined to the surface of the fibrils. Rubner (64) also responded that there was no such problem in his experimental materials, polyphenylacetylene. He said that all samples, after iodination, had been washed with 100ml nitromethane solution to remove residual  $I_2$  particles on the sample's surface. But, to a certain extent, the nitromethane solution might also extract some of the absorbed  $I_2$ . Therefore, the doping could become non-uniform due to the extraction process.

The damage problem has been widely observed by many researchers. For example Rabolt, et al., (40,41) reported structural changes and a deterioration in the conductivity in  $I_2$  and  $AsF_5$  doped polyparaphenylenesulfide. Similar

morphological changes in PPBT also have been observed. Figure 65 shows electron micrographs of an undoped PPBT fiber and an  $I_2$  doped PPBT fiber. The doped sample was placed in the vacuum chamber of Fig. 58 and then exposed to  $I_2$  vapor at  $135^\circ\text{C}$  for 30 minutes. As can be seen in the micrographs, the iodine appears to have produced structural damage in the PPBT sample.

10  $\mu$ m

(a) Undoped sample

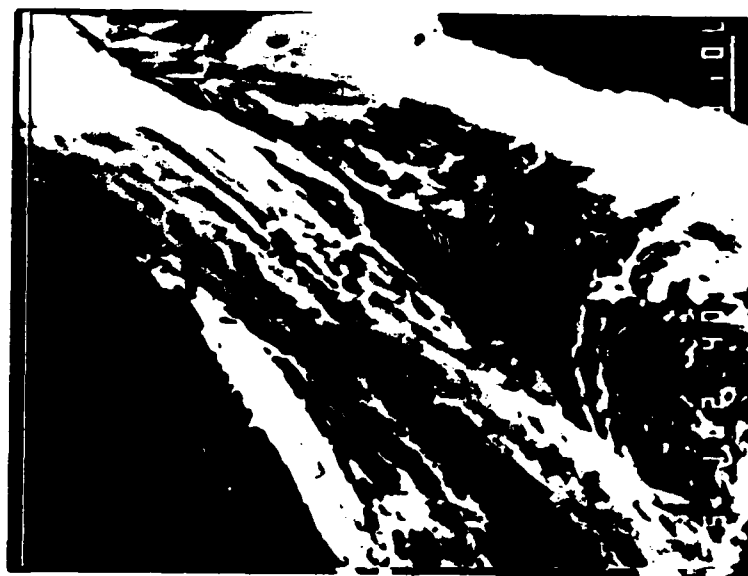
10  $\mu$ m(b) I<sub>2</sub> doped sample

Fig. 65. SEM micrographs of an undoped and a I<sub>2</sub> doped PPBT 28555-19-2 fibers.

## Chapter VII

### Future Research Possibilities and Applications

There are several practical motivations to understand the electrical behavior of polymers. For example, it would be very desirable to know the process of electrical breakdown on an insulator. To produce this understanding, it is essential to have a rather detailed description of the characteristics of the electrical processes in polymeric materials prior to breakdown and to then correlate severe electric potential (and radiation) conditions with their effect on the fundamental electrical nature of the insulator. Another practical motivation is engaging possibilities of creating inexpensive but effective polymeric semiconductors and plastic-metals. Current progress has proved encouraging and it is believed that the basic principle necessary to achieve the goal are beginning to be understood. In this chapter, certain special applications and future research possibilities relating to these two aspects will be discussed.

#### A. Electron-Microscopic Technique for Measuring $\sigma$ :

To overcome the difficult problems imposed by the nature of the currently available PPBT samples, a technique that looks promising has been conceived. Briefly, the

central idea for this technique is to charge one end of a polymer fiber by scanning the SEM (scanning electron microscope) beam across it and then to use the decaying deflection of the beam to measure the decrease of the surface charge as it leaks through the fiber to a conducting base in which the fiber is mounted. Figure 66 shows the arrangement of the sample in the SEM beam. Electrons leave the electron gun at a potential  $-V$  and move toward a spot on the sample holder platform. A short polymer fiber which protrudes a distance  $b$  out of a conducting base is rotated into the beam to have its end charged and is then rotated so that its axis is perpendicular to the original path of the electrons. The distance  $b$  is assumed small compared with the fiber radius  $r$ . For this condition, the electric field perpendicular to the beam will be

$$\epsilon_x = q_s / 2\epsilon_0, \quad (81)$$

where  $q_s$  is the charge per unit area of the end of the fiber. The change in momentum of an electric field will be given by

$$\Delta P_x = \int_0^t F_x \cdot dt \approx \int_0^t e \epsilon_x dt. \quad (82)$$

The effective interaction time for the force  $F$  is taken to be the transit time  $t \approx 2r/v_0$  of an electron moving past

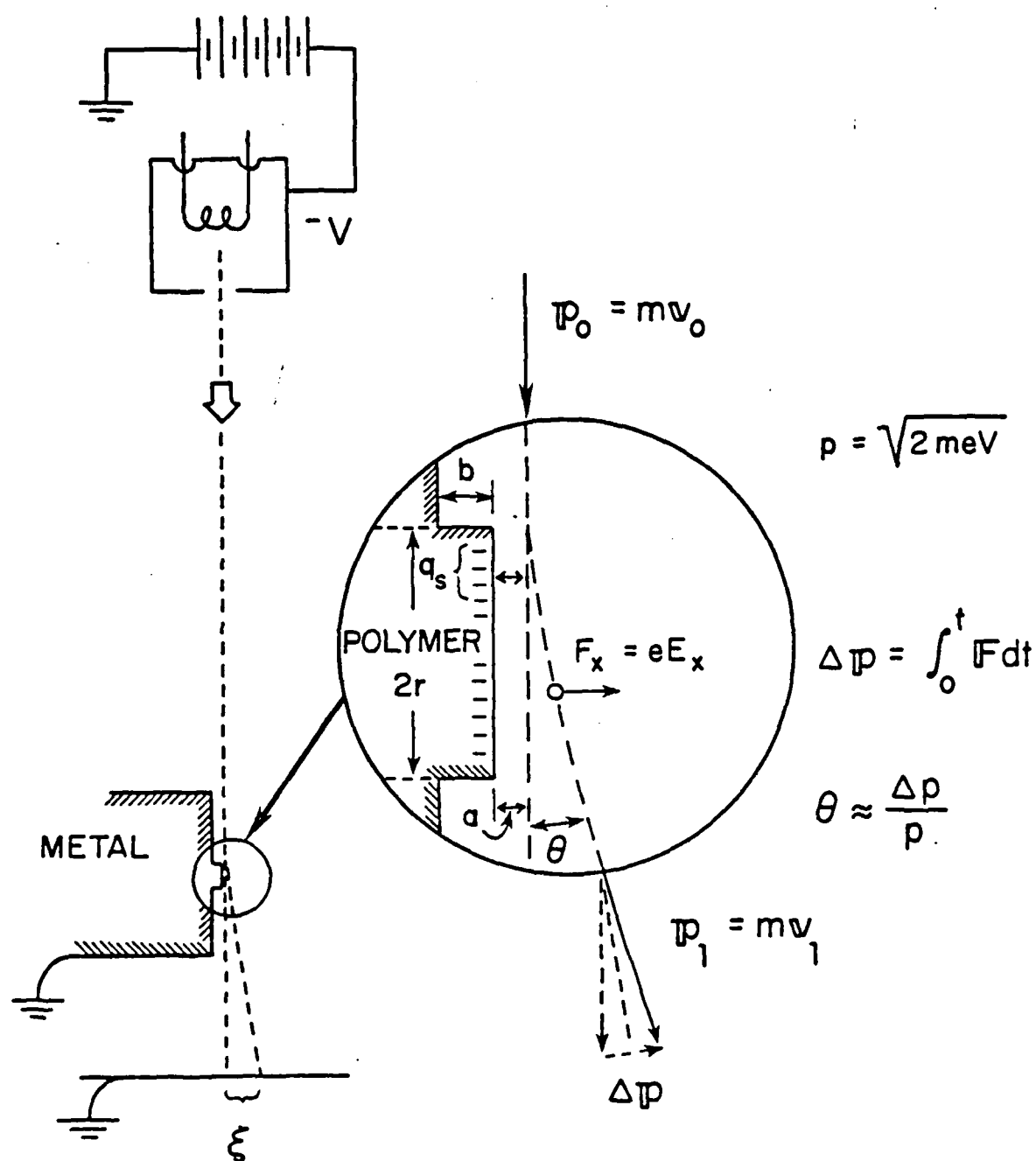


Fig. 66. Schematic of the principles involved in the use of the SEM to measure electrical conductivity.



the end of the fiber. Thus

$$\Delta P_x \approx \int_0^{2r/v_0} (eq_s/2\epsilon_0) dt \approx eq_s r / \epsilon_0 v_0. \quad (83)$$

The deflection angle  $\theta$  is given by

$$\theta \approx \tan^{-1}(\Delta P_x / P_0) \approx \Delta P_x / P$$

$$\frac{eq_s r / \epsilon_0 v_0}{m v_0} = \frac{eq_s r}{m \epsilon_0 v_0^2} \quad (84)$$

$$\frac{eq_s r}{m \epsilon_0} / \frac{(2Ve)}{m} = \frac{q_s r}{2 \epsilon_0 V} \quad (85)$$

To bracket the postulated magnitude of the deflection we can take the other extreme model for the interaction of the electron beam with the charged tip of the fiber, namely the assumption that the charge  $Q = \pi r^2 q_s$  is concentrated in a region that is small compared with the interaction distance  $R$  between the beam and the tip. In this model the mathematical problem is identical to the case of Rutherford

scattering by a nucleus of infinite mass. The classical result for the scattering of a point particle of mass  $m_1$  and charge  $q_1$  by one of mass  $m_2$  and charge  $q_2$  is (64) (66)

$$\tan \frac{\Theta}{2} = \frac{q_1 q_2}{(4\pi e_o)} \frac{m_1 + m_2}{m_1} \frac{1}{T_o a} \quad (86)$$

where  $T_o = (1/2)m_1 v_1^2 = Ve$  is the initial kinetic energy of the particle  $m_1$  in the laboratory coordinate system. The particle  $m_2$  is assumed to be initially at rest. The "impact parameter" (see Fig. 66) is denoted by  $a$ . In our case,  $q_1 = -e$ ,  $m_1 = m$  (mass of electron),

$$q_2 = \pi r^2 q_s \quad \text{and} \quad m_2/m_1 \gg 1. \quad (87)$$

Thus

$$\Theta = 2 \tan^{-1} \left[ \frac{\pi r^2 q_s e}{(4\pi e_o) 2eVa} \right] = 2 \tan^{-1} A. \quad (88)$$

Furthermore, for small angles

$$\tan^{-1} A \simeq A - (1/3) A^3 \quad (89)$$

so that, as a first approximation

$$\Theta \simeq \Theta_1 = 2A = \pi r^2 q_s / (4\pi e_o) Va \quad (90)$$

and as a second approximation

$$\Theta \simeq \Theta_2 = 2A - (2/3)A^3 = \Theta_1 - (\Theta_1^3/12). \quad (91)$$

The ratio of the first approximations for the two models is

$$\frac{(\text{plane charge})}{(\text{point charge})} = \frac{rq_s/2\epsilon_0 V}{r^2 q_s/4\epsilon_0 Va} \approx 2a/r. \quad (92)$$

Thus, since in the original model,  $a$  was to be less than  $r$ , it can be seen that the ratio is near unity. The planar charge model is preferred for  $a \ll r$  and the point charge model for  $a \gg r$ . If it becomes necessary to worry about the statistical distribution of electrons over a distance  $a$  from the fiber tip, the Rutherford scattering cross section concept could be utilized.

Within the charged fiber, it is assumed that the rate of current flow is proportional to the surface charge density, i.e. charge relaxation is

$$\frac{dq_s}{q_s} = -\frac{dt}{\tau}$$

giving

$$q_s = q_s^0 e^{-t/\tau}, \quad (93)$$

The time constant is analogous to an RC-circuit, but on a unit volume basis, therefore

$$\tau = \epsilon/\sigma. \quad (94)$$

This can, perhaps, best be seen by considering the contin-

uity theorem (67) for the current density  $J$

$$\nabla \cdot J = - \frac{\partial \rho}{\partial t} = \frac{\partial J}{\partial x} \text{ (in one dimension)} \quad (95)$$

but

$$J = \sigma \epsilon \text{ and } \partial \epsilon / \partial x = \rho / \epsilon, \text{ so}$$

$$- \frac{\partial \rho}{\partial t} = \frac{\sigma \partial \epsilon}{\partial x} = \sigma \rho / \epsilon \quad (96)$$

Consequently

$$\rho(t) = \rho(0) e^{-\sigma t / \epsilon} = \rho(0) e^{-t / \tau} \quad (97)$$

so that in a conducting medium, the initial charge at every point, and therefore near the surface, decays exponentially with a time constant  $\tau = \epsilon / \sigma$ . As a future part of the investigation, a more detailed study of the space charge limited conditions will be made.

Relative to Figure 66, the theoretical calculation indicates that the deflection  $\delta = \delta_{\max} e^{-t / \tau}$ , with a time constant  $\tau = (\epsilon / \sigma_0) e^{\Delta H^* / RT}$ , where  $\epsilon$  is the dielectric permittivity and  $\Delta H^*$  is the activation enthalpy for the conduction process.

A sample holder for the SEM was developed so that the PPBT film could be mounted in a conducting base and could be charged by the beam and then rotated to the configuration shown in Figure 66. A satisfactory mount was obtained by filling a very small bore copper tube with solder, then inserting the fiber, and allowing it to freeze in place.

No obvious evidence of thermal damage of the fiber has been noted at the  $\sim 200^{\circ}\text{C}$  temperature used to mount the samples. The technique for making a smooth cut in the fibers, to leave a short ( $\sim 10 - 100\mu\text{m}$ ) cylinder exposed proved to be extremely difficult due to the jagged fracture of the fiber and has not yet been perfected.

B. Interdigitated Electrode System for Measuring  $\sigma$   
Due to Pressure::

The interdigitated electrode system (see Figure 67) was proposed and used by Arthur Ruoff et al. at Cornell University (68). The effects of high-pressure (in hundreds of kilobars) on the measurement of  $\sigma$  can be studied. In Ruoff's experiments, some interesting phenomena related to the squeezing of xenon into a metal and sulfur into a superconductor have been discovered.

The device used in this kind of experiment has a flat diamond anvil upon which the experimenters press a diamond with a spherical tip. Figure 67 is a schematic of interdigitated electrodes. Actual electrodes should have 75 or more fingers which can be produced by photolithography. A thin sample is put on top of electrodes. Dashed circles show the circumference of the contact circle when the indenter is applied. Black center circles show two possible cases in which the sample has become conducting.

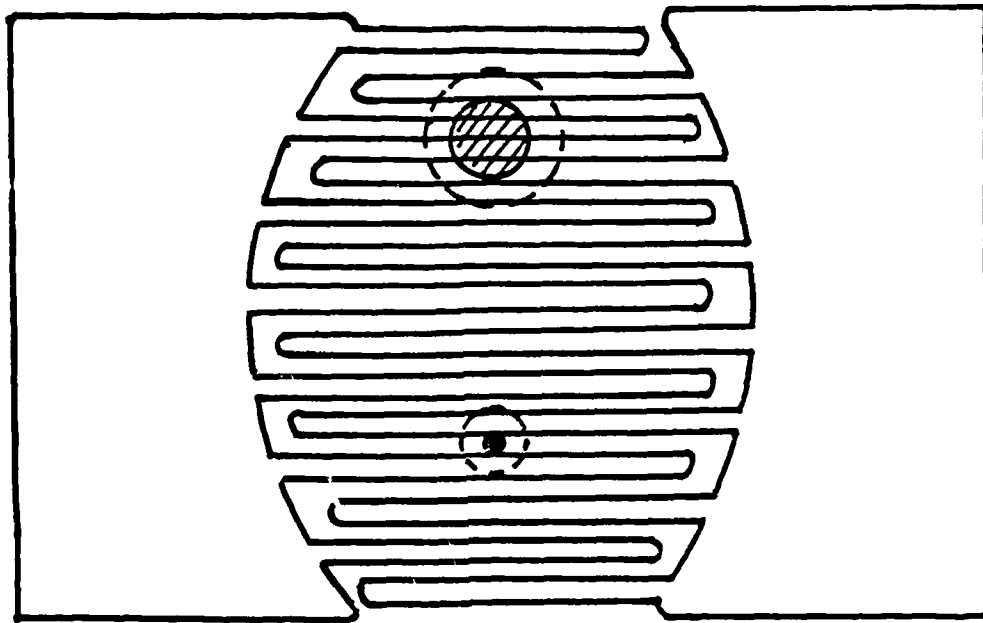


Fig. 67. Schematic diagram for an interdigitated electrodes system.

The pressure distribution and maximum pressure applied can be calculated from Hertz contact theory (69). For elastic deformation Hertz (1890) calculated (Fig. 68) that the contact radius  $r$  is given by

$$r = 1.11 \left( \frac{Na}{Y} \right)^{1/3}, \quad (98)$$

where  $N$  is the normal force,  $Y$  is Young's modulus and  $a$  is the radius of a spherical protuberance (in this case, the diamond indenter) from one of the surface. Pressure is maximum at the center of such a protuberance, and

$$P_{\max} = 1.5 N / \pi r^2. \quad (99)$$

Thus, it can be inferred that

$$\begin{aligned} P_{\max} &= 1.5(N/\pi) [1.11 \left( \frac{Na}{Y} \right)^{1/3}]^{-2} \\ &\approx (1.22/\pi) \left( \frac{NY^2}{a^2} \right)^{1/3} \propto N^{1/3}. \end{aligned} \quad (100)$$

By knowing the elastic constant of diamond, the applied force and the initial radius of the spherical tip, maximum pressure applied can be calculated.

Hopefully, the adoption of the interdigitated electrodes system and the experimental technique can lead to a solution of pressure dependence on  $\sigma$  in both axial and transverse direction of PPBT samples. The samples to be used for the  $\sigma_{||}$  measurements could possibly be discs

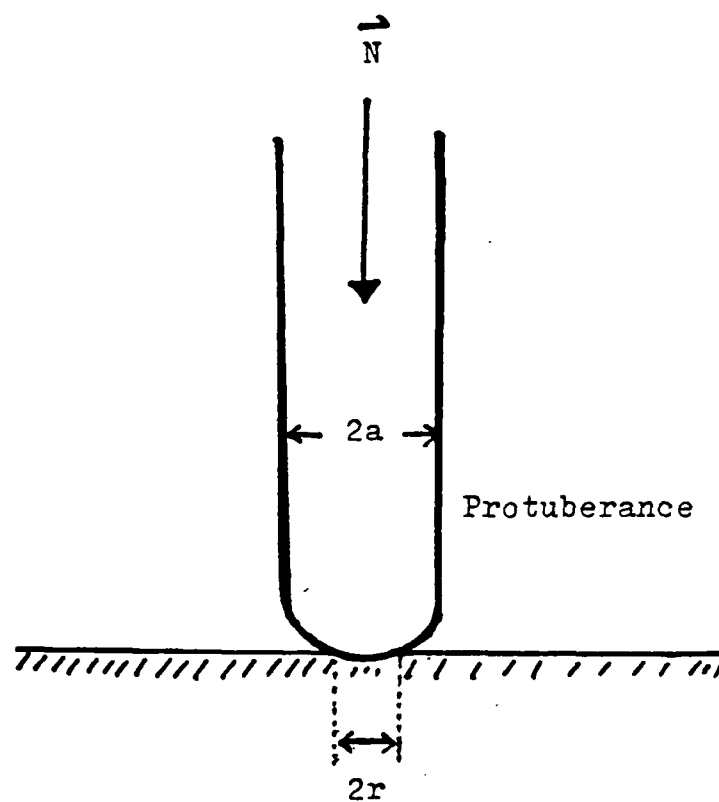


Fig. 68. Radius of contact.



microtomed from a PPBT fibers while the sample for  $\sigma_{\perp}$  measurements will be a small piece of a PPBT film.

C. The "Catwhisker" Technique for High-Electric-Field Studies:

Another topic that would be important for study on small discs of PPBT fibers, is the non-ohmic behavior and ultimate electrical breakdown in strong electric fields. Techniques similar to those used to prepare field-ion-microscope-probes (70) could be used to make a very sharply pointed electrode, about which the field is  $\epsilon_{\max} \approx V/r_{\min}$ , where  $r_{\min}$  is the minimum radius of the tip, and  $V$  is the potential difference between the probe and the sample.

Using 1 M KOH solution as the electrolyte (70), tungsten wire as the anode material, nickel wire as the cathode material (71), and the experimental setup in Fig. 69, several tungsten catwhiskers have been electrochemically produced. As depicted in Fig. 70, an electrode system similar to that used by Van Roggen (72) to study electronic conduction of the polymer single crystal will be used to conduct this sort of measurements.

For samples less than 50Å thick, some interesting tunneling effects are anticipated.

D. Thermally Stimulated Current (TSC) Studies:

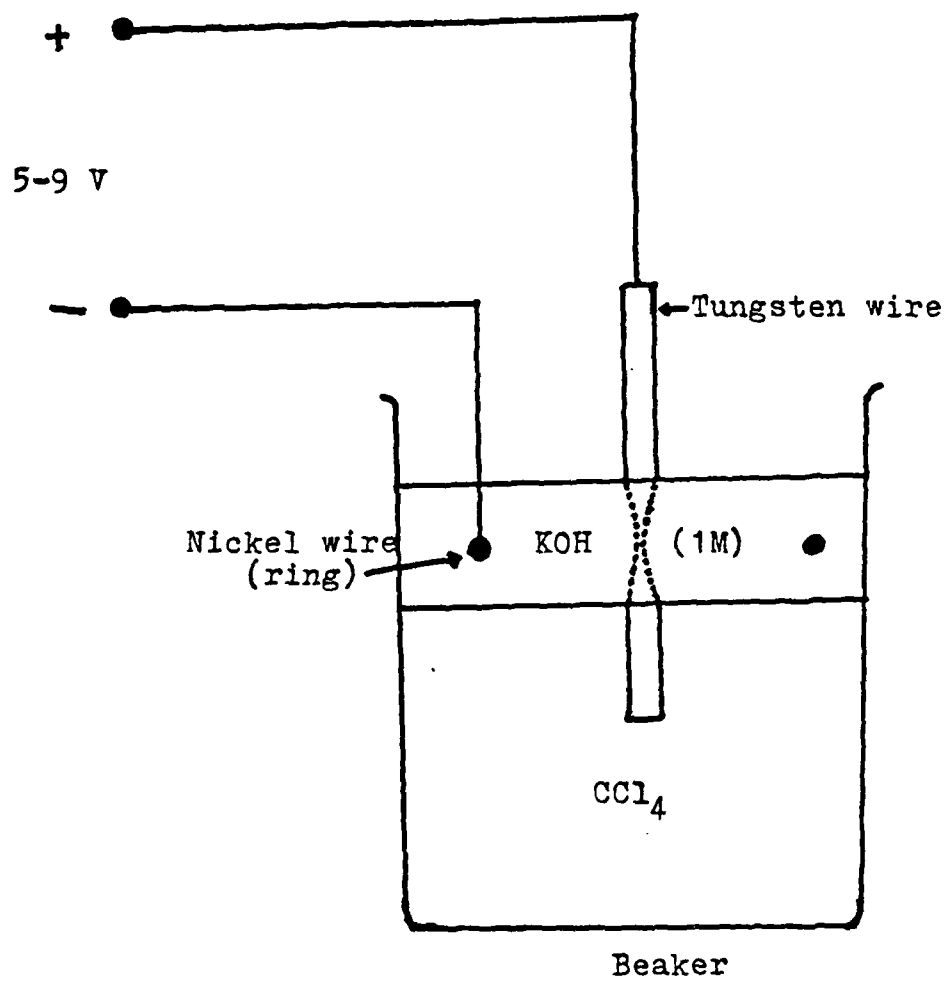


Fig. 69. Experimental setup for the preparation of a tungsten "catwhisker".

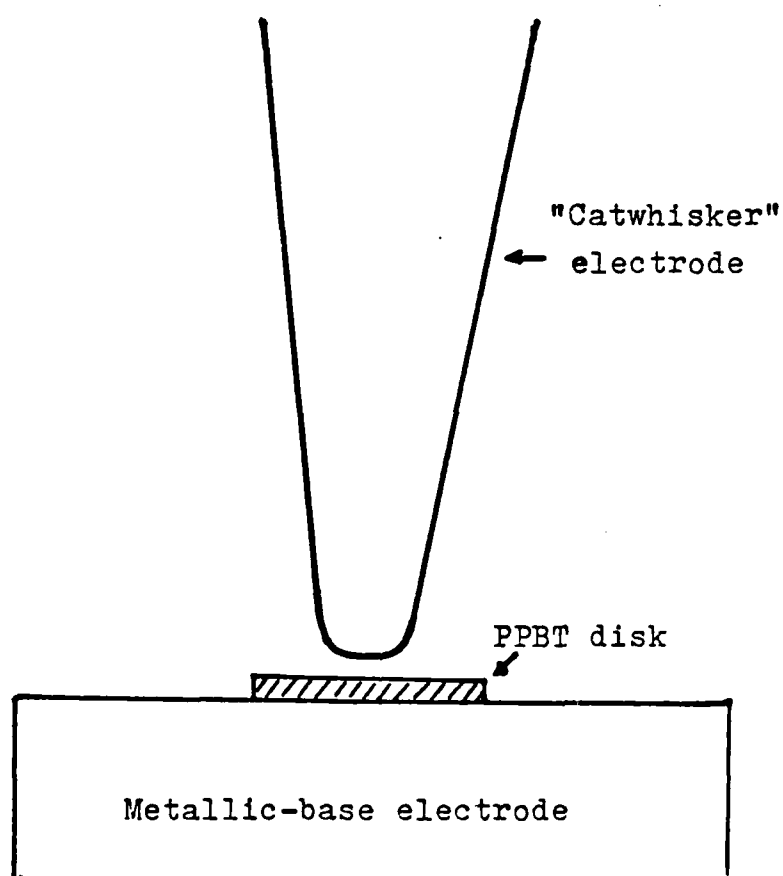


Fig. 70. Proposed electrode system for the study of strong electric fields.

From the experiments of transient phenomena, it is speculated that charge-carrier traps exist in PPBT. To further pursue this speculation, it would be worthwhile to apply an adaptation of the thermally stimulated current technique. The usual technique consists of cooling the sample to low temperatures ( $90^{\circ}\text{K}$ ), creating and trapping the charge carriers by illumination or by the prolonged application of potential. The current passing through the sample is then measured as the temperature is increased at a fixed linear rate. At a certain temperature, the charge carrier acquires sufficient thermal energy to escape from the trap and to contribute to the current flowing through the sample. The fate of the charge carrier will depend upon the number and state of the traps remaining in the solid. It may be swept completely out of the sample, it may be retrapped, or it may recombine with a carrier of opposite charge.

The current measured in such an experiment which is in excess of the normally observed dark current is called the thermally stimulated current. The trap depth can be calculated from the initial rate of current increase with temperature or the temperature at which the maximum current is observed (22). The area under the TSC vs. time curve gives the number of traps  $N_T$ , i.e.

$$N_T = \int_0^t I_{\text{stim.}} dt. \quad (101)$$

E. A Possible Application -- The Indirect Method to Determine the Diffusion Coefficient D of PPBT:

In the previous experiments of salt solutions treated PPBT samples,  $(\Delta I/I_{\min})$  vs.  $\sqrt{t}$  curves were plotted. The rising portion of such a curve was assumed to be due to the effect of water diffusion. This fact led us to think of the possibility of determining D from such measurements.

Figure 71 shows curves of  $\Delta I/\Delta I_{\max}$  vs.  $\sqrt{t}$  for both sorption and desorption cases in a 29022-39-1 PPBT film. Here the term sorption analogous to diffusion experiments means that moisture is diffusing into the experimental material, while the term desorption refers to the outward diffusion process. To estimate D from this figure, the following equation (73) will be used:

$$D = 0.04919 \left( \frac{b^2}{t_{1/2}} \right), \quad (102)$$

where b is the thickness of the sample and  $t_{1/2}$  is the time at which  $\Delta I/\Delta I_{\max} = 0.5$ . In Fig. 71,  $t_{1/2} = 10.24$  min and  $b = 10 \mu\text{m}$  for the PPBT 29022-39-1 film. Thus, the estimated value of D is equal to  $8.0 \times 10^{-11} \text{ cm}^2/\text{sec}$ . The value found experimentally by W.S. Huang (50) is  $9.68 \times 10^{-11} \text{ cm}^2/\text{sec}$ . Thus there is good reason to believe that the technique of measuring  $\Delta I/\Delta I_{\max}$  vs.  $\sqrt{t}$  can be used as

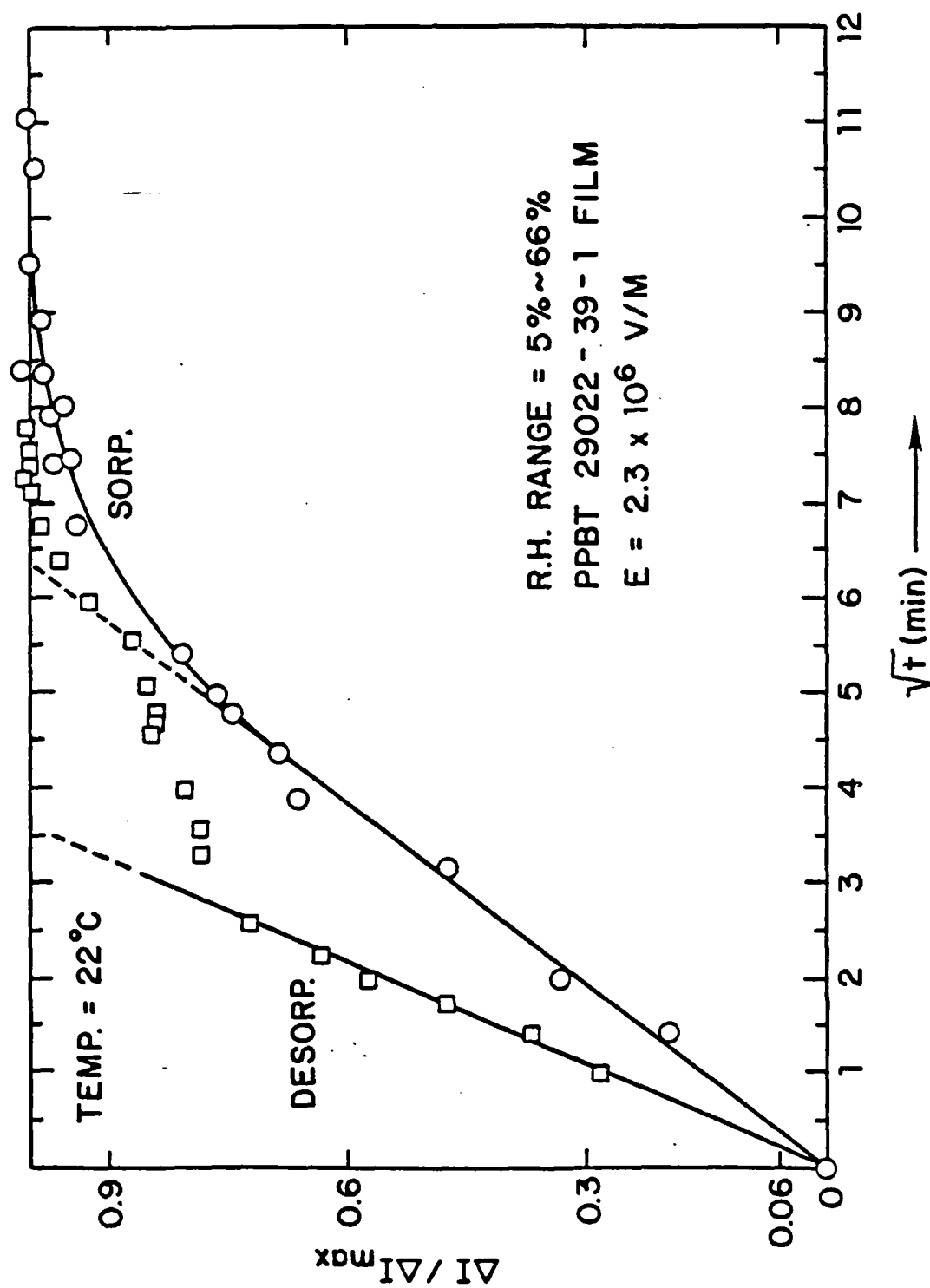


Fig. 71.  $\Delta I / \Delta I_{\max}$  vs.  $\sqrt{t}$  for PPBT 29022-39-1 film.

an indirect method to determine D. Although the preliminary experimental data show such good agreement, the theoretical work of developing a rigorous mathematical model remains to be done. This mathematical model should relate the diffusion process to the electrical conduction process.

In sum, it may be said that the study of electrical properties of PPBT and related polymers is a field rich in potential. The study of PPBT may also lead to important devices, such as a polymeric device similar to a molecular rectifier (74), or useful materials such as plastic-metals, or other applications by virtue of their wide variability of character, and their potential low cost.

## Chapter VIII

### Conclusions

In summary, the following experimental and theoretical accomplishments have been established.

(i) Special techniques have been developed for measuring the axial and transverse electrical conductivities of PPBT fibers and small pieces of film. These special techniques include the designs of the miniature guarded cell (MGC), the notched electrode system (NES), and the technique to separate surface conductivity from volume conductivity for a PPBT fiber.

(ii) Up to fields of  $1.2 \times 10^5$  V/m, the conductivity was observed to be ohmic.

(iii) The transient time of over six hours has been observed. It is proposed that it is due to the inhomogenous nature of PPBT samples, (i.e. the Maxwell-Wagner effect), and to the existence of microvoids inside PPBT samples.

(iv) A very large ratio of axial to transverse conductivity ( $\sigma_{||}/\sigma_{\perp} \sim 10^6$  at  $20^\circ\text{C}$ ) has been found. This is thought to be consistent with the molecular geometry of the PPBT polymer which leads to an extended chain conformation.



(v) Both the axial and transverse conductivities obey an Arrhenius type relation,

$$\sigma = \sigma_0 \exp (-E^*/RT), \quad (60)$$

with  $E_{||}^* = 0.38 - 0.43$  eV (8.8 - 9.9 kcal/mol) and  $E_{\perp}^* = 0.77 - 0.91$  eV (18 - 21 kcal/mol).

(vi) The electrical conductivity of PPBT is virtually independent of the processing history of samples that have thus been studied. Residual acids (MSA and PPA) in PPBT samples were found to be of a negligible amount by experiments involving  $\text{NH}_4\text{OH}$  solution treatment.

(vii) Moisture content increases the conductivity by the following empirical relations:

$$\sigma_{||}(R) = \sigma_{||}(0) 10^{R/36}, \quad (103)$$

and

$$\sigma_{\perp}(R) = \sigma_{\perp}(0) 10^{R/24}. \quad (104)$$

Both relations extrapolate to a finite value for  $R \rightarrow 0$ . This experimental fact leads to the conclusion that there exists dissociable ionic species and a mixture of ionic and electronic conduction mechanisms for PPBT.

(viii) Experimental results from ethyl alcohol treatment and salt solution treatments further support the conclusion of (vii).

(ix) By applying the Barker-Sharbaugh "weak electrolyte model" to experimental data, a mixture of ionic and electronic conduction process in PPBT were theoretically supported.

(x)  $I_2$  doping experiments have shown that charge transfer complex of  $I_2$ -PPBT, is formed upon iodination. This fact implies that the intrinsic electronic conduction can be enhanced by virtue of forming charge transfer complexes.

In conclusion, the study of electrical conductivity doubtless cast important light on the whole matter of the nature of charge transport in poly-(paraphenylene benzobis-thiazole). These results will be far reaching, extending well into our understanding of other important polymeric mechanisms.

## References

1. Chemical & Engineering News. 59, No. 41, 34, Oct. 12, 1981.
2. W.A. Little, Physical Review, 134, No. 6A, 1416, June 15, (1964).
3. L.B. Coleman et al., Solid State Communications, 12, 1125, (1973) Pergamon Press, printed in Great Britain.
4. D.A. Seanor, Adv. Polym. Sci., 4, 317, (1965).
5. Y. Miyoshi and N. Saito, J. Phys. Soc. Japan, 24, 1007 (1968).
6. R.E. Barker, Jr., Pure & Appl. Chem., 45, 157, Pergamon Press (1976), printed in Great Britain.
7. R.E. Barker, Jr. and C.R. Thomas, J. Appl. Phys., 35, No. 1, 87 (1964).
8. R.E. Barker, Jr. and C.R. Thomas, J. Appl. Phys. 35, No. 11, 3202 (1964).
9. R.E. Barker, Jr. and A.H. Sharbaugh, J. Polym. Sci., C10, 139 (1965).
10. A.H. Sharbaugh and R.E. Barker, Jr., Edition du Centre National de La Recherche Scientifique, Paris, No. 179, 349, (1970).
11. G.C. Berry, "Physical Chemical Properties of Complex Aromatic-Heterocyclic Polymers", Technical Report AFML-TR-71-2, Part VII, (1976).
12. E.L. Thomas, R.J. Farris, S.L. Hsu, "Mechanical Properties vs. Morphology of Ordered Polymers", Technical Report AFWAL-TR-80-4045, (1979).
13. A.J. Epstein and J.S. Miller, Scientific American, 241, No. 4, 52, Oct. 1979.
14. D.A. Seanor, J. Polym. Sci., C17, 195, (1967).
15. J.M. Schultz, Polymer Materials Science, Prentice-Hall, Inc., (1974), p. 419.
16. American Society for Testing Materials (ASTM), ANSI/ASTM D 257-76, p. 114.

17. E.L. Thomas, et al., "Mechanical Properties vs. Morphology of Ordered Polymers, Vol. II", Technical Report AFWAL-TR-80-4045, Vol. II (1980).
18. D. Bhaumik and J.E. Mark, Polymer Preprints, 23, No. 1., 105 (1982).
19. S. Glasstone, K.J. Laidler, and H. Eyring, "The Theory of Rate Process", McGraw-Hill, N.Y. (1947), p. 552.
20. H. Sasabe, Researches of the Electro Technical Laboratory, No. 721, Agency of Industrial Sci. and Tech. Tokyo (1971).
21. S. Saito et al., J. Polymer Sci., 6A-2, 1297 (1965).
22. D.A. Seanor, Polymer Science (edited by A.D. Jenkins), North Holland, Amsterdam (1972), p. 1187.
23. L.E. Amborskii, J. Polym. Sci., 62, 331 (1962).
24. Hewlett-Packard 16008A Resistivity Cell Operation Manual, Jan. 1980.
25. J.H. Calderwood, 1981 CEIDP (Conference on Electrical Insulation and Dielectric Phenomena) Annual Report, IEEE Electrical Insulation Society, p. 3 (Oct. 1981).
26. G. Stetter, 1964 CEIDP Annual Report, No. 1238, p. 21, Academy of Science: Washington, D.C. (1964).
27. F.P. La Mantia and D. Acierno, J. Appl. Polym. Sic., 25, No. 4, 554 (1980).
28. H. Scher and E.W. Montroll, Physical Review B, 12, No. 6, 2455 (1975).
29. V. Adamec and J.H. Calderwood, J. Phys. D: Appl. Phys., 11, 781 (1978).
30. F.P. La Mantia and D. Acierno, Polymer, 19, 851 (1978).
31. J.M. G. Cowie, "Polymer: Chemistry and Physics of Modern Materials", Van Nostrand, London (1973), p. 205.
32. Chemical Engineering News, 60, No. 8, 36, Feb. 22, 1982.
33. A.K. Doolittle, J. Appl. Phys., 22, 1471 (1951).

34. T. Miyamota and K. Shibayama, J. Appl. Phys., 44, No. 12, 5372 (1973).
35. J.H. Kallweit, J. Polym. Sci. A1, 4, 337 (1966).
36. F.P. La Mantia, Rheol. Acta. 16, 302, (1977).
37. A.E. Binks and A. Sharples, J. Polym. Sci. Part A-2, 6, 407 (1968).
38. S.D. Bruck, J. Polym. Sci., C17, 169 (1967).
39. Z.G. Soos and D.J. Klein, "Treatise on Solid State Chemistry", vol. 3 (edited by N.B. Hannay), Plenum Press, New York-London (1976), p. 679.
40. Chemical & Engineering News, 58, No. 14, March 31, 1981.
41. J.F. Rabolt, T.C. Clarke, K.K. Kanazawa, J.R. Reynolds, and G.B. Street, J. Chem. Soc., Chem. Comm., p. 347 (1980).
42. W.P. Su, J.R. Schrieffer, and A.J. Heeger, Phys. Rev. Lett., 42, 1678 (1979).
43. J.L. Bredas, R.R. Chance, and R. Silbey, Polymer Preprints, 23, No. 1, 82 (1982).
44. P. Cukor, J.I. Krugler, and M.F. Rubner, Polym. Preprints, 21, No. 1, 161 (1980).
45. L.B. Magnusson, J. Chem. Phys., 39, 1953 (1963).
46. R. Miles, Electronics, Sept. 27, 1979.
47. R. Erdman, Machine Design, Jan. 8, 1981.
48. Keithley 642 Electrometer Operation Manual, March 1980.
49. "Encyclopedia of Modern Plastics", 52, No. 10A, McGraw-Hill publication, 1975-1976.
50. W.-S. Huang, M.S. Thesis, University of Virginia, (1982).
51. J.F. Wolfe, B.H. Loo, and F.E. Arnold, ACS-Polymer Preprint, 19 (2), 1 (1978).
52. C. Kittel, Introduction to Solid State Physics (4th edition), John Wiley & Sons, Inc., New York, N.Y. (1971), pp. 370-371.

53. T. Kaura and R. Nath, *Polymer*, **22**, 1642 (1981).
54. T.E. Helminiak, AFWAL/MLBC/Wright-Patterson A.F.B., 1981, personal communication.
55. S.R. Allen, et al., *Macromolecular*, **14**, 1137 (1981).
56. *Handbook of Chemistry and Physics*, 60th edition, C.R.C. (1980).
57. L. Corrson, "Electromagnetic Fields and Waves", 2nd edition, W.H. Freeman and Company (1970), p. 115, p. 351.
58. E.A. Moelwyn-Hughes, "Physical Chemistry", Pergamon Press (1957), pp. 371-375.
59. Gutman and Daniels, "Outlines of Physical Chemistry", 7th edition, John Wiley and Sons, Inc. (1937), pp. 60-65.
60. P. Debye, "Polar Molecules", Dover Publication, Inc. (1929), pp. 19-22.
61. H.A. Liebhafsky, *J. Am. Chem. Soc.*, **61**, 3517 (1939).
62. A.S. Brill, Physics Dept., Univ. of Virginia (personal communication).
63. *Physics Today*, **32**, No. 9, 19, Sept. 1979.
64. M.F. Rubner, GTE Laboratories Inc., Waltham, MA. (personal communication).
65. A.E. Ruark and U.C. Urey, Atoms, Molecules and Quanta Dover publications, N.Y., 1964, pp. 46-51, 106-109.
66. J.B. Marion, Classical Dynamics, Academic Press N.Y. (1970) 2nd edition, p. 307.
67. W.K.H. Panofsky and M. Phillips, Classical Electricity and Magnetism, Addison-Wesley Publishing Co., Inc., Cambridge, Mass., 1955, p. 77, 98.
68. *Physics Today*, April, 1979, p. 17.
69. C. Zwikker, Physical Properties of Solid Materials, Interscience Publishers, Inc., N.Y. (1954) p. 266.
70. E.W. Muller and T.T. Tsong, Field Ion Microscopy, American Elsevier Publishing Co., Inc., 1969, pp. 23-25.

71. G.L. Cahn, Jr., Materials Science Department, University of Virginia (personal communication).
72. A. Van Roggen, Phys. Rev. Lett., 2, No. 9, 368 (1962).
73. J. Crank and S. Park, Diffusion in Polymers, Academic Press, N.Y. (1968).
74. A. Aviram and M.A. Ratner, Chem. Phys. Lett., 29, No. 2, 277 (1974).

## Appendix I : Preliminary Attempts

In this section a discussion will be given of (A) the ideal ASTM electrode system for films; (B) several systems which have been tried for PPBT-fibers and films; and (C) the microtome method.

### A. Standard Electrode System

The American Society for Testing Materials (ASTM-D257) electrode system and circuit are shown in Fig. I-1. This is known as a guarded electrode system because electrode no. 2 is concentric with no. 1 and separate from it by a gap  $g$  which serves two functions: first the guarding electrode bypasses the most significant part of the surface conduction about the edges of the sample, and second it prevents fringing of the electric field over the Area  $A_1 = \pi D_1^2/4$  used to collect the measured current through the sample of thickness  $b$ . Either silver paint electrodes or evaporated metal electrodes are recommended by ASTM-D257. Although this technique is the easiest way to obtain electrical conductivity, the application of this method was impossible because of the small size of available PPBT samples.



# ASTM (D-257) ELECTRODE SYSTEM & CIRCUIT

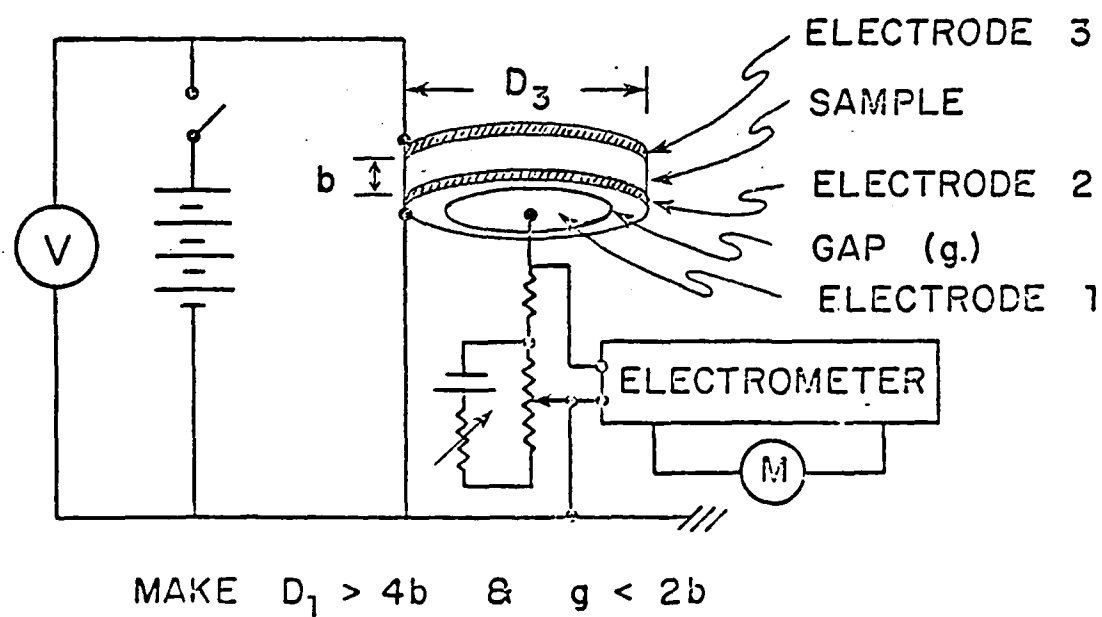


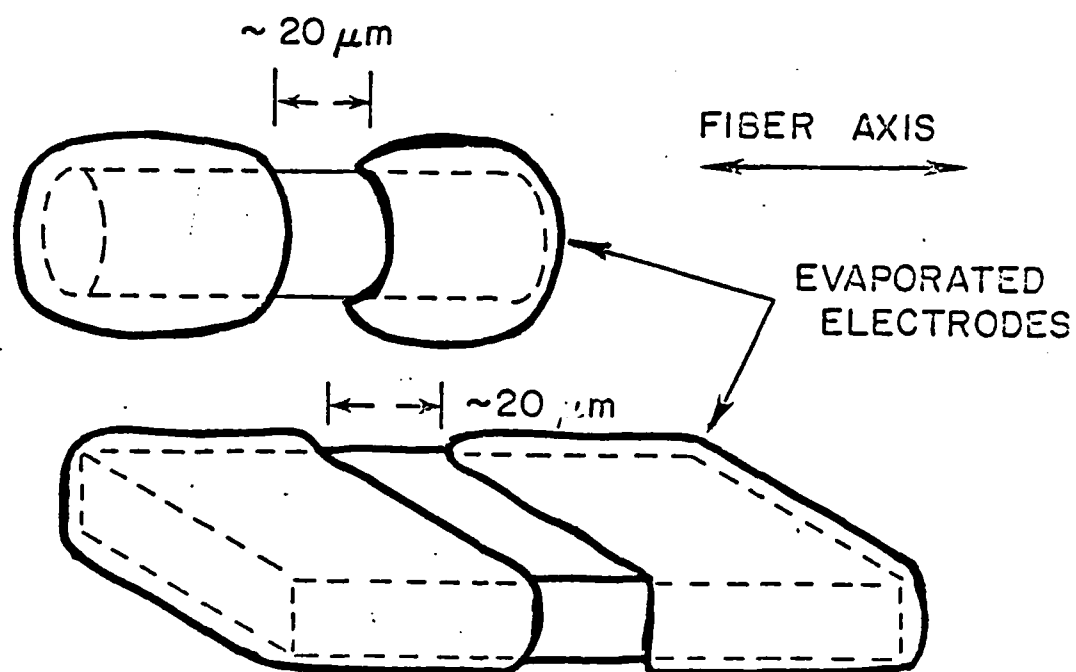
Fig. I-1. ASTM guarded electrode system.

### B. Electrode Systems for Axial Conductivities

Since it was not feasible to use the ASTM method for small diameter fibers, and since it was also desirable to measure conductivity along the chain axis as well as transverse to it, several electrode systems similar to those of Figure I-2 have been tried. A serious limitation of these electrode systems is the absence of a guarding electrode, so that separation of bulk and surface conductivities would require measurements on samples of several sizes. Our early attempts to detect conduction in PPBT with such electrodes were not successful. However, at that time a meter considerably less sensitive than the K642 was used. Some similar samples for a four probe technique have also been made. The fabrication of such samples was accomplished by using  $20\mu\text{m Al}_2\text{O}_3$  fibers to shield the polymer fibers to produce the  $20\mu\text{m}$  gap during the metalizing process by evaporation. In some earlier attempts, small spiderwebs were wrapped around the PPBT fibers but the metal just covered them over and it was too difficult to remove the web to leave a non-conducting gap.

### C. The Microtome Method

Another approach to overcome the difficulty of the small area of the PPBT fibers was to try to microtome the



## SAMPLES FOR AXIAL CONDUCTIVITIES

Fig. I-2. Preliminary electrode systems.

fibers into disks 0.1  $\mu$ m thick. This would then provide a current level about 1,000 times larger than that of the example in Chapter I (actually somewhat more than 1,000 due to the non-ohmic effects mentioned in Chapter II). This method has some serious problems. The fibers were first mounted in a resin, PMMA, which is soluble in benzene. The microtome was then used to cut off 1,000  $\text{\AA}$  slices which were collected in a beaker of benzene. An electrode system similar to Van Roggen's (72) was to be used and disks were supposed to settle randomly so that some would be in the correct position for measurement. Unfortunately, the resin also precipitated on the electrodes and the solution damaged the electrodes.

An attempt was made to separate the PPBT disks from the solution by an inhomogeneous electric field near the edge of a small capacitor. The separation was not effective, probably because the dielectric constant of the PPBT is too close to that of the benzene.

The force acting on a particle of size  $x$  and permittivity  $\epsilon_p$ , suspended in a liquid of permittivity  $\epsilon_1$  is (67)

$$F \approx 4\pi\epsilon_1 x^3 \frac{(\epsilon_p - \epsilon_1)}{\epsilon_p + \epsilon_1} \epsilon_0 \cdot \nabla \epsilon \quad (I-1)$$

The force is small if  $(\epsilon_{PPBT}/\epsilon_0) < 3$ ,  $(\epsilon_{Benzene}/\epsilon_0 \approx 2.27$  at 25°C). A third method, which showed promise but which needs some improvement of details, involves the use of Nucleopore filters to collect the thin samples and then

serve as an electrode system suitable for measuring current-voltage characteristics of microtomed PPBT disks. In this method an electrode is first vapor deposited on a Nucleopore filter which is then used to separate the microtomed polymer disks from a liquid. Subsequently a "catwhisker" type electrode is to be mounted on the upper surface of the disk (72).

## Appendix II : Calculation of $\Psi(t)$ (28)

The main steps in the computation of  $\Psi(t)$  will be outlined in this section. The first step is to consider an arbitrary site as the origin in a random medium and define  $Q(t)$  to be equal to the probability that a carrier remains on the site for a time interval  $t$  after arrival. This probability can decrease in time via all the parallel decay channels for it to transfer to surrounding sites:

$$\frac{dQ}{dt} = -Q \sum_j W(\vec{r}_j), \quad (\text{II-1})$$

where  $W(\vec{r})$  is the transition rate to a site located at  $\vec{r}$ . Solve (II-1) for the fixed (random) configuration  $\{\vec{r}_j\}$  and then compute the configuration average,

$$\begin{aligned} \Psi(t) &\equiv \langle Q(t) \rangle = \langle \exp[-t \sum_j W(\vec{r}_j)] \rangle \\ &= \exp\left(-\int d^3r p(\vec{r}) \{1 - \exp[-w(\vec{r})t]\}\right), \quad (\text{II-2}) \end{aligned}$$

Next determine  $\Psi(t)$  with the relation:

$$\Psi(t) = - \frac{d\Psi(t)}{dt} \quad (\text{II-3})$$

In Eq. (II-2),  $p(\vec{r})d^3r$  is the probability a site is located in a volume  $d^3r$  centered about  $\vec{r}$ . An excellent approximation to the integrand in Eq. (II-2), in the limit of large  $\tau$ , is a unit step function (28),

$$1 - \exp[-w(\vec{r})t] = \begin{cases} 1, & w(\vec{r})t > 1 \\ 0, & w(\vec{r})t < 1. \end{cases} \quad (\text{II-4})$$

Due to the general exponential dependence of  $W(\vec{r})$  on  $\vec{r}$ , the transition from 1 to 0 in Eq. (II-4) is very rapid as a function of  $\vec{r}$ . With

$$W(\vec{r}) = W_M \exp^{-r/R_d}, \quad (\text{II-5})$$

where  $W_M = \tau/t$  and  $R_d$  is the charge-localization radius (one-half the effective Bohr radius), the assumption of a totally random distribution

$$p(r) = N_D, \quad (\text{II-6})$$

and the use of Eq. (II-4), one obtains

$$\ln \Psi(t) = -4\pi N_D \int_0^{r_\tau} r^2 dr = -(\frac{4}{3})\pi N_D r_\tau^3, \quad (\text{II-7})$$

$$\text{where } W(r_\tau)t = \tau e^{-r_\tau/R_d} = e^{-\text{const.}} \approx 1, \quad (\text{II-8})$$

$$\text{or } r_\tau = R_d \ln e^{C\tau} \quad (\text{II-9})$$

Inserting Eqs. (II-7) and (II-9) into (II-3) and absorbing  $e^{C\tau}$  into  $W_M$ , one has

$$\frac{\Psi(t)}{W_M} = \frac{-d\Psi}{d\tau} = \frac{\eta (1m\tau)^2}{\tau [1 + (\eta/3)(1m\tau)^2]}, \quad \tau \gg 1, \quad (\text{II-10})$$

where  $\eta$  is the spatial bias factor. The long tail in  $\Psi(t)$  is related to the absence of a truncation of the transition rate spectrum, i.e., at an arbitrary  $t$  one can "find", with

a finite probability, a  $W(\vec{r})$  such that  $W(\vec{r})t \approx 1$ . The "smoothness" of the tail is related to the random assumption (II-6). If instead of Eq. (II-5) one used:

$$W(\vec{r}) = W_M \exp [-(r/R_d)^\gamma], \quad (\text{II-11})$$

$$\text{with } \gamma \geq 1, \text{ then } r_\tau = R_d (\ln \tau)^{1/\gamma} \quad (\text{II-12})$$

$$\text{and } \Psi(t) = \exp [-(\eta/3) (\ln \tau)^{3/\gamma}]. \quad (\text{II-13})$$

Hence for  $\gamma > 1$ , the time dependence of  $\Psi(t)$  would be slower than Eq. (II-10) for a given value of  $\eta$ .



### Appendix III : High Resistance Measurements

#### A. Measuring high resistance (47)

Two methods of measuring resistance will be considered: the constant voltage method and the constant current method. In the constant voltage method, a constant voltage is impressed across the resistance to be measured, and the resulting current flow is measured to indicate resistance. In the constant current method, a current source is connected to the resistance to be measured and the resulting voltage drop is measured to indicate resistance.

Electrometers usually employ the constant-current measurement technique which is represented in Fig. III-1. This constant-current technique is often preferred because it requires only one piece of test equipment, whereas constant-voltage tests require separate high-accuracy voltage sources and ammeters. Electrometers typically employ an amplifier containing a high input resistance to allow the accurate measurement of high resistances. The factor that usually limits measurement accuracy in these meters is the shunt resistance of the associated cables and the noise current generated in the interconnections.

To minimize error currents caused by these shunt resistances, the electrometer amplifier output can be used as a guard connection for insulators connected to the elec-

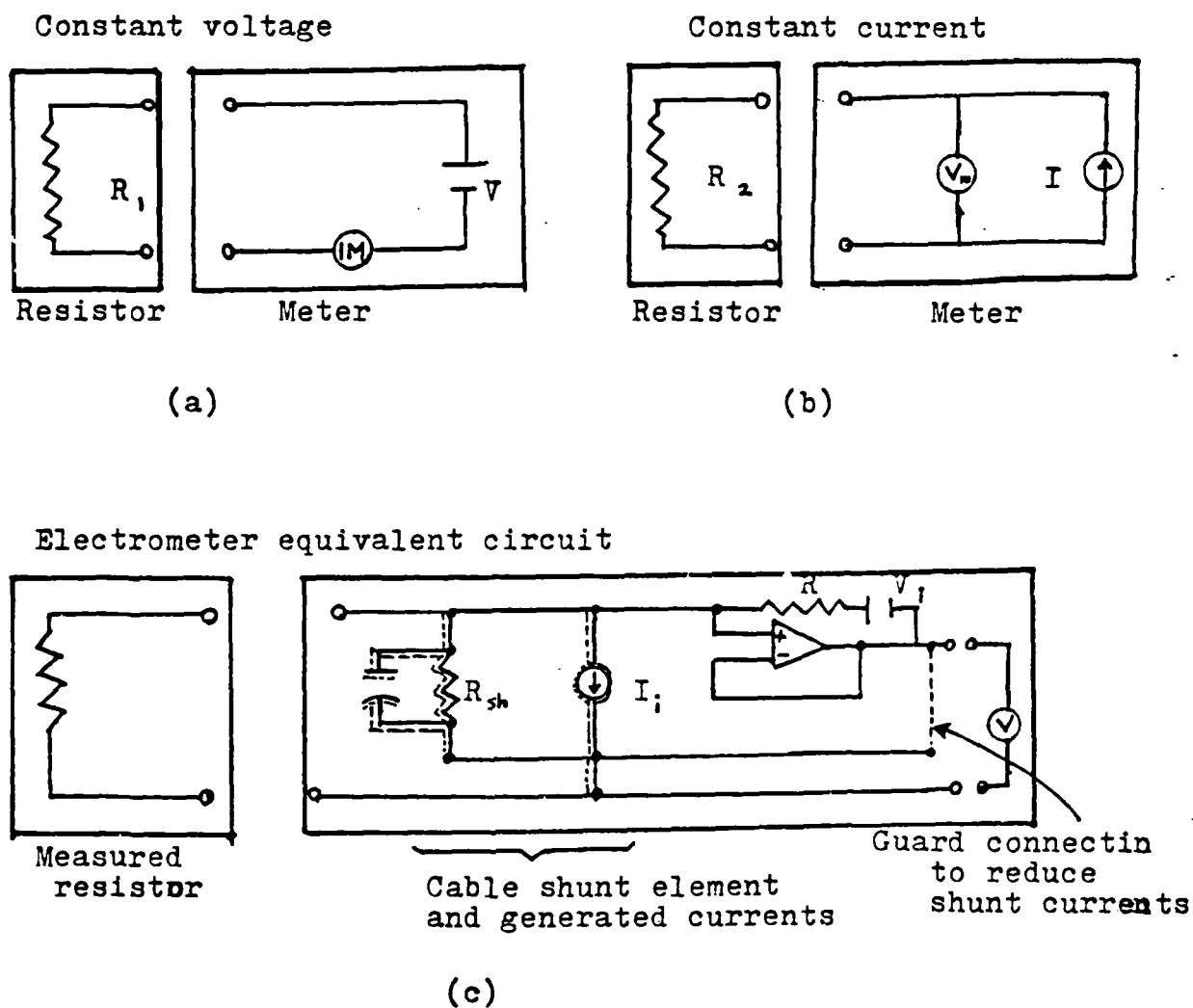


Fig. III-1. Techniques for measuring high resistance.

trometer input, Fig. III-1(c). This connection makes the voltage across the input insulators equal to the output voltage divided by amplifier gain. And amplifier gain is very high. Guarding also reduces the effective input cable capacitance, since this factor is also divided by amplifier gain.

#### B. Three measurement demons (46)

##### (i) Heat:

In a resistor, the kinetic energy of molecules produces random motion of electrical charges. These random charge movements result in what is known as Johnson noise (also called thermal or heat noise). In theory, the power available from this motion is constant and given by:

$$P_J = 4kT\Delta f \quad (\text{III-1})$$

where  $k$  = Boltzmann's constant,  $T$  = temperature in Kelvins, and  $\Delta f$  = the noise bandwidth in hertz over which the measurement is being made. Metallic conductors approach this theoretical noise level; other materials produce more noise than theory predicts. From the equation, the next mean square voltage noise developed in a resistor,  $R$ , can be found:

$$V_J = (P_J R)^{1/2} = (4kT\Delta f R)^{1/2} \quad (\text{III-2})$$

and Johnson current noise ( $I_J$ , in amperes rms) becomes:

$$I_J = (P_J/R)^{1/2} = (4kT\Delta f/R)^{1/2}. \quad (\text{III-3})$$

(ii) Pressure or stress

Piezoelectric currents are generated when mechanical stress is applied to certain insulating materials, notably ceramics and other crystalline materials. Teflon and some other plastics used for insulated terminals and interconnecting hardware exhibit what is known as a space charge effect, wherein an applied force creates a change in capacitance and thus a charge redistribution. The operational behaviour is the same as for piezoelectric materials, viz., a physical force creates a current.

(iii) Friction:

Triboelectrically generated currents result from the creation of charges at the interface between a conductor and an insulator due to frictional forces at the interface, for example, when a cable is moved. The mechanism involved is one of interfacial transfer of electrons, creating a charge imbalance and thus a transient current flow. Low noise cables are available with a conductive coating

(usually graphite) at the metal-insulators boundary, reducing this effect significantly. Currents down to 1 picoampere can be measured using cables treated in this manner. Rigidly securing a cable to prevent any movement will permit its use down to a few femptoamperes. Rigid airline coaxial cable such as GenRad GR874 series is suitable down to 0.1 fA. Below this current level, special connection schemes and the use of high quality insulators such as sapphire are required. For example, the sapphire-insulated input connector is used in the Keithley 642 electrometer. Table III-1 compares these properties for many commonly available insulating materials.

TABLE III-1

Material	Volume resistivity (ohm-centimeters)	Resistance to water absorption	Minimal pizoelectric effects	Minimal triboelectric effects
Sapphire	$10^{16} - 10^{18}$	V	V	M
Teflon	$10^{17} - 10^{18}$	V	W	W
Polyethylene	$10^{14} - 10^{18}$	M	V	M
Polystyrene	$10^{12} - 10^{18}$	M	M	W
Kel-F	$10^{17} - 10^{18}$	V	M	W
Ceramic	$10^{12} - 10^{14}$	W	M	V
Nylon	$10^{12} - 10^{14}$	W	M	W
Glass epoxy	$10^{10} - 10^{17}$	W	M	W
Polyvinyl chloride	$10^{10} - 10^{15}$	V	M	M
Phenolic	$10^5 - 10^{12}$	W	V	V

KEY V = Very good in regard to the property

M = Moderately good in regard to the property

W = Weak in regard to the property

## Appendix IV

## The Estimation of the Isotropic Dielectric Constant

## A. Semi-empirical estimation:

At optical frequencies, according to Maxwell's rule  $K \sim r^2$ , where  $r$  is the refractive index;  $K_{PPBT}$  can be calculated from values of  $r_{PPBT}$  listed in reference (12), Table IV-1. The average value of  $K = K_{iso}(0)$  from three different approaches is about 3.34.

## B. Theoretical estimation using Group Additivity

By defining a function  $\pi = (K-1/K+2)M/\rho$  (60), where  $M$  is the molecular weight and  $\rho$  is the mass density,  $K$  can be calculated from group contribution of the molar polarizability  $\pi$ , i.e.

$$\pi = \sum_i \pi_i \quad (IV-1)$$

$\pi_i$ 's value can be found in reference (56), (57), (58), and (59). Thus,

$$\begin{aligned} \pi_{PPBT} &= \pi_{\text{phenyl}} + \pi_{\text{ether}} + 2\pi_C + 2\pi_S + 2\pi_N \\ &= 61.39 \text{ cm}^3/\text{mol}. \end{aligned}$$

Table IV-1 ESTIMATION OF  $K_{PPBT}$ 

Approach	$\gamma_{PPBT}$	$K_{PPBT}$
Lorentz-Lorenz	1.865	3.48
Gladstone-Dale	1.836	3.37
Vogel	1.785	3.19

$$K = r^2$$



This value accompanied with  $\rho_{\text{PPBT}} = 1.60 \text{ g/cm}^3$  (12) and  $M_{\text{PPBT}} = 266.34 \text{ g/mol}$  implies that  $K_{\text{iso}}(0) \approx 2.75$ .

### C. Semi-quantitative estimation by comparison

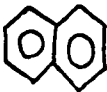
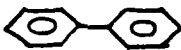

By examining  $K$  of several compounds which are structurally related to PPBT, Table IV-2 (56),  $K_{\text{iso}}(0)$  of PPBT can be roughly estimated to be about 2.60.

Furthermore, with data assembled by Sasabe (20), for ionic conducting polymers, electrical conductivity of  $10^{-18} \Omega^{-1} \text{cm}^{-1}$  corresponds to  $K \sim 2.5$  and electrical conductivity of  $10^{-12} \Omega^{-1} \text{cm}^{-1}$  corresponds to  $K \sim 8.0$  (Fig. IV-1). Thus, it is reasonable to say that  $K_{\text{iso}}(0)$  should be within the range of 2.5 - 8.0.

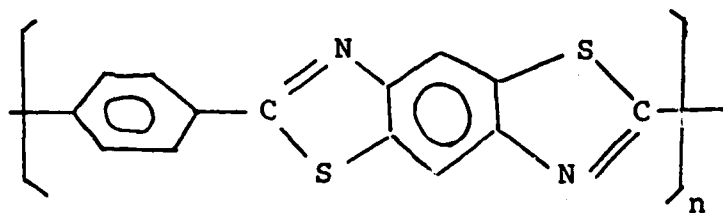
In conclusion, based on the above analysis,  $K_{\text{iso}}(0) \approx 3.0$  is chosen to be the estimated isotropic dielectric constant of PPBT.

TABLE IV-2

PPBT - STRUCTURALLY RELATED MATERIALS  
AND THEIR ISOTROPIC DIELECTRIC CONSTANTS

Material	Structure	K
Naphthalene		2.52 (22°C)
—		2.54 (85°C)
Diphenyl		2.53 (75°C)
Diphenylmethane		2.70 (22°C)

PPBT :



LOG (DC-CONDUCTIVITY) VS RECIPROCAL  
DIELECTRIC CONSTANT  $K'$  (100 Hz) FOR  
POLYMERS AT 25°C.

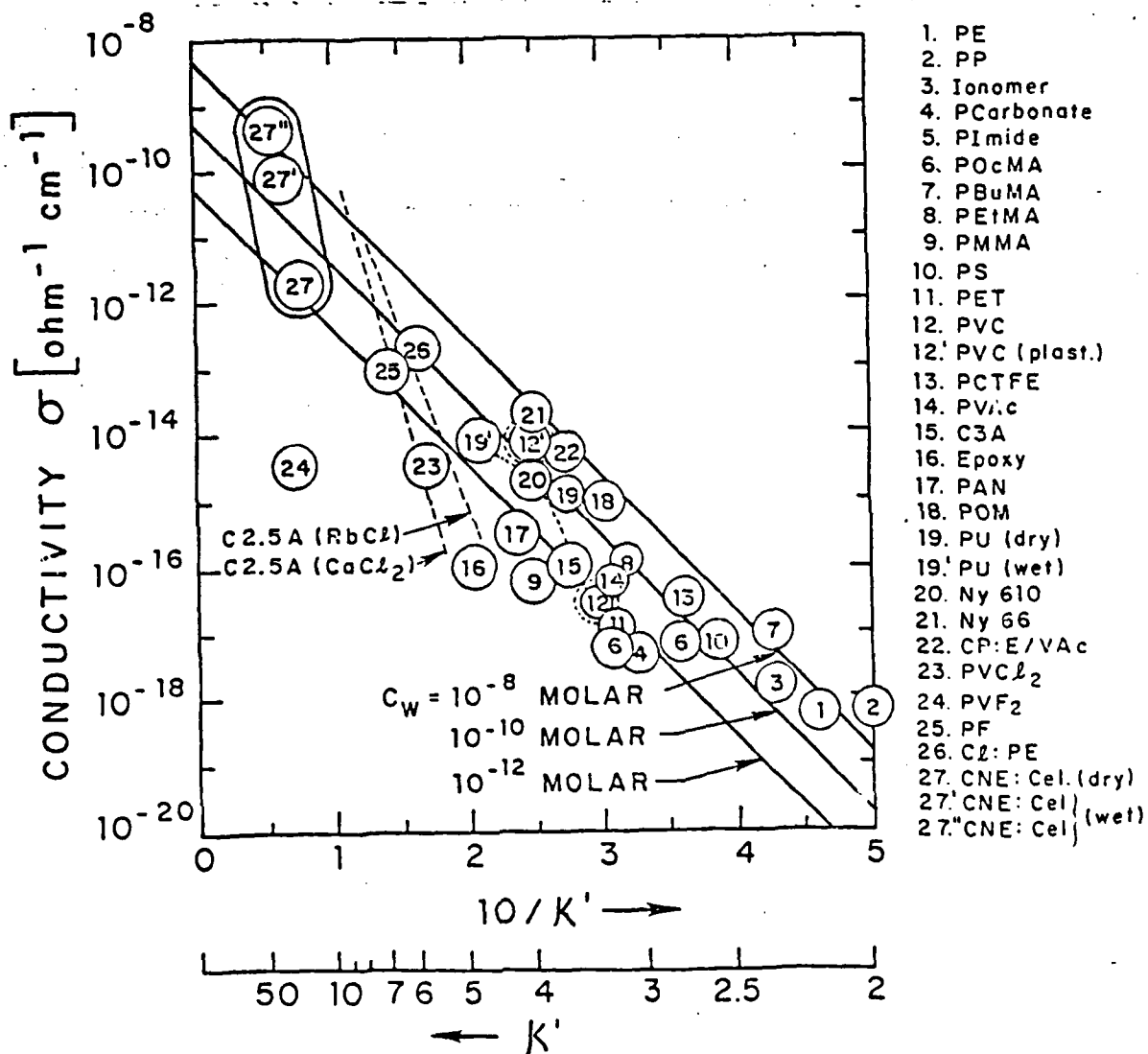


Fig. IV-1.

## DISTRIBUTION LIST

### Copy No.

1 - 16	U.S. Air Force Office of Scientific Research Bolling Air Force Base Washington, D.C. 20332 Attention: Mr. Donald R. Ulrich Building 410 NC
17 - 18	R. E. Barker, Jr.
19 - 20	K. R. Lawless
21	Dr. T. E. Helminiak AFML/MBP Wright-Patterson AFB, Ohio 45433
22	Dr. J. E. Mark Chemistry Department University of Cincinnati 2624 Clifton Avenue Cincinnati, Ohio 45221
23	Dr. E. C. Chenevey Celanese Research Co. Summit, New Jersey 07901
24 - 25	E. H. Pancake Clark Hall
26	SEAS Publications Files

**UNIVERSITY OF VIRGINIA**  
**School of Engineering and Applied Science**

The University of Virginia's School of Engineering and Applied Science has an undergraduate enrollment of approximately 1,450 students with a graduate enrollment of approximately 500. There are 125 faculty members, a majority of whom conduct research in addition to teaching.

Research is an integral part of the educational program and interests parallel academic specialties. These range from the classical engineering departments of Chemical, Civil, Electrical, and Mechanical and Aerospace to departments of Biomedical Engineering, Engineering Science and Systems, Materials Science, Nuclear Engineering and Engineering Physics, and Applied Mathematics and Computer Science. In addition to these departments, there are interdepartmental groups in the areas of Automatic Controls and Applied Mechanics. All departments offer the doctorate; the Biomedical and Materials Science Departments grant only graduate degrees.

The School of Engineering and Applied Science is an integral part of the University (approximately 1,500 full-time faculty with a total enrollment of about 16,000 full-time students), which also has professional schools of Architecture, Law, Medicine, Commerce, Business Administration, and Education. In addition, the College of Arts and Sciences houses departments of Mathematics, Physics, Chemistry and others relevant to the engineering research program. This University community provides opportunities for interdisciplinary work in pursuit of the basic goals of education, research, and public service.

**END**

**FILMED**

---

*1-86*

**DTIC**